Effects of Slab-Column Interaction in Steel Moment Resisting Frames with Steel-Concrete Composite Floor Slabs

A thesis submitted in partial fulfillment of the
requirements for the Degree of
Masters in Civil Engineering

by

Michael Hobbs

Supervised by
Associate Professor Gregory MacRae
Professor Desmond Bull

Department of Civil and Natural Resources Engineering
University of Canterbury
Christchurch, New Zealand

February 2014

Abstract

Composite construction is widely used worldwide and is undergoing significant technological development. New Zealand is part of this development, with new beam options incorporating multiple unstiffened web openings and new deck profiles supported by extensive testing. However, one area where relatively little research has been undertaken is in the interaction of the composite slab with the seismic resisting system under lateral loading.

In order to provide important new information in this area, a series of full scale beam-column-joint-slab subassemblies were tested at the University of Canterbury. Specimens tested had moment end plate connections and different combinations of deck tray direction, and isolation of the slab from the column. An additional test uses a sliding-hinge type connection to assess the effect of the floor slab in this type of low damage connection.

In these tests the lateral capacity of the seismic resisting system was increased by up to 25% due to the presence of the slab in contact with the column. The increase in capacity is 10% greater for decking running in longitudinal direction than in the transverse direction as a result of a more substantial full depth slab bearing on the column. The floor slabs of the subassemblies with the slab cast against the column all showed a higher level of damage than for those with the isolated column and the post ultimate strength degradation of the subassemblies without special detailing was significant. The subassembly with a section of full depth slab surrounding the column also exhibited a higher capacity but with an improved post ultimate strength degradation. All moment end plate subassemblies sustained drifts of up to 5% without significant strength loss.

The sliding hinge joint showed little signs of damage under testing to 5% drift. Some inelastic deformation of the connection and beams was noted above 5% drift.

Results from both testing and numerical modelling have shown that the current methods used to design these systems are conservative but within 15% of the values observed. Further testing and modelling will be necessary before any meaningful changes can be made to the way in which these systems are designed. Recommendations have been made regarding the placements of shear studs in plastic hinge zones and the provision of slab isolation around beam-column connections.

Acknowledgments

I would like to start by thanking my supervisors, Associate Professor Gregory MacRae and Professor Des Bull who have guided me throughout this project.

Thanks must also go to all the following people for your technical assistances:

- Professor Roberto Leon and Professor Charles Clifton for their assistance in the design of the specimens and testing protocol;
- Associate Professor Umarani Gunasekaran and Emeritus Professor Athol Carr for their assistance with Ruaumoko modelling;
- Peter Coursey, Gavin Keats, Russell McChonchie, John Maley, Tim Perigo and the other laboratory technicians for their assistance in the testing associated with my thesis. Also to Andrew Dunbar, Mustafa Marshall, Wouter van Beerschoten and Sam White for their assistance.

Without your valuable and timely assistance, the project could not have been a success.

Finally I would like to thank all of my family, friends and colleagues who have supported me throughout this project, I owe a great deal of gratitude to you all.

Table of Contents

Figures

1 Introduction

1.1 Background

The use of composite steel-concrete construction techniques in design is common practice in New Zealand, particularly in medium to high rise construction. The idea of using different construction materials in such a way that the benefits of each are fully utilised has been utilised by engineers for many years for the design of strong, yet cost effective, buildings. A primary example of this is reinforced concrete, where both the concrete and the steel reinforcement are combined such that each elements strength is used to compliment the others weakness. The concrete mass forms a strong compressive element with limited tensile capacity. The tensile strength is provided by the steel which is strong in tension but is susceptible to buckling under compressive loads.

In recent times, more innovative uses of composite design have been sought for low cost structural steel-concrete composite construction (SSCCC). These include members such as concrete filled steel tubes for columns and braces, I-beams or columns with concrete cast into the web cavity to restrain buckling and, most commonly, the use of cast-in-situ concrete floor slabs on sheet steel decks.

Composite floor slabs are usually cast in-situ over a flat or ribbed sheet steel deck tray hence eliminating the need for boxing and reducing the need for propping. The slab is connected to the steel frame via steel shear studs welded to the beams as shown in Figure 1-1. This connection allows the slab to contribute to the flexural strength of the beam hence increasing its strength. Reinforcing is provided in the concrete slab to limit slab cracking and to assist in the transfer of forces around openings in the slab such as the column in Figure 1-1. The slab can also be cast either with a gap around the column (isolated) or in direct contact with the column flanges.

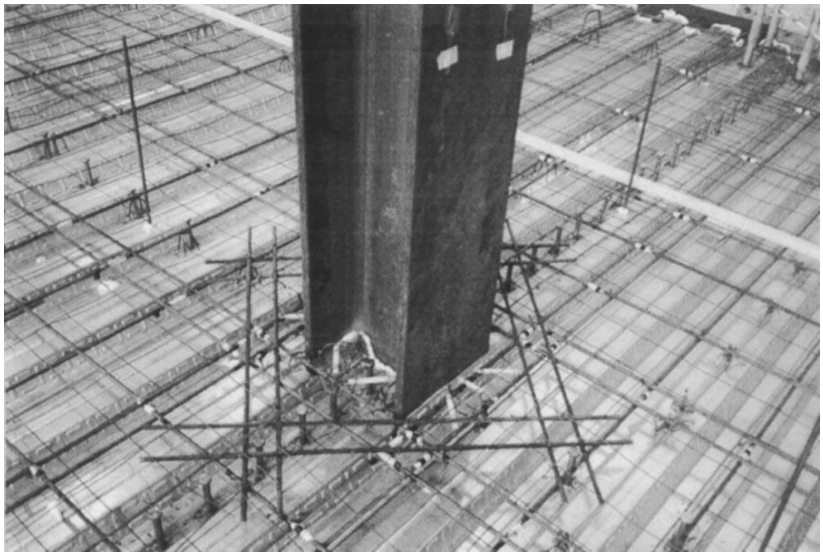

Figure 1-1: Typical slab detailing around column

The use of this SSCCC may provide designers with an opportunity to reduce overall costs by reducing the beam size. Under gravity loading the concrete acts as a compression element, raising the neutral axis (as shown in Figure 1-2), allowing the steel beam to devote a larger portion of its area to resisting the tensile forces. As such a smaller beam with composite slab can sustain the same level of gravity load as a larger beam without a slab. Design processes for gravity loading are well documented.

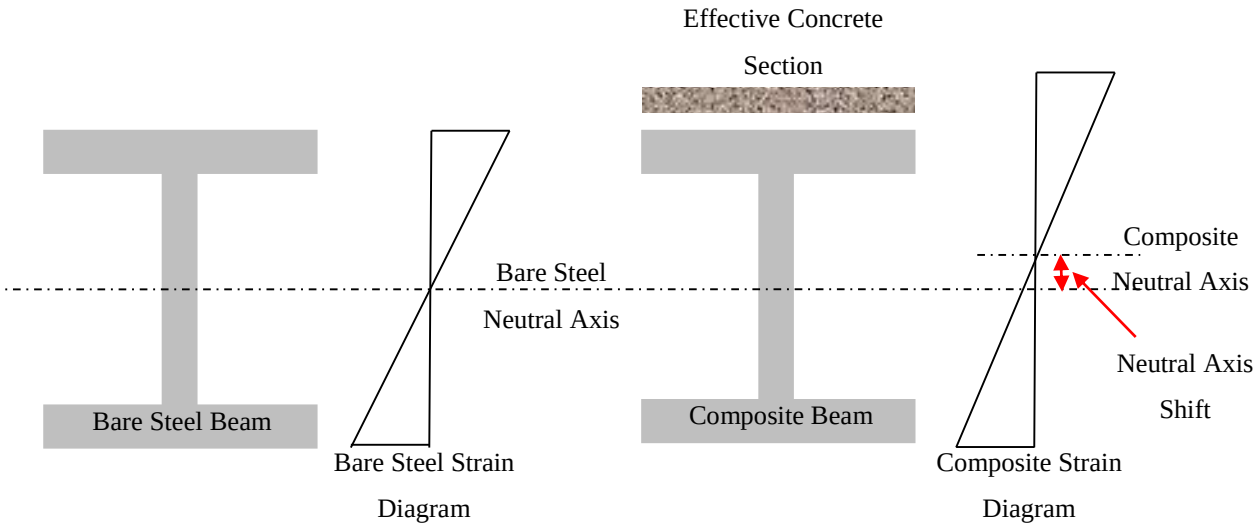

Figure 1-2: Composite action effect on beam neutral axis.

Significantly less work has been conducted for the design of composite beams for lateral loading. When the concrete slab is poured in contact with face of the column flanges, direct bearing can occur when the slab is in compression against the column as shown in Figure 1-3. This bearing implies that the slab resists seismic loads. However, in current New Zealand and worldwide practice the steel beam without the slab is considered to carry the seismic loads when designing for beam size. This results in a larger beam size than if composite action with the slab were considered.

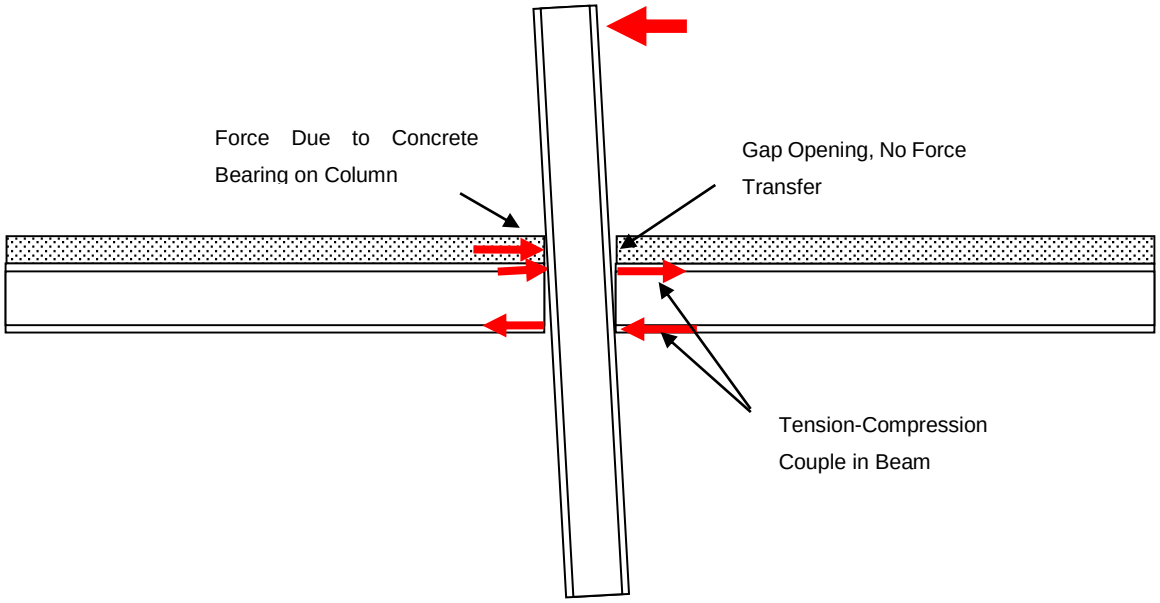

Figure 1-3: Evaluation of subassembly showing slab bearing forces on column flange.

A possible reason as to why the beam-slab composite effects are not considered in design is that the bearing interaction is relatively unknown and is not considered to be dependable. Whilst contact between the slab and the column is one obvious load path, the presence of the reinforced slab surrounding the column may allow for force transfer around the column as shown in Figure 1-4. As such the effect of the slab may affect the likelihood of panel zone and column yielding. Other issues such as stiffness differences and displacement incompatibility may also have an effect on these systems.

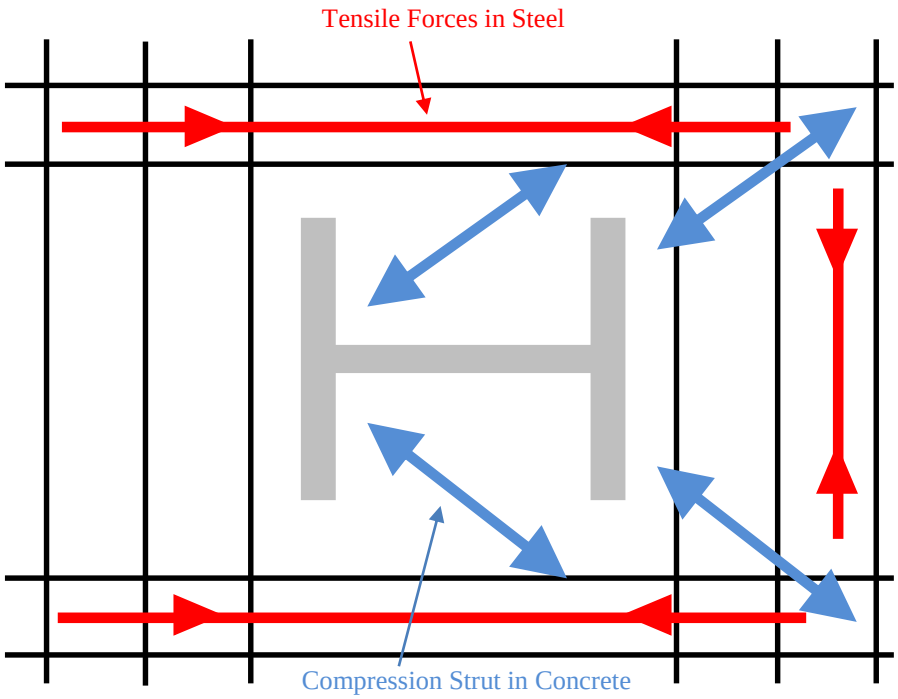

Figure 1-4: Forces in concrete and reinforcing steel around column.

The only code worldwide which explicitly considers these possible detrimental effects of interaction is the New Zealand steel code. Background studies in the area of slab-column interactions have little in terms of experimental test data and whilst past studies have concluded that the composite slab does have an effect on lateral resistance this has yet to be fully utilised in design.

Slab-column interaction does not only affect traditional fully restrained moment connections, but it can also affect newer "low damage" connections such as the sliding hinge joint. In such connections damage to the slab may be restricted to a smaller area, resulting in more intensive damage.

Also after the 2010-2011 Christchurch earthquake sequence, significant slab damage was observed in reinforced concrete structures owing to beam elongation. This beam growth caused gapping at either end of the beams which in turn caused separation in the floor slab. The question has been asked as to whether this same beam growth is likely to occur in steel beams both with and without composite slabs.

1.2 Need for Research

Based on the discussion above, it is clear that there is a need to evaluate the New Zealand design approach to determine whether slab effects are significant and if they can be considered both for the design of the beam itself as well as for the design of the panel zone and column for traditional and newer beam-column moment connections.

1.3 Scope and Objectives

The aim of this study is to address the need outlined above. In particular, answers are sought to the following questions:

a) What is the effect of isolating the floor slab from the column on flexural strength of the subassembly?

b) What is the effect of the direction of the deck tray on the performance of the subassembly?

c) Does the concrete slab contribute significantly to the strength loss of the non-isolated subassemblies and what are the strength loss mechanisms?

d) What effect does the provision of a full depth slab around the column slab have on the performance of the subassembly?

e) What are the modes of steel strength loss in the subassemblies with fully restrained moment connections?

f) Can steel section and material properties and dimensions be used to predict the strength of a subassembly where the slab is separated (isolated) from the column face?

g) Is it possible to model this slab column interaction using simplified modelling techniques?

h) Are the effects of beam elongation significant in this type of steel moment resisting frame?

i) What is the effect of the slab on low-damage sliding hinge connections?

j) Do the current methods used in NZS3404 result in a reasonable approximation of the effects of the composite slab and if not what changes could be made to improve the accuracy of the code calculations?

2 Literature Review

2.1 Design Codes

2.1.1 New Zealand Structural Steel Code (NZS3404)

The New Zealand Steel code, NZS 3404 (2009) [1] does not consider the effects of slabs in sizing the beams for seismic loading. However slab effects must be considered when computing overstrength moments at the column face. Consequently, connection and column detailing must be such that all other components have capacity to withstand the overstrength action of the beams. Clause C12.10.2.4 of NZS3404 (2009) states that the overstrength method in is based on the assumption that the slab is infinitely rigid and strong axially and carries compression forces which arise from bearing over a defined contact area on the outer face of the column flange.

The process for determining overstrength moments in category 1, 2 and 3 moment resisting frames (fully ductile, limited ductility and nominally ductile) is described in NZS3404 (2009) section 12.10.2.4. The overstrength moment capacity, M^o_{bi}, of each steel beam is calculated by applying an overstrength factor, ϕ_{oms} (given in clause 12.2.8), to the nominal member flexural capacity of the steel beam, $M_{bi,}$ as shown in Equation 1.

$$\boldsymbol{M^o_{bi} = \varphi_{oms} M_{bi}}$$

Equation 1

To account for the axial forces resulting from the slab-column contact shown in Figure 2-1, the sum of the overstrength moment of the beams, M^o_i, is reduced using the moment-axial force interaction shown in Figure 2-1. The slab participation factor is given as the slab axial force N_{slab} divided by the sum of the gross area of the steel beams, A_g, multiplied by the yield strength of the beams, f_y. The steel beam moment-axial force interaction is shown in Equation 2.

$$\sum \boldsymbol{M^o_i = min}\left\{\boldsymbol{1.18} \times \left(\boldsymbol{1 - {N_{slab}}/{\sum (A_g f_y)_i}}\right) \times \sum \boldsymbol{M^o_{bi}}; \sum \boldsymbol{M^o_{bi}}\right\}$$

Equation 2

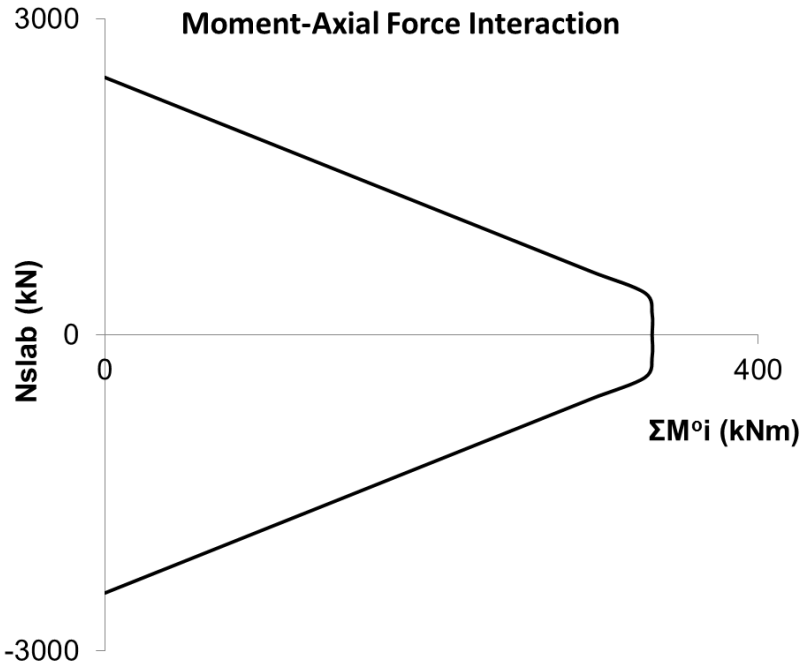

Figure 2-1: NZS3404 moment-slab axial force interaction example for 310UB32 section.

The slab axial force, N_{slab}, is assumed to be shared between all of the beams framing into the joint and is calculated based on the compressive capacity of the slab, f'_c, in contact with an area on the column. This is subject to the condition that the slab axial force must not exceed the axial capacity of the beams given by $A_g f_y$ as shown in Equation 3. The effective contact width, b_{sef} is based on the size, type and orientation of the column whilst the effective thickness of the slab, t_{ef}, is determined by the type and layout of the deck tray and slab. The strength of concrete is also increased to account for both initial increases in strength using the f'_{cos} factor (taken as 10MPa) and for long term hardening with a factor of 1.3.

$$N_{slab} = min\left\{1.3 t_{ef} b_{sef} (f'_c + f'_{cos}); \sum (A_g f_y)_i\right\}$$

Equation 3

The overstrength moments at the column face, M^O, are then calculated by taking the sum of the overstrength capacities of the composite beams framing into a joint and adding the moment caused by the axial load of the slab acting over a lever arm between the effective slab centroid and the beam centroid ($d_b/2+t_o-t_{ef}/2$) as shown in Figure 2-2 and Equation 4 where d_b is the depth of the beam and t_o is the full thickness of the slab.

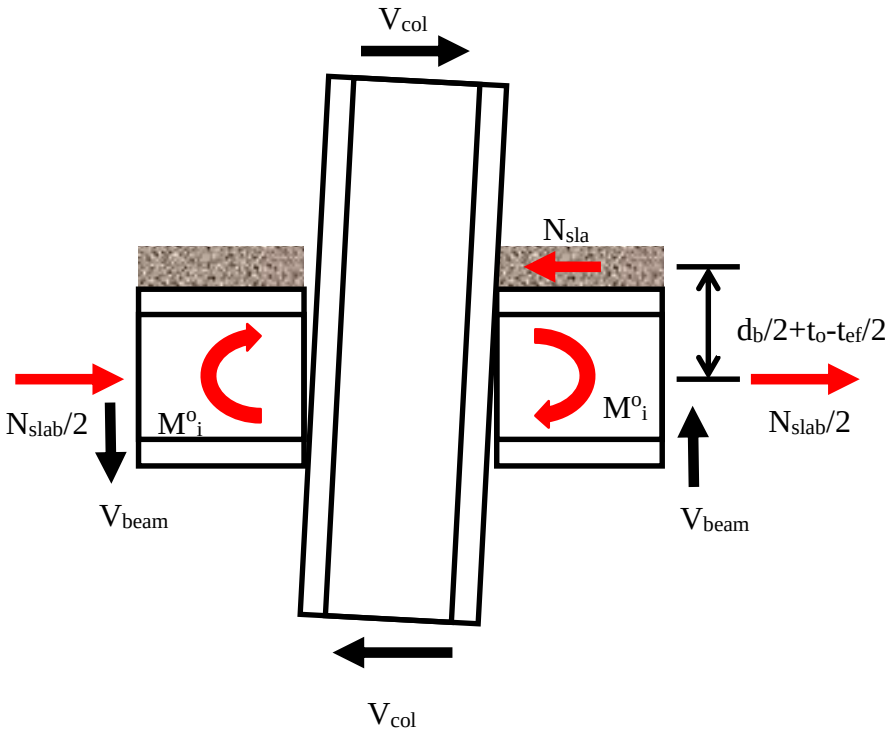

Figure 2-2: Slab interaction mechanism assumed by NZS3404.

$$M^o = \sum M_i^o + N_{slab}\left({d_b}/{2} + t_o - {t_{ef}}/{2}\right)$$

Equation 4

Alternatively, for I section beams framing into the flanges of I section columns a simplified method may be used wherein the section capacity of the beam (M_s) is multiplied by a modified overstrength factor which takes into account the effect of the slab. This method (Equation 5 and Equation 6) is based on empirical data and was shown to have at most a 3% loss of accuracy over a practical range of t_{ef}/d_b.

$$M^o = \varphi_{omss} M_s$$

Equation 5

$$\varphi_{omss} = \varphi_{oms}\left(1.0 + 1.08\,{t_{ef}}/{d_b}\right)$$

Equation 6

2.1.2 American Steel Design Codes

a) AISC341 (2010)

Composite seismic design in the United States of America is governed by the steel seismic design code AISC341 (2010) [2]. Unlike the New Zealand code, no clear design methods are given to determine the effect of slab-column interactions on the column. However, the presence of slab effects are alluded to in multiple parts of the code.

Section D1 Clause 4a-2 specifies that the strength of the column must be greater than *the maximum load transferred to the column by the system including the effects of material overstrength and strain hardening in those members where yielding is expected*. As such the column is required to have the capacity to resist the forces generated by the composite beams framing into it or the sum of the resisting moments of the connections if partial strength connections are used.

Section D1 Clause 5a specifies that, in composite slab diaphragms, *details shall be provided to transfer loads between the diaphragm and boundary members, collector elements and elements of the horizontal framing system*. No mention is made as to the transfer of loads between the slab and the column.

Section D1 Clause 7 details the requirements for composite connections. Force transfer mechanisms between steel and concrete components are specified as being *(a) Direct bearing from internal bearing mechanisms; (b) Shear connection; (c) Shear friction with the necessary clamping force provided by reinforcement normal to the plane of shear transfer; or (d) A combination of these means.*

Additionally Clause 7 states that *Reinforcement shall be provided to resist all tensile forces in reinforced concrete components of the connections* and requires the use of ACI318 [3] for the determination of development lengths in reinforcing.

The commentary for Section D1 Clause 7 acknowledges that in connections where the slab bears against the column such as partially restrained connections *the force transfer between the concrete slab and the steel column requires careful detailing*. The commentary also recommends that only the section of slab above the ribs be counted in design and with the nominal bearing strength of the concrete limited to no more than 1.2fc'. Reinforcement layouts such as that in Figure 2-3 are recommended to ensure that strut-and-tie mechanisms can form to handle the large compressive struts that form between the slab reinforcing and the column face.

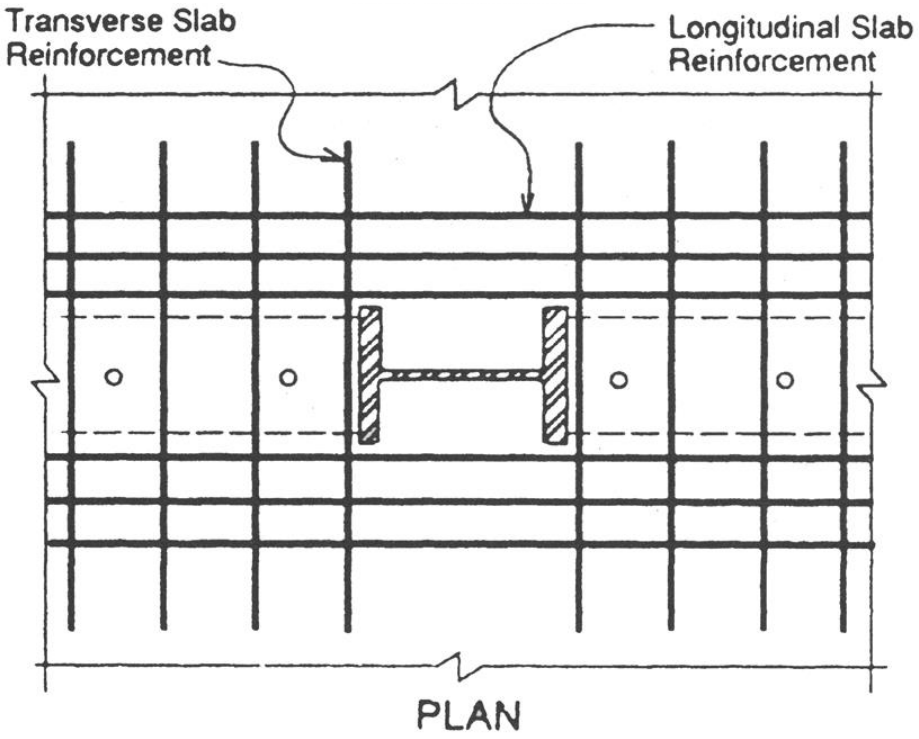

Figure 2-3: Reinforcing layout demonstrated in AISC341-10.

Section G4 describes slab detailing for Composite Partially Restrained Moment Connections however these are described in more detail in the AISC Design Guide for Partially Restrained Composite Connections [4] below.

b) AISC360 (2010)

The composite strength of the beams and/or the strength of the connections are calculated from AISC360 (2010) [5]. Section I3 details the design practices for composite beams under both positive and negative bending moments including specifications for shear stud placement and reinforcing. The effects of deck tray orientation are discussed in clause 2c with the concrete below the ribs only being considered when the deck tray is run parallel to the primary beams. Force transfer between the slab and the moment resisting frame is described in clause 2d however only transfer of force between the slab and the beam are considered. As such floor diaphragms are designed in accordance with section I7 to transfer forces through the shear studs into the beams.

Whilst both AISC341 [2] and AISC360 [5] acknowledge that force can be transferred between the concrete slab and steel members through direct bearing, neither code makes direct recommendations for the increase in column demand resulting from the of slab bearing on the column face. Likewise neither publication provides details for isolating the slab from the column face.

c) AISC Design Guide for Partially Restrained Composite Connections

In addition to these two codes, the AISC Design Guide for Partially Restrained Composite Connections [4] offers guidance for the use of composite slabs in structures with partially restrained connections. The design guide focuses on structures using bolted angles on the bottom flange and web of the beam with the composite slab used to transfer forces from the top flange as shown in Figure 2-4.

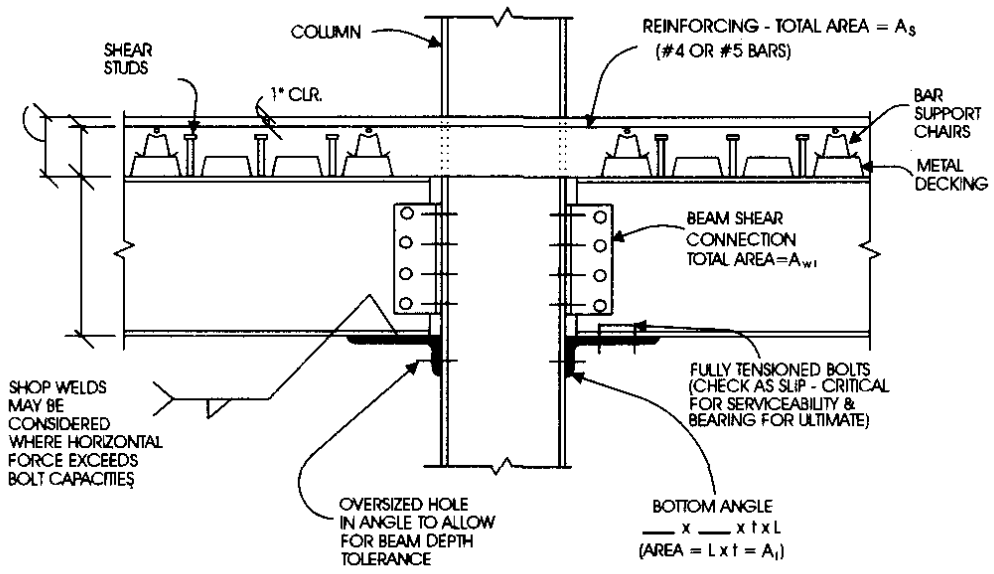

Figure 2-4: Typical AISC partially restrained composite connection (PR-CC) detailing.

The moment capacity of the composite connection under gravity loading with the slab in tension at the column face, M_n^-, is given in Equation 7. This is based on the capacity of the steel reinforcing and the web angle connections multiplied by a lever arm from the bottom of the girder to the centroid of the reinforcing. Here *d* is the girder depth, *Y3* is the distance from the top flange of the girder to the centroid of the reinforcement, A_s and A_{wl} are the gross areas of the reinforcing and the double web angles respectively and F_{yrb} and F_y are the yield stresses of the reinforcing and the seat and web angles.

$$M_n^- = 0.245\left(4A_sF_{yrb} + A_{wl}F_y\right)(d + Y3)$$

Equation 7

The moment capacity of the composite connection with the slab in compression at the column face, M_n^-, is given in Equation 8. In this case the slab is not considered to be critical with the capacity instead being based on the areas of the web angle connections, A_{wl}, and the bottom flange angle connection A_l. Here moments are taken about the slab centroid which is where rotation is assumed to occur.

$$M_n^+ = 0.25(1.25A_{wl} + 1.35A_l)\left(F_y\right)\left(d + \frac{Y3}{2}\right)$$

Equation 8

The beam ultimate capacity is checked using a beam load factor λ_b which must be greater than 1.0. The load factor is given in Equation 9 where P_u and w_u are the design point and uniformly distributed loads, L is the beam length, $M_{p,c1}$ and $M_{p,c2}$ are the connection strengths at each end of the beam given by Equation 7 and $M_{p,b}$ is the ultimate moment capacity of the composite beam. The factors a, b and c are given in tables and are dependent on the loading conditions. The failure mechanism expected here is not clearly described.

$$\lambda_b = \frac{d}{(P_u \; or \; w_u L)L}\left[\left(aM_{p,c1}\right) + \left(bM_{p,c2}\right) + \left(cM_{p,b}\right)\right]$$

Equation 9

Similarly the ultimate capacity of the frame is checked using the frame load factor λ_f given in Equation 10. In this equation P represents the story axial load, δ is the interstory drift, ΣM_n is the summation of the design moments and S_p is a sway parameter based on the interstory height and the number of stories. While it looks as though this could be a P-delta check, the background for this equation is not clearly defined.

$$\lambda_f = \lambda_p - S_p\lambda_p^2\left(\frac{\sum P\delta}{\sum M_n}\right)$$

Equation 10

λ_p is the first order rigid plastic load factor given by Equation 11 where V_i and h_i are the factored lateral force and the height of story i.

$$\lambda_p = \frac{\sum \phi M_n}{\sum V_i \, h_i}$$

Equation 11

$\Sigma\phi M_n$ is the sum of the moment capacity of the column hinges and the partially restrained connections and is given in Equation 12 where N is the number of bays and "Inte" and "Exte" represent the interior and exterior frame connections.

$$\sum \phi M_n = \sum \phi M_{n,col}(R) + \sum [(N-1)(\phi M_n^+ + \phi M_n^-)_{Inte}] + \sum [(\phi M_n^+ + \phi M_n^-)_{Exte}]$$

Equation 12

$\phi M_{n,col}(R)$ is the reduced design plastic moment capacity of the columns at the base of the structure given in Equation 13. This is obtained by taking the moment capacity of the columns, $\phi M_{n,col}$, and reducing it to account for the factored axial load and the columns axial capacity P_y.

$$\phi M_{n,col}(R) = min\left[1.18\left(1 - \frac{P_u}{P_y}\right)\phi M_{n,col};\ \phi M_{n,col}\right]$$

Equation 13

Guidance is also given as to the placement of reinforcing steel to ensure force transfer around the column. The basic requirements, as shown in Figure 2-5, are that small bar sizes should be used with at least three bars on each side of the column. Full anchorage must be developed in the bars and at least two bars must be run along the length of the beam.

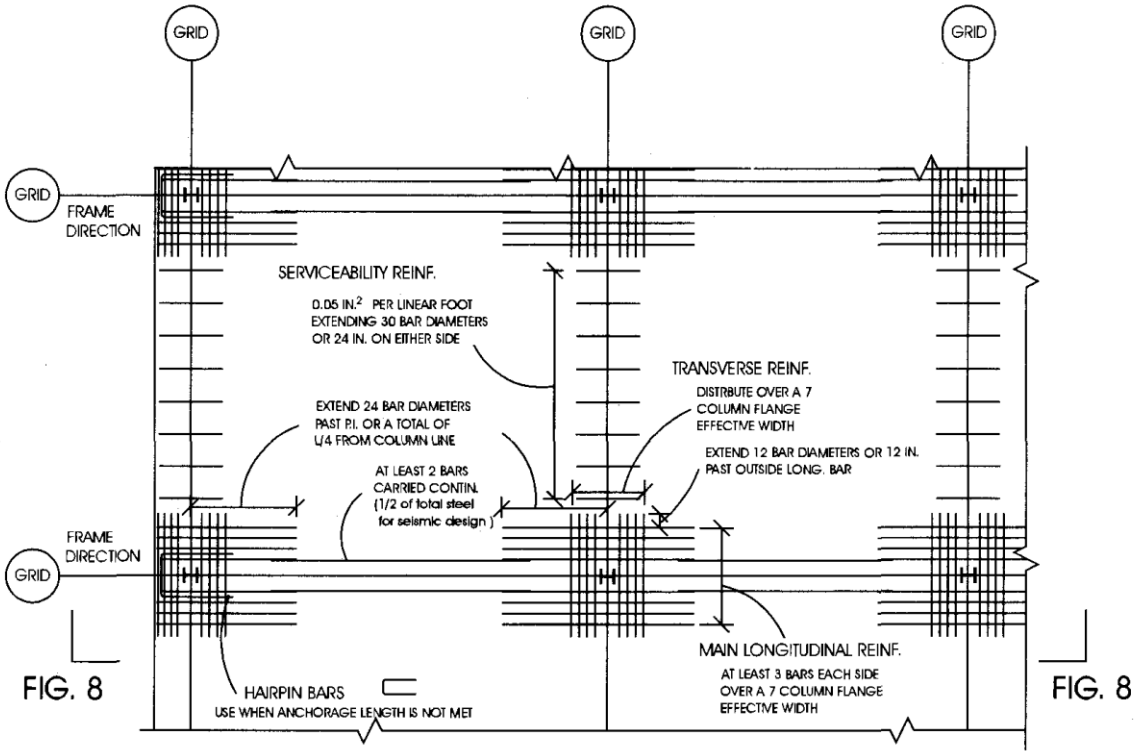

Figure 2-5: Reinforcing layout specified for partially restrained composite connections.

2.1.3 European Steel Design Codes (Eurocodes 3, 4 & 8)

Design of steel-concrete composite buildings for European countries follows Eurocode 4 (2004) (Composite Construction) [6] and Eurocode 8 (1998) (Seismic Design) [7]. Eurocode 4 (EC4) covers the general design of composite structures for resistance and serviceability under primarily static loading. EC4 can also be used for composite structure seismic design with an appropriate seismic design code.

Composite beam-column connections are covered in Section 8.4.2 of EC4. Like the American partially restrained connection provisions, the force transfer is computed based reinforcing in the slab. The EC4 method assumes that *the effective area of longitudinal reinforcement in tension is stressed to its design yield strength* f_{sd}. This implies that there is no force the column when the slab force on both sides of the column is equal. Force transfer between the slab and the column only occurs with unbalanced forces as shown in Figure 2-6 when $F_{t1} \neq F_{t2}$. In this case strut and tie methods are specified to determine the forces applied to the column.

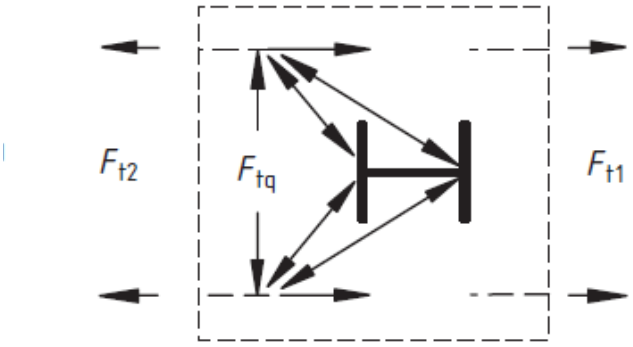

Figure 2-6: Strut and tie mechanism in the slab recommended by EC4 for unbalanced forces.

EC4 [6] Clause 8.1 specifies that the design of the beam-column connections be undertaken as per the procedures set out in Eurocode 3 (2005) (Steel Connections) [8]. Eurocode 3 (EC3) gives no specific guidance is given for the detailing of composite beam-column connections. Column web compression failure is mentioned in Clause 6.1.3 however this only relates to the forces imposed on the column by the steel beam connections. Direct bearing effects of the concrete slab against the column face are not specifically covered in either EC3 or EC4.

The seismic design of composite moment resisting frames is covered in Eurocode 8-1 [7] (EC8). Like the US codes, no explicit method is given for the design of the column considering slab column effects. Annex C of EC8 specifies the slab and beam requirements around the column necessary to allow slab-column interactions in design and gives some guidelines for the layout of the seismic reinforcing surrounding the column. For exterior columns with the slab in tension slab-column interactions are only allowed to be considered when a façade beam is present or if the slab is cantilevered beyond the column. In exterior joints with the slab in compression and in all interior joints the slab effect may be considered if the slab is in contact with the column.

Despite allowing for slab-column effects, no guidance is given about how the design of the lateral load resisting system incorporating slab effects should be conducted. The primary purpose of the reinforcing layouts described in EC8 is to ensure the development of the strut-and-tie mechanism shown in Figure 2-6. In non-isolated specimens EC8 specifies that *the integrity of the concrete must be maintained at all times* although no guidance is provided as to how to achieve this.

Detailing recommendations for the isolation of the slab from the column (Clause 7.7.5) specify that the slab must be totally disconnected from the steel frame within a distance equal to the effective width of the beam, b_{eff}, from each column face. The effective width, given in Clause 5.4.3.1.1, is dependent on the conditions at the beam-column joint as is shown in Figure 2-7.

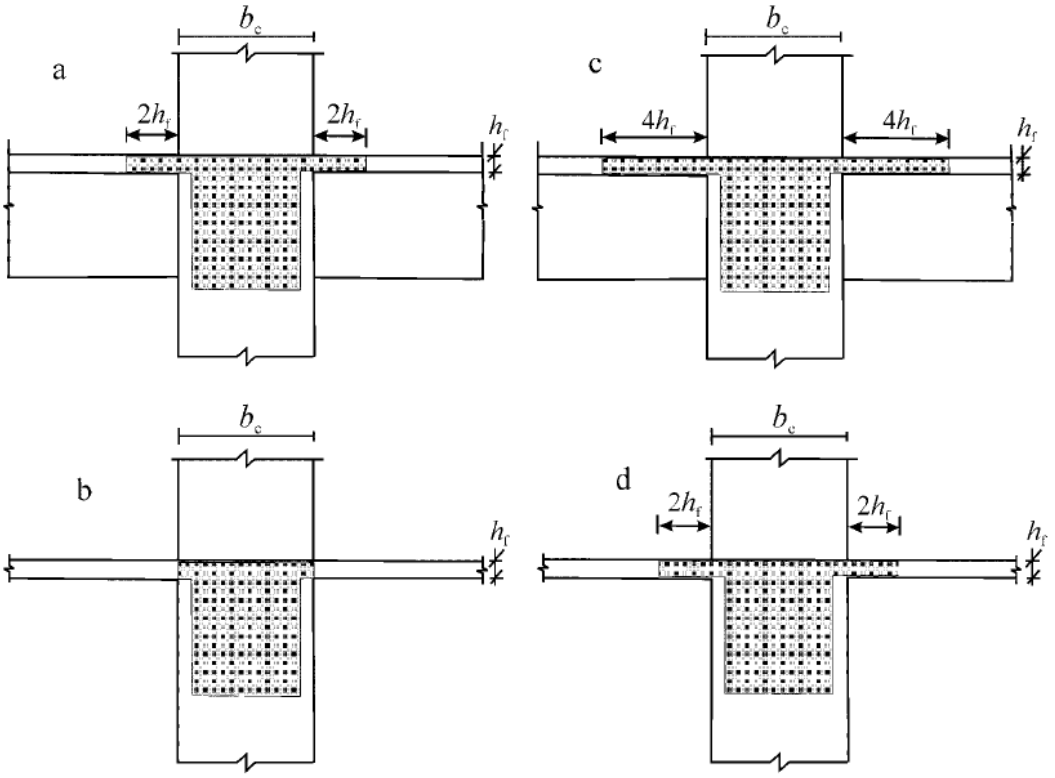

Figure 2-7: Effective beam widths as defined by EC8.

Columns a and b in Figure 2-7 are exterior columns whilst columns c and d are interior columns. Columns a and c have secondary beams framing into them.

2.2 Previous Research

2.2.1 Testing of Composite Subassemblies Under Lateral Deformation

Du Plessis and Daniels (1974) [9-11] studied the effects of floor slabs on multi-storey buildings testing four welded beam subassemblies with composite full depth reinforced concrete slabs considering wind loading. The each beam was welded to a steel plate representing the column face which was then bolted to a stiff reaction frame. Force was applied to the end of the beam to represent wind loading. The floor system increased the strength of the beam-column connection by up to 87% and the stiffness by up to 70% over those of a bare steel frame. The author states this effect was particularly noticeable when the stiffness of the beams and columns were similar however given that a rigid reaction frame was used in these tests this comment is dubious. Similar tests with slabs poured on ribbed steel deck showed that the slab effect still resulted in a strength increase of 61% over the bare steel frame. Du Plessis and Daniels modelled this interaction using simple bi-linear approximations as shown in Figure 2-8. They concluded that the ultimate strength of the test beams could be effectively bounded with upper and lower bounds obtained using plasticity theory with the following assumptions:

- Steel and concrete obey the Tresca yield criterion
- The stress-strain law for both steel and concrete is rigid-perfectly plastic
- The yield stress of the concrete in compression is equal to the crushing strength
- Plain strain conditions exist in the steel beam and concrete slab at the end plate

The upper bound limit was determined by equating the rate of external work in terms of load applied to internal dissipation resulting from a mechanism formed by a single hinge near the beam-column joint. The lower bound limit was calculated by assuming an internal equilibrium based on section properties which satisfied yield criterion.

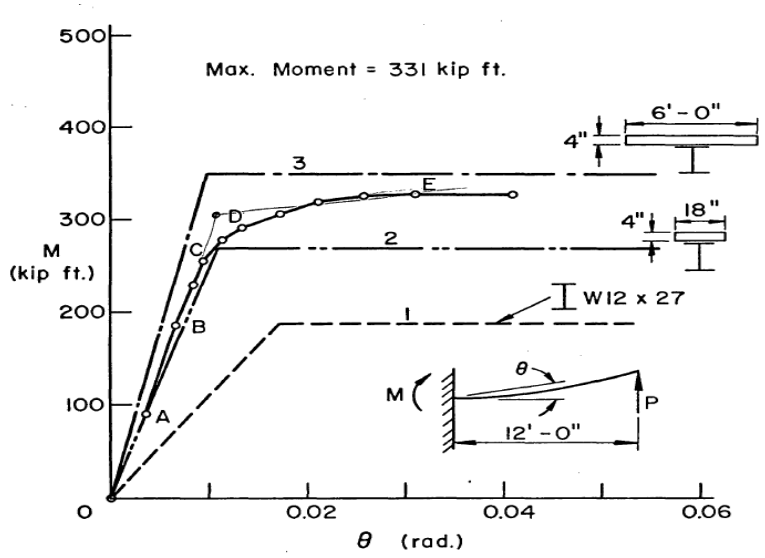

Figure 2-8: Moment-rotation plot showing test data, bi-linear model for bare steel and bi-linear models for upper and lower bound composite sections.

Du Plessis and Daniels also considered the presence of a gap between the column face and the slab which may be formed by shrinkage of the concrete. They stated that, if a shrinkage gap was present, the initial stiffness of the subassembly changed at the point at which rotation was sufficient to close the gap and bring the slab into contact with the column. Furthermore the spalling of the slab in contact with the column shown in Figure 2-9 tended to occur after the peak strength was reached. It therefore did not affect the overall subassembly strength.

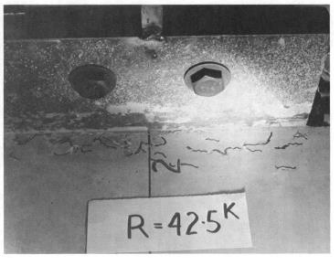

FIG. 17a B-44: SPALLING AT END PLATE

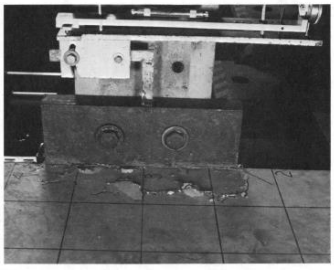

FIG. 17b B-66: SPALLING AT END PLATE

Figure 2-9: Damage to floor slab around column face.

Lee and Lu (1989) [12] tested three full-scale beam-column joint subassemblies incorporating composite floor slabs under cyclic loading. Two of the specimens used a single beam to represent exterior columns whilst the third had a beam on either side of the column to represent an interior joint. All subassemblies used W18×35 beams (beam depth 450mm) with bolted web angles and welded flanges as per AISC 1978 specifications. No slab depth measurement was given in the paper however the shear studs are 130mm long indicating that the slab was probably 140mm-150mm deep. Results from an exterior joint test, shown in Figure 2-10, showed that under positive bending (slab in compression against the column) the composite action significantly increased the strength and stiffness of the subassembly. The composite beam exhibited 10% more strength and a 6% increase in stiffness over what was observed under negative bending. From Figure 2-10 it can be clearly seen that under positive displacement a higher level of force was required to attain the same displacements at high levels of drift. It was stated that the design of the subassemblies was such that deformation of the panel zone was likely to occur before the beams yielded. It is therefore unsurprising that the panel zones of the steel columns in two of the three tests sustained damage during testing in addition to severe yielding of the bottom flanges of the steel beams. The hysteresis loops produced were very stable with any pinching being due to the opening and closing of concrete cracks. Han and Li (2010) [13] also observed similar increases in strength and stiffness in their tests on composite beam-column joints with concrete filled steel tube columns.

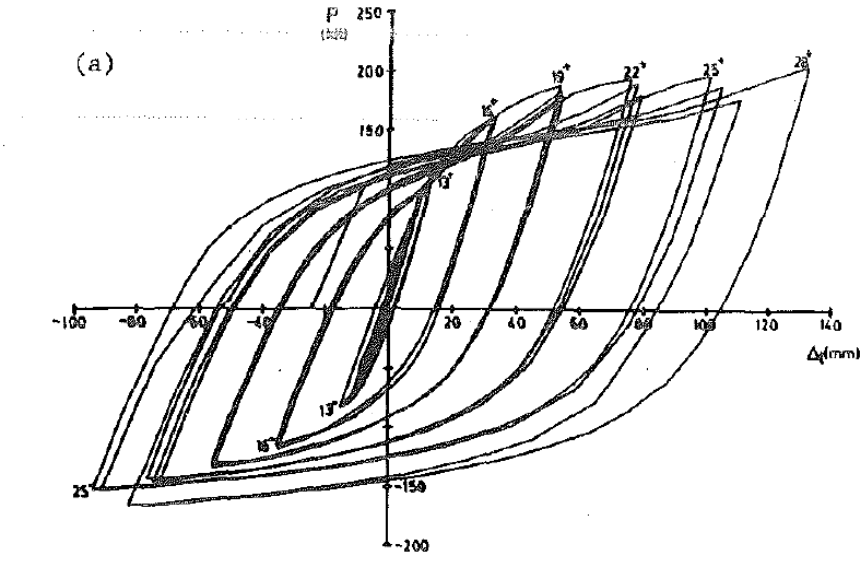

Figure 2-10: Force-rotation plot for exterior beam-column joint (Lee and Lu 1989).

Leon (1994) [14] considered using the slab to form part of the beam-column connection with partially restrained steel connections. The concept involved using the slab to transfer axial

forces from the top flange of the beam to the column whilst shear forces and axial forces in the bottom flange were transferred through an angle bolted to the web and/or bottom flange. Under gravity loading the slab acted in tension hence by using force equilibrium as shown in Figure 2-11 and varying the amount of reinforcing in the slab Leon theorised that the design strength of the connection could be adjusted to suit the demand. Under reversed loading (top flange in compression) Leon considered the steel components of the connection to carry all tensile loads.

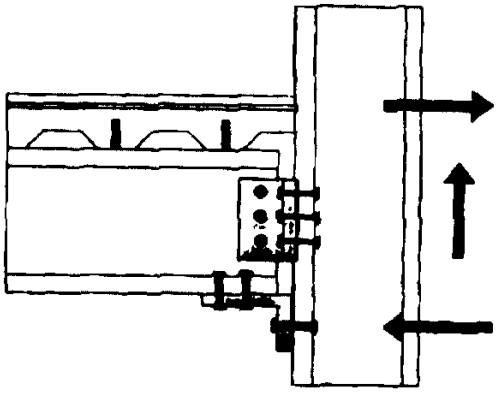

Figure 2-11: Force equilibrium for partially restrained connection with slab participation (Leon 1994).

In response to damage to beam-column connections following the Northridge earthquake, Leon, Hajjar, Gustafson and Shield (1998) [15, 16] ran a series of experiments to determine the effects of partially composite floor slabs on steel moment connections. Three full scale interior steel moment resisting frame joints were tested utilising pre-Northridge connections with bolted angle plates to the beam web and beam flanges welded to the column. W14×145 columns and W27×94 beams (beam depth 684mm) were used in all tests with a 127mm thick slab. The authors state that the columns were sized to ensure a higher capacity than the bare steel beams and connections however no mention is made as to whether they were designed to account for composite actions. Each subassembly was tested under cyclic loading at drifts of up to 3.0% with forces being applied at the beam ends and the column being pinned at its top and base. The composite beam plastic moment capacity was up to 43% greater under positive loading than that of the corresponding bare steel specimens however this increase in capacity was significantly less under negative load due to steel strength degradation. Although the specimens with composite slabs were calculated as having a plastic moment capacity up to 54% higher than the corresponding bare steel specimens none of the subassemblies tested managed to reach the calculated capacity as shown in Figure 2-12. This was due to brittle

failures in both the beam-column connection (mainly weld failures) and the beam itself in the form of a fatigue crack running from the cope cut in the web to allow access to the bottom flange for welding. Furthermore the presence of the concrete slab caused a strain difference between the top and bottom beam flanges, a result which was partially attributed to bearing of the concrete slab on the column. This strain difference implies that the neutral axis is not in the centre of the steel section, so the beam may be prone to elongation and shortening which causes greater strains in the bottom flange than if the slab were not present.

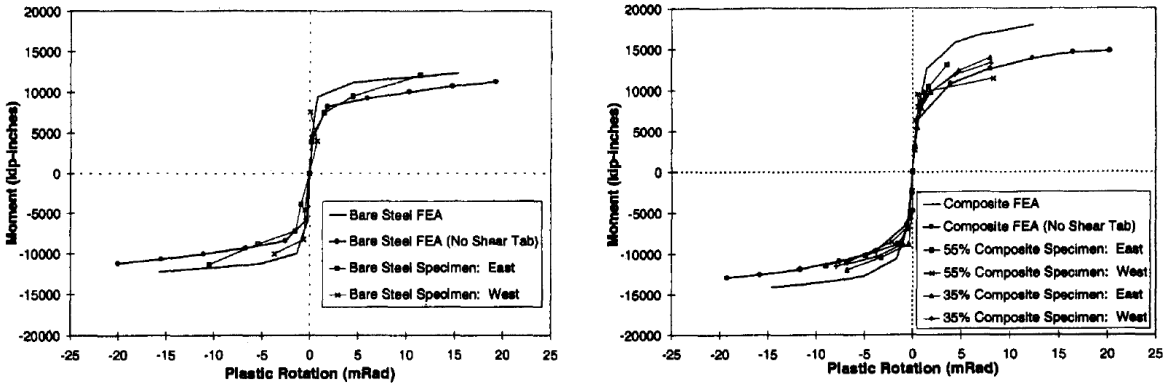

Figure 2-12: Bending moment vs. plastic rotation curves for bare steel (left) and composite (right) beams (Leon et al 1998)

Civjan, Engelhardt and Gross (2001) [17] performed tests on six subassemblies with pre-Northridge connections with loads being applied at the top of the column. From their test results, Civjan, Engelhardt and Gross stated that even during elastic deformation, the stiffness of the composite beams was up to 10-30% higher than the bare steel. Throughout testing the strains in the top flange were observed to be smaller in the composite section than in the bare steel specimen however those in the bottom flanges did not differ much between composite and bare steel specimens. As a result of this, the neutral axis was observed to have moved to the top of the steel sections resulting in some beam elongation or shortening as shown in Figure 2-13 and Figure 2-14. However comparing the two figures it is apparent that the bare subassembly has a higher overall level of shortening with one beam elongating whilst the other elongates at a slightly lesser rate. The composite subassembly exhibited a reduced level of movement with a resultant net elongation of less than 1mm. In both figures positive on the beam shortening axis represents beam shortening whilst negative indicates beam elongation. The first cycle at 10mm displacement (0.3% drift) is missing from Figure 2-13 hence the initial elongation on the west beam.

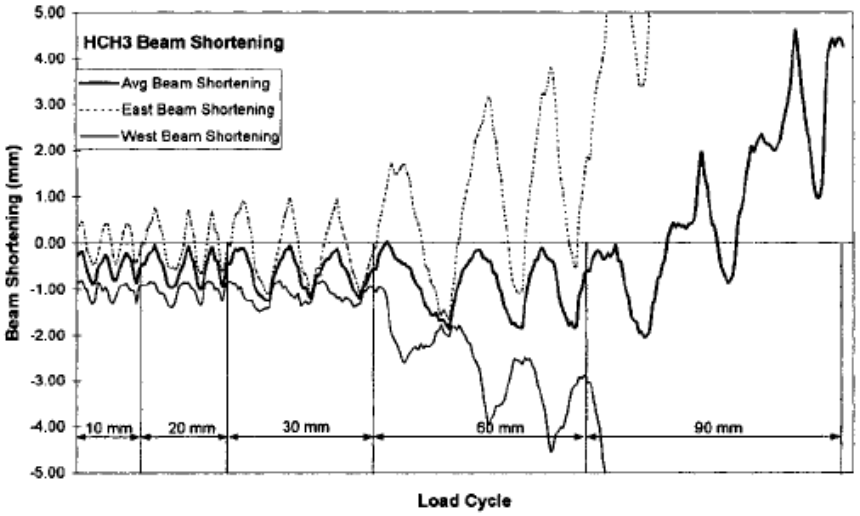

Figure 2-13: Beam elongation of bare steel subassembly during cyclic testing (Civjan 2001).

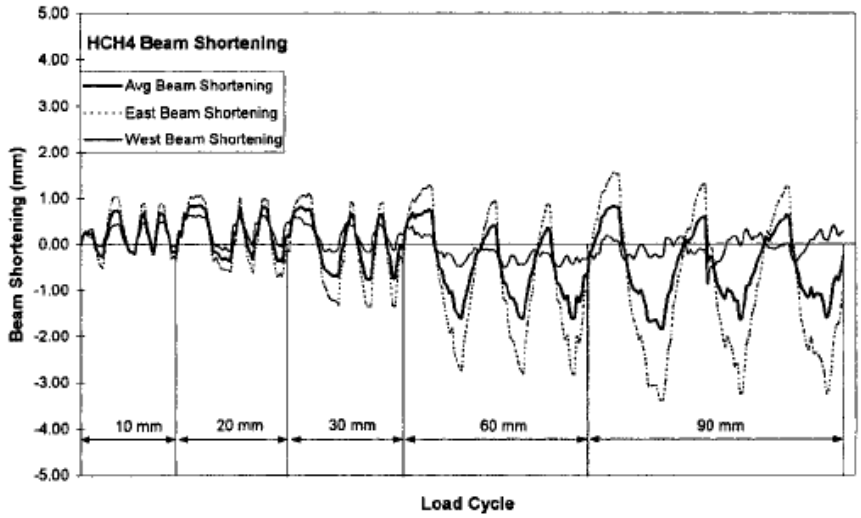

Figure 2-14: Beam elongation of composite subassembly during cyclic testing (Civjan 2001).

In addition to this Civjan, Engelhardt and Gross observed the transfer of strains in the concrete slab near the column and identified that the concrete compression zone started at the far column flange, peaked at the column face and dispersed rapidly beyond the column face. The maximum strain profile beyond the column face is shown in Figure 2-15 however because of overlap the strains at the far column flange are not included (each half of the plot comes from a different loading direction).

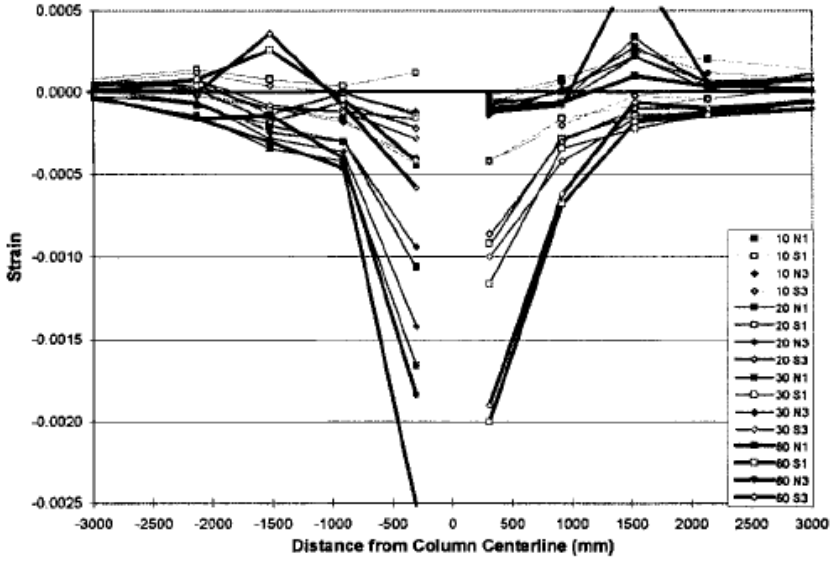

Figure 2-15: Strain profile in the concrete slab beyond column face (Civjan 2001).

Sumner, Mays and Murray (2002) [18] tested bolted endplate connections in steel moment resisting frames with composite slabs. The specimens were designed to withstand the demands imposed by the steel beams without consideration of the slab. Although the beams initially showed local flange buckling in the bottom flange the ultimate, and unexpected, failure mechanism was tension rupture in the bottom flange bolts. Murray and Seek (2009) [19] further expanded on this research testing beam column arrangements in which the floor slab was isolated from the column faces by means of foam packing and the effects of the slab on the beam-column joint experienced in the earlier testing were eliminated.

Green, Leon and Rassati (2004) [20] ran a series of bi-directional tests on a single large subassembly constructed with partially restrained bolted angle connections. The testing was primarily aimed at determining the interaction between slab-column force transfer in the strong and weak bending directions. The test subassembly comprised of a single column with two W18×40 primary beams (beam depth 455mm) connected with both web plates and bottom flange T-stubs and two W24×55 secondary beams connected by web plates only. The slab was 6.7m×9.1m×82.6mm with shear studs attached to both the primary and secondary beams. Under cyclic loading the connections showed elastic behaviour up to 1% drift with significant yielding and panel zone damage occurring from 1.5% drift. The beams on the subassembly acted compositely up until 1.5% drift at which point localised crushing and spalling of the slab around the column occurred. At maximum moment the subassembly exceeded the design

plastic moment of the composite partially restrained connections on the primary beams by up to 8% under positive loading. Under negative loading however, concrete degradation resulted in the observed plastic moment being 21% lower than the predicted plastic capacity. The design plastic moment capacity for the composite connection was 4-5 times higher than that of the bare steel connection. The concrete slab was shown to cause both an increase in stiffness (amount unspecified) and an 8% increase in strength up until around 2-3% drift after which localised slab crushing adjacent to the column faces decreased the effect of the slab.

Liu and Astaneh-Asl (2004) [21, 22] investigated the effects of a composite slab on the behaviour of simple shear connections under lateral loading. The slab increased the moment capacity of the connection by up to 45%. This was accompanied by higher levels of fracturing in both the beams and the shear connections, which were subjected to 2.5 times their design plastic capacity. Because of the upward neutral axis shift in positive bending (slab in compression), the primary beams were noted as having higher levels of out-of-plane deformation particularly in the lower flange. Following spalling of the slab at 4% drift, the specimens were observed to revert back to the strength of the bare steel specimens. Liu and Astaneh-Asl also noted a 20% increase in strength in specimens with concrete poured between the column flanges in the web cavity above that with a slab and a gap between the flanges, however this was accompanied by an earlier failure of the beam-column connection.

Braconi et al (2008) [23, 24] tested composite beam column joints in a two bay, two storey 3D moment resisting frame structure with composite beams, columns and moment end plate type connections. The testing was primarily focused on the assessment of various design methods particularly those used in the European and American design codes Eurocode 8 (1998) [7] and AISC341 (2010) [2]. Pseudo dynamic testing showed little damage below 2% drift and drifts up to 3.5% were not sufficient to induce collapse. Damage to the frame was limited to cracking in the concrete and localised crushing of the concrete against the column faces. They stated that the Eurocode 8 strut and tie mechanism 2 for transferring forces to the column and shown in Figure 2-16 below could not be activated and that all force was transferred by mechanism 1. This is contrary to that found by Liu and Astaneh-Asl (2004) [22].

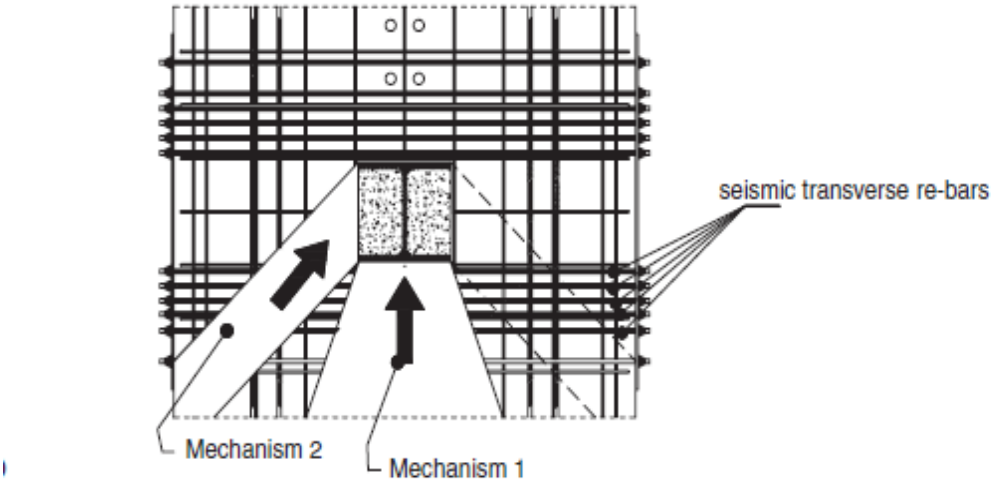

Figure 2-16: Slab mechanisms inferred by Eurocode 8 (1998)

Braconi, Elamary and Salvatore (2010) [25] performed a series of tests on ten composite beam-column joint assemblies with bolted endplate connections. Their aim was to determine the effects of concrete slab type, connection system and the contribution of the column web panel on the beam-column joints. Results from this testing concluded that high strength concrete negatively influenced the behaviour of the beam-column joint causing a 30% reduction of the maximum resistance and increasing strength degradation in the samples tested. The authors state that this was mainly due to the steel beams yielding earlier in specimens with high strength concrete. Full depth slabs (those with a constant depth across the whole slab) provided improved performance in terms of stability and strength degradation in comparison to slabs cast on ribbed steel decks. Finally it was observed that there were benefits, in terms of strength and ductility, in the introduction of shear systems (such as stud anchors or steel reinforcing) for connecting slabs and columns as shown in Figure 2-17. Specimens which utilised shear studs welded to the columns showed a higher peak strength and less reduction in strength than those without.

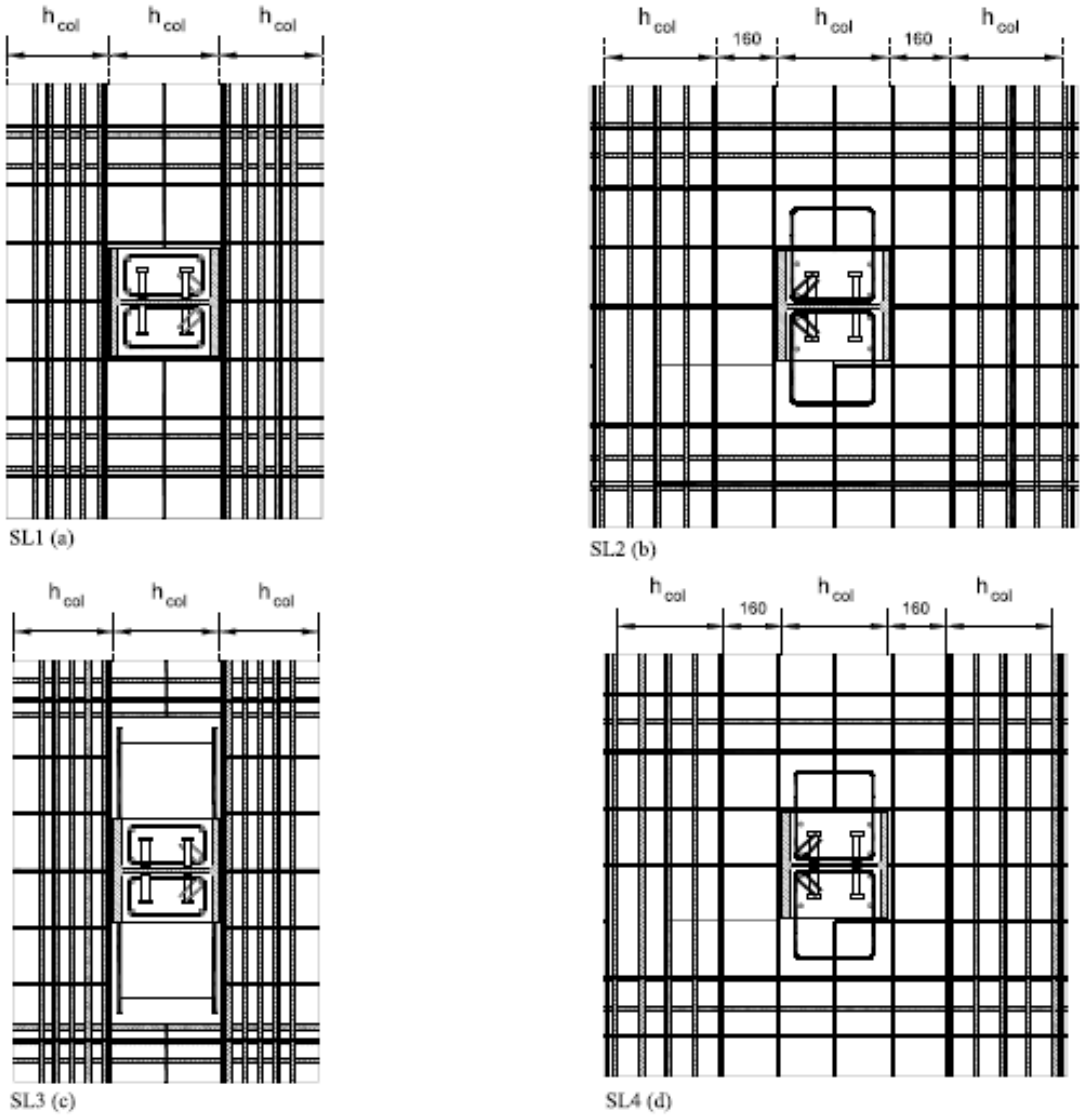

Figure 2-17: Examples of column reinforcement tested by Braconi et al (2010).

Yamada et al (2010) [26] performed shake table testing on a full scale four storey structure with concrete filled tube columns and composite I section beams. The objectives of the test were to evaluate the performance of the structure under design-level ground motions however during testing a soft storey mechanism formed when the ground floor columns buckled. Although no data was recorded, the authors stated that slab-column interaction was likely a contributing factor to the premature collapse.

2.2.2 Computer Modelling

As part of their research on composite floor effects Leon, Hajjar and Gustafson (1998) [15] created finite element models of beam-column joints with bare steel and floor slabs. After analysis using ABAQUS, the results showed distinctive non-linear behaviour in the frames fitted with composite floor slabs and an upward migration of the neutral axis of the beam. This resulted in more yielding in the bottom flange than the top flange as a result of slab participation.

Gunasekaran and MacRae (2007) [27] developed a simple model to determine the effects of the slab in concrete moment resisting frames. The model, shown in Figure 2-18, is a modified version of the Kim, Stanton and MacRae model (2004) [28] for considering the effect of beam elongation. It assumes that the presence of slab reinforcing steel transfers forces around the column. These force transfers were considered by the addition of a spring element, with the properties of the effective width of the concrete slab, connecting the slab elements on either side of the column. Contact between the beam/slab concrete and the column was represented by contact (gap) elements which only acted in compression. The model did not consider the effects of bending of the slab or the effects of contact between the slab and the side of the column. The model was run using the structural analysis programme RUAUMOKO (Carr 2004). It was shown that the slab caused an increase in the lateral resistance of the structure as well as an increase in the overstrength moments placed on the column. The model described the behaviour of the subassembly strength well.

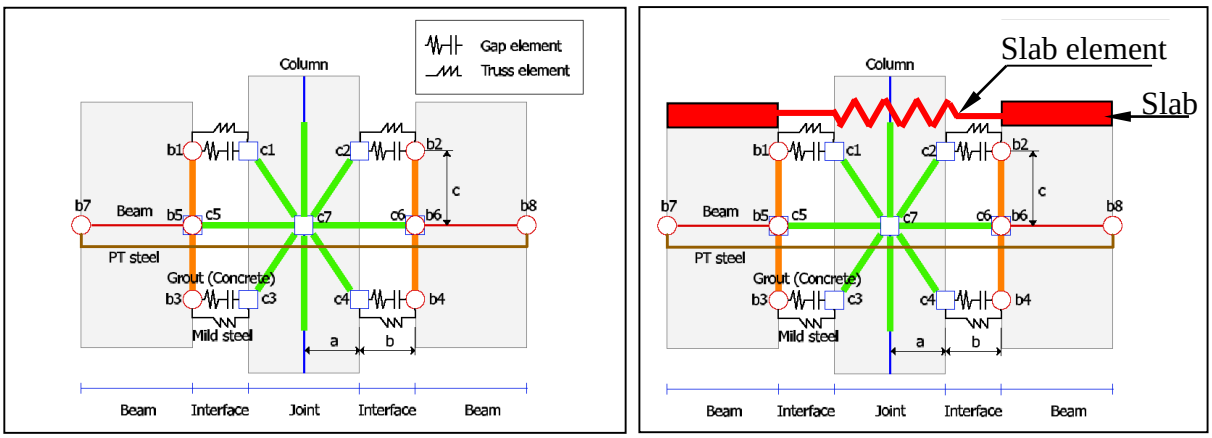

Figure 2-18: Kim's model for beam elongation (left) and modified to consider slab effects (right).

Mago and Clifton (2008) [29] developed 3D models of typical beam column joints using the ABAQUS computer suite and ran a finite element analysis to determine the effect of a number of parameters on the slab behaviour. The results from the finite element analysis showed that the percentage of reinforcing and the slab concrete compressive strength had a negligible effect on the performance of the beam-column joint. The effect of the width of the compression face of the universal columns was more important than between the column flanges.

MacRae, Mago and Clifton (2007) [30] also stated that the slab increased the demands on the column and the panel zone. It was concluded that the increase in panel zone demands was proportionally less than the moment increases as the slab increased both the panel zone demand and capacity. It was also noted that slab causes contact stresses to occur on both the inner and outer faces of the column flanges as shown in Figure 2-19, however the compressive stress on the inside face of the flange were far less than those on the outer face.

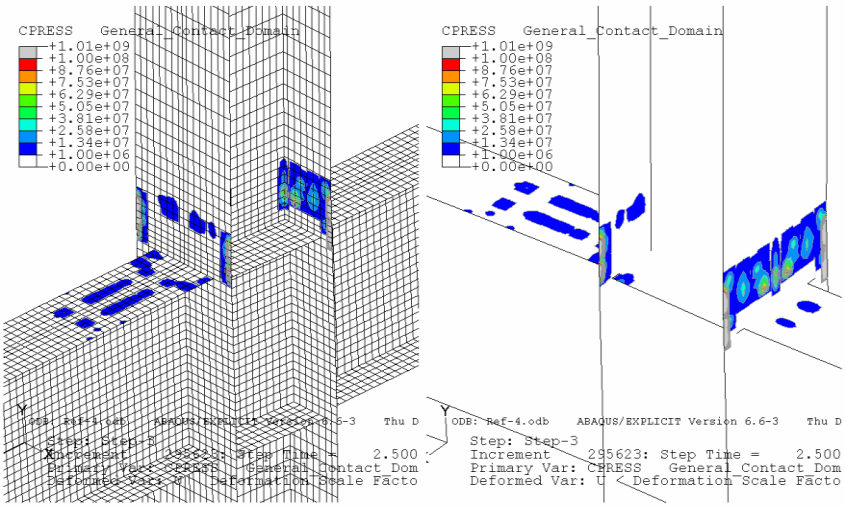

Figure 2-19: FEA output of contact pressure on the steel members

2.2.3 Sliding Hinge Joints

The sliding hinge joint uses a low damage friction type connection developed by Clifton (2005) [31]. The connection is designed to pivot about the pinned top flange of the beam as shown in Figure 2-20 whilst slotted holes in the bottom flange and web allow these elements to slide. Energy dissipation is achieved through friction created by the sliding of the web and bottom flange against their corresponding column and cap plates. While some early testing utilised a composite slab, the effect of the slab on the performance of a sliding hinge joint is still unclear. In particular the effect of the slab in raising the neutral axis, and hence the point of rotation of the beam, is not particularly well understood. Other issues such as plate bending and displacement incompatibilities are yet to be fully quantified.

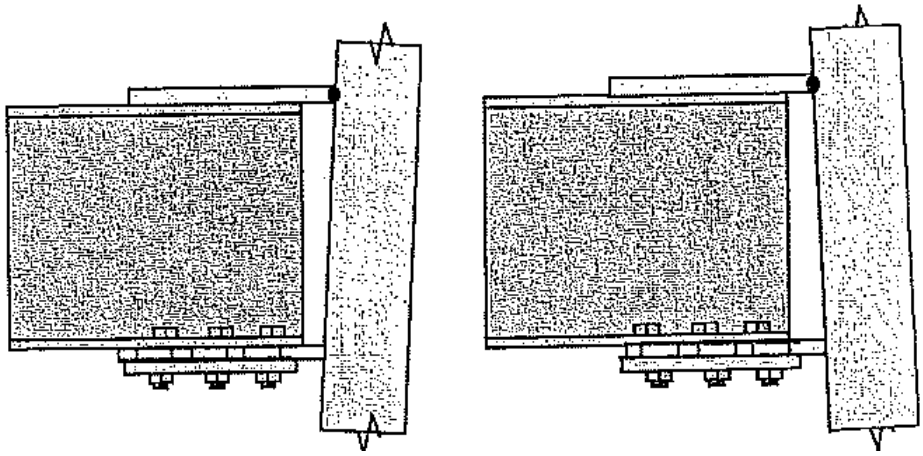

Figure 2-20: Typical sliding hinge joint behaviour

MacRae et al (2010) [32] introduced guidelines for the design of sliding hinge connections. The capacity of the connection was based on the sliding forces generated by movement at each of the bolt groups, multiplied by a lever arm about the top flange of the beam. An overstrength factor is applied to account for the forces needed to overcome static friction before the joint can slide. Further consideration is then given to the bolt holes in the bottom beam flange and in the bottom row of bolts in the beam web which are elongated to prevent binding up to the design drift.

Khoo et al (2011) [33] further developed the sliding hinge joint concept by proposing the addition of ring springs as shown in Figure 2-21 to encourage re-centring of the structure. Khoo ran a series of analytical experiments using five different combinations of self-centring sliding hinge joints (SCSHJ) in 10 storey structures under recorded ground motions. It was found that although the springs did reduce the final displacement to within construction tolerances (0.2%) the costs associated with providing sufficient springs was excessive. Khoo also recognised that there was only a small difference between the optimal spring force and a level of force that would lead to inelastic deformation of the beams.

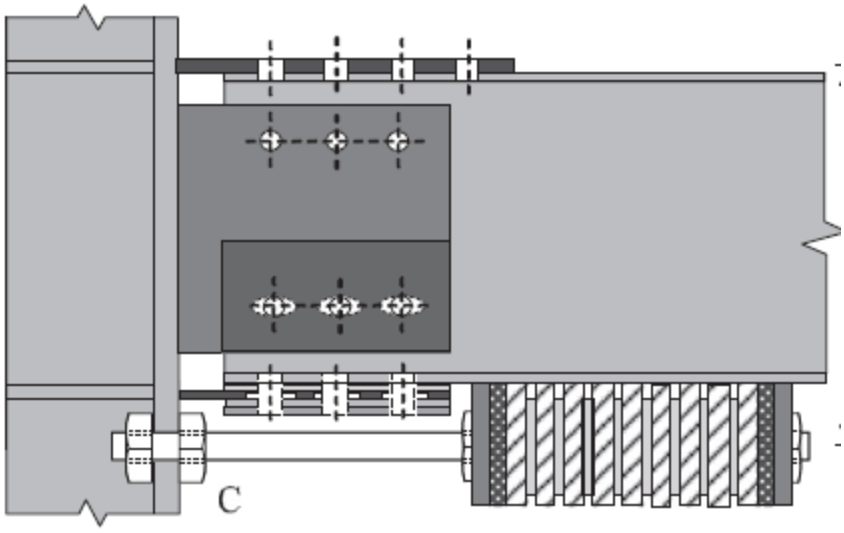

Figure 2-21: Self-centring sliding hinge joint (SCSHJ) developed by Khoo (2012)

Recent testing of asymmetric friction connections (AFC) by Chanchi et al (2013) [34] has focused on the effect of bolt tension, shim materials, surface coatings and corrosion on energy dissipation during sliding and overall performance of the sliding connection. The tension of the bolts used in the connection had a direct effect on the sliding force of the connection as shown in Figure 2-22. It was noted that 50% of the maximum sliding force of the connection was achieved with snug tightened (defined by NZS3404 as *the full effort of one man on a hand wrench tightening the bolt*).

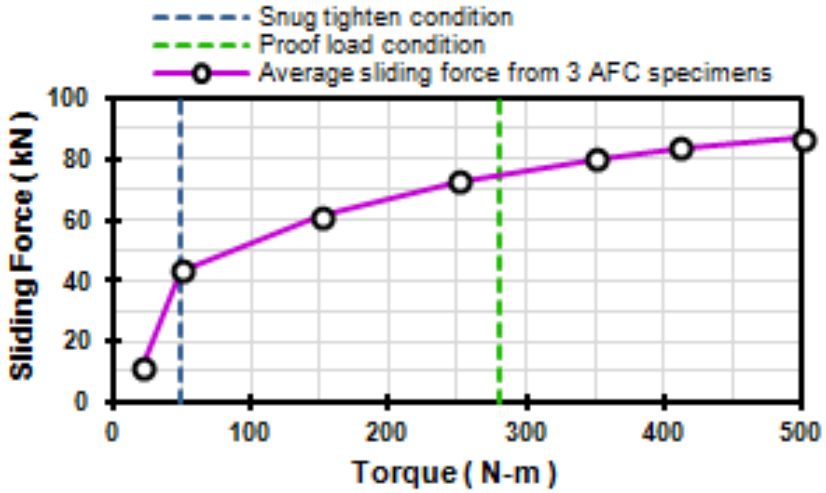

Figure 2-22: Effect of bolt tension on the sliding force of friction connection (Chanchi 2013).

Chanchi determined that the AFC specimens developed a predictable and stable hysteresis loop when shims with a material hardness well above or well below that of the steel beams and connection plates was used. Materials with a similar hardness to the steel beams or connection plates tended to exhibit an unstable hysteresis loop. A similar result was experienced when Zinc and Alkyd primer were used with the hysteresis loop becoming unstable and the sliding force of the connection being reduced. Corrosion of the plates tended to increase the initial sliding strength of the connection however once sliding had been initiated little further effect was noticed.

2.2.4 Slab and Tray Deck Behaviour

A number of tests have been performed by the manufacturers of profiled steel deck trays to establish the properties of their systems. Comflor produces both a Composite Floor Decking manual [35] along with Load Span Tables [36] for their products. In addition to this, Tata steel commissioned a Heavy Engineering Research Association (HERA) report into the performance of its decking system. HERA report SSTR015 (2008) [37] tested 6 composite slab sections recording the moment capacity and the slip between the deck tray and the slab at the end of the section. In all cases the slip in each slab was minimal to a point after which movement began to occur, usually accompanied by a drop in strength.

Khanlou (2013) [38] investigated the performance of concrete slabs poured over ribbed steel decks under shrinkage stress, flexural load and punching shear. Sixteen two bay and eight one bay slabs were cast and measured for shrinkage strain before being loaded in either flexure or shear. Khanlou found that only slabs with heavy reinforcing (deformed bar) showed signs of shrinkage cracking and that all specimens regardless of reinforcing exceeded predicted values for punching shear from both European and American codes by anywhere between 30% and 130%.

3 Test Subassemblies and Methods

3.1 Design of Test Subassemblies

3.1.1 Test Subassemblies

Physical tests of the five full size beam-column subassemblies in Table 1 were conducted. The first test utilised a moment end plate type connection, deck tray running transverse to the main beams and a 25mm gap between the column flanges and the concrete slab created using sheet polystyrene. The second test subassembly used the same layout without the gap between the column and the slab. The third test was similar to the second but with the deck tray oriented longitudinally (parallel to the main beams) with the deck trough running along the length of the primary beam. The fourth and fifth test subassemblies were also similar to the second subassembly however the fourth test subassembly used an asymmetric friction connection (sliding hinge joint) in place of the moment end plate type connection. The fifth test subassembly had a full depth slab block extending 300mm (12 in.) from each face of the column as specified by AISC341 (2010) [2].

Table 1: Summary of test subassemblies

Specimen	Deck Tray Direction (to main beams)	Beam Connection	Concrete Detailing
1 (Isolated)	Transverse	Bolted Moment End Plate	Separated from column
2 (Transverse)	Transverse	Bolted Moment End Plate	Poured up to column
3 (Longitudinal)	Longitudinal	Bolted Moment End Plate	Poured up to column
4 (Sliding Hinge)	Transverse	Sliding Hinge Joint	Poured up to column
5 (Full Depth)	Transverse	Bolted Moment End Plate	Poured to column, large full depth block

3.1.2 Subassembly Details

Each test subassembly consisted of a 310UC158 column which was 2m from the centre of the base pin to the line of applied force at the top of the column. Two 310UB32 half beams, each of 3m length, were attached to the column and supported by pinned connections 3m out from the column centreline as shown in Figure 3-1 and Appendix A. These connections were to represent the point of contriflexure in the beams of a structure with a 6m span between column centrelines. With this arrangement and assuming Grade 300 steel the predicted moment at first yield of the extreme fibres, M_y (=Zf_y), of the bare steel beams was 229kNm, the plastic moment, M_p (=Sf_y), was 304kNm and the ultimate moment, M_u (=Sf_u), was 441kNm. This corresponded to applied lateral forces of 149kN, 171kN and 205kN respectively at the top of the column. These values were calculated based on the assumption that beam hinging in flexure occurred close to the tips of the gusset plates. Discussions with practicing engineers revealed that the beams used could be full scale representations of those expected in the upper levels of frames or in short buildings. They could also represent scaled down versions of larger sections. Larger sections may have exceeded the capacity of both the column and the testing equipment. Detailed calculations for this can be found in Appendix B.

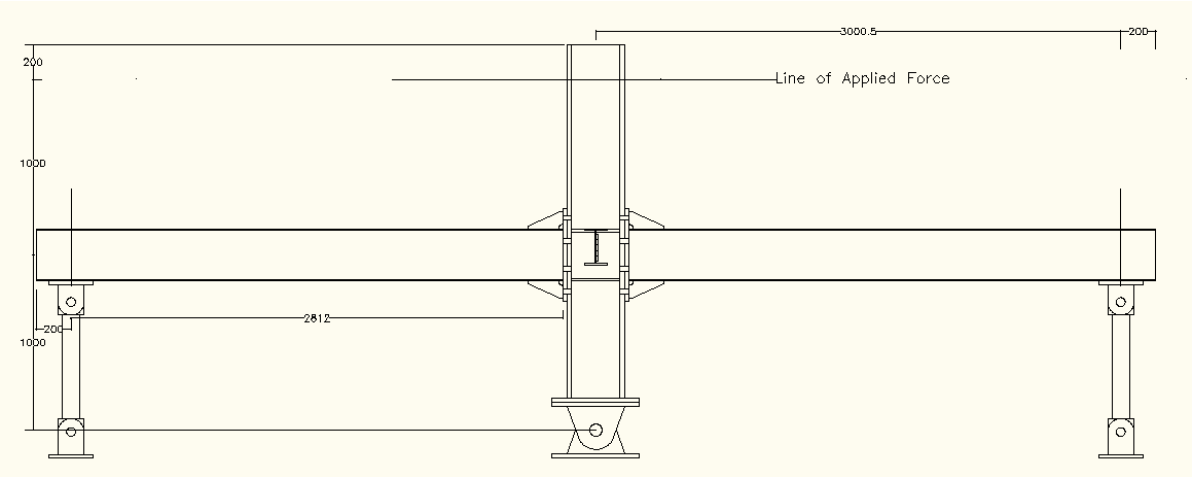

Figure 3-1: Steel subassembly elevation for subassemblies 1, 2, 3 and 5.

3.1.3 Slab Details

The concrete slab was 6m long, 3m wide and 150mm thick and was poured over a Comflor 80 deck tray with the dimensions given in Figure 3-2. The Comflor deck tray was laid out in 3m lengths for tests with transverse ribs and 6m for longitudinal ribs. In tests with a transverse deck tray the 3m sheets were centred over the primary beams with the edges were temporarily propped for casting. In the longitudinal test (Subassembly 3) the 6m sheets were laid over the secondary beams with a trough running the length of the primary beam. Comflor deck trim was used to enclose the edge of the area to be poured whilst around the column sheet steel was cut and fitted. Any remaining small gaps were filled with silicone sealant. The deck was attached to the beams using two 125x19mm diameter shear studs per trough on the primary beams and one per trough on the secondary beams. No shear studs were used within 1.5 times the depth of the beam from the column face in accordance to NZS3404 Clause 13.4.11.3.3 [1] to minimise the likelihood of low cycle fatigue of the beams.

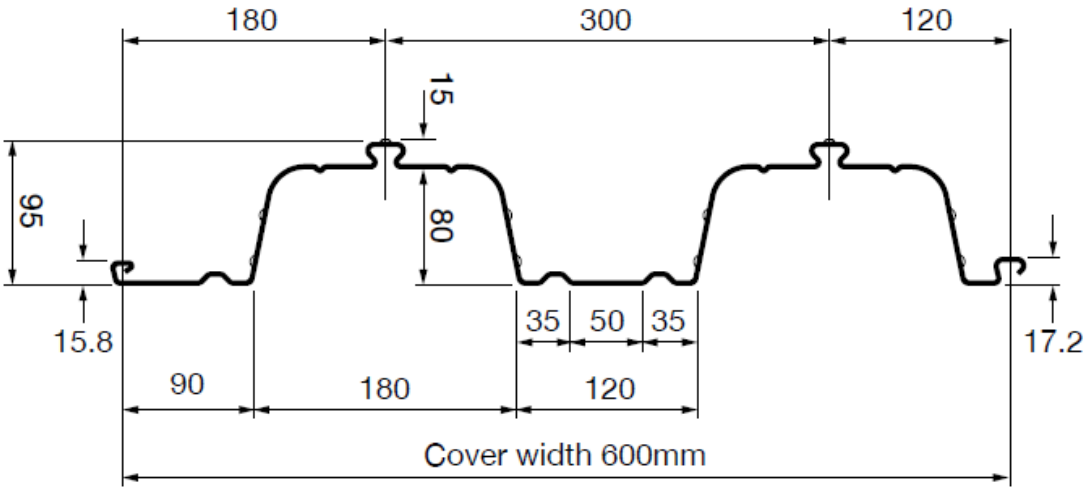

Figure 3-2: Comflor 80 section profile.

The slab was poured using 30MPa concrete with a maximum aggregate size of 19mm and a 100mm requested slump. Reinforcement comprised of SE82 [39] seismic mesh (Grade 500 Steel, 8mm round bar in a 200mm×200mm grid) placed 30-40mm below the slab surface and D10 Grade 500 bar tied below the mesh in each deck trough. Further D10 bars were used around the column opening in accordance to recommendations on page 9 of the Comflor 80 design guide [35] as shown in Figure 3-3. This requires a minimum of two bars in a strip of width $d_o/2$ along each face of the column opening where d_o is the width of the opening

transverse to the direction of the deck tray. Recommendations for the size of bar to use are not given.

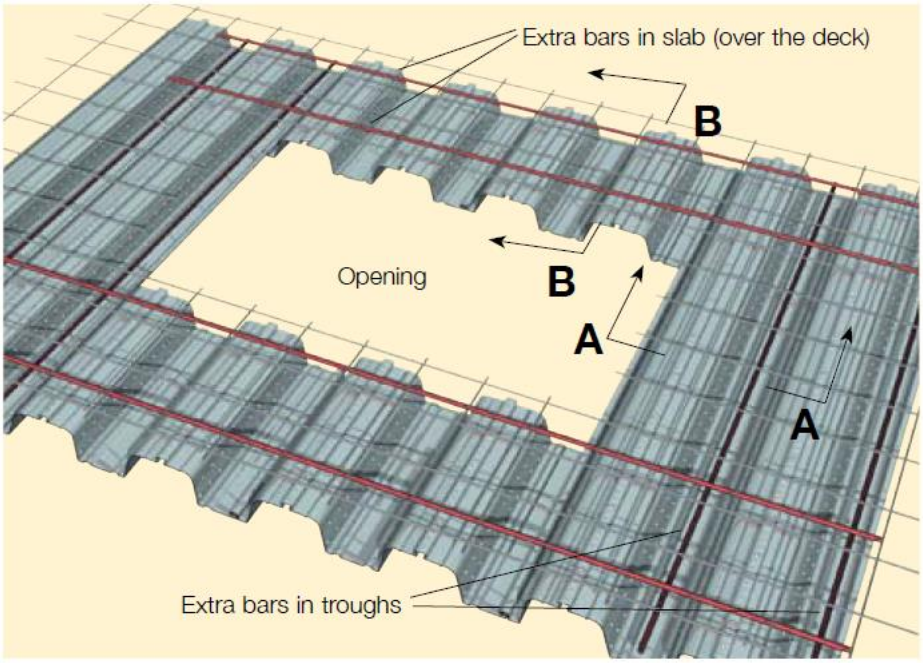

Figure 3-3: Comflor recommendation for opening detailing.

Using the methods set out in NZS3404 Clause 13.4.5 [1], the capacity of the composite beam section under gravity loading was 280kNm. This was based on 51% composite action which represents an economic level of composite action with over 85% of the strength of a fully composite beam being generated. Furthermore an upper bound on the design overstrength moment generated by the composite beams at the end of the gusset plate assuming full depth slab bearing with a concrete stress of 40MPa and an ultimate steel stress, f_u, was calculated according to Clause 12.10.2.4 of NZS3404 to be 286kNm (see Appendix B for calculations).

3.1.4 Connection Details

Test subassemblies 1, 2, 3 and 5 all utilised the moment end plate type connection shown in Figure 3-4 and Appendix A. This connection was designed to resist the overstrength capacity of the composite beam in accordance to HERA report R4-100 [40] which specified the plate thickness, hole layout, bolt sizes, welding details and gusset plate detailing. Additionally HERA report R4-142 [41] was utilised to ensure the capacity of the column web and flanges were sufficient to resist prying and deformation of the flanges. Detailed calculations and drawings for the moment end plate connections are given in Appendix B. The end plates were

25mm thick steel and eight Grade 8.8 M24 bolts, with flat washers, were used for each connection. The connection moment capacity at the column face was approximately 300kNm.

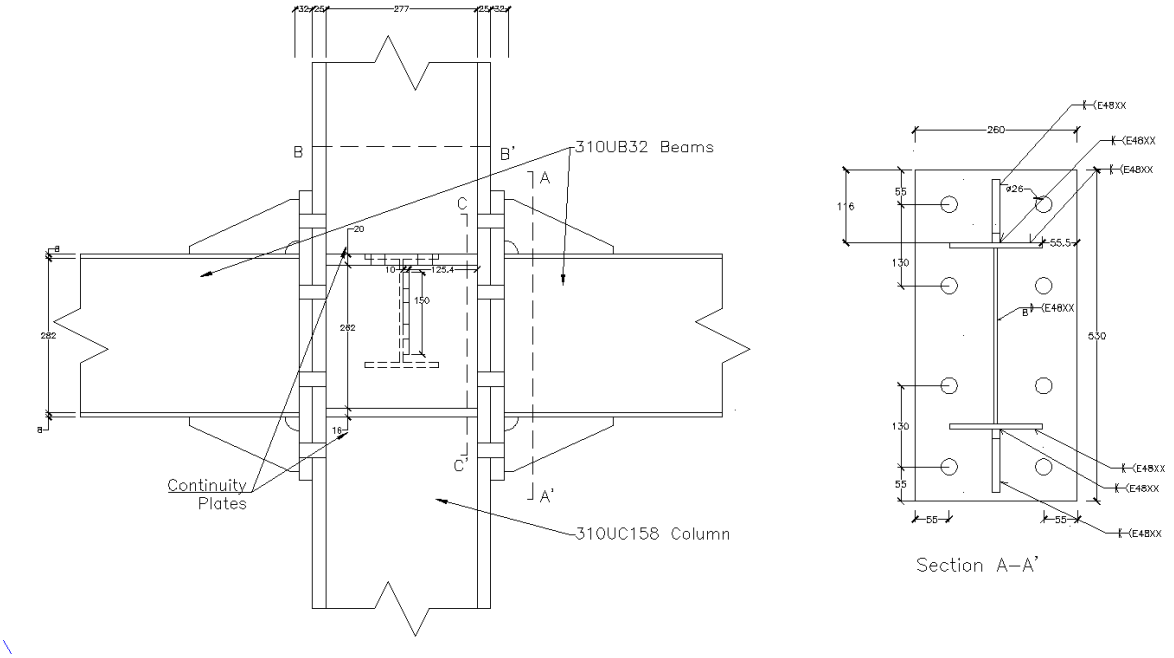

Figure 3-4: Moment end plate connection details.

Shear tabs were attached to the web of the column as shown in Figure 3-5 and Appendix A so as to allow the use of secondary beams when the deck tray was run longitudinally (parallel to the main beams). The secondary beams were only used in subassembly 3 and had a 200UB29.8 section. They were bolted to shear tabs which had been designed to HERA report R4-100 [40] and welded to the webs of the column and the ends of the primary beams. Because of tight clearances between the secondary beams and the column flanges only snug-tightening was possible. A pair of plates were attached to the top flange of each secondary beam and the column continuity plate/primary beam flange to provide moment resistance. This was necessary as the secondary beams were only supported at one end as opposed to the usual shear connections at both ends of the beam. Detailed calculations for this connection can be found in Appendix B.

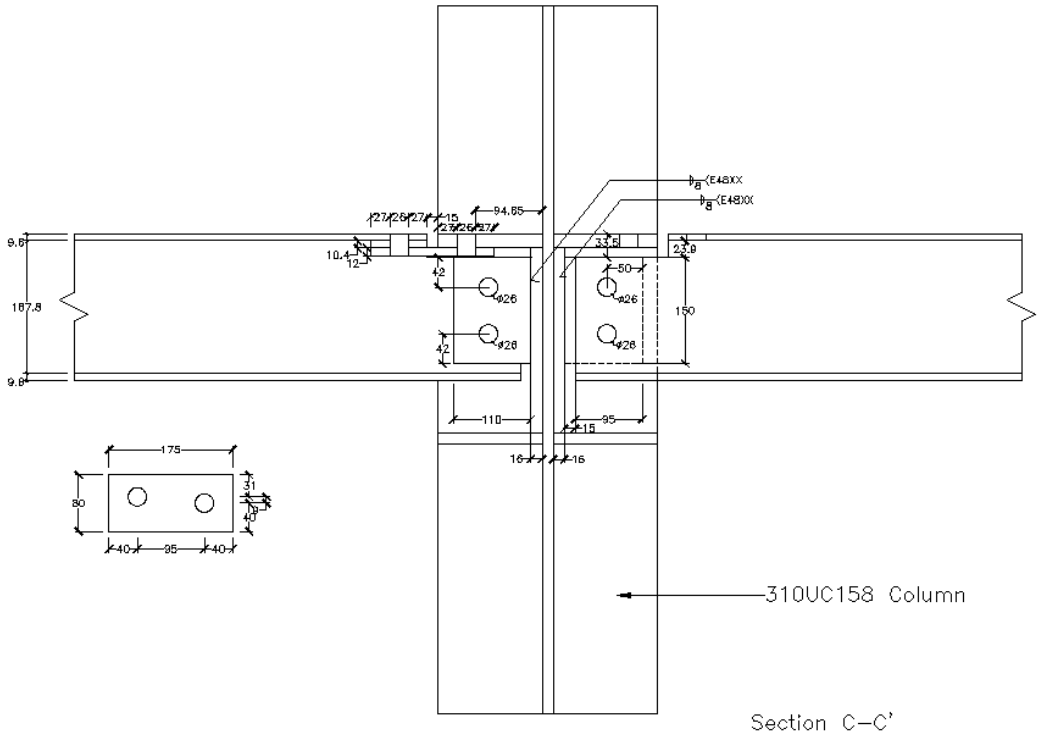

Figure 3-5: Secondary beam connection detail.

3.1.5 Sliding Hinge Joint

The fourth test subassembly used a Sliding Hinge Joint connection designed in accordance with principles set by MacRae et al (2010) [32]. To avoid the need for welding plates to the columns, the top and bottom flange plates and the web plate were welded to a 25mm think end plate as shown in Figure 3-6 and Appendix A. This end plate was then bolted to the column face in the same manner as the moment end plate beams. The bolt layout was chosen to ensure the overstrength capacity of the joint came as close as possible to the first yield strength of the bare steel beam. Eight Grade 8.8 M20 bolts were used for the top flange connection, 5 Grade 8.8 M16 bolts for the web and 4 Grade 8.8 M16 bolts for the bottom flange. Two Grade 4.6 Positioning bolts were also used in the bottom flange. Belleville washers were not available at the time of testing so flat washers were used on all structural bolts. One minor difference in the design from that of MacRae et al (2010) was the use of slotted holes for the top web bolts to allow drifts of up to 5% without binding horizontally. This resulted in slotted holes with a length of 30mm for the top web bolts and 60mm for the bottom web and bottom flange bolts. Bisalloy 500 [42] was used for the shims because it resulted in the most stable hysteresis loops

when tested by Chanchi [34]. The connection capacity computed at first sliding according to the methods of MacRae et al (2010) [32] and utilising a friction coefficient of between 0.2 and 0.4 (Chanchi [34]) was 132kNm at the outer edge of the moment end plate which was less than the computed first yield moment of the beams, M_y, at 229kNm considering the full section contribution. The beam yield moment considering the holes made for the sliding hinge joint bolts, M_{yh}, was 200kNm (see Appendix B for calculations)

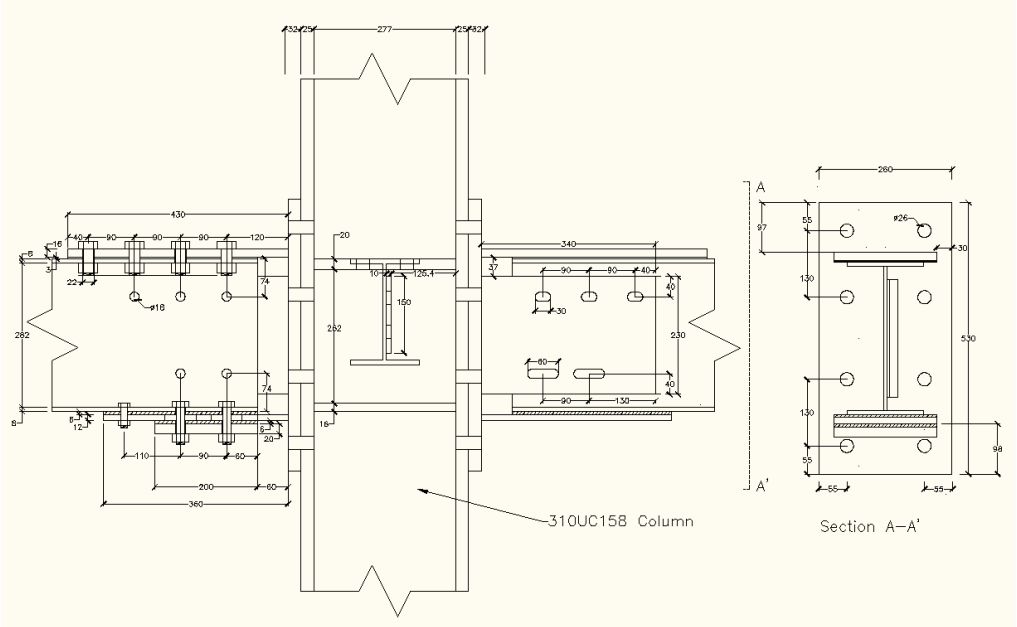

Figure 3-6: Sliding hinge joint (SHJ) connection details.

3.2 Test Setup

Each subassembly used an identical test setup to apply load. The base of the column was supported on a pinned connection attached to the strong floor by four M40 bolts which were tightened using an air impact wrench at its maximum torque rating of approximately 800Nm. The pinned connection was designed such that the distance from the centre of the pin to the steel beam centreline was 1000mm. Past experience indicated that each anchor point on the strong floor had a combined axial and shear capacity of at least 50kN each when applied together hence four bolts gave a total capacity of 200kN in both shear and axial loading.

The beam end supports utilised pinned connections both under the beams and at floor level as shown in Figure 3-7 with a 150kN load cell between the pinned connections. Because of the

imperial measurements used on the strong floor, the end supports of the primary beams were moved to ensure the supports were vertical at zero displacement and avoid transferring moments through the load cell. This resulted in the length between column centre and the end support centreline being 3048mm.

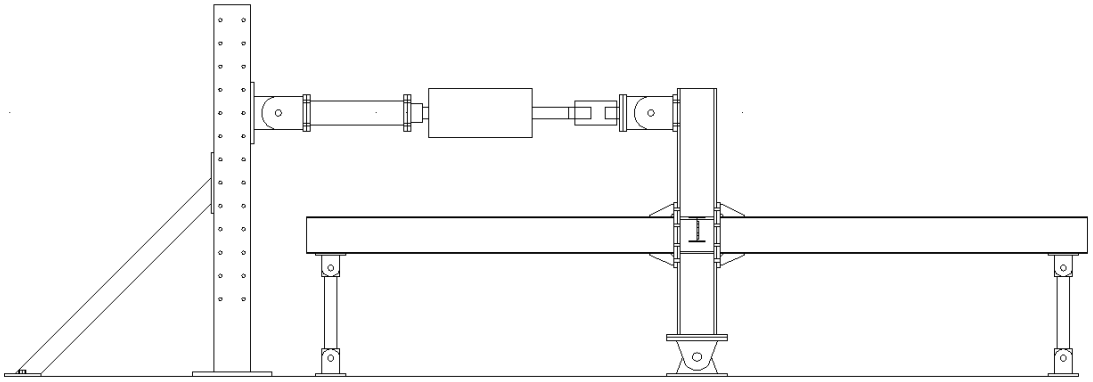

Figure 3-7: Test subassembly in reaction rig.

Torsional lateral support was provided by two 150kN actuators with one attached to the end of each beam and connected to a 200UC46.2 stub column clear of the floor slab as illustrated in Figure 3-8. The actuators were pinned horizontally at both the beam and the support with the distance between pins being approximately 1840mm. During the largest displacement cycles the beam ends were expected to move 50mm horizontally in-plane. This would result in less than 1mm extension of the actuators. Because of the small movements it was decided to lock the actuators to a fixed length by removing the hydraulic oil supply hoses and simply monitor the forces induced.

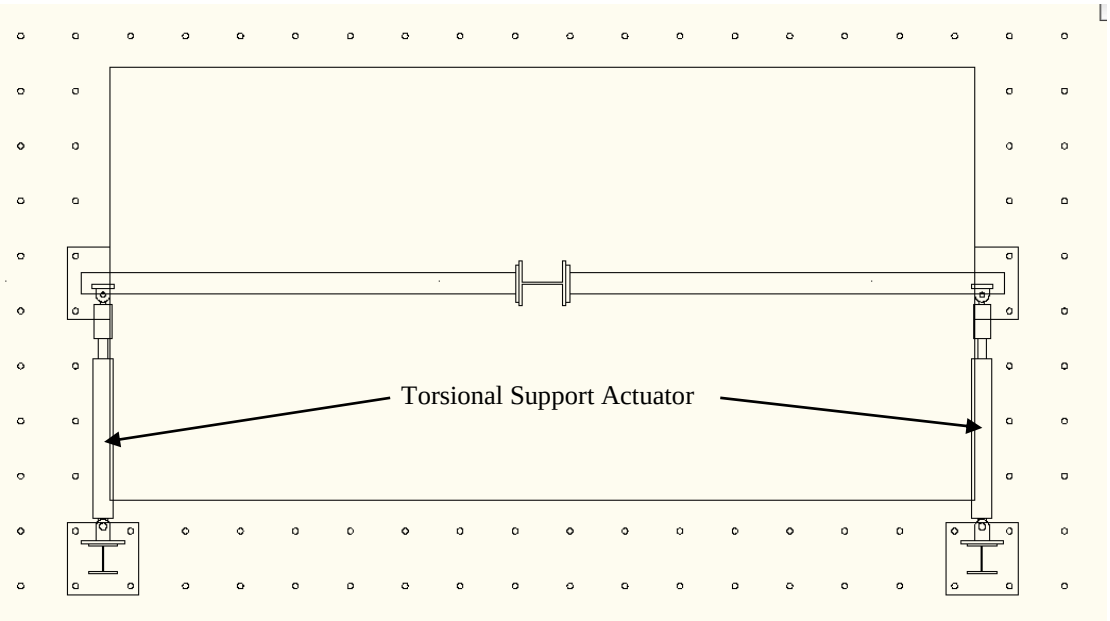

Figure 3-8: Birds eye view showing torsional supports.

Lateral displacements were applied to the subassembly using a 1000kN actuator mounted between the top of the column and a reaction frame. The first two tests used a smaller 440kN actuator however this was found to be under capacity for subassemblies without isolated slabs.

3.3 Construction

The following construction procedures were used for the subassemblies. The steel components were assembled in place with the ends of the beams temporarily propped. The beam-column connections were fastened using the NZS3404 [1] turn-of-the-nut method to ensure proof loading. This method, described in Clause 15.2.5.2, required the bolts to be first tightened using a hand wrench. The moment end plate bolts were then marked as shown in Figure 3-9 and tightened a further 1/3 turn as were all but the top web bolts in the sliding hinge joint. The top web bolts in the sliding hinge joint required a 1/2 turn. This was to reach the proof load. Any extra turning above this results in only a small increase in strength as shown by Chanchi et al [34] in Figure 2-22.

Figure 3-9: Beam-column connection showing bolt proof loaded markings.

The tray deck was then laid on top of the beams and positioned such that the distance between the column face and the first rib of the deck tray, d_t, was equal on both sides of the column as shown in Figure 3-10. In test subassemblies 1 and 2, d_t was approximately 20mm.

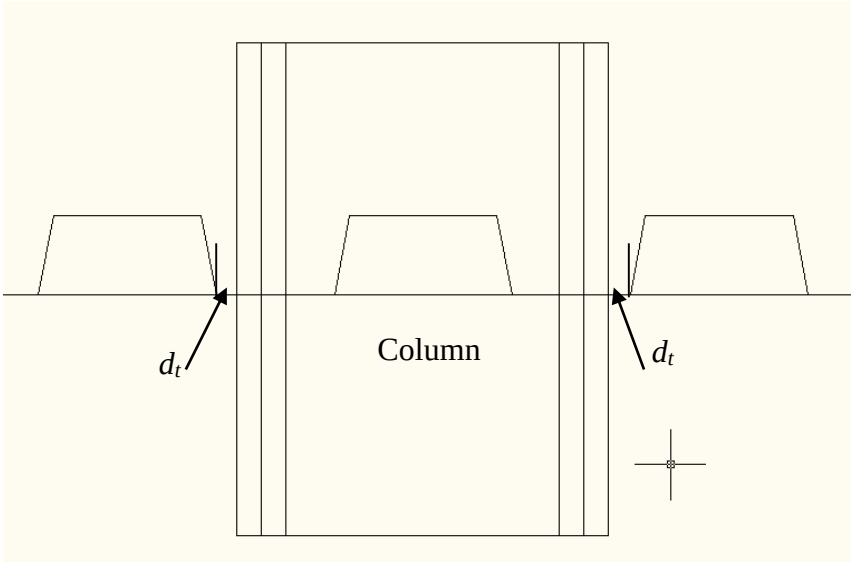

Figure 3-10: Placement of transverse deck tray around column in test subassemblies 1 and 2.

Parts of the tray were cut to accommodate the column, end plate and beam gussets with the gaps being filled with flat plate and silicon sealant. The deck tray sheets connected together

using hook and tab joints folded into the edges of the sheets and were fastened together using tec screws at 400mm spacing. The completed deck was then attached to the beam with shear studs. Edge trims were added using tec screws and sections of flat bar were used as restraint straps to secure the top of the edge trim as shown in Figure 3-11 to avoid it being pushed out by the weight of the concrete.

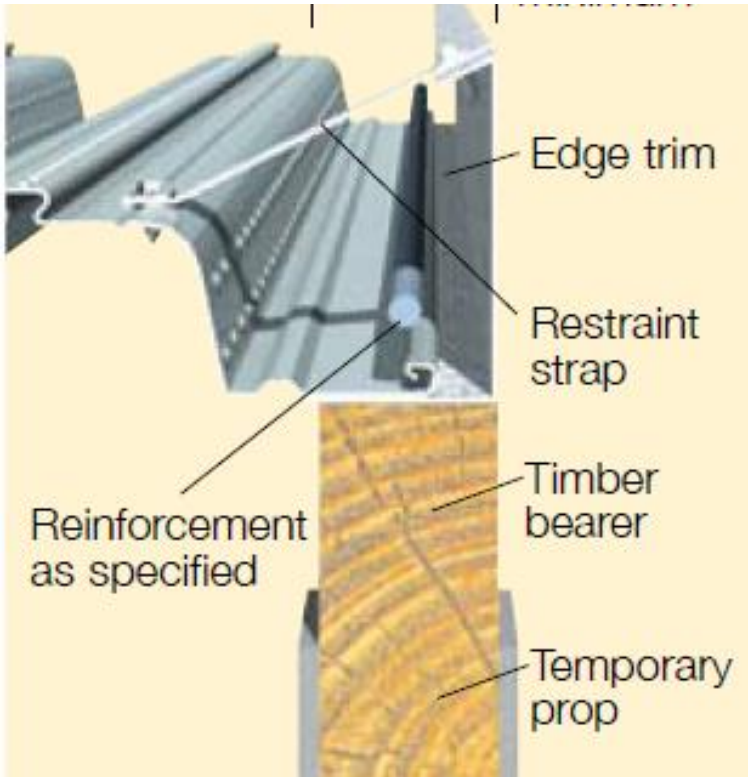

Figure 3-11: Example of edge trim detail from Comflor80 design guide.

Finally all remaining gaps were filled with silicone sealant. In cases where a large full depth slab was required around the column, sheet steel was used as shown in Figure 3-12 and sections of angle were attached under the slab to prevent sagging whilst pouring (these were removed before testing).

Figure 3-12: Tray deck detailing around column for longitudinal (left) and full depth (right) subassemblies.

The slabs were each poured in one cast and the concrete was vibrated and screeded to the top of the edge trim as illustrated in Figure 3-13. A 4m screed was used to set the level of the slab to the top of the edge trim however hand screeding was required around the column. Final finishing was done with a bull float two to three hours after the initial screed.

Figure 3-13: Finished concrete slab before curing compound was applied.

To reduce the risk of shrinkage cracking due to excessive bleed Sika Antisol E, a wax based curing compound, was sprayed over the slab once the final finishing had been completed as shown in Figure 3-14.

Figure 3-14: Finished slab after curing compound was applied.

To assist in crack identification, two coats of white water based undercoat paint were applied to the slab after excess wax from the curing compound had been removed. This was done 2-3 weeks after the pour to allow time for the curing compound to break down.

3.4 Loading Regime

Each sub-assembly was subjected to a displacement controlled quasi-static loading regime based on ACI report T1.1-01 [43]. Subassemblies were first subjected to 0.2% drift (4mm displacement at the loading point) followed by increased drifts (as shown in Table 2) up to 5.0% (100mm displacement). The increase in drift levels was such that each new drift level was between 1.25 and 1.5 times larger than the previous drift level as specified by ACI T1.1-01.

Table 2: Control drift levels.

Drift (%)	Displacement (mm)	Increase in step size*
0.2	4	-
0.25	5	1.25
0.35	7	1.40
0.5	10	1.43
0.75	15	1.50
1	20	1.33
1.5	30	1.50
2	40	1.33
2.5	50	1.25
3.5	70	1.40
5	100	1.43
* Current drift level/Previous drift level		

Three fully reversed cycles were performed at each drift level as shown in Figure 3-15. Between each set of drift cycles a single cycle of approximately half the drift level of the previous cycle was run in accordance with ACI recommendations to observe the residual stiffness of the structure.

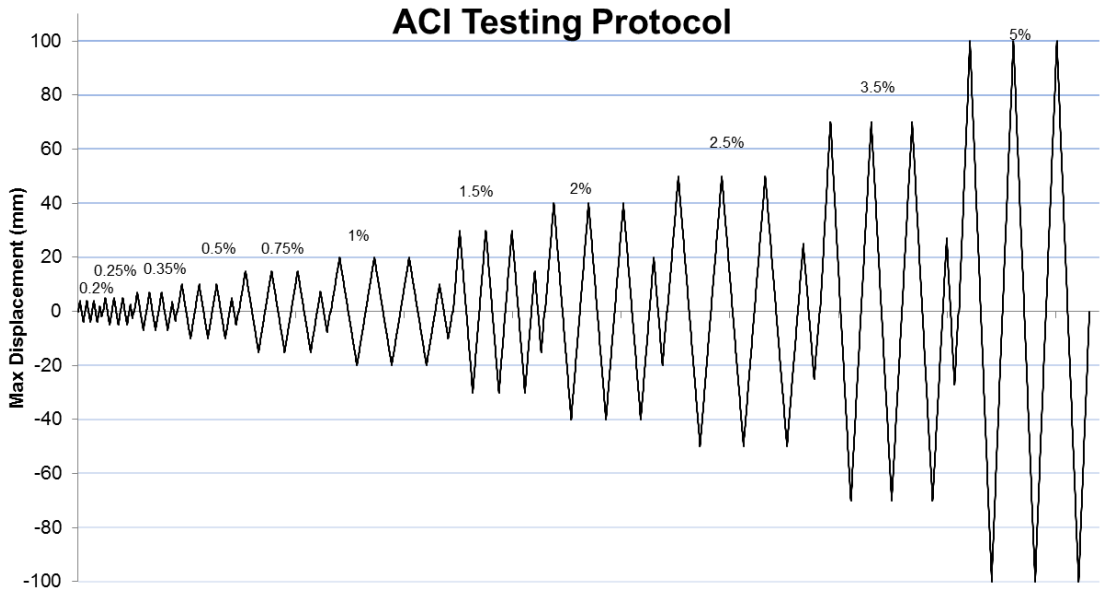

Figure 3-15: ACI displacement protocol for testing (ACI report T1.1-01).

3.5 Instrumentation

3.5.1 Load and Control

Load cells were used on all rams and supports to measure force as shown in Figure 3-16. A single 1000kN load cell was used in conjunction with the main actuator whilst smaller 150kN load cells were used for both the vertical support at the beam ends and the torsional restraint actuators. Rotary potentiometers were used to record the total displacement of the frame and to control the loading. Two of these were used, one recording displacements in the line of applied force (at the top of the column) while the other was used to record displacements at the centre of the panel zone. Both rotary potentiometers were mounted on a separate tower to ensure movement of the reaction frame did not affect readings.

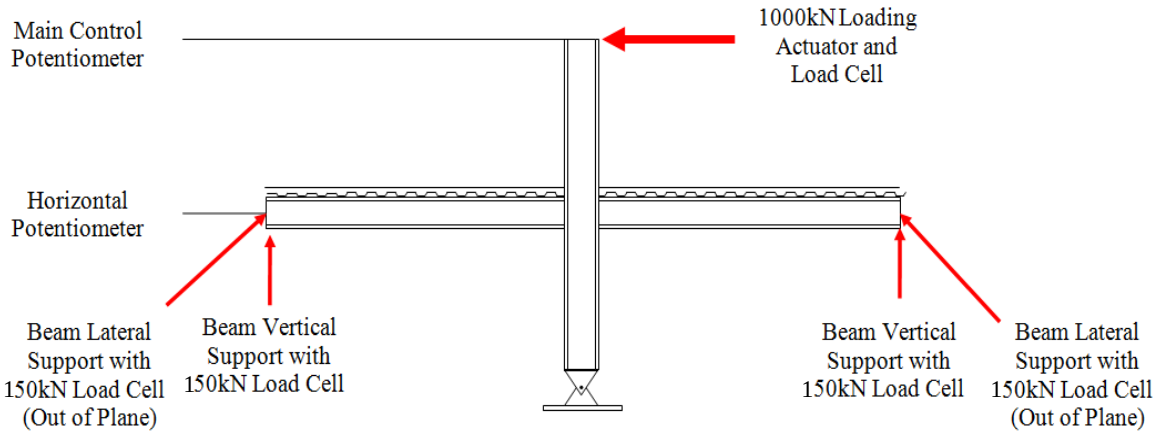

Figure 3-16: Loading and control instrument layout.

3.5.2 Panel Zone

The column panel zone and beam-column joint were both instrumented with linear potentiometers as shown in Figure 3-17. Four potentiometers were used to outline the panel zone, one in line with both the top and bottom flange continuity plates and the other two in line with the column flanges. A further two potentiometers were used to cross the panel zone diagonally.

From the column flange two linear potentiometers were placed in line with the top and bottom beam flanges. One of these was attached to the beam at a distance equal to the beam depth from the column face and the second was attached to the beam at one-and-a-half times the depth of the beam from the column face. Finally to monitor gap opening in the moment end plate connection, spring potentiometers were mounted on the beam end plate in contact with the column flange. Because of the presence of the secondary beams in subassembly 3, the top continuity plate potentiometer and the two diagonal potentiometers, numbers 6, 10 and 11 in Figure 3-17, had to be removed.

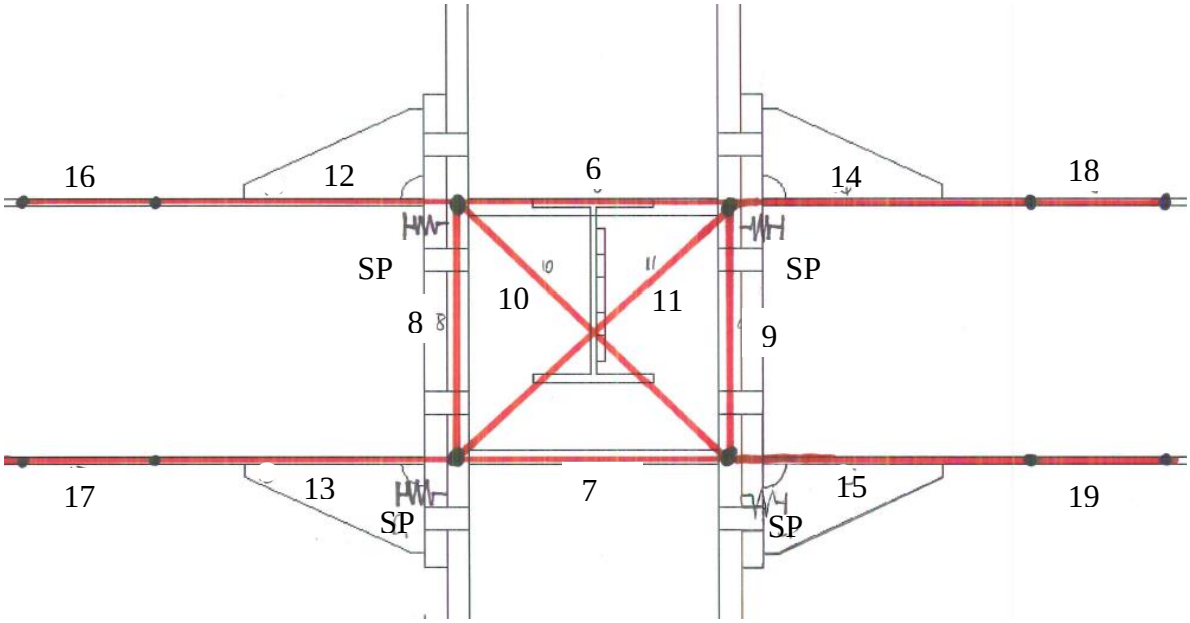

Figure 3-17: Beam-column joint instrumentation.

3.5.3 Slab

Deformations on the surface of the slab were recorded using a grid of linear potentiometers spread across one half of the slab. A 250mm by 250mm grid was used up to 1m out from the column centreline with the remainder of the instruments placed in a 500mm by 500mm grid as shown in Figure 3-18. Near the edges of the slab the grid length was adjusted to fit the placement of the slab with 450mm instruments being used in most cases. Diagonal (shear) instruments were only used in grids along the primary and secondary beams as shown Figure 3-18.

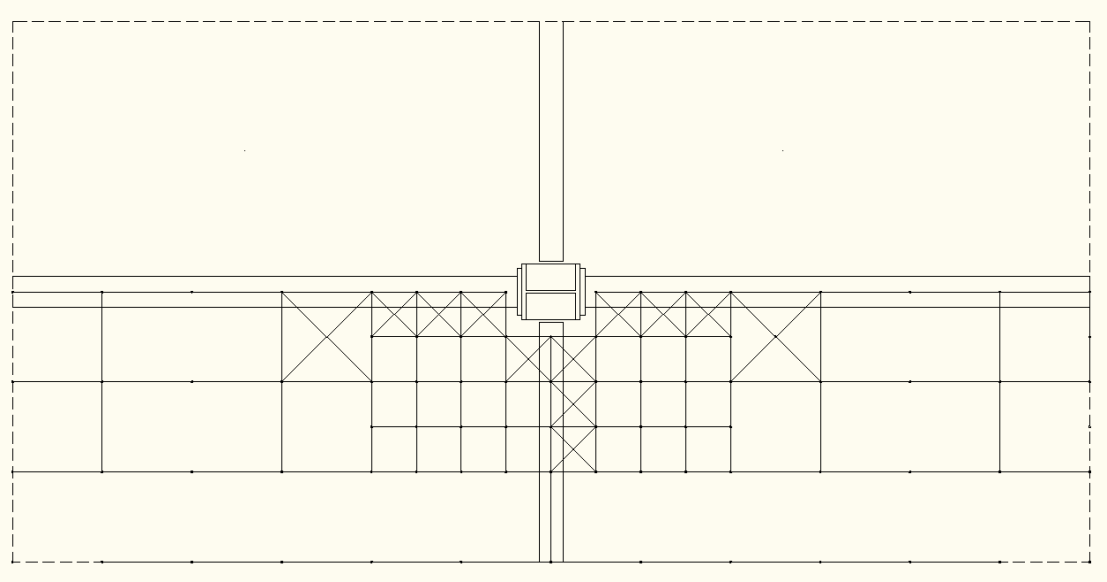

Figure 3-18: Linear potentiometer grid layout on the slab.

To ensure that both sides of the slab were acting in a similar manner, a line of Demec (Demountable Mechanical Strain Gauge) points were placed 500mm from the column centreline. Demec measurements were taken at the maximum drifts (positive and negative) in the third cycle at each drift level.

Leaving half of the slab with only a line of Demec points allowed for the observation and recording of crack patterns. Crack lines were marked on the surface on the slab when they appeared. Crack widths were recorded when the crack appeared and during the first and last cycles at each level of drift thereafter. After completing all cycles the linear potentiometers were stripped off the slab and the crack pattern drawn based on the visible cracks. The whole slab was then photographed in 500mm by 500mm grids which were then rearranged to give a detailed image.

3.6 Modelling the Subassemblies

In order to provide a point of comparison for the physical results, the beam-column subassemblies were modelled using the Ruaumoko structural analysis package. 2D models of the isolated, transverse and longitudinal subassemblies, as illustrated in Figure 3-19, were created with sub models being used to provide hysteretic data for the column panel zone and the concrete strut connecting the slab on either side of the column. Input files and model plots can be found in Appendix C.

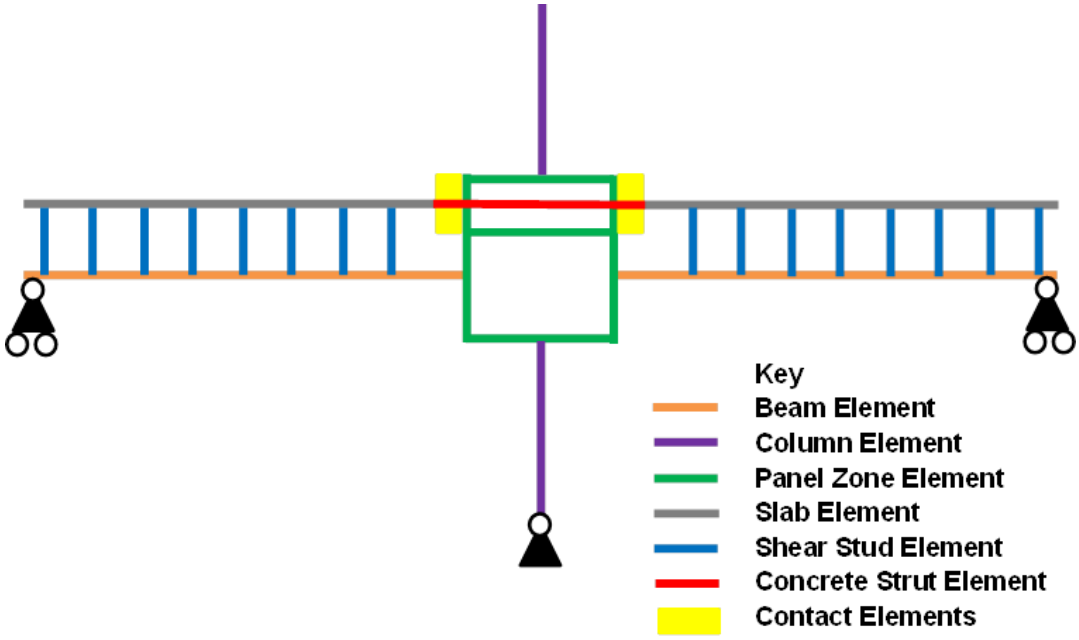

Figure 3-19: Layout of elements in the Ruaumoko model (not to scale).

The steel columns were modelled using a steel beam-column type member with fixed ends, no strength degradation and a bi-linear hysteresis with an initial assumed bi-linear factor of 0.01. In the area above the panel zone where the slab is in contact with the column, the column was modelled as two members each with half the strength of the full column. These members were joined using rigid links. The panel zone itself was modelled as shown in Figure 3-20 with four rigid links attached by pinned connections and with a pair of rotary springs to provide resistance.

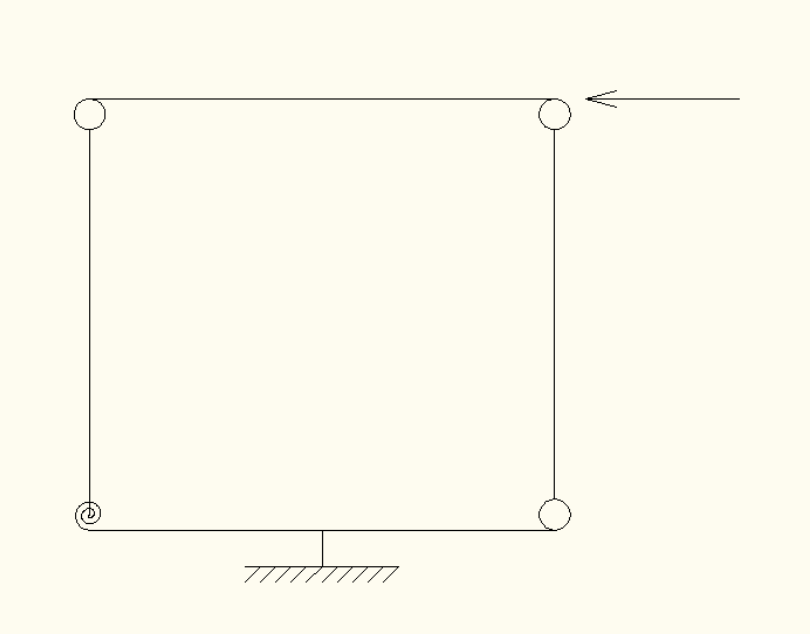

Figure 3-20: Panel zone model layout.

These springs were calibrated to match predictions given by NZS3404 clause 12.9.5.3.2 (see Appendix C) with both an elastic and an inelastic component to form the tri-linear hysteresis shown in Figure 3-21.

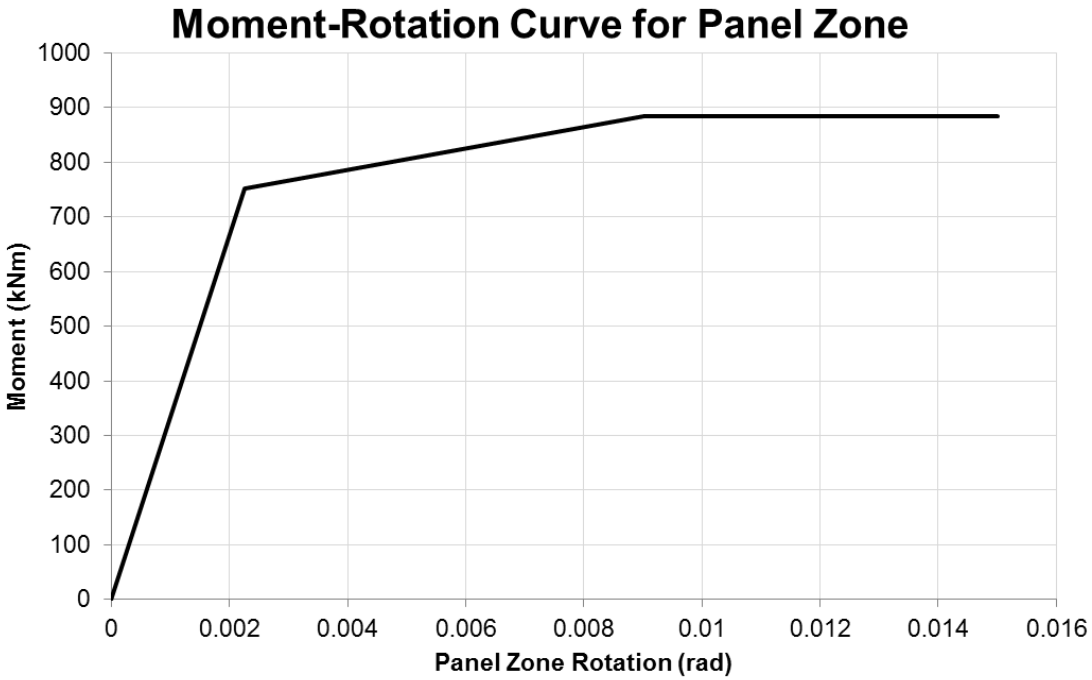

Figure 3-21: Moment rotation curve for panel zone.

The steel beams are represented by steel beam-column type members with fixed ends, no strength degradation and an elasto-plastic hysteresis. Because of the presence of the gusset plates near the beam-column joint, the section of beam over which the gusset plates covered was assumed to be significantly rigid so as to ensure and buckling occurred beyond the gusset plates. As such this section of the beam was represented by a rigid link. The plastic hinge length for all beam members was assumed to be equal to the depth of the beam.

The beam-column connection was initially planned to include endplate detailing, contact elements between the beam and the column for compression and bolt elements for tension. In practice however these elements made no appreciable difference and were replaced with a direct connection between the beam and the column with a rigid link to represent the end plate.

The slab surrounding the column was modelled using a pinned strut between the slab elements on either side of the column. To account for the effect of any strut-and-tie mechanisms formed between the concrete and reinforcing steel, the strut was calibrated using the component model shown in Figure 3-22. In this model tension ties, shown in red, were used to simulate various combinations of mesh, deformed bar and deck tray as required for each individual test. In this model the deck tray was only considered to act parallel to the ribs whereas all other tension members were considered to act when present. Rigid concrete strut elements, shown in black, and column flange elements, in grey, were used to apply load to the tension members hence completing the strut and tie model. Loading was applied to one of the flange elements whilst the other was fixed. This was to simulate the effect of column displacement applying compressive forces to the slab.

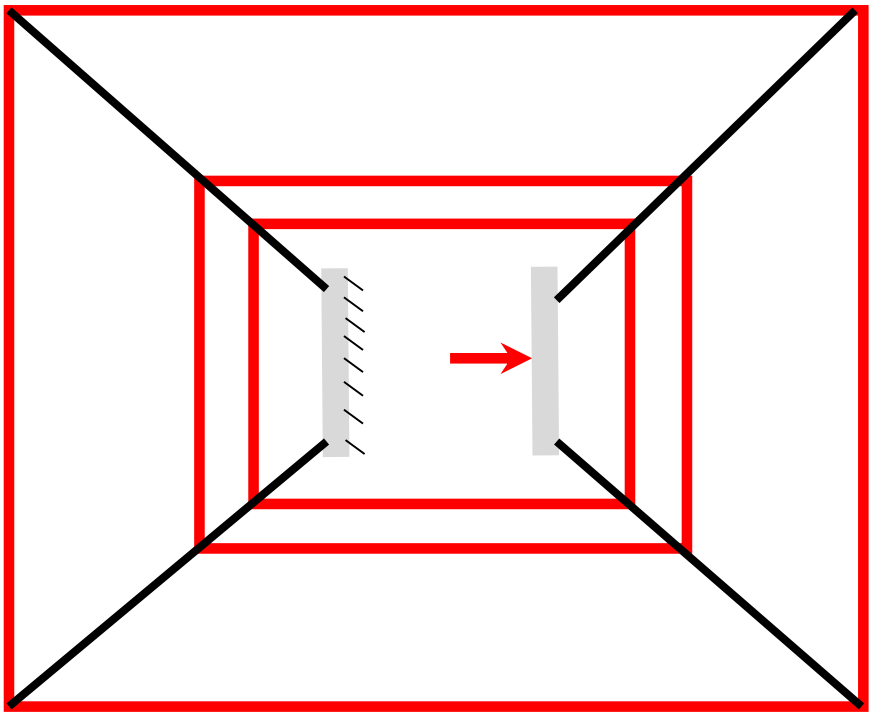

Figure 3-22: Strut-and-tie component model for concrete strut element.

Four component models were run, two with the deck tray in each direction. In each of these sets one subassembly had the deck effects included whilst the second did not. Comparison of the component models showed that the deck tray increased the strength for both tray layouts however without the deck both the parallel and perpendicular tray models were similar. From these tests, tri-linear hysteresis curves were created as shown in Figure 3-23 to be applied to the strut elements.

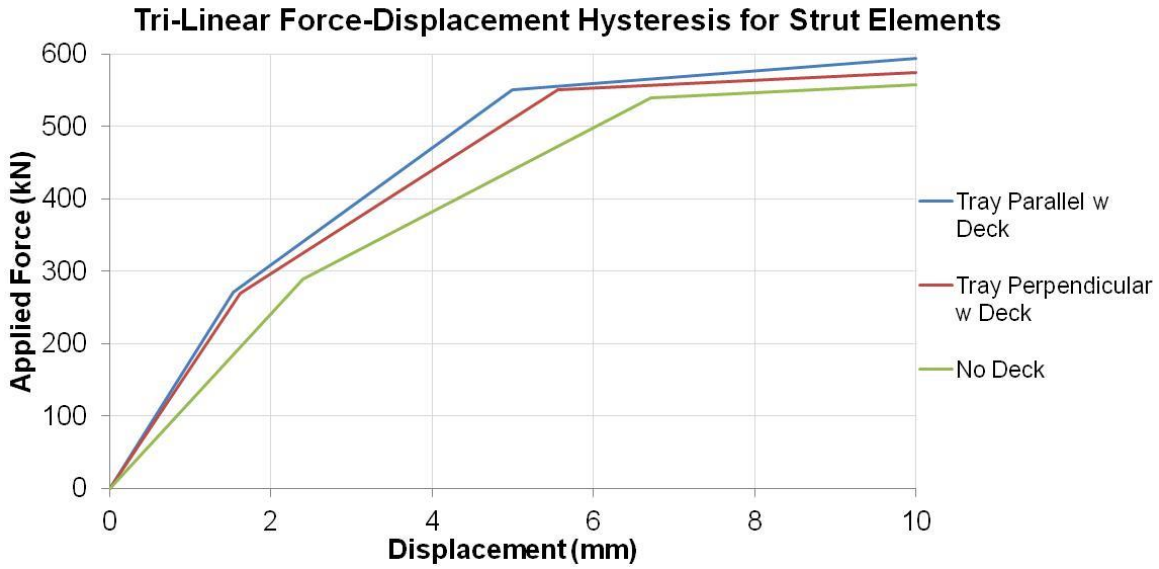

Figure 3-23: Tri-linear hysteresis for concrete strut elements.

The concrete slab was modelled as a pair of one component (Giberson) type members, one representing the concrete and one representing the mesh. The concrete elements were modelled as compression only struts with pinned ends and an elasto-plastic hysteresis. Strength degradation based on maximum ductility was introduced to reduce the strength of the concrete to near zero following crushing. Only the area of slab above the deck ribs was considered in subassembly models with a transverse deck tray whereas the average concrete depth was used for the longitudinal model. Shearing of the concrete parallel to the direction of loading was not explicitly considered. The mesh was also modelled as a tension-compression strut with pinned ends and an elasto-plastic hysteresis.

The concrete in contact with the column was modelled with a full depth of 150mm although the length of the contact element was not specifically matched to the actual length between the column face and the first deck rib. This section of the slab was modelled using beam elements with near zero tensile strength. Fifteen of these elements were used with a 10mm spacing to allow for progressive failure of the slab in compression. Like the main slab these elements used strength degradation based on maximum ductility to allow for crushing failure of the slab. The strength of these contact elements was multiplied to account for the bearing surfaces on both the inside and outside faces of the column.

The slab was fixed to the steel beam using a number of shear stud elements. These had a rigid length set to represent the depth of half of the beam. The concrete slab and mesh elements were attached to the top of these shear stud elements. Near the column face, where studs were not present, the vertical movement of the slab had to be fixed to represent the depth of the slab bearing on the beam.

It had been desired to test the beams under displacement controlled cyclic loading. Unfortunately a suitable loading type was not able to achieve this as the cyclic adaptive pushover option terminated when stiffness reached zero and single ground input option was unable to cope with the decrease in strength of the subassembly after peak strength was reached. As such it was decided to use a force controlled pushover, which was shown to produce identical results to the displacement controlled pushover. The isolated subassembly, which remained elasto-plastic after peak, was run to 5% drift levels and the remaining subassemblies

were run to their peak strength. At this point the subassemblies were assumed to revert to the elasto-plastic behaviour of the isolated subassembly.

4 Material Properties

4.1 Steel Properties

4.1.1 Section Sizes and Dimensions

The steel sections used in testing were standard sized universal beam (UB) and universal column (UC) type sections produced by OneSteel Manufacturing in Australia. Nominal section sizes from the OneSteel Hot Rolled and Structural Steel Products handbook [44] are reproduced in Table 3 below. The steel sections were stated as being produced to exceed the minimum strength, chemical and dimensional requirements of AS/NZS3679 [45] which are compared below.

Table 3: Section sizes for steel members.

	Column	Primary Beam	Secondary Beam	
Size	310UC158	310UB32	200UB29.8	
d	327	298	207	mm
b_f	311	149	134	mm
t_f	25	8	9.6	mm
t_w	15.7	5.5	6.3	mm
d_1	277	282	188	mm

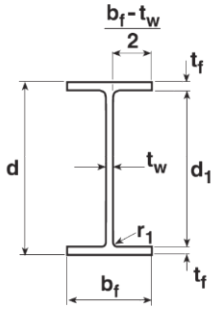

Eighteen thickness measurements from the top and bottom flanges and the web gave the average thicknesses shown in Table 4 below. These values were within the tolerances of 0.7mm for the web and 1.0mm for the flange set by AS/NZS3679.

Table 4: Beam thickness data.

	Top Flange Thickness (mm)	Bottom Flange Thickness (mm)	Web Thickness (mm)
Maximum	8.02	7.99	5.70
Minimum	7.58	7.70	5.59
Average	7.81	7.89	5.65
Specified	8	8	5.5

The flanges of both columns were noted as having some variations in the cross section from the manufacturing process. The sum of the measurements a_1+a_0 from Figure 4-1 for both columns was 5mm which fell within the tolerance of 8mm set by NZS3404.

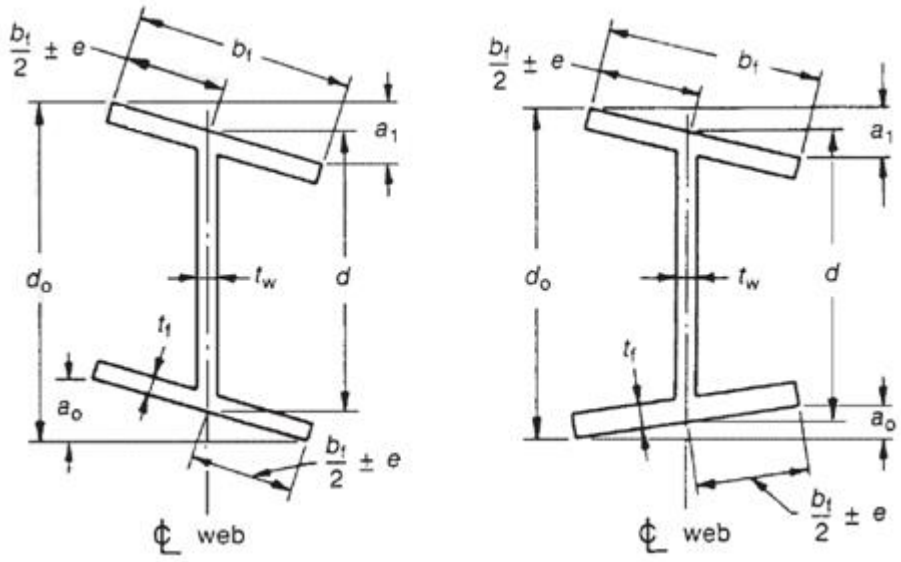

Figure 4-1: Flange out of square terminology as per NZS3404.

4.1.2 Steel Section Strengths

Grade 300 steel was specified throughout. The steel sections were tested by OneSteel (the manufacturer) prior to shipment and selected steel tests were performed in the laboratory.

The primary beam sections had a specified minimum yield stress of 320MPa and an ultimate stress of 440MPa (for both the flange and the web). Initial factory tensile testing performed by OneSteel (see the mill certificate in Appendix D) indicated that the primary beams had a yield strength of 385MPa and an ultimate strength of 520MPa. This gave an increase over the specified minimum strength of 1.2 times at yield and 1.18 times at ultimate. The beams were of AS/NZS3679.1-300 specification [45].

Further tensile testing was carried out on coupons cut from undamaged portions from the beams of the second, third, fourth and fifth tests with the results shown in Table 5 and Table 6 below. It can be seen that the average first yield strength of both top and bottom flanges was 368MPa which is less than that from the OneSteel tests by 17MPa and gives an increase over the

minimum specified yield strength of 1.15. The ultimate strength was approximately 518MPa which is comparable with the OneSteel mill test value of 520MPa. The strength of the web steel was significantly higher and gave a strength increase of 1.24 times the minimum yield and 1.21 times the minimum ultimate strengths ordered.

Table 5: Yield strengths from tensile testing.

	Top Flange	Bottom Flange	Web
	Yield Strength	Yield Strength	Yield Strength
1	362.7	362.2	399.2
2	362.1	368.3	380.2
3	371.0	366.2	407.8
4	381.4	360.1	376.5
5	364.3	375.9	409.7
6	370.1	375.6	400.0
Average	368.6	368.0	395.6
	MPa	MPa	MPa

Table 6: Ultimate strengths from tensile testing.

	Top Flange	Bottom Flange	Web
	Ultimate Strength	Ultimate Strength	Ultimate Strength
1	514.8	512.5	535.8
2	510.3	515.8	523.6
3	516.1	510.8	536.7
4	523.6	523.2	526.0
5	516.6	520.4	546.8
6	525.8	526.6	536.5
Average	517.9	518.2	534.2
	MPa	MPa	MPa

The column sections were of 300PLUS S0 specification and had a specified minimum yield strength of 280MPa for the flanges and 300MPa for the web. The specified ultimate strength was 440MPa. Factory testing produced a yield strength of between 310MPa and 335MPa (322MPa average) and an ultimate strength of between 470MPa and 490MPa (480MPa average) as shown in the mill certificate in Appendix D. This gave an increase over the

specified minimum strength of 1.15 at first yield and 1.09 at ultimate. Because the columns were to be reused for further testing no further tensile tests were conducted.

The secondary beams had a factory tested yield strength of between 350MPa and 395MPa and an ultimate strength of between 500MPa and 530MPa as shown in the mill certifications in Appendix D. Because these were not lateral load resisting elements and were subjected to very little force no further tests were conducted.

4.2 Concrete Properties

The concrete specified for testing required a 28 day compressive strength of at least 30MPa and a maximum aggregate size of 19mm. Each subassembly required 1.9m^3 and an extra 0.2m^3 was added to allow for test cylinders and pooling. The concrete supplier, Allied Concrete, provided a 3019 grade mix with the component quantities given in Table 7 below. This mix had a target 28 day compressive strength of 36MPa.

Table 7: Component quantities of 3019 mix.

Cement	265kg
Water	155kg
19mm Aggregate	660kg
13mm Aggregate	440kg
Sand (5mm)	880kg
Water Reducer (SP500)	795ml
Water : Cement Ratio	0.585
Minimum 28 Day Strength	30MPa
Target 28 Day Strength	36MPa
Target Slump	100mm

Batch records supplied by the provider are shown in Appendix D along with calculations of the water to cement ratio and the after batching predicted 28 day compressive strength. The supplier also provided details on the capacity of the trucks used for delivery and these are shown along with the water to cement ratio and after batching predicted strength in Table 8.

Table 8: Truck capacity, predicted water to cement ratio and after batching predicted 28 day strength.

	Truck Volume (m^3)	Water : Cement Ratio	After Batching Predicted 28 day Compressive Strength
Isolated	5	0.571	37.8MPa
Transverse	6	0.697	27.9MPa
Longitudinal	5	0.590	36.0MPa
SHJ	6	0.637	32.0MPa
Full Depth	10	0.680	29.0MPa

Compressive testing, in accordance to procedures set out in NZS3112-2 [46], was performed on all batches with 3 standard cylinders tested after 7 days, 14 days, 28 days and on the day of testing (see Appendix D for detailed results). The average concrete compressive strength (fc') for 28 days and the day of testing is shown in Table 9 along with the measured slump at the time of casting. As can be seen all specimens tested fell short of the target 28 day strength, some by a large margin. Batch records displayed in Table 8 showed that only the transverse and full depth subassembly strengths were compromised by poor mix quantities with the remaining subassemblies all having predicted 28 day strengths above 30MPa. The strength loss is thought to be mainly due to excess wash water compounded by the use of large trucks for small loads as is shown in Table 8.

Table 9: Concrete compressive strength at 28 days and on day of testing.

Subassembly	Slump	28 Day Compressive Strength	Test Day Compressive Strength
Isolated	100	26.2	26.4
Transverse	70	23.7	27
Longitudinal	120	23.1	23.8
SHJ	120	24.4	24.2
Full Depth	120	17.2	19.7
	mm	**MPa**	**MPa**

4.3 Fastener Properties

Bolts for the moment endplate connections and the sliding hinge joint were structural grade 8.8 type. Grade 4.6 bolts were only used as sacrificial positioning bolts in the sliding hinge joint connection and these were accounted for in the design. Bolts were sized to ensure threads were excluded from any interface and suitable flat washers were used on all bolts. Bolt sizes for various connections are shown in Table 10 along with the proof load and breaking load as specified by the manufacturer. All structural bolts were stated as complying with AS1252 [47].

Table 10: Bolt sizes and strengths.

Location	Grade	Bolt Size	Total Length	Grip Length	Specified Proof Load (min)	Specified Breaking Load (min)
Moment End Plate	8.8	M24	90	36	212	293
Secondary Beam	8.8	M24	60	-	212	293
	8.8	M24	50	-	212	293
Sliding Hinge Joint	8.8	M20	70	24	147	203
	8.8	M16	90	52	94.2	130
	8.8	M16	80		94.2	130
	8.8	M16	60	22	94.2	130
	4.6	M12	40	-	-	-
			mm	mm	kN	kN

Tensile testing of such bolts by Chanchi [34], using bolts from the same supplier, had shown that the M16 bolts used in the sliding hinge joint tended to yield between 110kN and 115kN. Ultimate loads for the bolts tested ranged between110kN and 125kN for 90mm bolts and 130kN and 142kN for 75mm bolts. Testing by the University of Auckland [48] on M24 bolts resulted in a yield stress of approximately 867MPa and an ultimate stress of 953MPa, over a reduced area of around 40mm^2, in comparison to the specified yield strength of 660MPa and ultimate strength of 830MPa.

The composite beams utilised 19mm diameter, 125mm tall Nelson mild steel shear studs with a minimum specified tensile strength of 415MPa. Approximately one in every ten studs was

bent one way to a 15 degree angle after installation to check weld quality as recommended by AS/NZS1554 [49].

5 Predictions and Interpretation of Results

5.1 Predicted Behaviour

Before conducting the physical testing, a set of predictions were made. These predictions formed a hypothesis for this study to which the results could be compared to. It was considered that a possible way to better incorporate slab effects in design could be to consider:

- For slabs isolated from all faces of the column flanges, that slab effects should not be considered in beam strength design to resist the lateral forces nor in overstrength design.

- For slabs which are full depth for a significant distance (say equal to the beam depth) from the column face, that the slab effect could be considered both in beam strength design to resist the lateral forces and in overstrength design.

- For slabs which are placed in contact with the column face, but without special care, that the current NZ design approach continue to be used where the slab effect is not considered for beam strength design to resist the lateral forces but it is considered in overstrength design.

5.2 Analytical Comparisons

5.2.1 Design Strength

Strengths Used in Analysis

The design strength subassembly models, described in Section 3.6, utilised the strength values for steel and concrete assumed in the initial design of the physical subassemblies. This was Grade 300 Steel for the steel elements and a target 30MPa crushing strength for the concrete elements. Each of the three subassemblies, isolated, transverse and longitudinal, was analysed twice with the concrete strut element being changed to incorporate or ignore the presence of the deck tray as described in chapter 3.6. Overstrength of the beams due to strain hardening was not considered in this analysis.

Isolated Subassembly

The isolated subassembly model utilised the basic model components described in Section 3.6 with the contact elements removed. An essentially elasto-plastic envelope was formed from the analysis as shown in Figure 5-1. The model was linear up to 1.18% drift at which point the steel beam elements reached their plastic flexural strength, after which no further resistance was encountered. Data from the analysis, shown in Appendix C, indicated that the concrete strut element, shown in Figure 3-19, between the slab on either side of the column was carrying less than 15N of axial force at the time of beam yielding. This is less than 5% of the beam flange yield force and as such the response was assumed to be that of the steel beams alone.

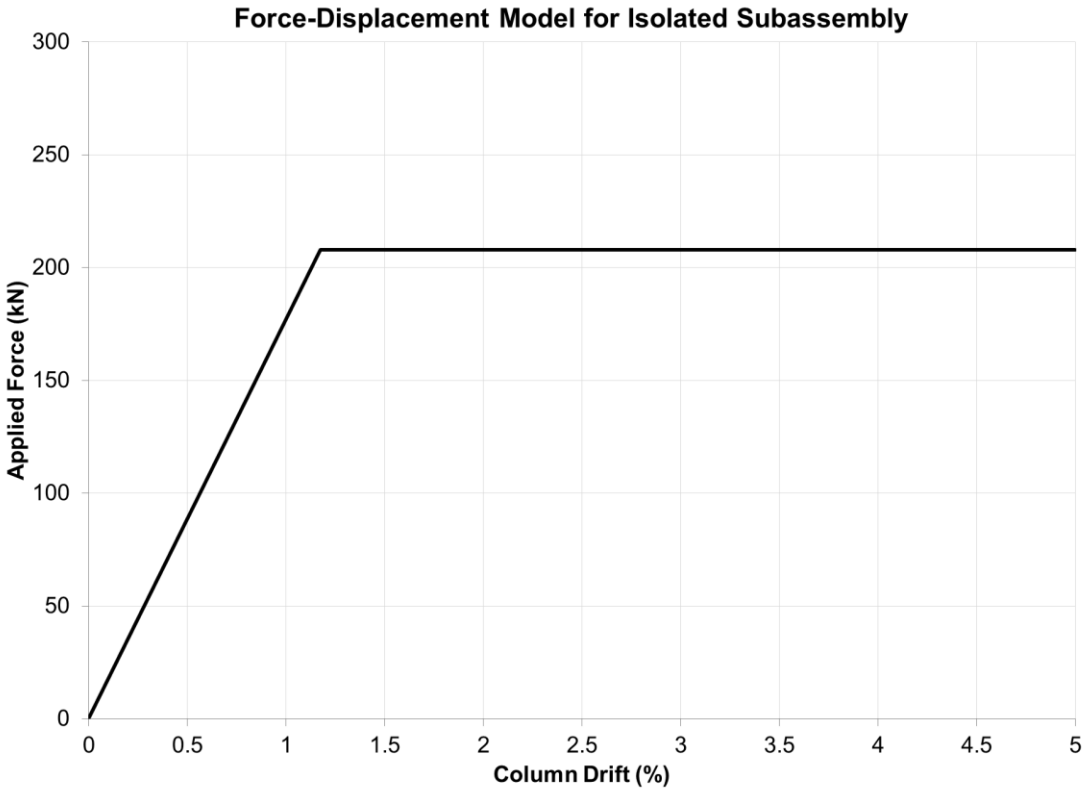

Figure 5-1: Force-displacement hysteresis model for isolated subassembly using nominal material strengths.

The presence of the deck tray elements in the slab strut made no appreciable difference to the overall performance of the subassembly. As such the deck tray was not considered in the isolated subassembly model.

Transverse Subassembly

The transverse subassembly used the Ruaumoko model described in chapter 3.6 with a modelled slab thickness of 70mm. It was analysed monotonically up to 1.35% drift at which time the stiffness of the subassembly dropped to zero and the analysis was terminated. The envelope remained linear up to 1.2% drift at which time the steel beam elements yielded. This was followed by a rapid failure of the concrete contact elements and the concrete slab at 1.35% drift, at which point the tangent stiffness of the subassembly went to zero. To simulate behaviour at larger drifts the envelope was assumed to reduce to the post-yield resistance of the isolated subassembly as illustrated in Figure 5-2. The final strength was that of the isolated subassembly of 208kN as shown in Figure 5-1. This was a reduction of 13% from the peak strength and was taken as the slab contribution on the overall system.

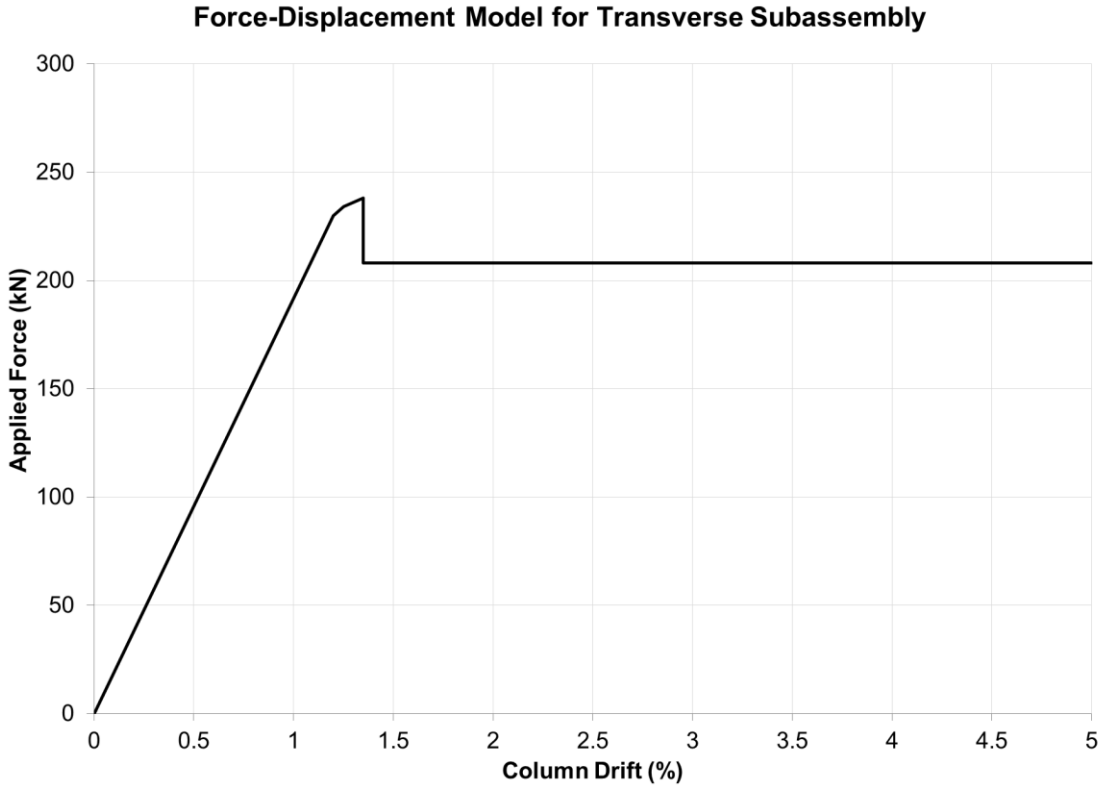

Figure 5-2: Force-displacement hysteresis model for transverse subassembly using nominal material strengths.

Data from the output file, shown in Appendix C, indicated that the concrete contact elements provided resistance from the beginning of the analysis. The force on these elements drastically increased following the yielding of the beams leading to the eventual failure of these elements. The outer most element, that representing the top surface of the slab, was the first to fail by spalling however once this element failed additional stresses were put on the elements below

in a cascade effect which caused these elements to fail in rapid succession. Likewise the slab strut element showed an increase in axial load which spiked after the beams yielded and dropped rapidly when the slab contact elements failed. Like the isolated subassembly, the presence of the deck tray in the slab strut had no effect and was ignored in further analyses.

Longitudinal Subassembly

The longitudinal subassembly used a near identical model setup to the transverse subassembly but with an average slab depth of 106mm as described in chapter 3.6. It was analysed monotonically to 5% drift and exhibited a similar pre-yield stiffness to the transverse subassembly. The envelope remained linear up to 1.2% drift at which time the steel beams yielded. Beyond this point a more gradual failure of the concrete contact elements occurred due to gradual spalling of the contact elements with the subassembly reaching zero stiffness just beyond 5% drift as shown in Figure 5-3. Longitudinal shear failure of the concrete was not considered by this model.

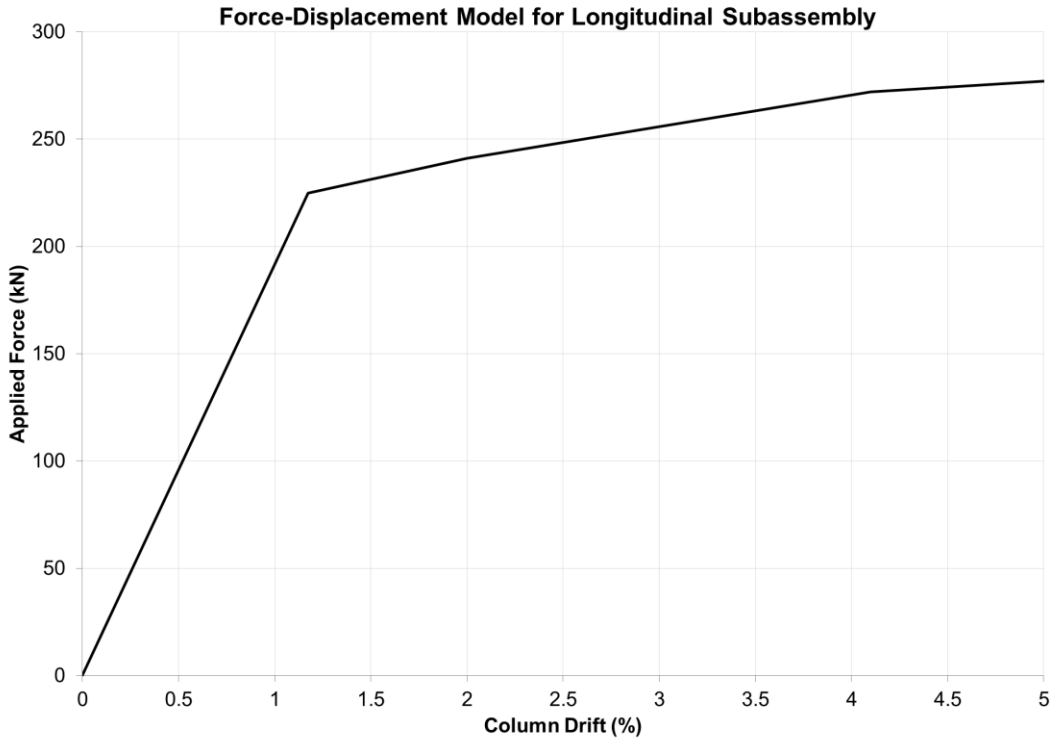

Figure 5-3: Force-displacement hysteresis model for longitudinal subassembly using nominal material strengths.

Data from the output file again showed that the concrete contact elements provided compression resistance from the beginning of the analysis. However, unlike the transverse subassembly, the force on this group of elements tended to be more evenly spread over all of the individual elements. As such the cascade effect which caused the failure of these elements in the transverse subassembly wasn't observed until a much higher drift level. Data from the output files, shown in Appendix C, also showed the slab strut element carrying an increased axial load which spiked after the beams yielded and dropped rapidly when the slab contact elements failed. Again the presence of the deck tray in the slab strut had no effect and was ignored in further analyses.

5.2.2 Actual Strength

After material testing had been completed, the three subassembly models were re-analysed with the measured material properties given in Section 4. In all three subassemblies, shown in Figure 5-4, 5-5 and 5-6, the behaviour remained much the same however the ultimate strength was increased. In most cases this was purely due to the increase in the resistance provided by the beams with the concrete contribution being reduced on account of the sub-strength concrete provided.

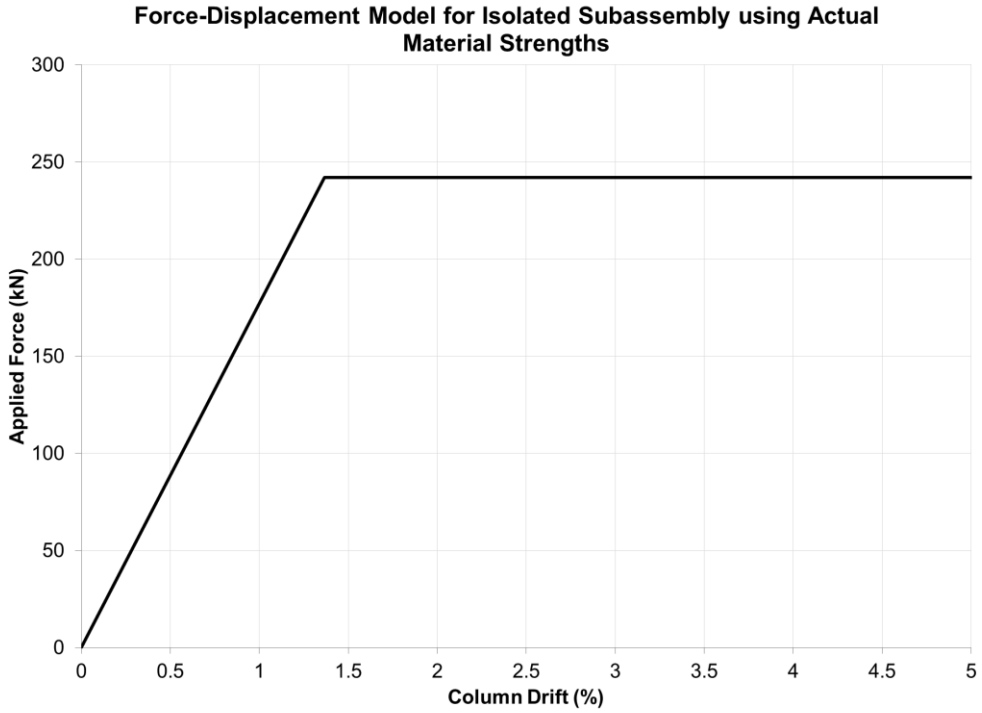

Figure 5-4: Force-displacement hysteresis model for isolated subassembly using actual material strengths.

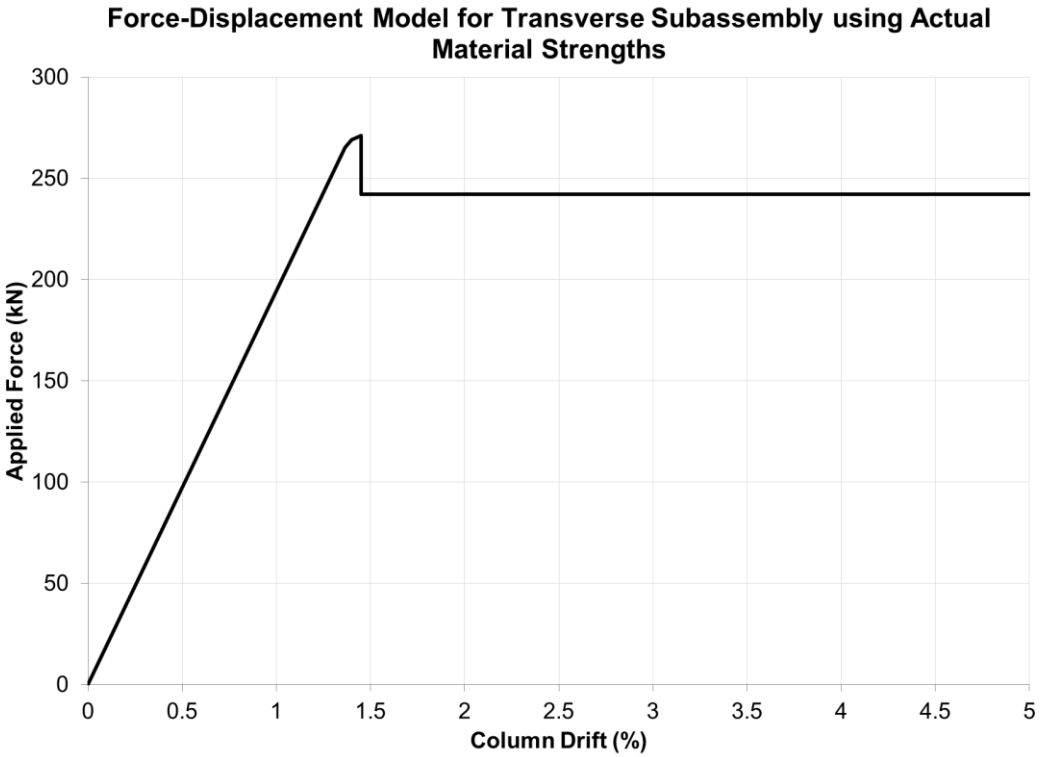

Figure 5-5: Force-displacement hysteresis model for transverse subassembly using actual material strengths.

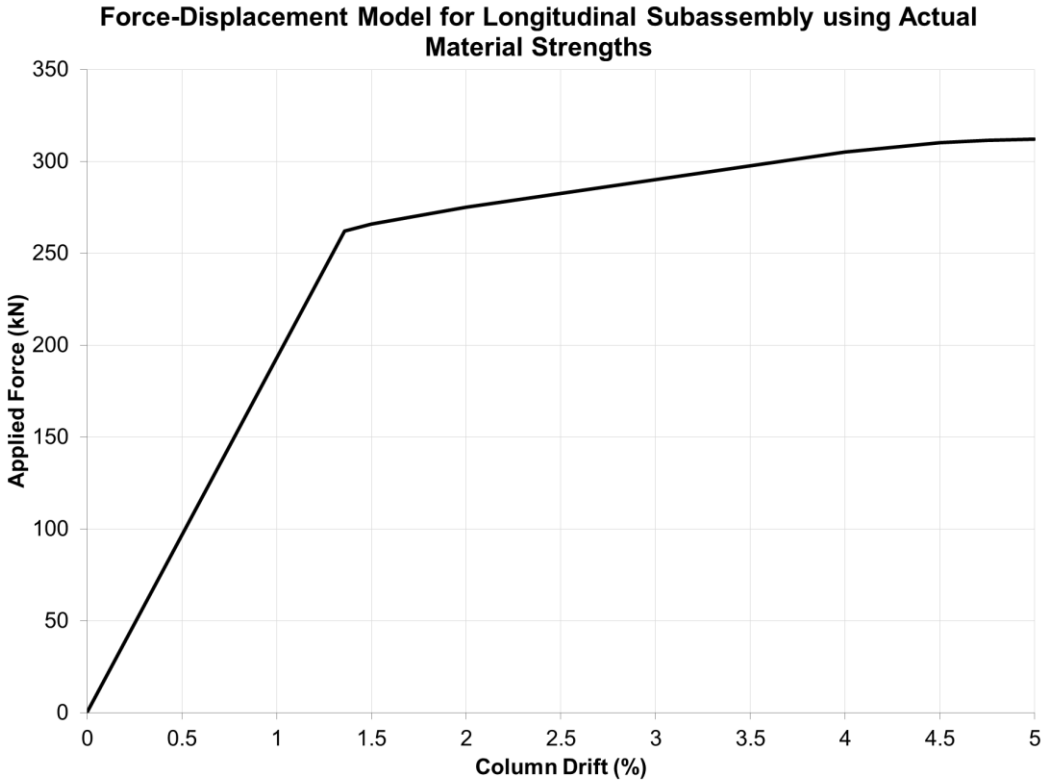

Figure 5-6: Force-displacement hysteresis model for longitudinal subassembly using actual material strengths.

5.3 Data Processing

Hysteresis

Hysteresis data was plotted in the form of a force-displacement plot for both the column top and column mid-height displacements. Force and displacement data from the output files were zeroed against the first value of the file. The data was then plotted to form both the full hysteresis and hysteresis loops for each drift cycle. Where present, data from the column to base connection was subtracted from the displacement data to remove the displacement caused by slip in this region.

Panel Zone and Beam End Plates

Panel zone displacement data was taken straight from the output file and zeroed to the first recorded value. The maximum and minimum values from each instrument were identified and the sum of these recorded in a figure to give an indication of the extent of movement in the panel zone. The deformation due so shearing of the panel zone was then calculated based on the assumption that the top and bottom flange continuity plates remained perpendicular to the upper and lower sections of the column whilst the section between deformed as illustrated in Figure 5-7.

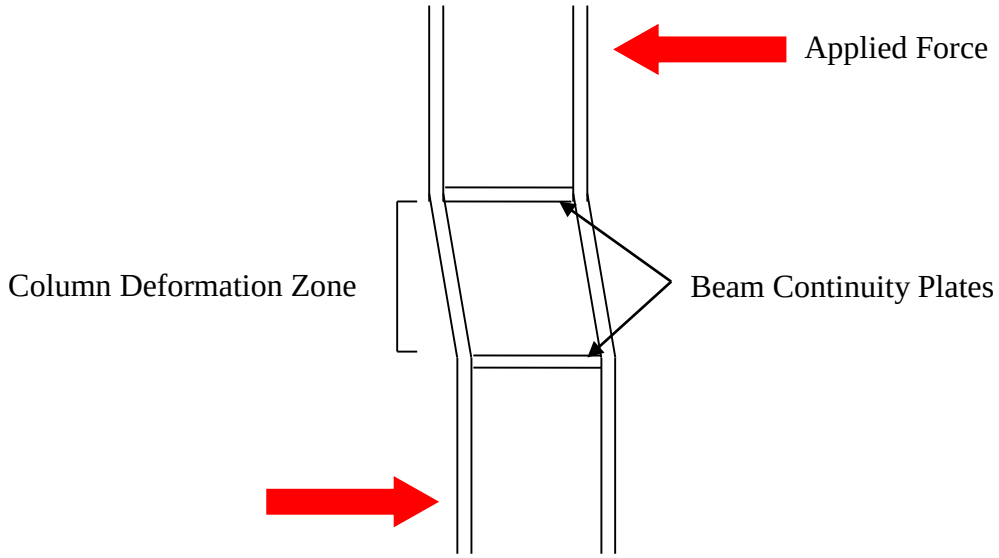

Figure 5-7: Assumed panel zone deformation mechanism.

Using this assumption the panel zone deformation was calculated using the following trigonometric equations, developed from first principles using triangle rules, where Δ_{pz} was the panel zone deformation, *a* was the measured length of the column flange within the deformation zone, *b* was the measured length of the top flange continuity plate and *c* was the measured corner to corner diagonal length of panel zone.

$\Delta_{pz} = a \sin(|90-\gamma|)$

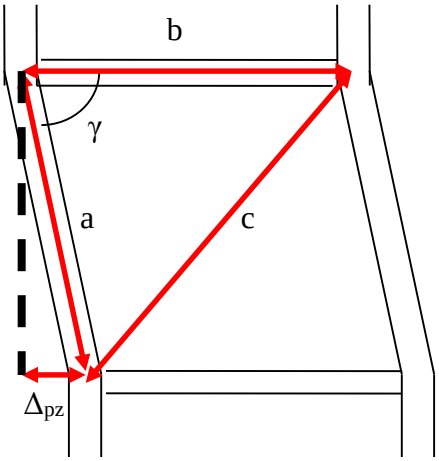

$\gamma = \cos^{-1}((a^2+b^2-c^2) / 2ab)$

Figure 5-8: Calculation of panel zone deformation from trigonometry.

The column top displacement due to panel zone deformation was derived empirically with the derivation being set out in Appendix E.

The beam end plate lift off was recorded throughout the testing. It was theorised that the total displacement due to gap opening at any one time would be the sum of the values of the four spring pots (SP) in Figure 3-17. This assumes that at any time two of these would be located on compression flanges (the top flange of one beam and the bottom flange of the other) and would give zero readings whilst the other two would be on the tension flanges of the beams as shown in Figure 5-9.

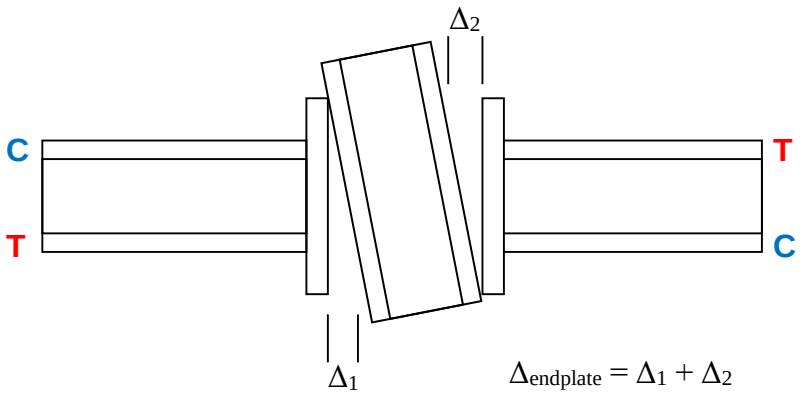

Figure 5-9: Assumed moment end plate lift-off behaviour.

These values were added to the panel zone deformation to give the total participation of the beam-column connection. This was then subtracted from the total column top deformation and plotted against the total deformation to illustrate the effect of the beam-column joint deformations on the system. In all cases two sets of data was plotted, continuous data from the length of the testing and residual data from points where the applied force was zero.

Beam Elongation

Beam elongation was measured using the linear potentiometers located on the top and bottom flanges of the primary beam described in Section 3.5.2. To reduce the risk of measurements being disrupted by flange deformations in the plastic hinge zone the potentiometers running 1.5 times the beam depth from the column face, numbers 16 to 19 in Figure 3-17, were chosen for plotting beam elongation. As such it was assumed that all elongation in the beam fell within the plastic hinge zone which was taken as being less than 1.5 times the beam depth. The centreline elongation at each data recording point was computed by averaging the displacement of the linear potentiometers on the top and bottom flange. This was then plotted against the loading step number to provide a plot of beam elongation over time. Again both continuous data and residual data from points where the applied force was zero were plotted.

Column Bending Displacement

The column bending displacement for the top half of the column was to be obtained by talking the difference between the main control potentiometer and the horizontal potentiometer shown in Figure 3-16. Unfortunately a defect was present in the horizontal potentiometer at beam level

(non-controlling) which resulted in a calibration error at higher drifts. This defect only tended to increase the drift measurement in one direction and as such remained unnoticed until the instrument failed during the testing of the fourth subassembly. As such only the data from the fifth subassembly was able to be recovered for analysis.

To provide some indication of the column bending displacement it was decided to use the data from the fifth subassembly to produce a linear force-displacement model to determine the expected column deflection. The data from the full depth subassembly and visual inspection of the columns indicated that there had not been significant inelastic deformation so this method was reasonable. The linear relationship is shown in Figure 5-10. The offset of the data at zero displacement was due to the slip observed between the base plate and the pin connection. The data had to be calibrated to account for this however because the slip did not occur at low drift levels the displacement data at these points was reduced to below the actual displacement. Because both the positive and negative loading cycles were effected in the same way the linear relationship produced is still accurate.

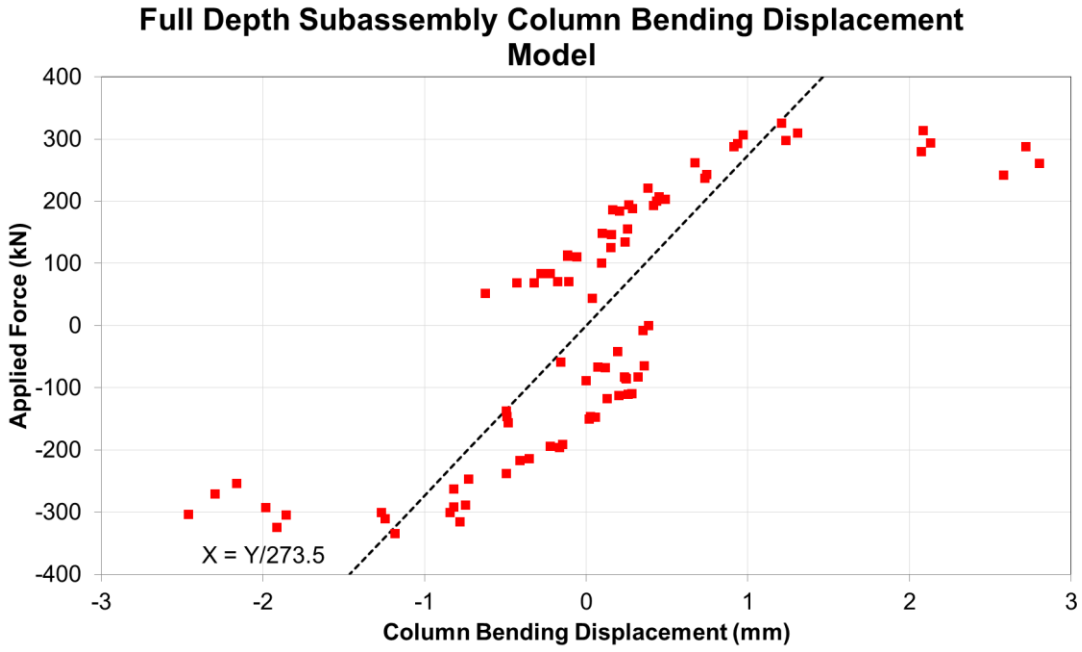

Figure 5-10: Linear model used for determining column bending displacement.

The force applied to the column (Y) was used to determine the corresponding bending displacement in the top half of the column (X). This value was then multiplied by two to

estimate the bending displacement of the whole column. Both continuous data and residual data from points where the applied force was zero were plotted.

Slab

The in-plane displacement measured on the surface of the slab was plotted in a series of 2D contour plots using Matlab. The area covered by linear potentiometers was set as a grid with the column centreline being the zero point and the x and y axis following the lines of the primary and secondary beams respectively. Because only one side of the slab was instrumented this was taken as the positive y axis and the contour profile was mirrored across the x axis to form the negative y axis. The centreline of the column also formed the absolute zero point for comparing displacements to. All points along the primary beam lines were set to zero y displacement whereas all points along the secondary beam line were set to zero x displacement. Beyond this, each individual data points movement was calculated by taking the extension of the potentiometer framing into it and subtracting the extensions from all the potentiometers in the line back to the nearest zero point as shown in Figure 5-11. As such the displacements produced are relative to the starting position of each individual point and the total displacement, relative to the column centreline, is obtained by summing the individual point displacements between the column and the point of interest.

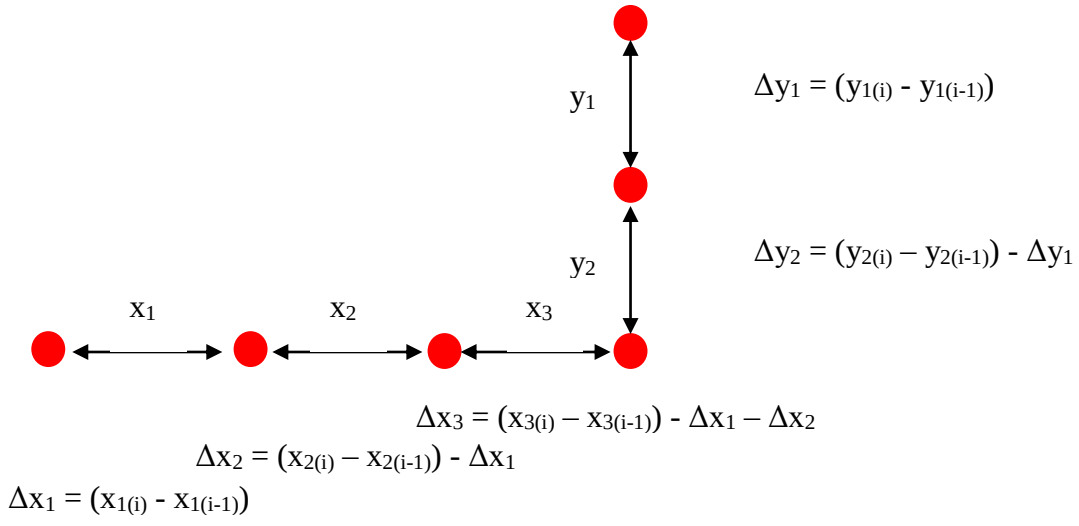

Figure 5-11: Calculation of slab surface deformation from raw data.

Once the x and y displacements at each data point were calculated, the net displacement was obtained by taking the square root of the sum of the squared x and y data. This value then

formed the z displacement for a filled contour plot with the x and y positions being given as the initial location of the point on the grid. To ensure a constant grid spacing linear interpolation was used between points over 250mm apart to form a uniform with the distance between points being 250mm. This grid along with the displacement data was then plotted in using the Matlab code in Appendix E. This created a 2D coloured contour similar to the example shown in Figure 5-12 with contours being placed every 0.5mm.

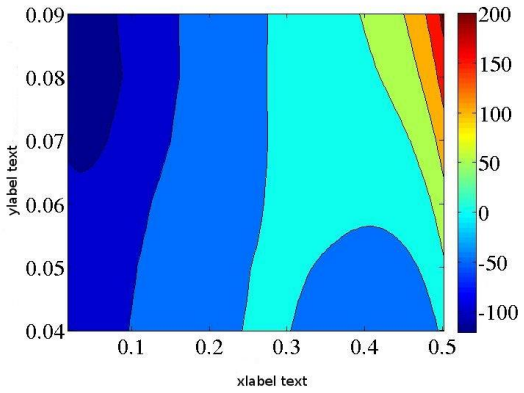

Figure 5-12: Example of a Matlab filled contour plot.

6 Subassembly Behaviour

6.1 Observed Behaviour

6.1.1 Isolated Subassembly

Testing of the isolated subassembly occurred over 3 days with cycles to 1.0% drift (20mm) tested on the first day and cycles to 1.5% drift (30mm) on the second day. During the 1.5% drift cycles a control software issue developed. The subassembly was returned to zero displacement (some residual force was present) to allow the fault to be rectified and the 2%-5% (40mm-100mm) drift cycles were completed on the third day.

Cracks in the concrete slab began to appear from 0.35% drift (7mm displacement) with initial cracking being confined to transverse cracks running across the width of the slab. These transverse cracks appeared to form either at or beyond the second deck rib which was approximately 600mm from the column centreline as shown in Figure 6-3. The majority of the transverse cracks observed tended to form over the ridges of the profiled decking, where the slab was shallowest. Further transverse cracks appeared as the testing progressed along with longitudinal cracking in the vicinity of the primary beams from around 1.5% drift. Photographs of the full slab crack pattern can be found in Appendix G.

During the 0.5% drift (10mm displacement) cycles some slipping was noticed between the column baseplate and the pinned connection as well as between the connection and the strong floor. This tended to occur at approximately 90-100kN under positive loading and 50-60kN under negative loading and resulted in 5-6mm of displacement with minimal change in force in each direction of loading.

During the first cycles to 3.5% drift (70mm displacement), the bottom flanges of both beams began to buckle just beyond the tips of the gusset plates. This buckling was more prominent during the 5% drift (100mm displacement) cycles with some deformation of the lower web was also noticed. Upon completion of testing the bottom flanges of the east beam had developed a 22mm (vertical) buckle as shown in Figure 6-1 whilst the west beam developed a 33mm buckle in the bottom flange.

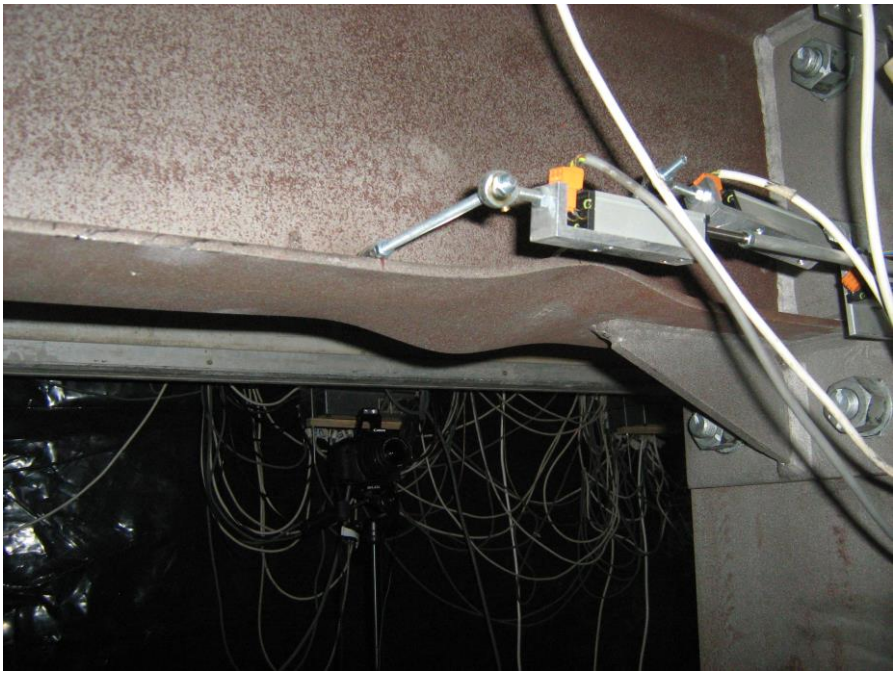

Figure 6-1: Residual buckling in the bottom flange of the east beam, isolated subassembly after the 5% drift cycles.

The top flanges did buckle but to a much lesser extent with a maximum of 14mm of residual buckle observed as shown in Figure 6-2.

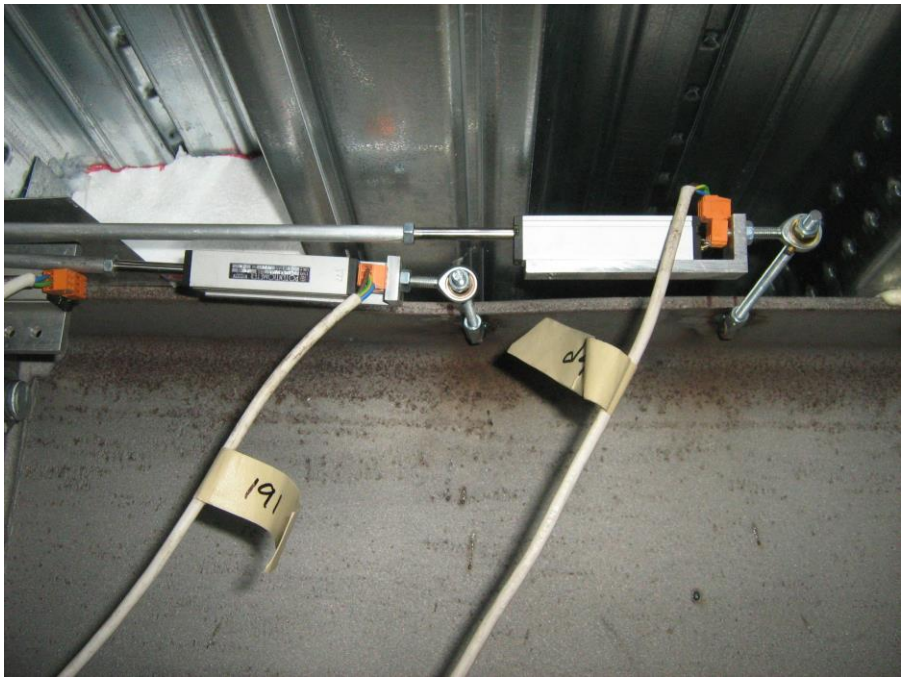

Figure 6-2: Residual buckling in the top flange of the west beam, isolated subassembly after the 5% drift cycles.

From 3.5% drift localized spalling and diagonal cracking occurred at the column faces and around the edges of the column flanges. As shown in Figure 6-3, damage to the slab

surrounding the column was comparatively minimal with only spalling of the surface concrete which had stuck to the polystyrene spacer blocks. Spalling along the east column face occurred in the top 10-20mm of the slab (depth) and there was almost no slab damage on the west column face.

Positive Loading Direction

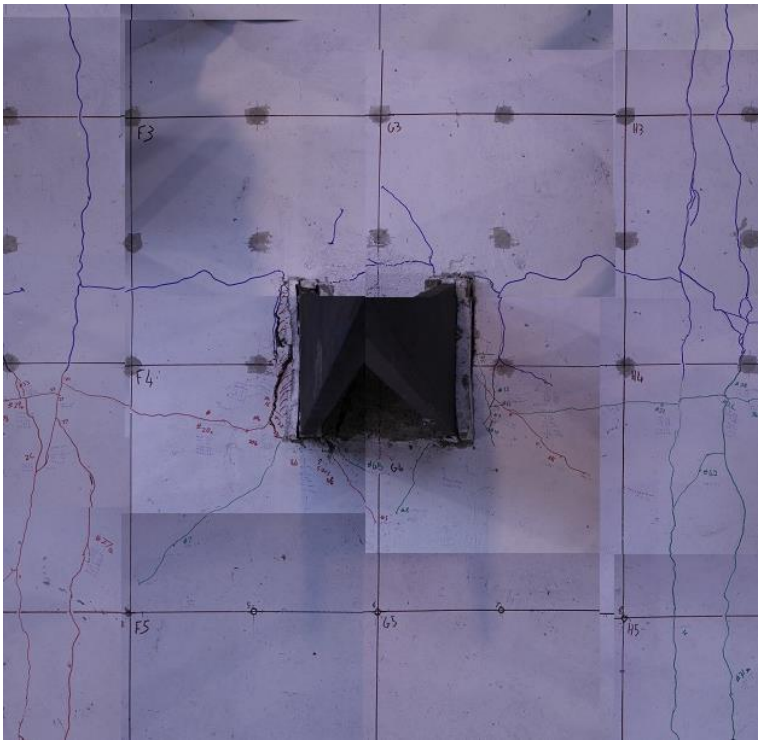

Figure 6-3: Compilation photo of slab damage around the column, isolated subassembly after testing to 5% drift.

The transverse and longitudinal cracks widths were less than those observed in subsequent tests with average crack widths rarely exceeding 0.5mm. Crack records, given in Appendix G, show that the largest recorded crack widths were between 1.2 and 1.5mm during the 5% drift cycles.

The panel zone of the column remained intact with no visible sign of yielding or deformation in the column flanges or continuity plates. No separation was observed in the moment end plate connection. Further images of damage observed during testing of this and other subassemblies can be found in Appendix F.

6.1.2 Transverse Subassembly

Testing of the second subassembly occurred over 2 days with cycles to 1.5% drift (30mm) tested on the first day and cycles to 5% drift (100mm) on the second day. Further controller issues were experienced with manual control required to complete the peak displacements in the 2% and 2.5% drift cycles. After these cycles were completed the automatic controller was used.

First cracking of the slab in the transverse subassembly slab occurred during the 0.25% drift (5mm displacement) cycles with diagonal cracks of around 0.1mm width propagating from the edges of the column flanges. This was followed by transverse cracking above the slab ribs and longitudinal cracks along the beam as shown in Figure 6-7 (further images in Appendix G). Unlike the isolated subassembly, transverse cracks formed above the ribs closest to the column faces and multiple longitudinal cracks were present on both sides of the primary beams. The diagonal (horizontal) cracks from the column flanges propagated at 45° for a distance of 500-600mm and generally terminated at an intersection with a transverse crack.

Despite additional tightening of the column base connection bolts, slipping still occurred between the column baseplate and the pinned connection as well as between the connection and the strong floor. Similar to the isolated subassembly, this slip tended to occur at lateral forces of approximately 90-100kN under positive loading and 50-60kN under negative loading. It resulted in 5-6mm of displacement with minimal change in force in each direction of loading.

During the first cycles at 2.5% drift (50mm), the bottom flanges of both of the beams began to buckle beyond the tips of the gusset plates as shown in Figure 6-4 and Figure 6-5. Again this buckling was more prominent during the 3.5% and 5% drift cycles than in earlier drift cycles with deformation of the lower web of both of the beams under higher drift levels. The residual buckling deformation of the bottom flanges, at zero displacement after 3 cycles at 5% drift, was 21mm (vertical) in the east beam, as shown in Figure 6-4, and up to 47mm in the west beam, Figure 6-5. The buckling of the top flange and the web was more prominent than in the first subassembly with 17mm residual deformation in the east beam and 7mm in the west beam.

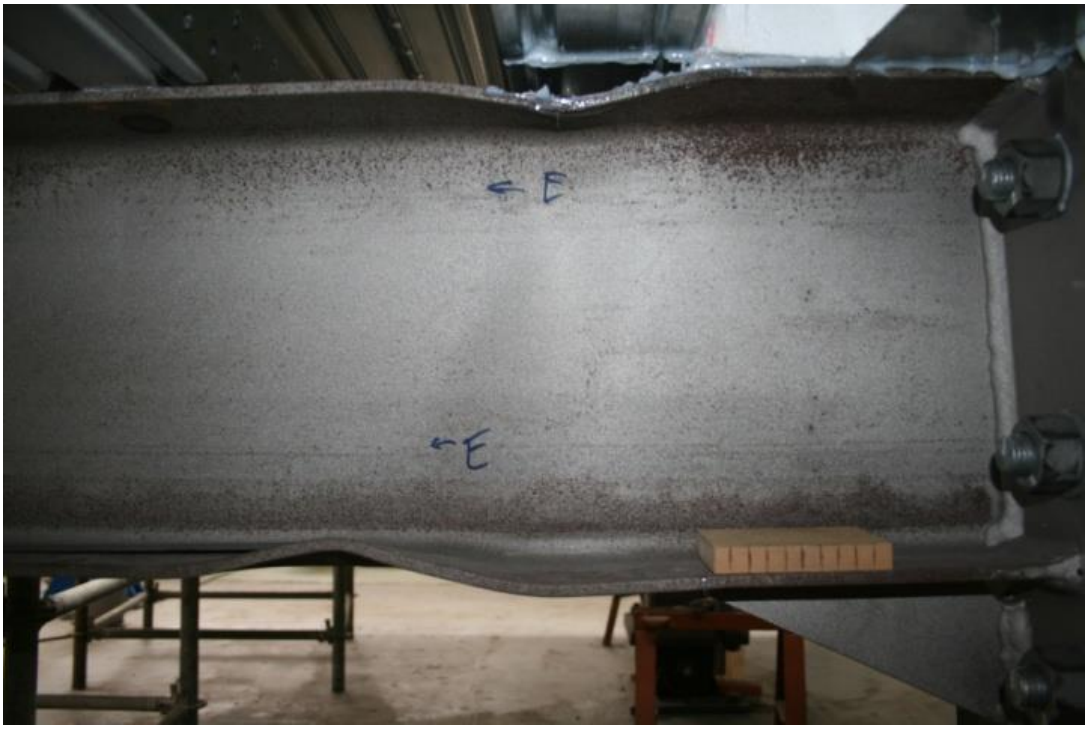

Figure 6-4: Residual buckling in the top and bottom flanges of the east beam, transverse subassembly after testing to 5% drift.

Figure 6-5: Residual buckling in the top and bottom flanges of the west beam, transverse subassembly after testing to 5% drift.

Spalling of the concrete in contact with the column faces occurred during the first cycle at 3.5% drift (70mm displacement). This was confined to the concrete between the column face and the first rib and was predominately spalling of the concrete above the deck rib, a distance of 70-100mm from the column face as shown in Figure 6-6. The area of concrete between the column flanges sheared away from the rest of the slab at 3.5% drift and was accompanied by a sudden loss of strength of the overall system. Following the shearing of the concrete between the flanges the vast majority of the remaining cracks on the slab decreased in width to levels closer to those experienced in the isolated subassembly with the slab separated from the column.

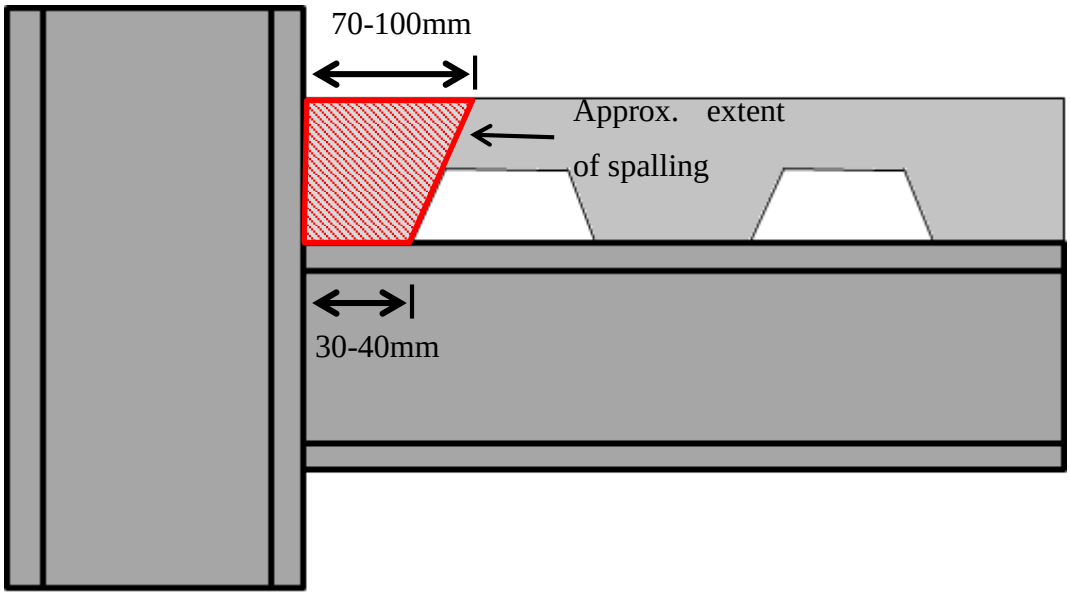

Figure 6-6: Observed extent of spalling in the transverse subassembly.

Again no damage was observed in the column panel zone and no separation was observed in the moment end plate connection. Damage to the slab surrounding the column as shown in Figure 6-7. In comparison to the isolated subassembly, the extent of both the cracking and the spalling at the column faces is significantly greater as is the propagation of the diagonal cracks from the flange tips.

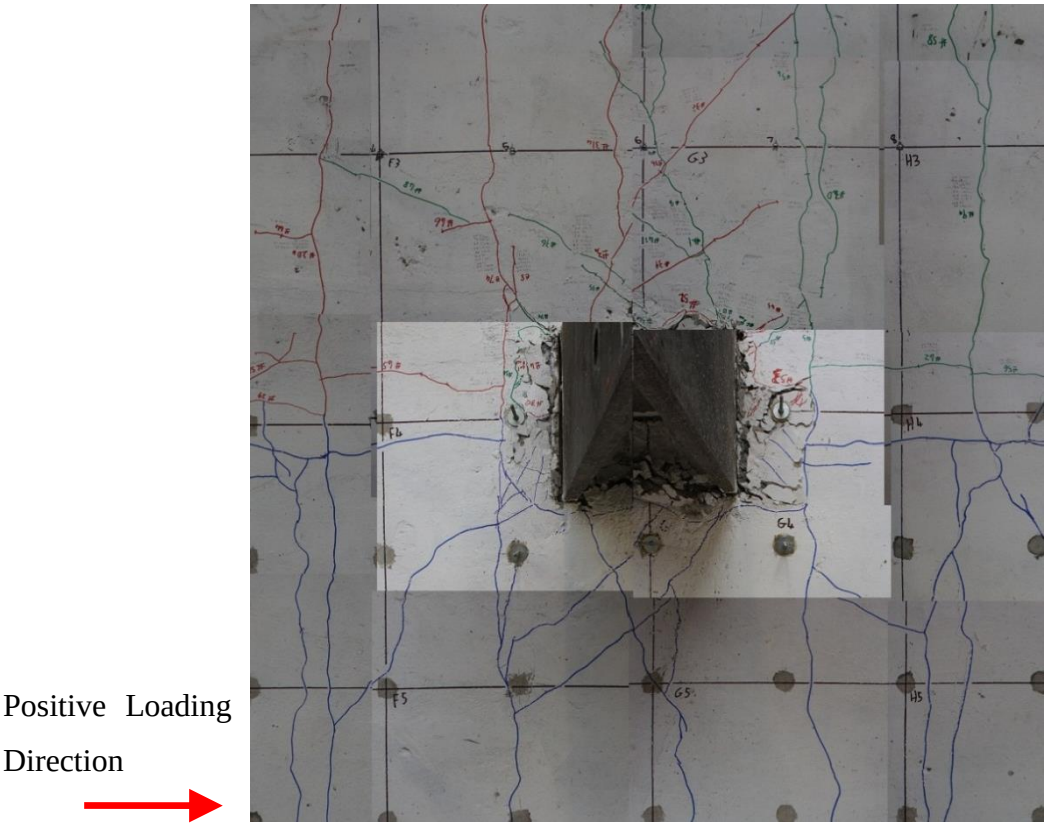

Figure 6-7: Compilation photo of slab damage around the column, transverse subassembly after testing to 5% drift.

Crack records, given in Appendix G, indicate that the average crack width was higher than in the first test.

6.1.3 Longitudinal Subassembly

Like the transverse subassembly, testing of the longitudinal subassembly occurred over 2 days with cycles to 1.5% drift (30mm) tested on the first day and cycles to 5% drift (100mm) on the second day. Slip between the column, pinned connection and the strong floor was again noted from 0.5% drift (10mm displacement) however instruments were placed to record this.

As in the transverse subassembly, first cracking of the slab in the longitudinal subassembly occurred during the 0.25% drift cycles with diagonal cracks propagating from the edges of the column flanges followed by transverse cracking above the slab ribs as well as longitudinal cracking. The extent of both the longitudinal and diagonal crack patterns, as shown in Figure 6-10 (further images in Appendix G), was greater than those experienced in the isolated and

transverse subassemblies. Diagonal cracking was observed both at the column and near the ends of the primary beams with multiple cracks at each location. Longitudinal cracks were observed next to the primary beam as well as approximately 500mm from the centreline of the beam. These were roughly centred over the first and second deck ribs either side of the main beams.

The buckling of the bottom flanges of both of the beams occurred at 2.5% drift and was again more significant than the previous two tests especially in the west beam as shown in Figure 6-8 and Figure 6-9. The residual buckling deformation of the bottom flanges after the 5% drift cycles was up to 27mm (vertical) in the east beam and up to 43mm in the west beam with both of the beams showing double curvature on at least one side of the flange. The residual buckling of the top flange was 7mm on the east beam and 6mm on the west beam.

Figure 6-8: Residual buckling in the bottom flange of the west beam, longitudinal subassembly after testing to 5% drift.

It was noted that one side of the bottom flange on both of the beams buckled with double bending at the end of the gusset plate as shown in Figure 6-9. This double bending resulted in the buckle extending beyond 1.5 times the depth of the beam from the end plate. As such the buckle extended beyond what would be classified as the plastic hinge zone.

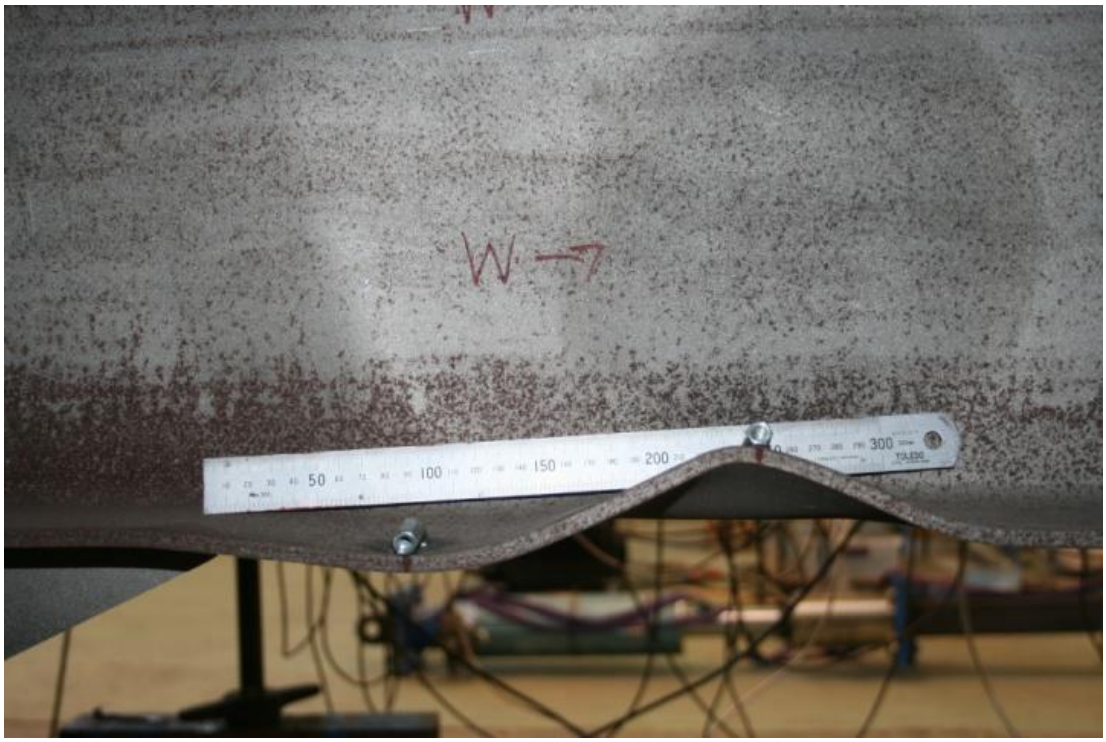

Figure 6-9: Residual buckling in the bottom flange of the west beam, longitudinal subassembly after testing to 5% drift.

Compression failure of the concrete in contact with the column faces also began during the 2.5% drift cycles. In the direction of loading this extended up to 750mm from the column centreline. Perpendicular to the direction of loading the extent of the spalling was more significant than had been observed in previous subassemblies, extending up to 500mm from the primary beam centreline as shown in Figure 6-10. Again the area of concrete between the column flanges sheared away from the rest of the slab at 3.5% drift and was accompanied by sudden strength loss. In comparison to the first two tests, the extent of both the cracking and the spalling at the column faces was noticeably higher with the area of spalled concrete extending over 500mm from the column centreline in almost all directions. Once again no damage was observed in the column panel zone or end plate connection.

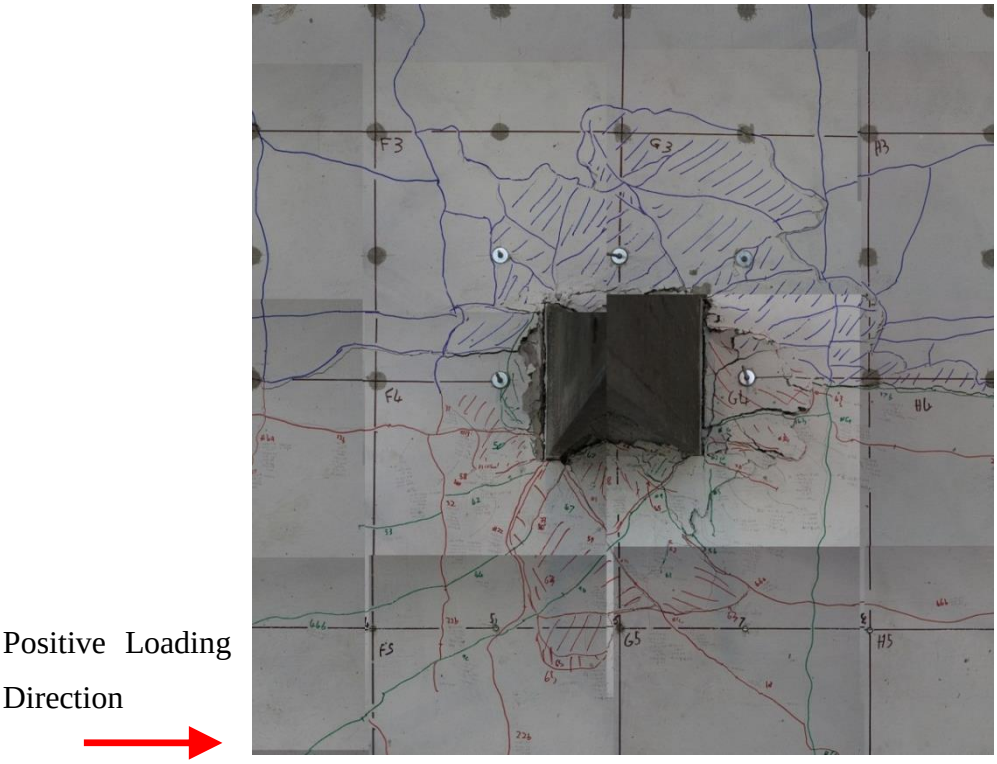

Figure 6-10: Compilation photo of slab damage around the column, longitudinal subassembly after testing to 5% drift.

Following completion of the test and removal of the slab beside the beams (the slab was saw cut and removed) cracking was noticed approximately 50mm from the top of the slab. Upon closer inspection it was discovered that the top 50mm of concrete above both of the beams had delaminated from the remainder of the slab, as shown in Figure 6-11 and 6-12.

Figure 6-11: Slab surface delamination along primary beam in longitudinal subassembly after testing.

Figure 6-12: Slab surface delamination along primary beam in longitudinal subassembly after testing.

Average crack widths were higher than in previous tests with multiple cracks exceeding 0.8-0.9mm. Crack records, given in Appendix G, show that the largest recorded crack width was 2.5mm with several others recorded at 1.5mm.

6.1.4 Sliding Hinge Joint Subassembly

The fourth subassembly was used to test an asymmetric friction type connection with slab attached. The first part of the testing was to put the sliding hinge joint through the displacement protocol applied to the other subassemblies.

As in the two previous non-isolated subassemblies, first cracking of the slab in the SHJ subassembly occurred during the 0.25% drift cycles with diagonal cracks propagating from the edges of the column flanges followed by transverse cracking above the slab ribs as well as longitudinal cracking. The extent of both the longitudinal and diagonal crack patterns was greater than in the isolated subassembly but less than that observed in the transverse and longitudinal subassemblies as can be seen by comparing Figures 6-3, 6-7, 6-10 and 6-14.

The SHJ connection performed well with the only visible damage being the shearing of the Grade 4.6 positioning bolts in the bottom web plate at 2.5% and 3.5% drifts (50mm and 70mm) owing to horizontal displacement incompatibility of the circular holes, and the shearing one top web plate bolt at 5% drift, as shown in Figure 6-13, due to vertical displacement incompatibility. This vertical displacement incompatibility was bought about by the rotation of the beam relative to the web plate which exceeded the 2mm of vertical slack in the bolt holes.

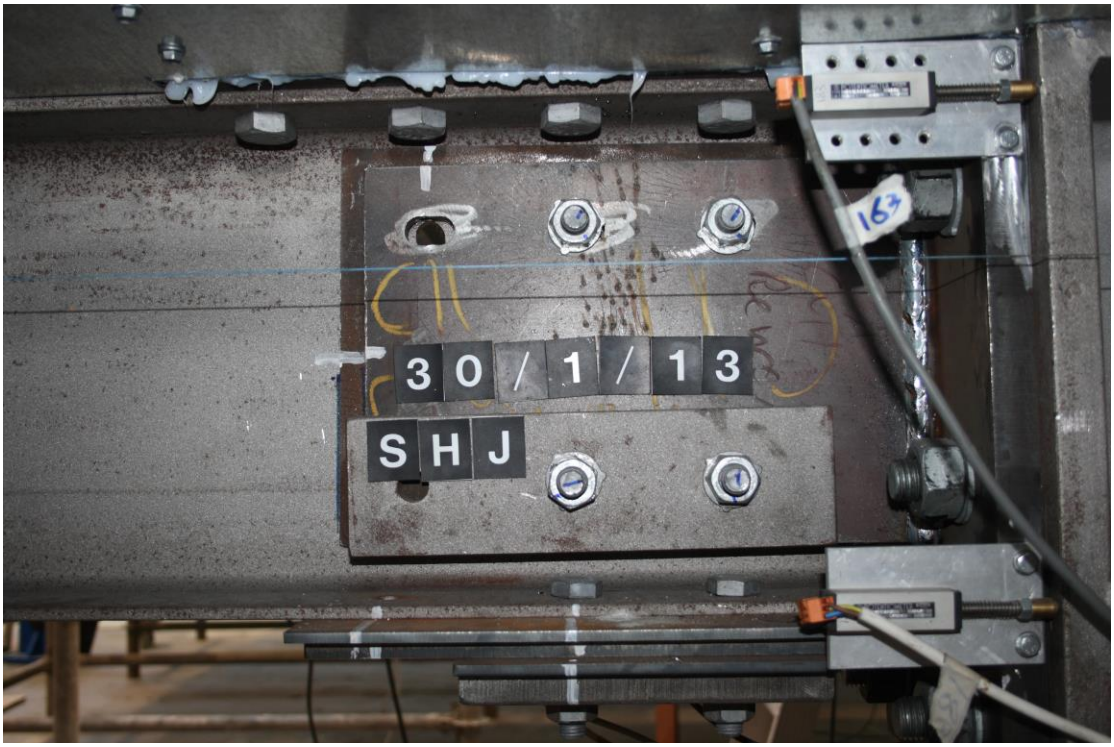

Figure 6-13: Missing top web bolt on the east beam, SHJ subassembly after 3 cycles at 5% drift.

As in the transverse and isolated subassemblies, the slab surrounding the column spalled at 3.5% drift with a corresponding loss of strength. As shown in Figure 6-14 (with further images in Appendix G), the spalling of the concrete in contact with the column faces was reduced from the levels observed in the transverse and longitudinal subassemblies and, like the transverse subassembly, it was restricted to the area between the column face and the first deck rib. Crack widths were also reduced with the largest recorded crack width being 1.3mm in the vicinity of the sliding hinge beam-column connection. This reduction in slab damage is likely due to the lack of bending and elongation in the primary beams with most damage occurring in the section of the slab between the tips of the sliding hinge connections. Panel zone deformations were again negligible as was separation of the moment end plate connection.

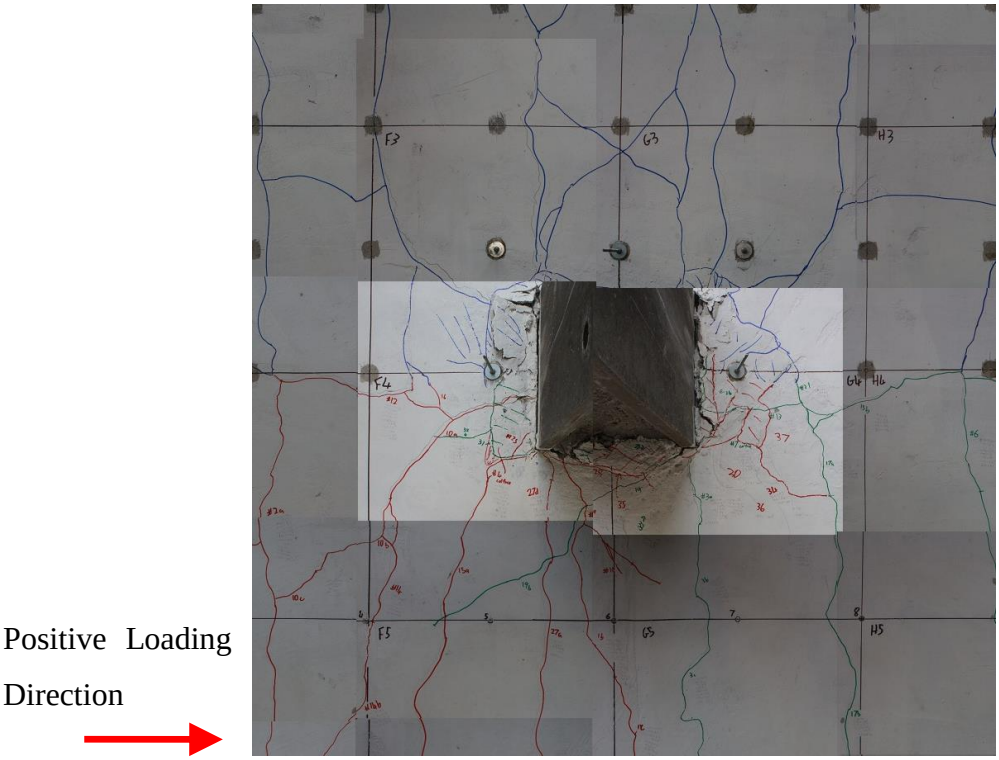

Figure 6-14: Compilation photo of slab damage around the column, SHJ subassembly after testing to 5% drift.

Following on from this, the subassembly was put through 50 cycles at 2.5% drift, 7 cycles at 5% drift and 1 cycle at 10% target drift (although the ram ran out of travel at 8.5% drift in the positive cycle). At these higher drifts a further 2 web plate bolts, the outer-most top web bolt on the west beam and the outermost bottom web bolt on the east beam, sheared off and some permanent flexural deformation of between 8mm and 10mm was noticed in the flange plates of the sliding hinge joint and the bottom flange of the beam as shown in Figure 6-15 and 6-16.

Figure 6-15: Bending in the top flange plate of the east connection, up to 10mm of deflection, SHJ subassembly.

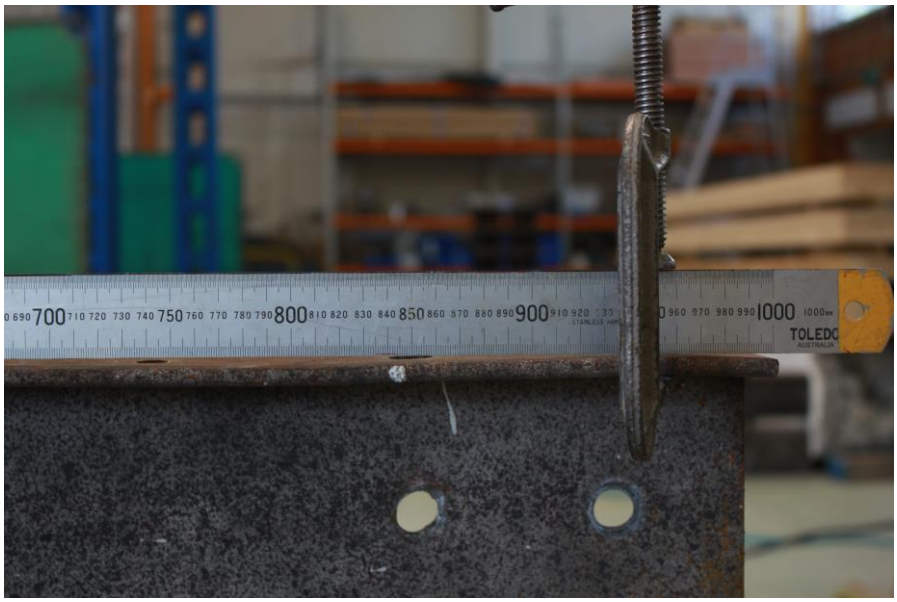

Figure 6-16: Buckling in the bottom flange of the west beam, up to 5mm deflection, SHJ subassembly.

Further investigation following on from testing revealed several holes in the beams elongated owing to vertical displacement incompatibility as shown in Figure 6-17. Several of the bottom flange and web bolts were also bent during testing as shown in Figure 6-18 and Figure 6-19.

Figure 6-17: Elongation of the top bolt holes in the web of the west beam, SHJ subassembly.

Figure 6-18: Bending of a middle top web plate bolt, SHJ subassembly.

Figure 6-19: Bending and shearing of one row of bottom flange bolts, SHJ subassembly.

As observed in the first stage of testing, panel zone deformations and end plate lift off were not noticeable.

6.1.5 Full Depth Subassembly

As with the previous three subassemblies, testing of the second subassembly occurred over 2 days with cycles to 1.5% drift (30mm) tested on the first day and cycles to 5% drift (100mm) on the second day.

First cracking of the concrete slab in the Full Depth subassembly occurred during the 0.25% drift (5mm displacement) cycles. Longitudinal cracks started forming beyond the edges of the full depth section and were accompanied by hairline diagonal cracks propagating from the edges of the column flanges. The number of longitudinal cracks was greater than in the isolated specimen but less than that observed in the transverse and longitudinal subassemblies as shown in Figure 6-22. It was also observed that the extent of diagonal cracking in the slab was greater than in the four pervious subassemblies with multiple diagonals crack forming at each of the column flange tips compared to the usual single diagonal crack observed in the other test subassemblies.

The buckling of the bottom flanges of both beams was greater than that observed in the previous four subassemblies, especially in the west beam as shown in Figure 6-20 and Figure 6-21. The residual buckling deformation of the bottom flanges was up to 37mm (vertical) in the east beam and up to 48mm in the west beam with both beams showing a residual (after cycles at 5% drift) double curvature on at least one side of the flange. The residual buckling of the top flange was 4mm on both the east beam and the west beam. As in the longitudinal subassembly one side of the bottom flange on both beams, the south face of the west beam and the north face of the east beam, buckled with double bending with the buckle extending beyond 1.5 times the depth of the beam from the end plate. As such the buckle extended beyond what would be classified as the plastic hinge zone.

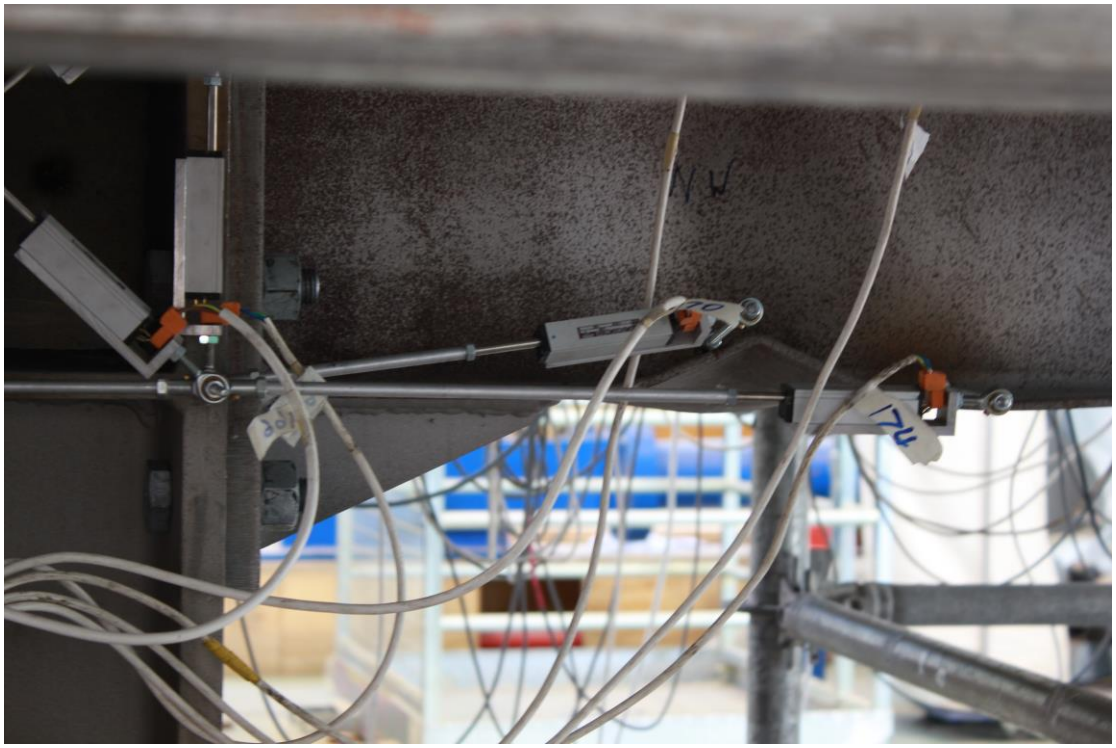

Figure 6-20: Residual buckling in the bottom flange of the west beam, full depth subassembly after testing to 5% drift.

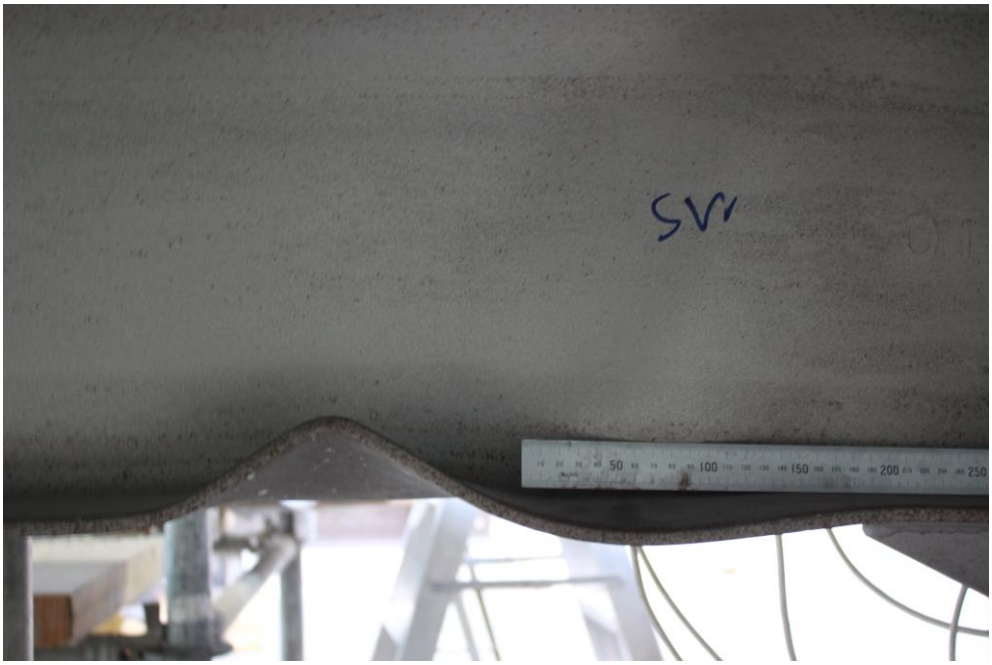

Figure 6-21: Residual buckling in the bottom flange of the west beam, full depth subassembly after testing to 5% drift.

Degradation of the concrete in contact with the column faces was slow to develop with no visible signs of spalling appearing until the 5% drift cycles. Although spalling was observed up to 250mm from the column face, the depth of the spalling, shown in Figure 6-22 and Appendix G, was less than had been observed in previous tests with only the top 10-20mm of concrete spalling. Additionally there was no sudden shearing of the area of concrete between the column flanges although some localised spalling was noted during the 5% drift cycles. The spalled section of the slab terminated near the edges of the full depth section indicating that the area of full depth section provided was sufficient. Crack width measurements, given in Appendix G, indicated an increase in average crack widths in the area surrounding the column in comparison to the isolated and longitudinal subassemblies and a reduction near the outer extremities of the slab. The highest recorded crack widths were between 1.5mm and 2.5mm, all of which were located near the column, possibly indicating an increase in the levels of force being carried in the slab via strut and tie mechanism.

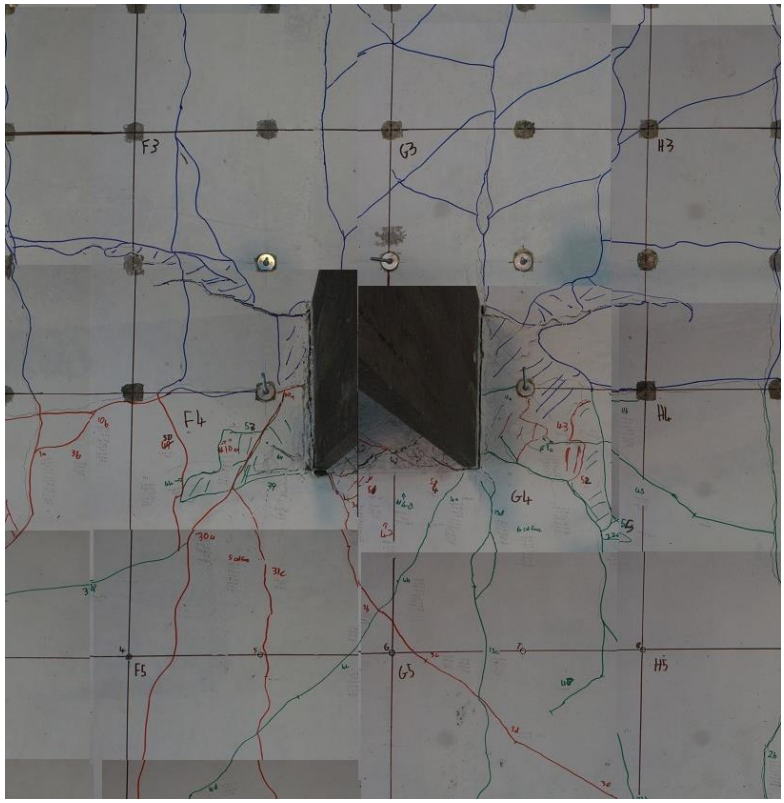

Positive Loading Direction

Figure 6-22: Slab damage around the column, full depth subassembly.

Panel zone deformation and separation of the moment end plate connection was again negligible.

6.2 Recorded Measurements

6.2.1 Global Hysteresis

Unit 1 (Isolated):

As shown in Figures 6-23 & 6-24 the force-displacement hysteresis for the isolated subassembly was predominantly linear up to 0.5% drift (10mm displacement) followed by a long yield curve up to 3.5% (70mm displacement). The base plate slip experienced from 0.5% drift (10mm displacement) accounts for the plateau in the hysteresis at 100kN of applied force in each direction. The hysteresis tended to plateau for 5-6mm of displacement before the applied force increased again once the bolts have reached the edge of their holes.

From the 0.75% drift (15mm displacement) cycle, the peak strength of the subassembly was noted to decrease after the first cycle at each drift level owing to crack formation and inelastic beam deformation. This was generally followed by a smaller decrease in strength between the second and third cycles. Beyond the first cycle at 3.5% drift the strength of the subassembly began to plateau and decrease owing to buckling of the beams.

The maximum force applied to the column was 251kN during the first cycle at 3.5% drift. This equates to an end plate moment of 502kNm. The peak force applied during the final cycle at 5% drift was recorded as 231kN or 92% of the peak strength. As a reduction of strength to below 85% of peak is generally used as a limit for dependable ductility (Park 1975 [50]), the structure could still be considered to have some residual ductility.

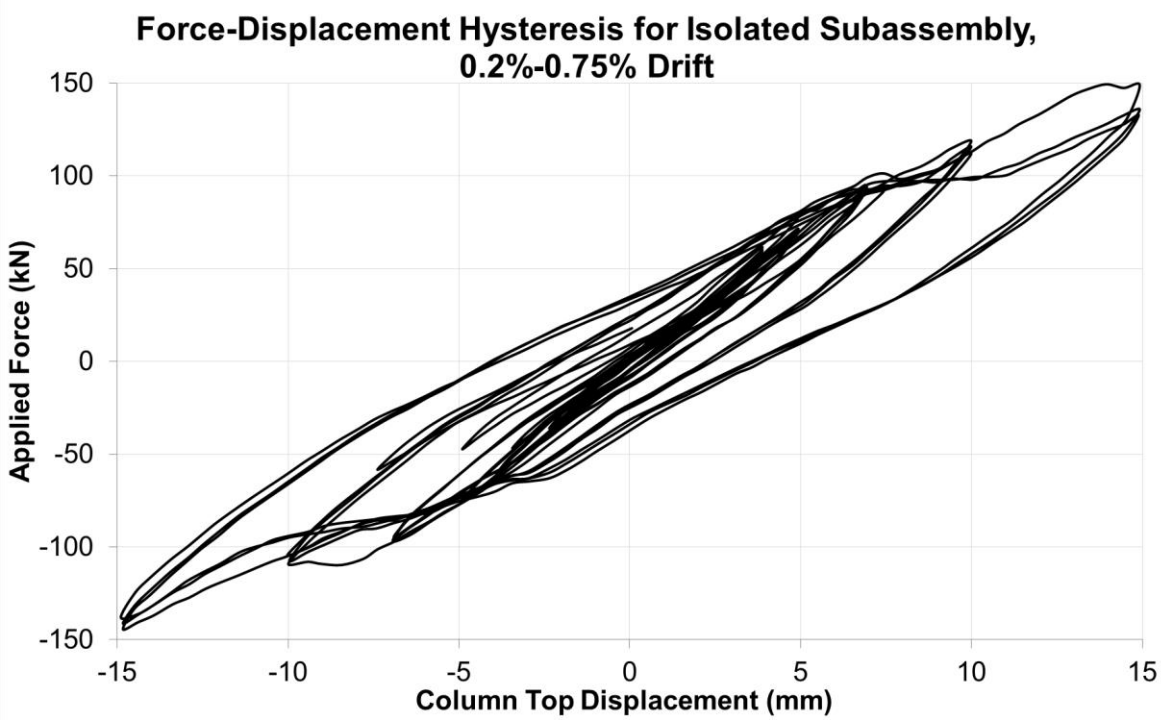

Figure 6-23: Force-displacement hysteresis for the isolated subassembly, 0.2%-0.75% drift (4mm-15mm).

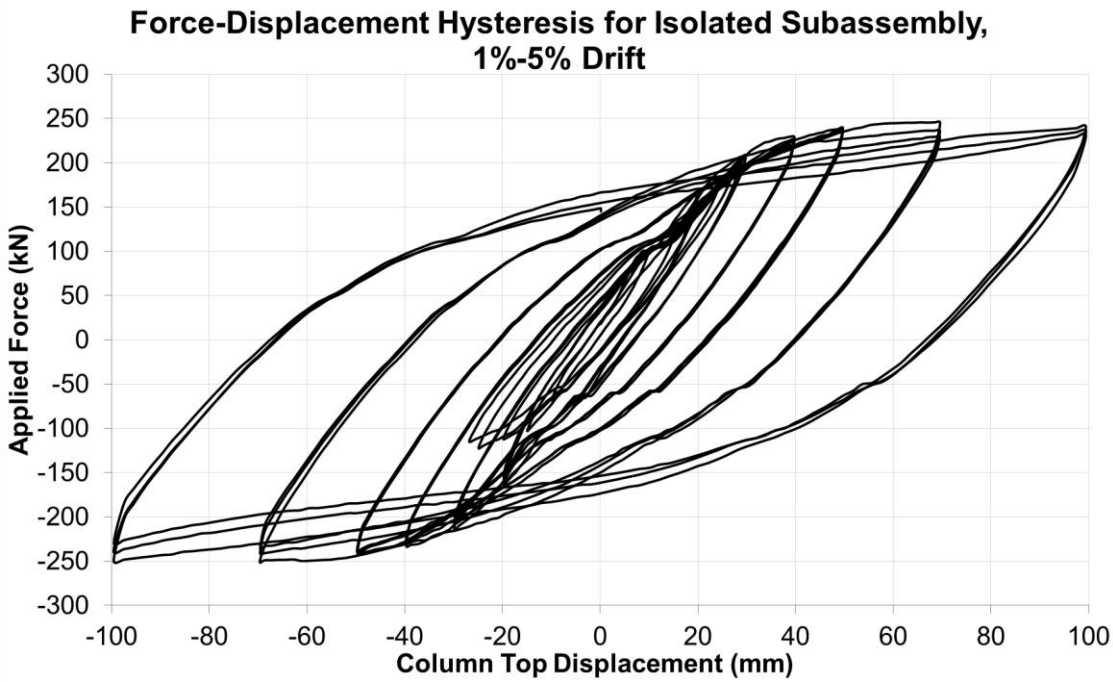

Figure 6-24: Force-displacement hysteresis for the isolated subassembly, 1.0%-5.0% drift (20mm-100mm).

.

Unit 2 (Transverse):

As shown in Figures 6-25 and 6-26 the force-displacement behaviour, like that of the isolated subassembly, was predominantly linear up to 0.5% drift (10mm displacement) followed by a long yield curve up to 2.5% (50mm) at which point buckling of the beams occurred. Base plate slip was experienced from 0.5% drift (10mm displacement) resulting in a plateau (of the applied force) for 5-6mm of displacement at approximately 100kN of applied force.

Again a decrease in the peak strength during each set of drift cycles was noticed from 0.75% drift (15mm displacement) although in many cases no reduction in strength was noticeable between the second and third cycles. The stiffness of the transverse subassembly beyond 0.75% drift was noticeable higher than that of the isolated subassembly owing to the slab participation. As the beams began to buckle during the first cycle at 2.5% drift a corresponding drop in strength was noticed particularly in the negative cycles. During the first cycle at 3.5% drift (70mm) the strength of the subassembly dropped rapidly when the concrete at the column face spalled and the concrete between the column flanges sheared off. This shearing accounted for the majority of the strength loss in the subassembly. Following this the strength of the subassembly dropped to a level similar to that of the isolated subassembly (231kN).

The maximum force applied to the column was 324kN during the first cycle at 2.5% drift. This equates to an end plate moment of 648kNm. The peak force applied during the final cycle at 5% drift was recorded as 212kN or 65% of the peak strength (<85%). As such this subassembly was considered to have no remaining ductility.

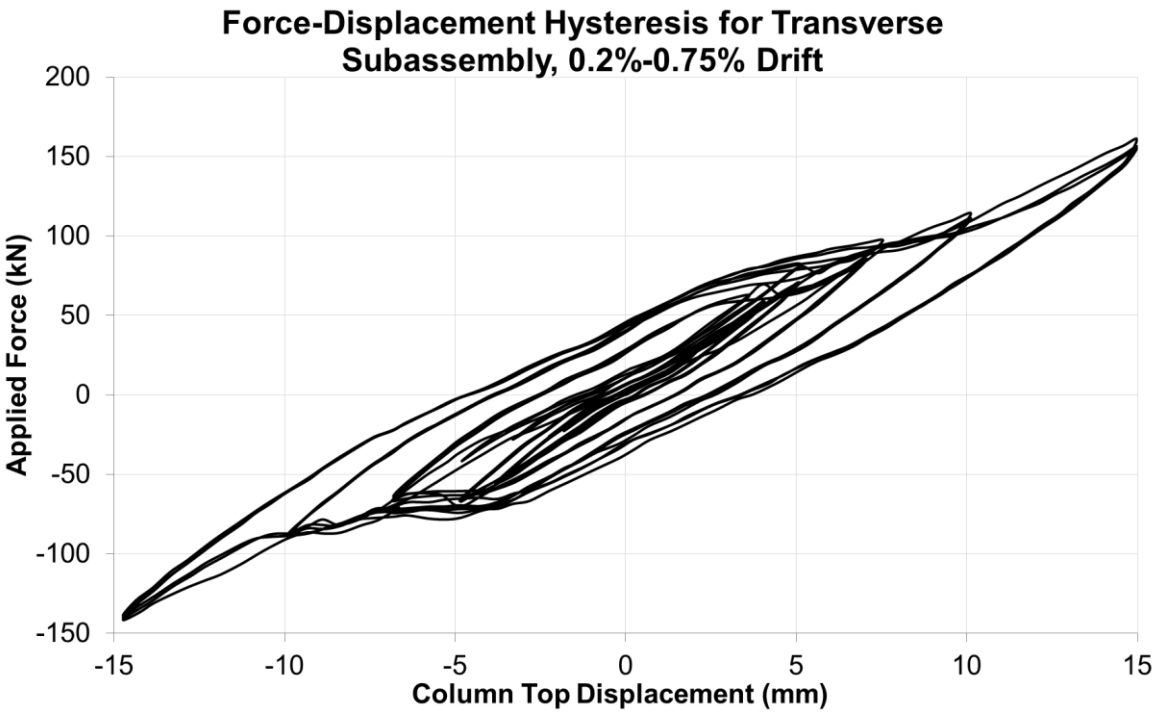

Figure 6-25: Force-displacement hysteresis for the transverse subassembly, 0.2%-0.75% drift (4mm-15mm).

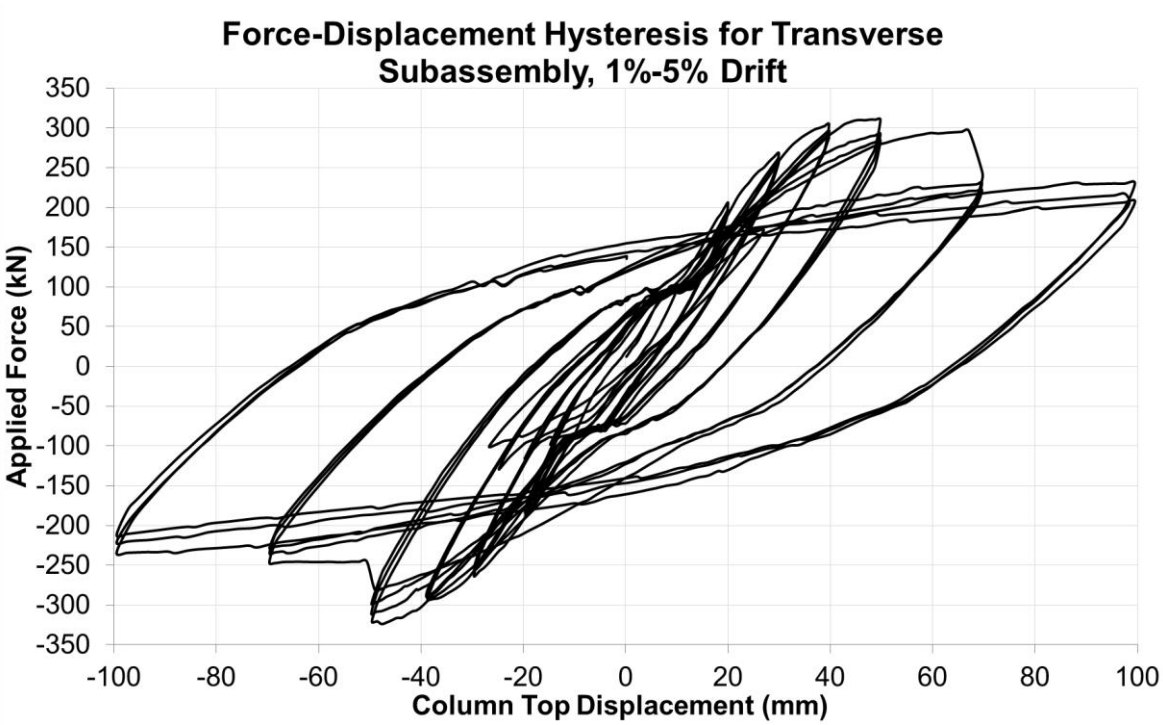

Figure 6-26: Force-displacement hysteresis for the transverse subassembly, 1.0%-5.0% drift (20mm-100mm).

Unit 3 (Longitudinal):

Like the isolated and transverse subassemblies the hysteresis for the longitudinal subassembly, shown in Figures 6-27 & 6-28, remained linear up to 0.5% drift (10mm displacement). Again the yield curve up to 2% (40mm displacement) drift exhibited a higher stiffness than the previous two subassemblies and strength loss between cycles at each drift level was noticeable from 0.75% (15mm). Base plate slip occurred from 5% drift (10mm) however the plateau was corrected in the resulting plots.

The beam bottom flanges began to buckle during the first cycle at 2% drift with the east beam buckling under positive loading and the west beam buckling under negative loading. This corresponded to compression forces in the bottom flanges. The buckle magnitude continued to increase for the remainder of the 2% and 2.5% drift cycles. This buckling resulted in a reduction of the applied forces by 10-15kN. Spalling of the concrete around the column and shearing of the slab between the column flanges at roughly 3% drift resulted in a further drop in the strength of the subassembly down to isolated levels.

The maximum force applied to the column was 365kN during the first cycle at 2% drift. This equates to an end plate moment of 729kNm. The peak force applied during the final cycle at 5% drift was recorded as 240kN or 66% of the peak strength. The displacement at which 85% of the peak strength was reached was 3% drift.

In Figure 6-28 (1-5%) a number of small cycles are present around 150kN applied force and 20mm displacement. These are the small cycles which were inserted between each drift level as described in Figure 3-15. Each of these was recorded after a different level of drift and as such the stiffness of these intermediate cycles tended to reduce as the subassembly was subjected to higher drift levels and damage.

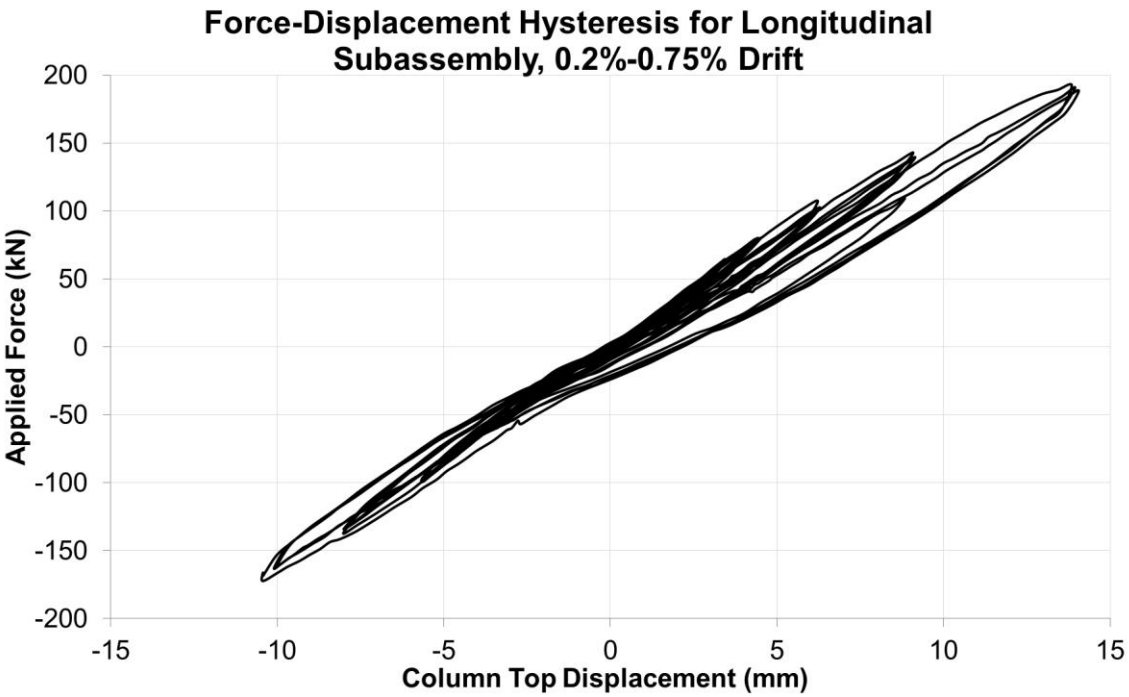

Figure 6-27: Force-displacement hysteresis for the longitudinal subassembly, 0.2%-0.75% drift (4mm-15mm), corrected for base plate slip.

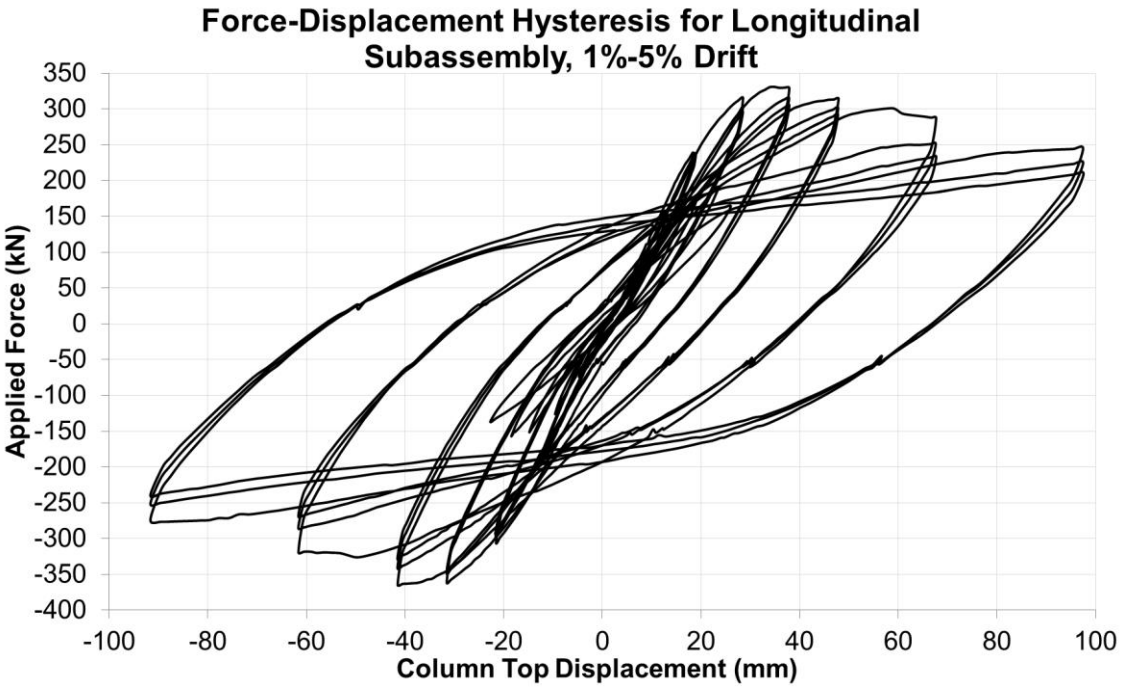

Figure 6-28: Force-displacement hysteresis for the longitudinal subassembly, 1.0%-5.0% drift (20mm-100mm), corrected for base plate slip.

Unit 4 (SHJ):

The hysteresis for the SHJ subassembly, shown in Figures 6-29 & 6-30, also remained linear up to 0.5% drift (10mm displacement). Beyond 0.75% drift (15mm displacement) sliding began to occur in the SHJ connection although the strength of the subassembly continued to increase due to the participation of the slab.

Peak strength was reached at 2% drift (40mm) followed by localised spalling of the concrete at the west column face and shearing of the east beam positioning bolts at 2.5% drift (50mm). This was followed by spalling of the concrete on the east column face and column centre concrete and shearing of the west beam positioning bolts at 3.5% drift (70mm).

The maximum force applied to the column was 207kN during the first cycle at 2% drift. This equates to an end plate moment of 414kNm. The peak force applied during the final cycle at 5% drift (100mm) was recorded as 150kN or 72% of the peak strength. These losses were predominantly due to slab compressive deformation and localised spalling while the SHJ connection continued to increase resistance between the 3.5% and 5% drift cycles.

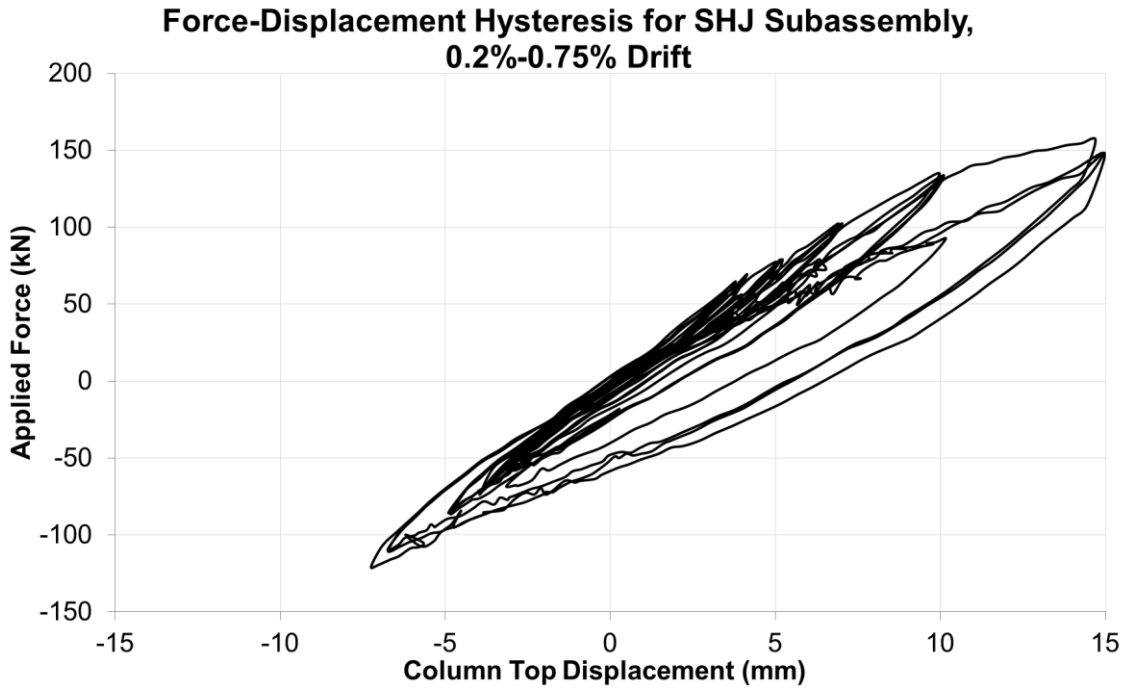

Figure 6-29: Force-displacement hysteresis for the SHJ subassembly, 0.2%-0.75% drift (4mm-15mm), corrected for base plate slip.

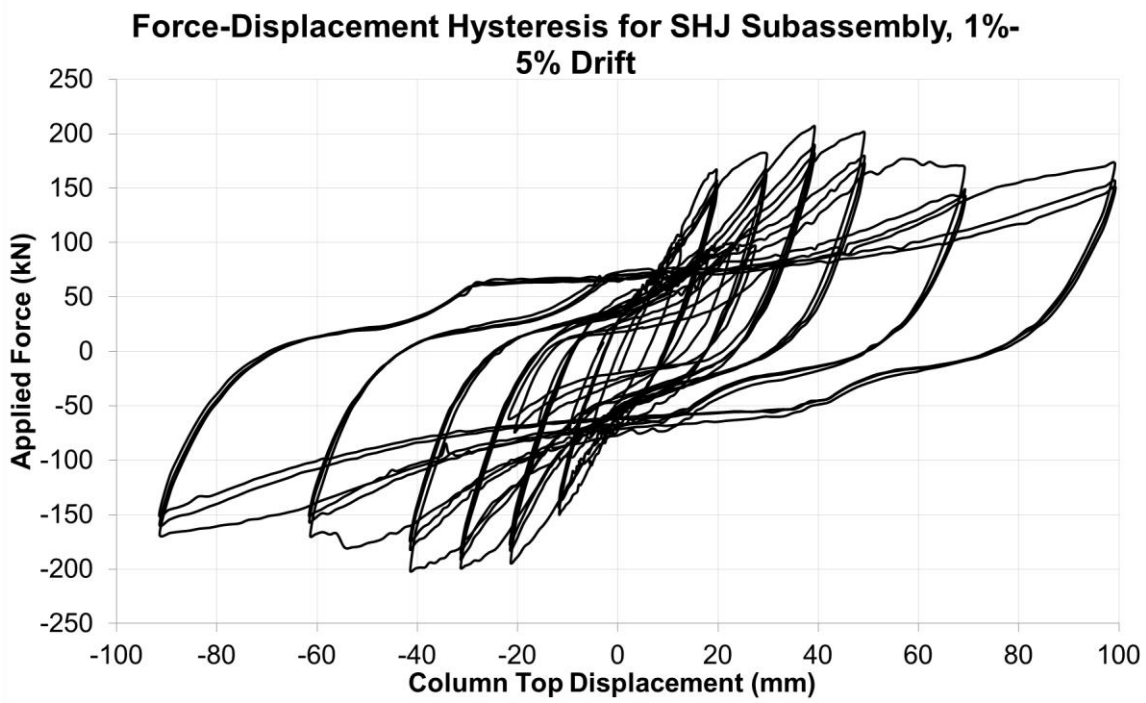

Figure 6-30: Force-displacement hysteresis for the SHJ subassembly, 1.0%-5.0% drift (20mm-100mm), corrected for base plate slip.

Extended testing of the SHJ subassembly, 50 cycles to 2.5% drift, 8 cycles to 5% drift and 1 cycle to 10% drift, resulted in a very stable hysteresis loop with a relatively low strength as shown in Figure 6-31. Without significant slab interaction, sliding tended to occur at around 50kN of applied force in each direction. Beyond 2.5% drift (50mm of column top displacement) the strength of the subassembly began to increase owing to bending of the top and bottom flange plates due to prying by the beam. As such the 2.5% drift (50mm) cycles generally reached a peak strength of around 50kN whereas similar drift levels in the first stage of testing resulted in a peak strength of around 200kN at 2.5% drift. Similarly the 5% drift cycles reached a peak strength of around 100kN whereas similar drift levels in the first stage of testing reached 150kN of peak strength. As such it was apparent that a portion of the long term strength loss was due to degradation of the steel connection elements however this was not as large as the slab contribution. Pushing the SHJ beyond 5% drift also showed an increase in the subassembly strength up to 250kN. This was greater than the peak strength observed in the first stage of testing indicating that, that the strength degradation in the smaller cycles is unlikely to result in failure of the connection.

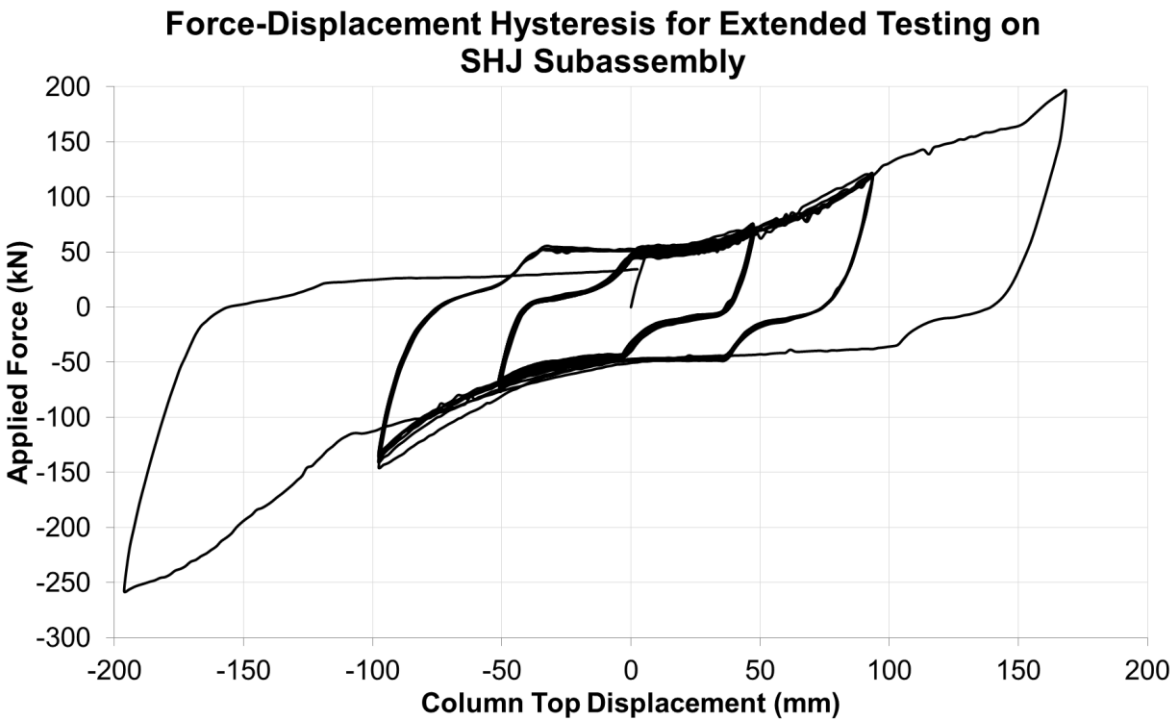

Figure 6-31: Force-displacement hysteresis for the SHJ subassembly under extended testing, corrected for base plate slip.

Unit 5 (Full Depth):

As with all the subassemblies tested, the hysteresis for the full depth subassembly, shown in Figures 6-32 & 6-33, remained linear up to 0.5% drift (10mm displacement) followed by yielding up to 2.5% drift (50mm). The beams began to buckle during the first cycle at 2.5% drift and spalling of the concrete around the column occurred at 3.5% drift (70mm).

Unlike in the other non-isolated subassemblies, the full depth subassembly did not exhibit a rapid drop in strength due to shearing of the concrete between the flanges of the column. This resulted in a more gradual loss of strength due to concrete degradation than was previously observed as a result of buckling and concrete compression.

The maximum force applied to the column was 337kN during the first cycle at 2.5% drift. This equates to an end plate moment of 674kNm. The peak force applied during the final cycle at 5% drift was recorded as 254kN or 75% of the peak strength.

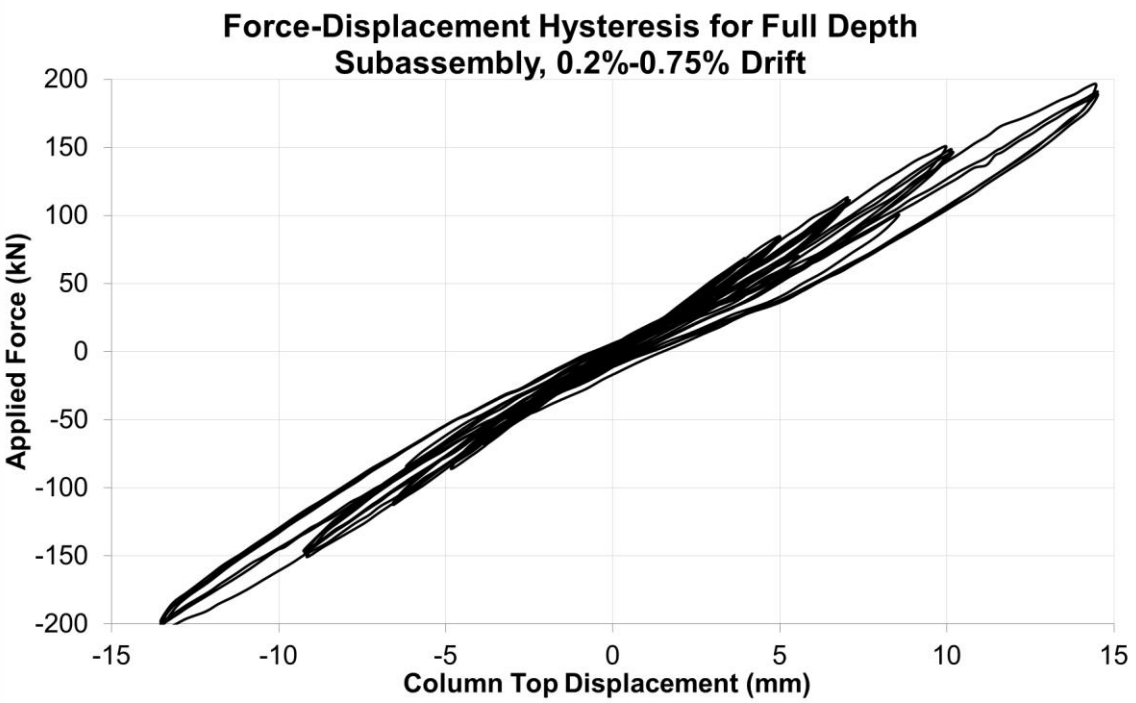

Figure 6-32: Force-displacement hysteresis for the full depth subassembly, 0.2%-0.75% drift (4mm-15mm), corrected for base plate slip.

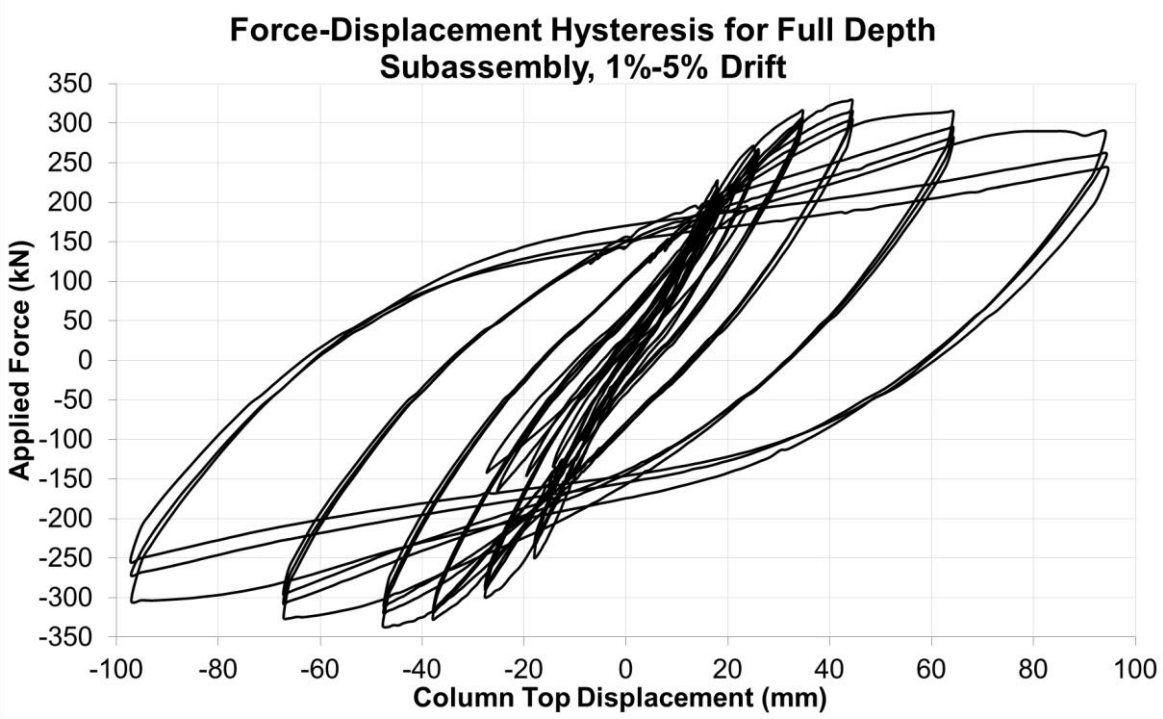

Figure 6-33: Force-displacement hysteresis for the Full Depth subassembly, 1.0%-5.0% drift (20mm-100mm), corrected for base plate slip.

6.2.2 Panel Zone and End Plate

Unit 1 (Isolated):

Data from the instrumentation on the column panel zone showed that the absolute maximum displacement between measured points, taken as the sum of the maximum positive and negative displacement values over all drift cycles, was less than 1mm as is illustrated in Figure 6-34. The panel zone tended to show most displacement across the two diagonal instruments indicating that the behaviour was consistent with the assumed displacement shape in Section 5.3.

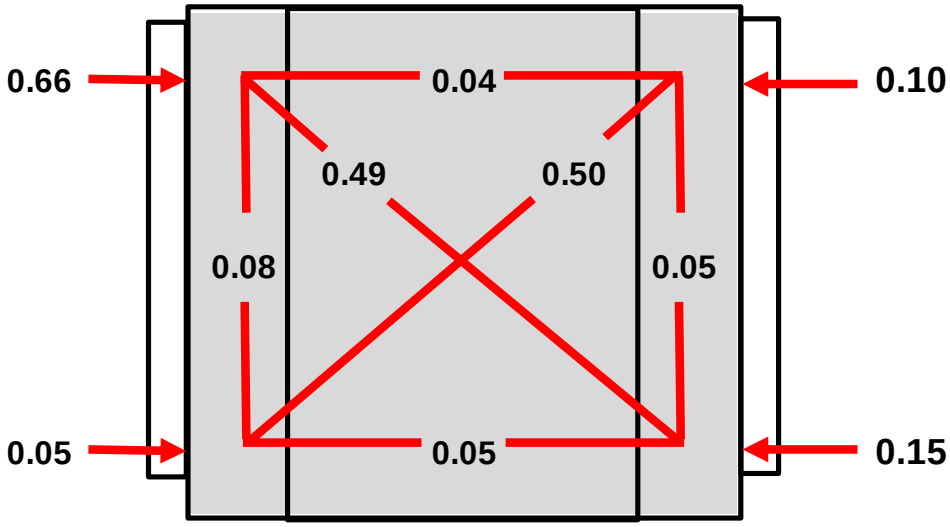

Figure 6-34: Isolated subassembly maximum panel zone deformation and end plate gap opening (mm)

The horizontal panel zone deformation, shown in Figure 6-35, resulted in a very minor residual deformation during high drift cycles. The maximum residual deformation was less than 0.5mm in either direction. The sudden drop in displacement at 5% drift, around the 4200th load point, may have been due to instrument issues however the level of displacement makes it difficult to be certain. If instrument failure is the cause it is unlikely the result would have exceeded 0.5mm.

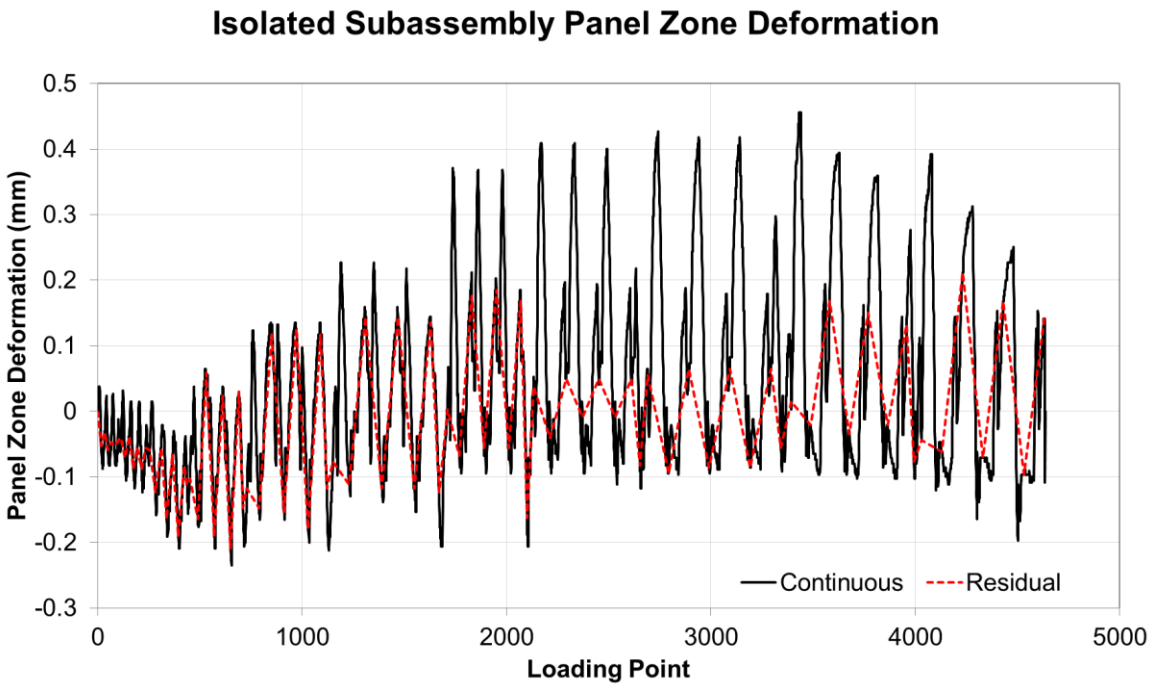

Figure 6-35: Isolated subassembly panel zone horizontal deformation (mm)

The maximum deformation of the panel zone was 0.46mm during the 3.5% drift cycle (around load point 3300). Over the panel zone depth of 300mm this equates to a steel strain of 0.0015. Given that the nominal yield strain of Grade 300 steel is 0.0015 (0.00175 for Grade 350 steel) the panel zone steel in the isolated subassembly is likely to have come close to yielding.

Lift-off of the moment end plates is shown in Figure 6-36. A gradual increase in the displacement due to lift-off is evident suggesting that some separation of the connection did occur. The magnitude of this prying however was minimal when compared to the panel zone deformation (less than 0.1mm) and as such the end plate prying is unlikely to have a significant effect on the performance of the structure.

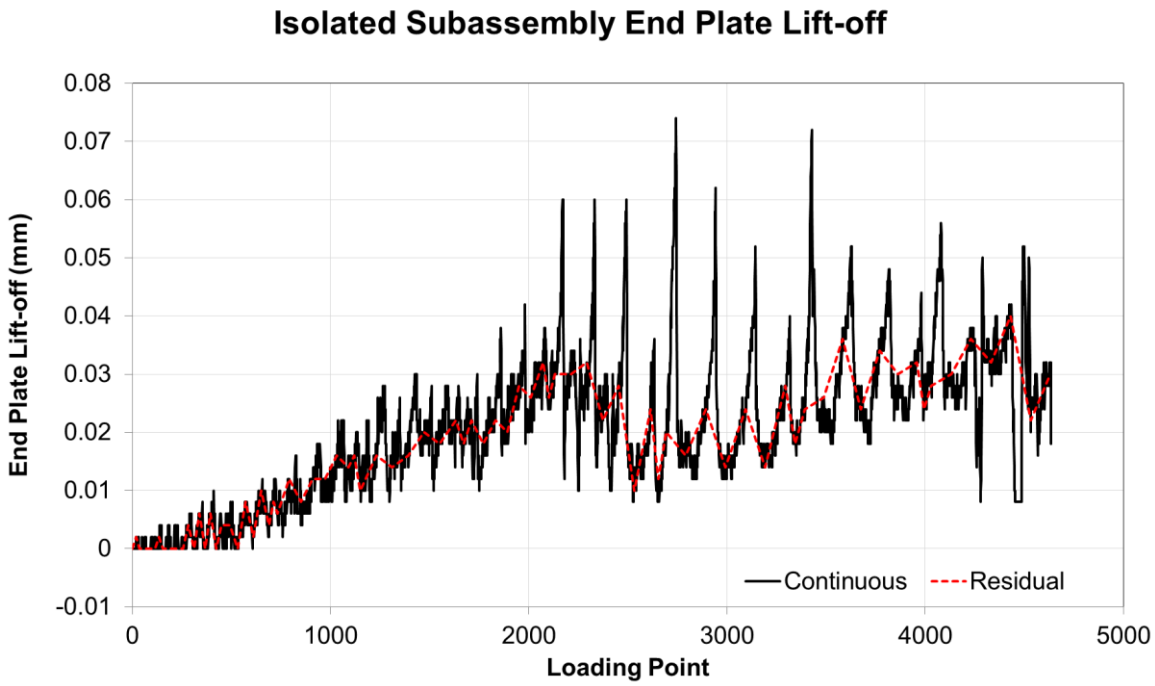

Figure 6-36: Isolated subassembly displacement due to end plate lift-off (mm)

The effect of the panel zone deformation on the overall deformation of the structure is shown in Figure 6-37 (end plate lift-off was considered to be too small to be considered). As can be seen the panel zone accounted for at most 1.5mm of column top displacement (0.075% drift).

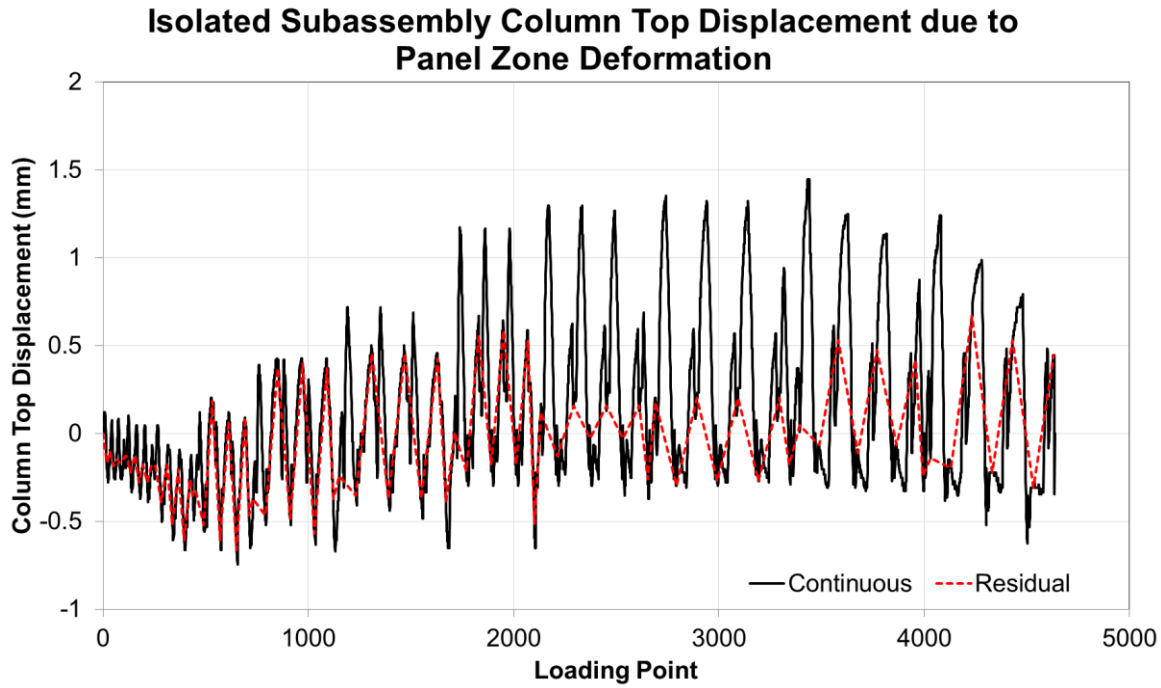

Figure 6-37: Isolated subassembly column top displacement due to panel zone deformation (mm)

Unit 2 (Transverse):

The absolute maximum displacement between measured points in the transverse subassembly was less than 0.5mm as is illustrated in Figure 6-38. Again the panel zone tended to show most displacement across the two diagonal instruments. The two top endplate instruments tended to show a higher level of gap opening than in the first subassembly although this was still less than 1mm.

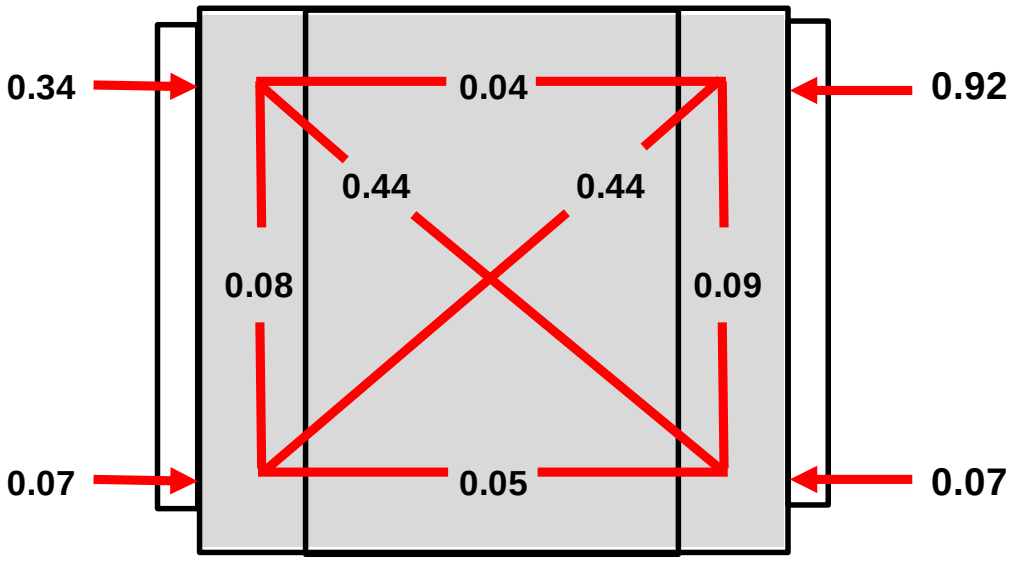

Figure 6-38: Transverse subassembly maximum panel zone deformation and end plate gap opening (mm)

The horizontal deflection of the panel zone in the transverse subassembly was more uniform than that observed in the isolated subassembly as shown in Figure 6-39. Again a very minor residual deformation was observed during high drift cycles although maximum residual drift was less than 0.3mm in either direction. During the lower drift cycles the residual displacements tended to be similar to the maximum displacements observed in the continual data. This indicates that the panel zone displacements tended to occur during the peak displacements through the lower drift cycles.

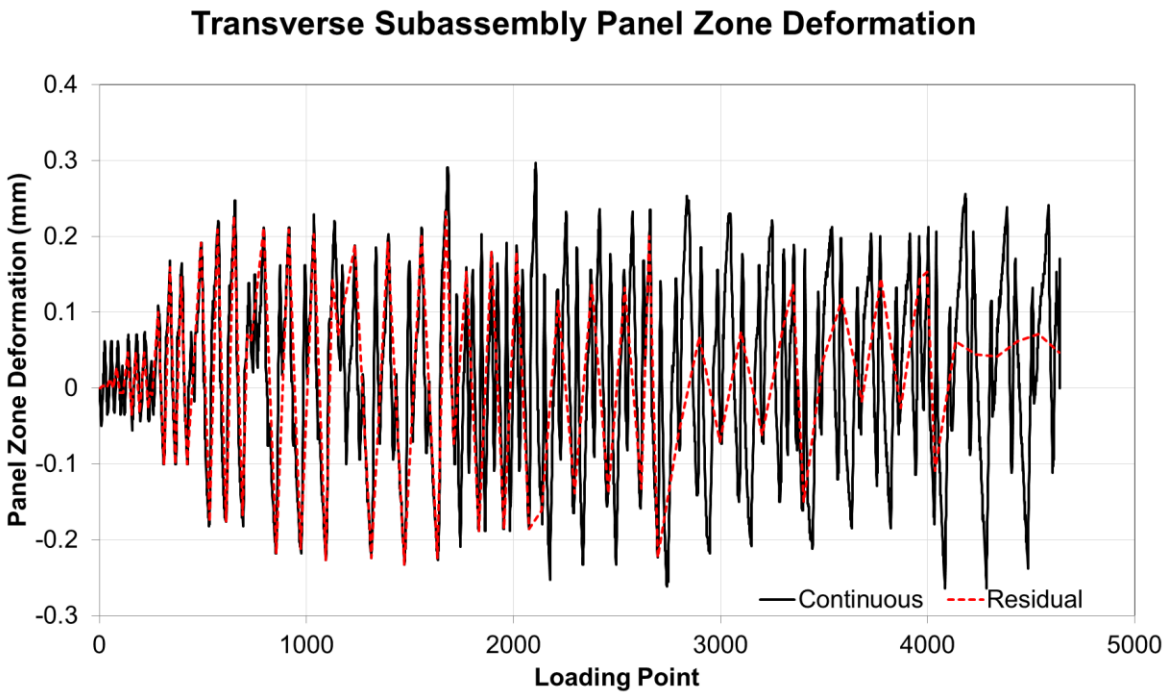

Figure 6-39: Transverse subassembly panel zone horizontal deformation (mm)

The maximum deformation of the panel zone was 0.3mm during the 0.75% drift cycle (around load point 2000). Over the panel zone depth of 300mm this equates to a steel strain of 0.001. Given that the nominal yield strain of Grade 300 steel is 0.0015 (0.00175 for Grade 350 steel) the panel zone steel in the transverse subassembly is likely to have remained elastic.

Plotting the moment end plate lift-off, shown in Figure 6-40, again shows a gradual increase in the displacement due to lift-off. The sudden increase in lift off at the 3600th load step is believed to be due to instrument failure. Prior to this the magnitude of this prying was again minimal in comparison to panel zone deformation (less than 0.1mm) and the end plate prying is unlikely to have a significant effect.

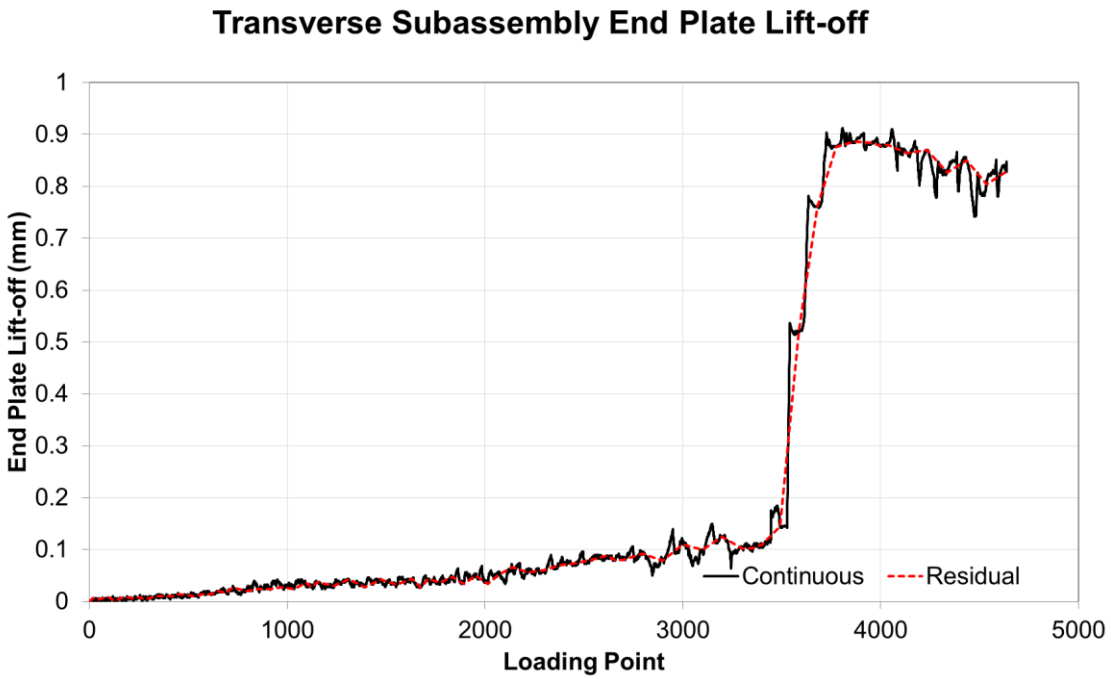

Figure 6-40: Transverse subassembly displacement due to end plate lift-off (mm)

The effect of the panel zone deformation on the overall deformation of the structure is shown in Figure 6-41. Again end plate lift-off was considered to be too small to be considered. As can be seen the panel zone accounted for at most 0.95mm of column top displacement (0.048% drift).

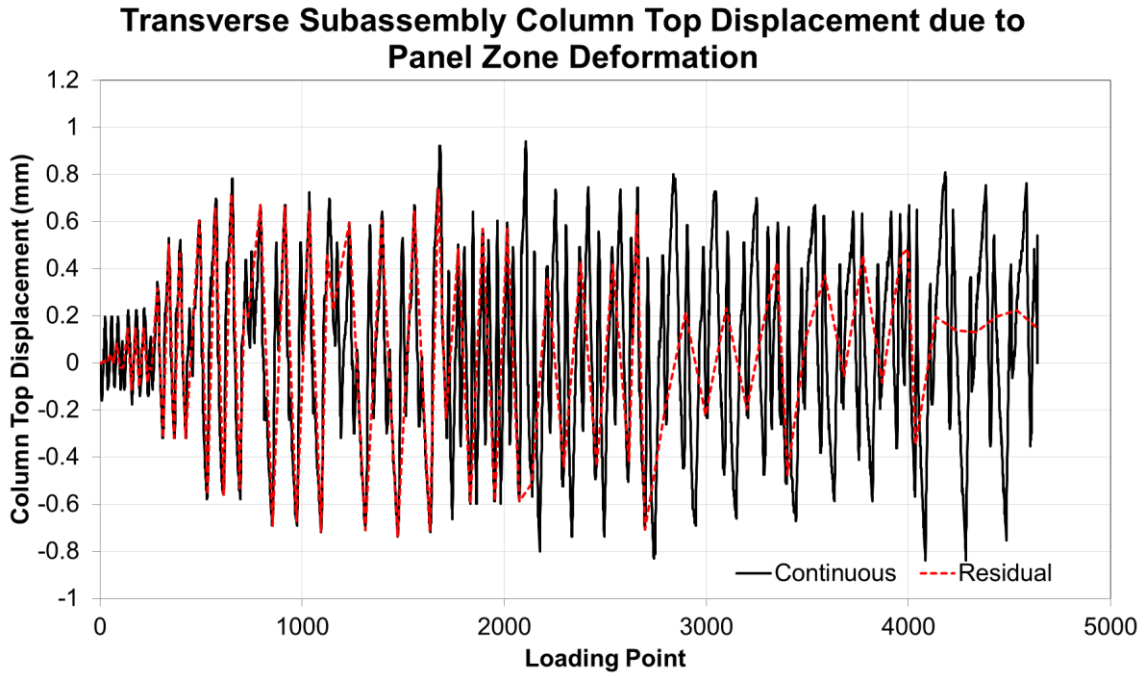

Figure 6-41: Transverse subassembly column top displacement due to panel zone deformation (mm)

Unit 3 (Longitudinal):

The panel zone instrumentation for the longitudinal subassembly was reduced owing to the presence of the secondary beam. As such only the results for the two side and the base potentiometer, along with those for the end plates, are illustrated in Figure 6-42. Again the two top endplate instruments, numbers 12 and 14 in Figure 3-17, tended to show a higher level of deformation than in the first subassembly with the right hand potentiometer recording 1.21mm of maximum deflection. A portion of this may have been due to instrument failure or pressing of the potentiometer against the underside of the deck tray which may have led to the uncharacteristic increase in displacement observed in Figure 6-44.

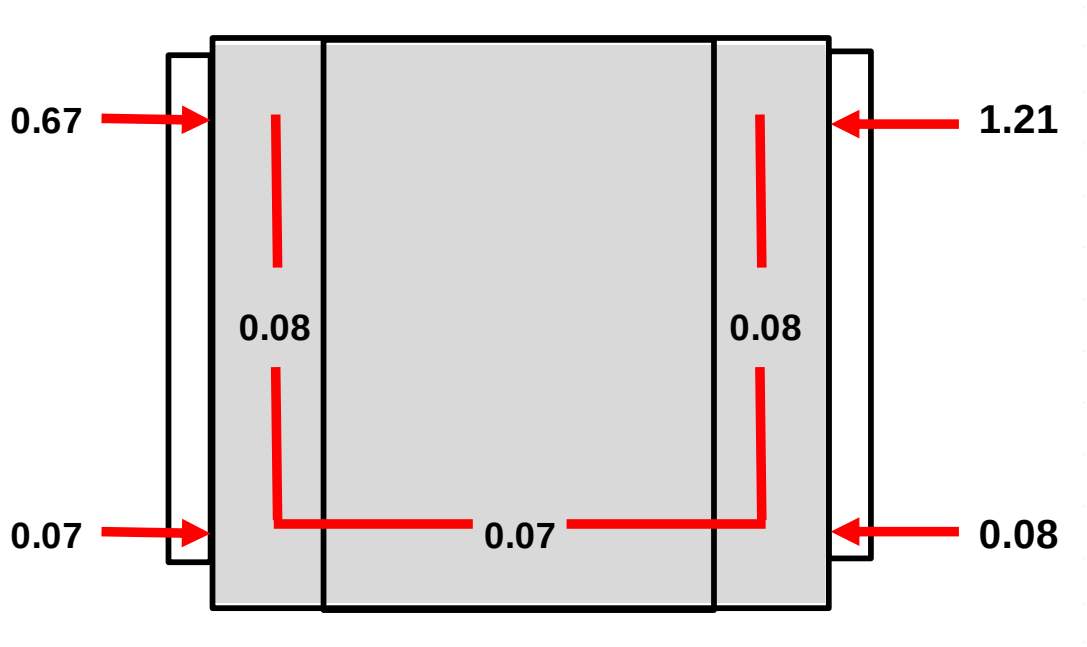

Figure 6-42: Longitudinal subassembly maximum panel zone deformation and end plate gap opening (mm)

Because of the missing instruments the only panel zone deformation measured was that of the bottom potentiometer. As such the panel zone deformation displayed in Figure 6-43 is far less than the actual deformation.

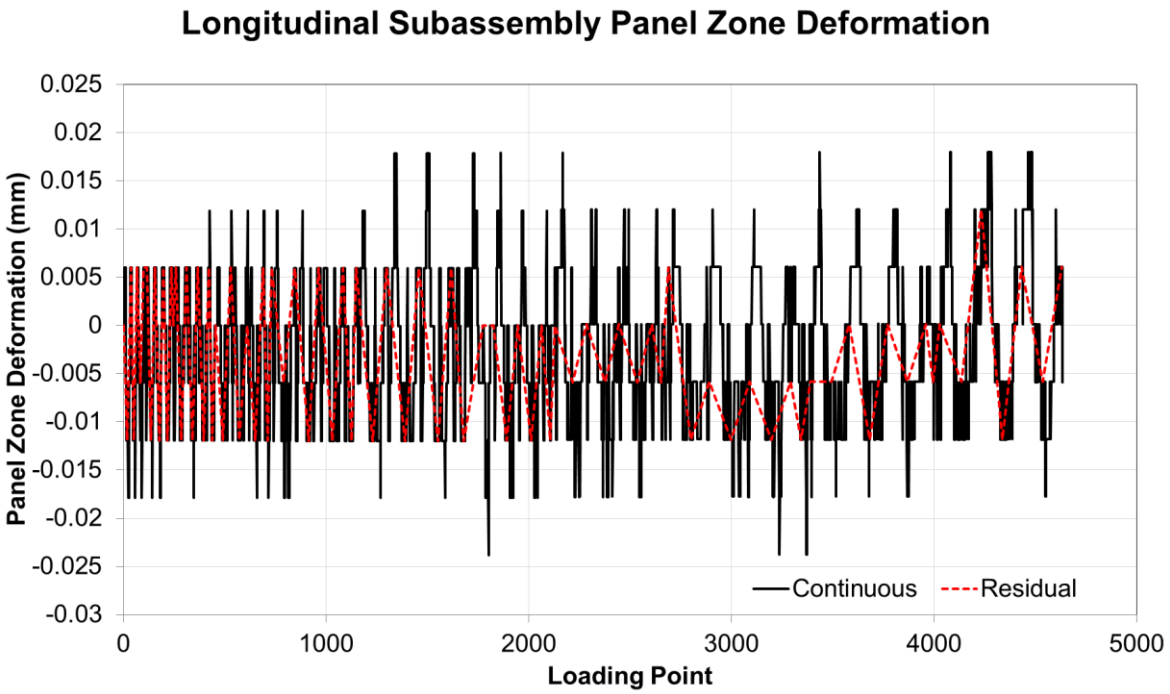

Figure 6-43: Longitudinal subassembly panel zone horizontal deformation (mm)

The moment end plate lift-off, shown in Figure 6-44, again shows a gradual increase in the displacement due to lift-off. The sudden increase in lift off at the 3400th load step is again due to instrument failure. Prior to this the magnitude of separation was less than 0.3mm and is unlikely to have a significant effect.

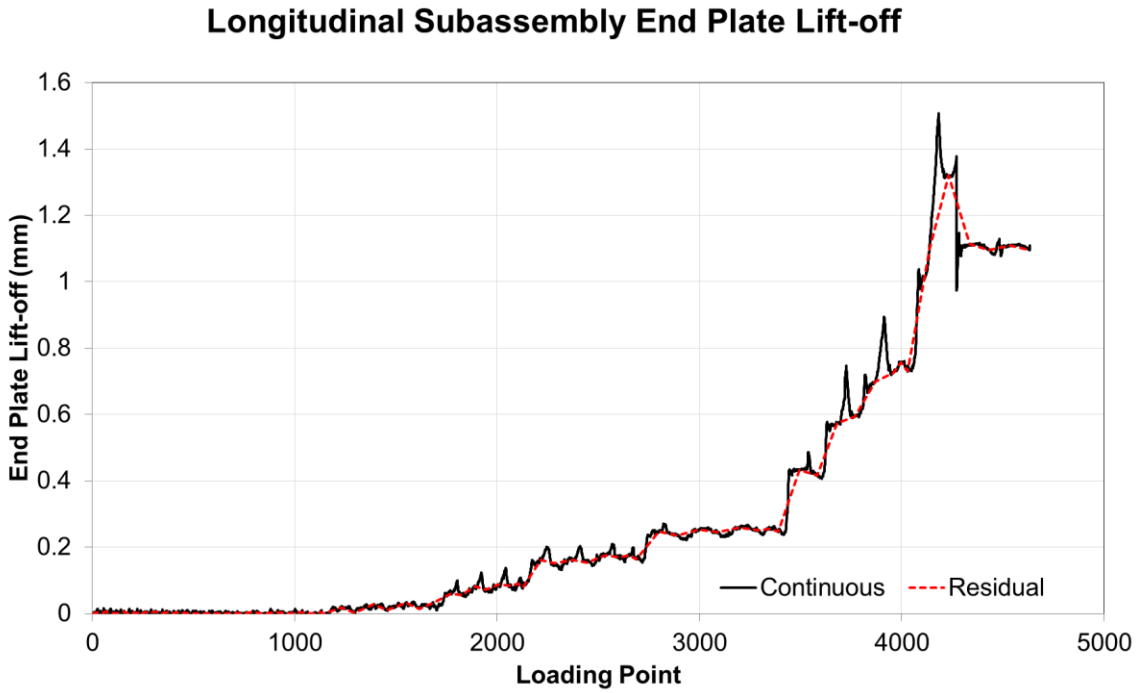

Figure 6-44: Longitudinal subassembly displacement due to end plate lift-off (mm)

The effect of the panel zone deformation on the overall deformation of the structure is shown in Figure 6-45, however this is also smaller than the actual displacement due to incomplete instrumentation.

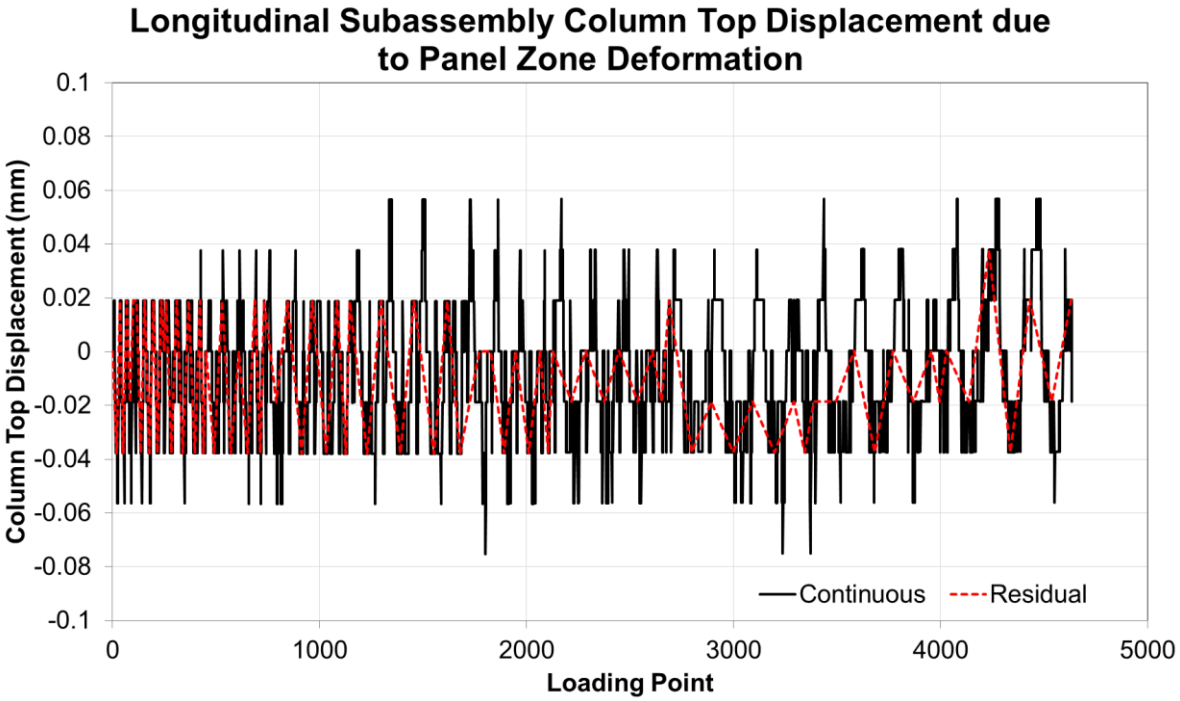

Figure 6-45: Longitudinal subassembly column top displacement due to panel zone deformation (mm)

Unit 4 (SHJ):

The SHJ subassembly exhibited reduced panel zone and end plate deformations in comparison to the first three subassemblies. The absolute maximum displacement measured by the two diagonal instruments peaked at 0.34mm as is illustrated in Figure 6-46. The two top endplate instruments showed a lower level of deformation than in the first subassembly with maximum displacements of less than 0.3mm. It should be noted that instrument failures meant that the top left contact value and the bottom continuity plate value are based on incomplete sets of data.

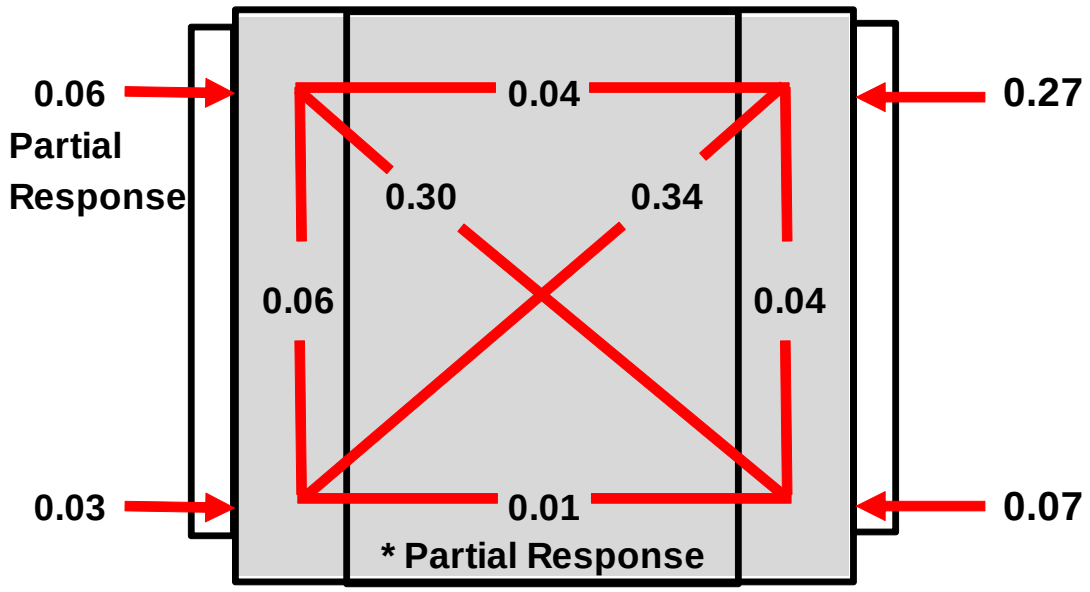

Figure 6-46: SHJ subassembly maximum panel zone deformation and end plate gap opening (mm)

The horizontal deflection of the panel zone in the SHJ subassembly was less than 0.3mm throughout the testing and, like the transverse subassembly, the residual displacements tended to be similar to the maximum displacements observed in the continual data during the lower drift cycles.

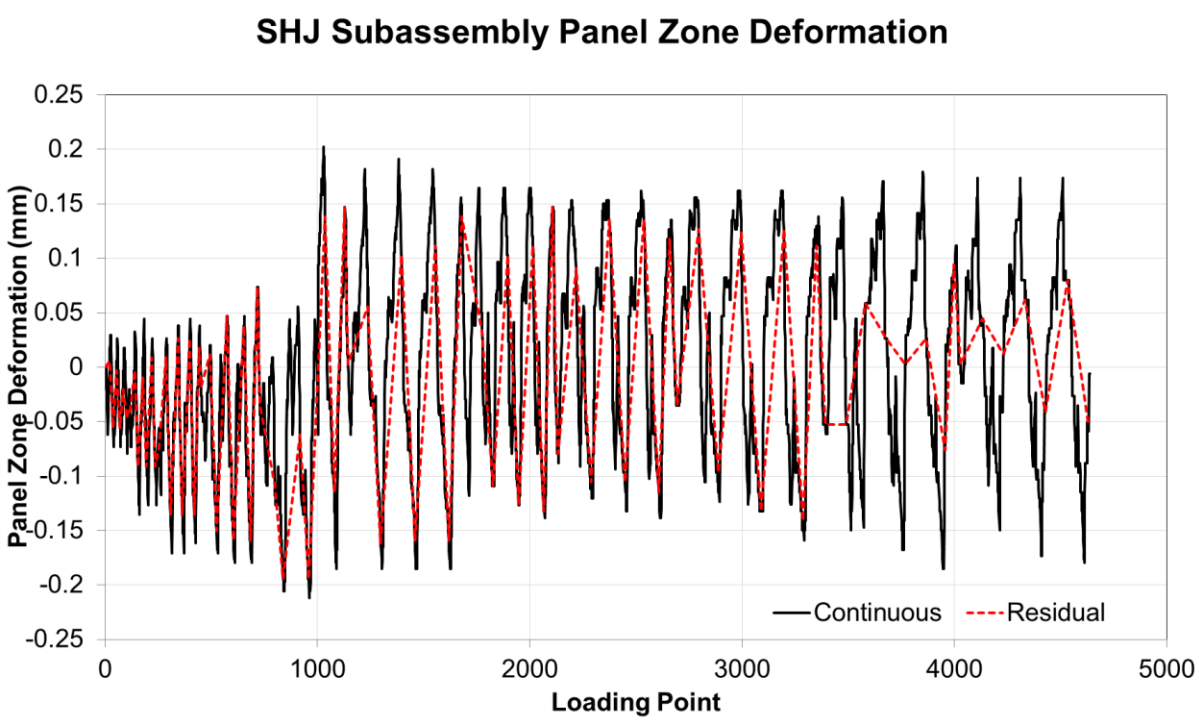

Figure 6-47: SHJ subassembly panel zone and end plate horizontal deformation (mm)

The maximum deformation of the panel zone was 0.21mm during the 0.5% drift cycle (around load point 1000). Over the panel zone depth of 300mm this equates to a steel strain of 0.001. Given that the nominal yield strain of Grade 300 steel is 0.0015 (0.00175 for Grade 350 steel) the panel zone steel in the SHJ subassembly is likely to have remained elastic.

Moment end plate lift-off, shown in Figure 6-48, gradually increase during testing however the magnitude of prying was again minimal in comparison to panel zone deformation less than 0.2mm. As such end plate prying is unlikely to have a significant effect.

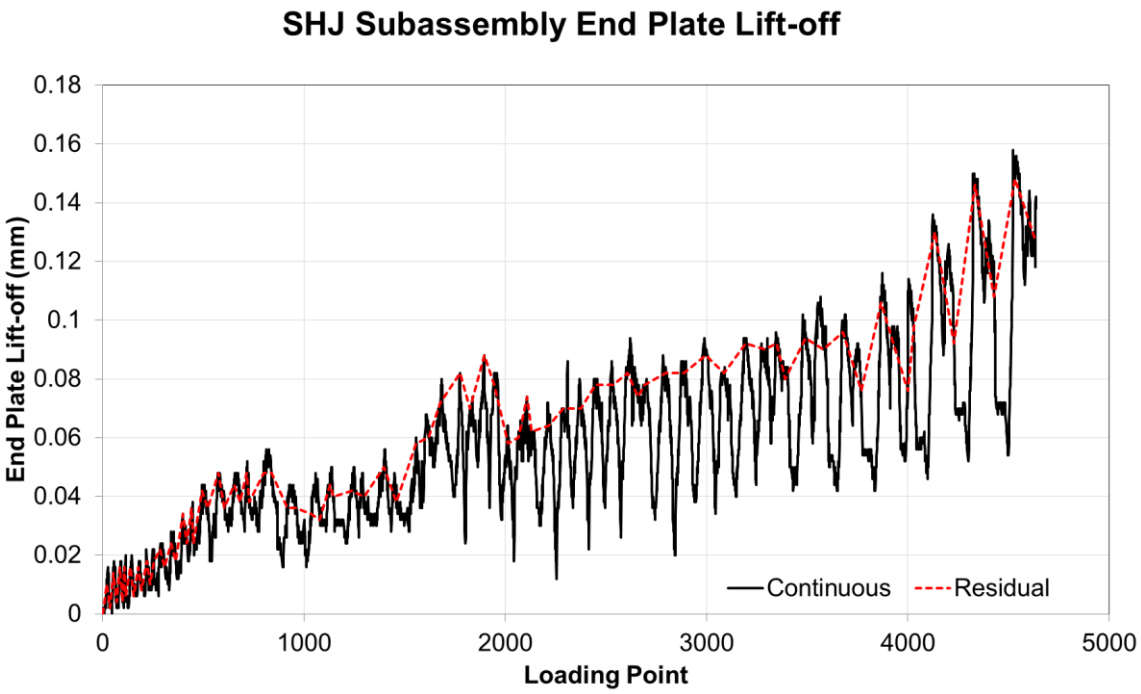

Figure 6-48: SHJ subassembly displacement due to end plate lift-off (mm)

The effect of the panel zone deformation on the overall deformation of the structure is shown in Figure 6-49. As can be seen the panel zone accounted for at most 0.7mm of column top displacement (0.035% drift).

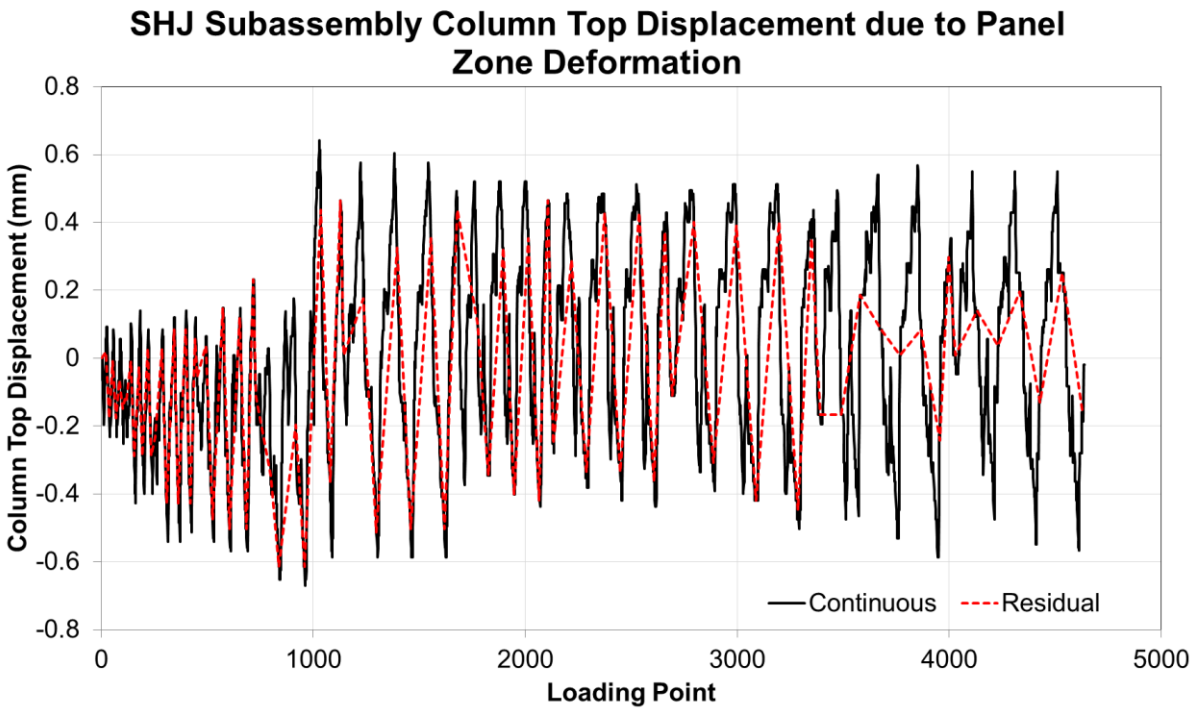

Figure 6-49: SHJ subassembly column top displacement due to panel zone deformation (mm)

The extended testing cycles produced similar levels of panel zone displacement and a slightly increase level of end plate deformation as shown in Figure 6-50.

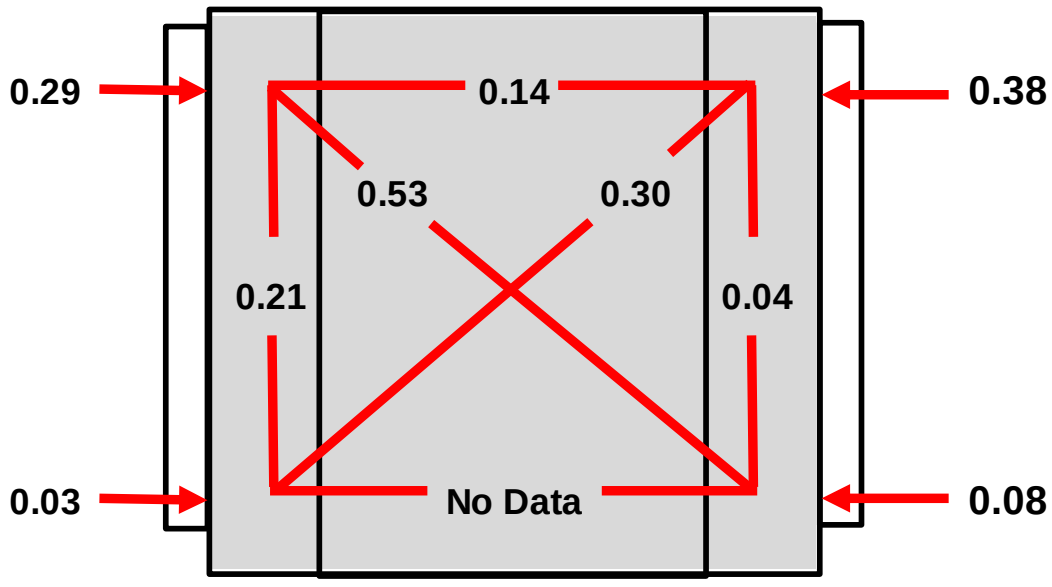

Figure 6-50: SHJ subassembly extended testing maximum panel zone deformation and end plate gap opening (mm)

The total horizontal panel zone displacement for the extended testing, illustrated in Figure 6-51 showed a reduction in deformation during the 2.5% drift cycles in comparison to similar levels of drift in the initial testing. This was most likely due to the reduction in joint capacity. Throughout the higher drift cycles the residual deformation remained less than 0.3mm.

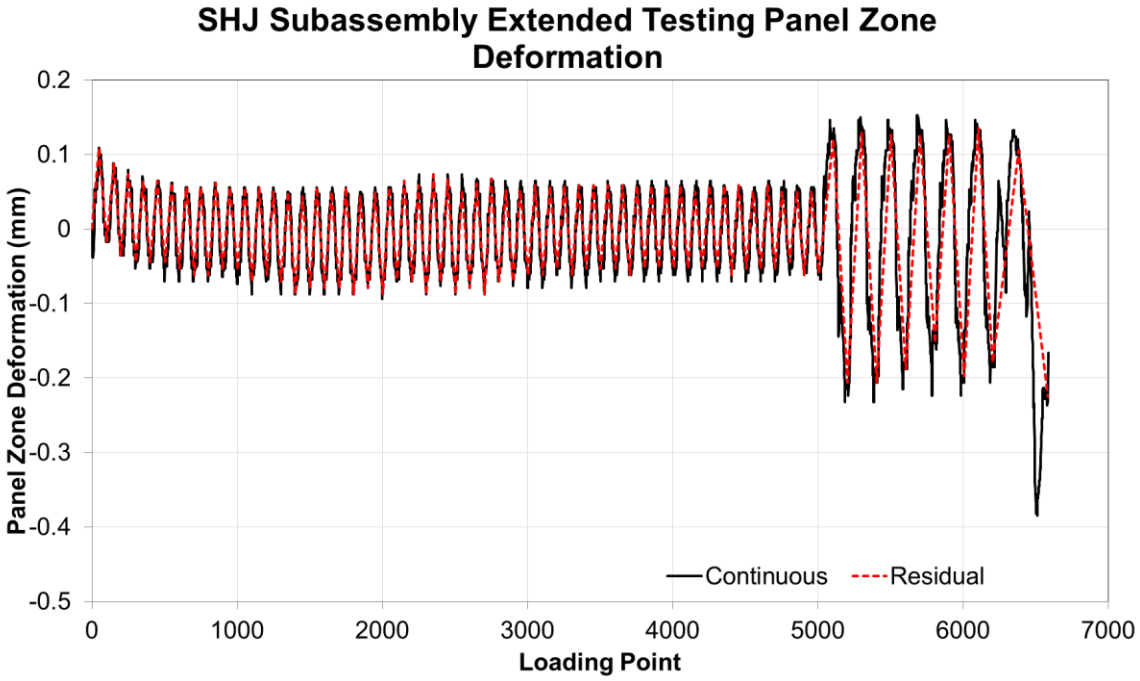

Figure 6-51: SHJ subassembly panel zone horizontal deformation under extended testing (mm)

The maximum deformation of the panel zone was 0.38mm during the 10% drift cycle (around load point 6500) which equates to a steel strain of 0.0013. Given that the nominal yield strain of Grade 300 steel is 0.0015 (0.00175 for Grade 350 steel) the panel zone steel in the SHJ subassembly is likely to have remained elastic.

Moment end plate lift-off, shown in Figure 6-52, remained constant during the 2.5% drift cycles but increased over the 5% and 10% drift cycles. The magnitude of prying was similar to panel zone deformation but less than 0.5mm.

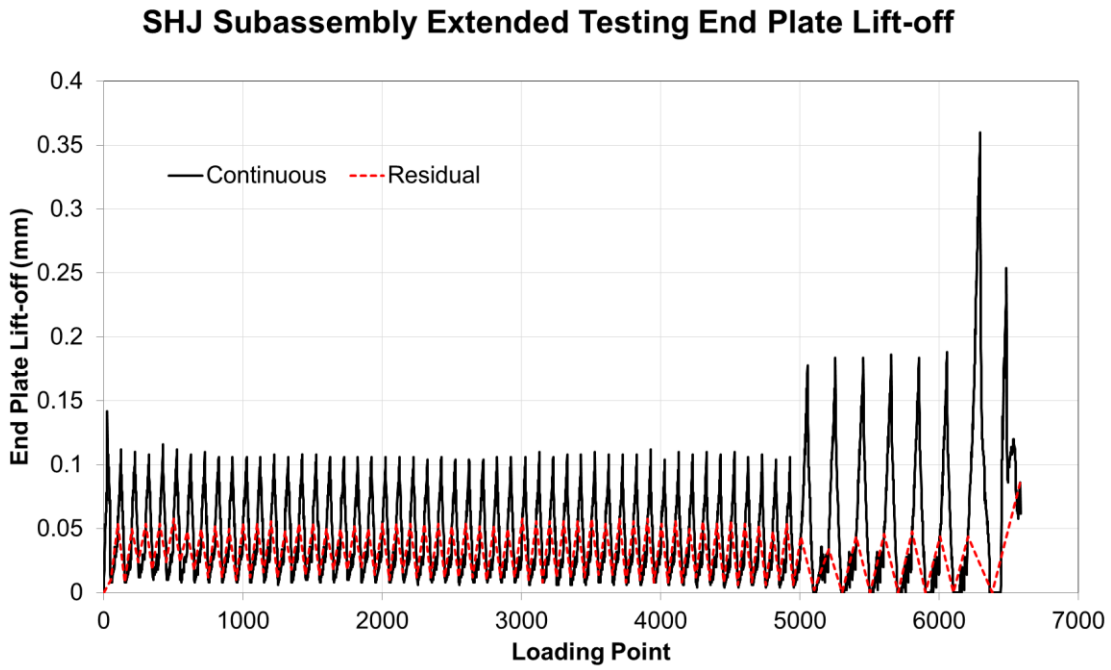

Figure 6-52: SHJ subassembly displacement due to end plate lift-off under extended testing (mm)

The effect of the panel zone deformation on the overall deformation of the structure is shown in Figure 6-53. As can be seen the panel zone accounted for at most 1.2mm of column top displacement (0.06% drift).

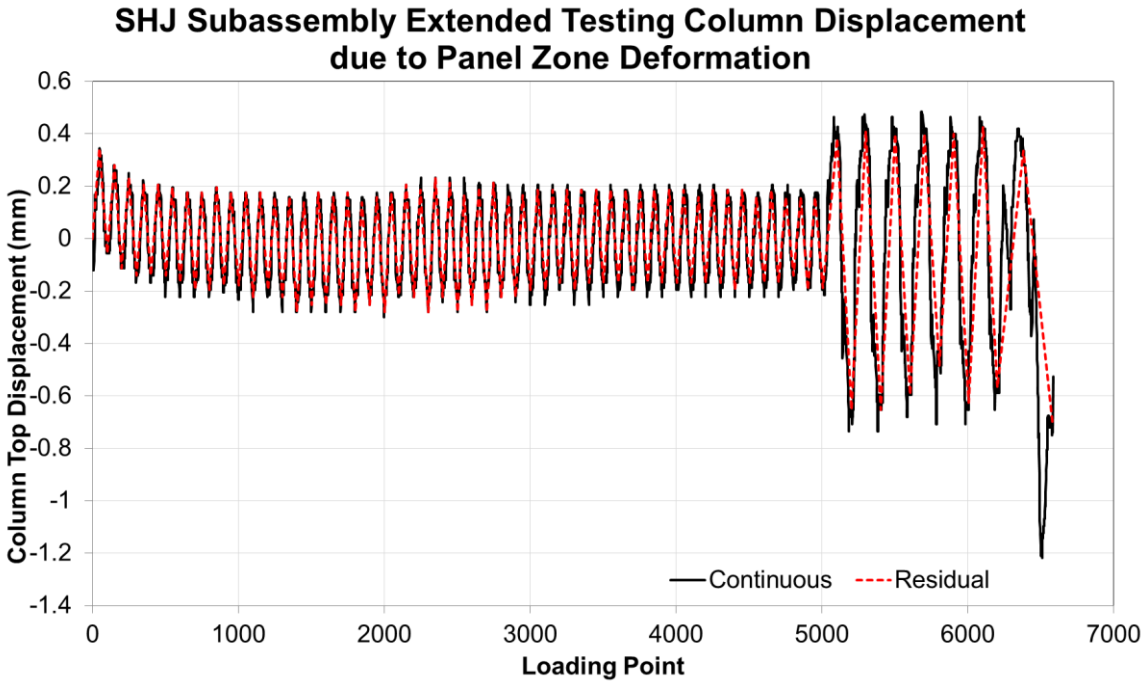

Figure 6-53: SHJ subassembly column top displacement due to panel zone deformation under extended testing (mm)

Unit 5 (Full Depth):

The SHJ subassembly exhibited the highest level of panel zone deformation of all of the subassemblies tested however the end plate deformations were comparatively low. The absolute maximum displacement measured by the two diagonal instruments peaked at around 0.6mm as is illustrated in Figure 6-54. The two top endplate instruments showed a lower level of deformation than in the other subassemblies with maximum displacements of less than 0.05mm.

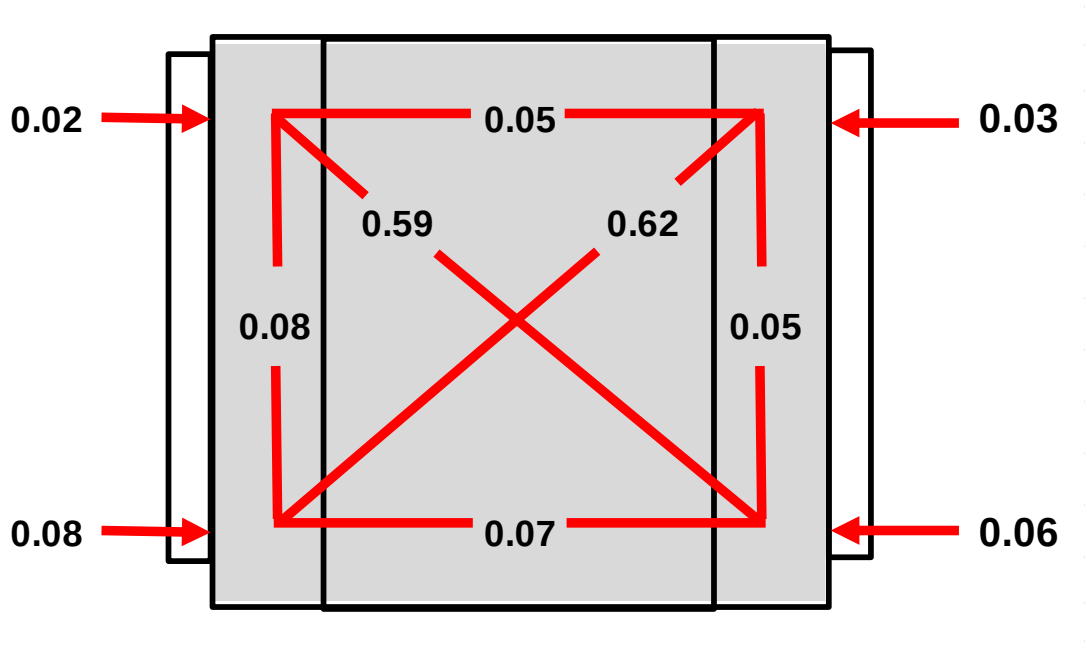

Figure 6-54: Full depth subassembly maximum panel zone deformation and end plate gap opening (mm)

The horizontal deflection of the panel zone in the full depth subassembly was less than 0.5mm throughout the testing. Unlike the transverse and SHJ subassemblies, the residual displacements tended to stay near to zero during the lower drift cycles.

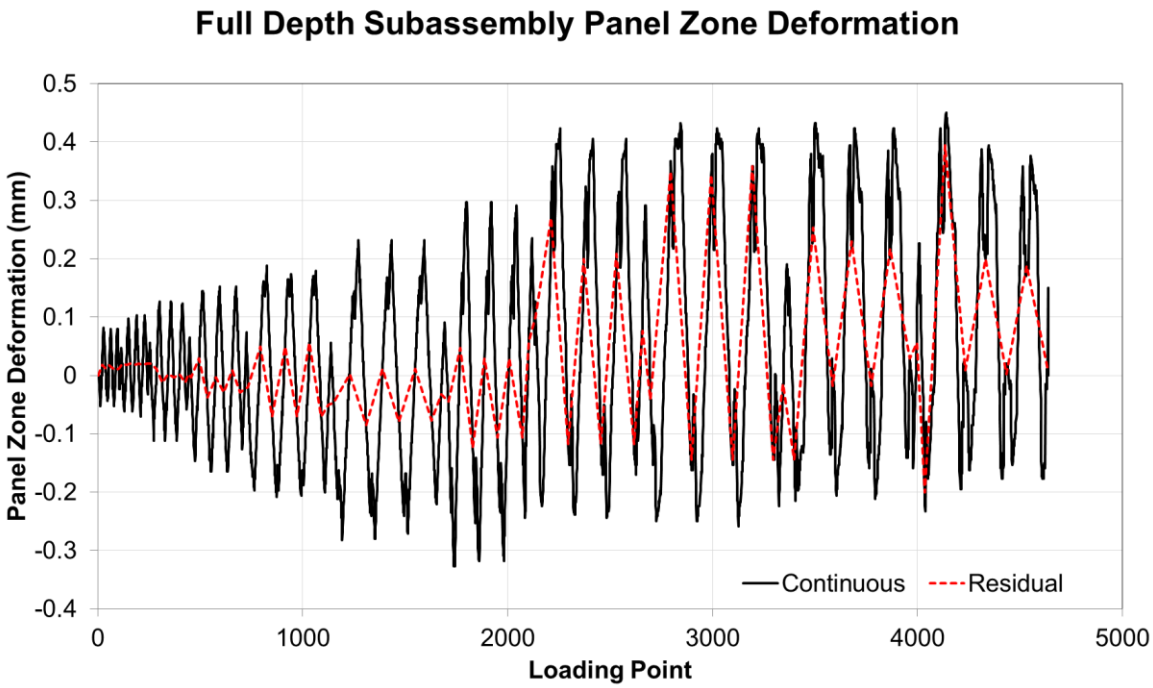

Figure 6-55: Full Depth subassembly panel zone and end plate horizontal deformation (mm)

The maximum deformation of the panel zone was 0.45mm during the 5% drift cycle (around load point 4100) which equates to a steel strain of 0.0015. Given that the nominal yield strain of Grade 300 steel is 0.0015 (0.00175 for Grade 350 steel) the panel zone steel in the full depth subassembly is likely to have come close to yielding.

Moment end plate lift-off, shown in Figure 6-56, gradually increase during testing however the magnitude of prying was again minimal in comparison to panel zone deformation (around 0.1mm). As such end plate prying is unlikely to have a significant effect.

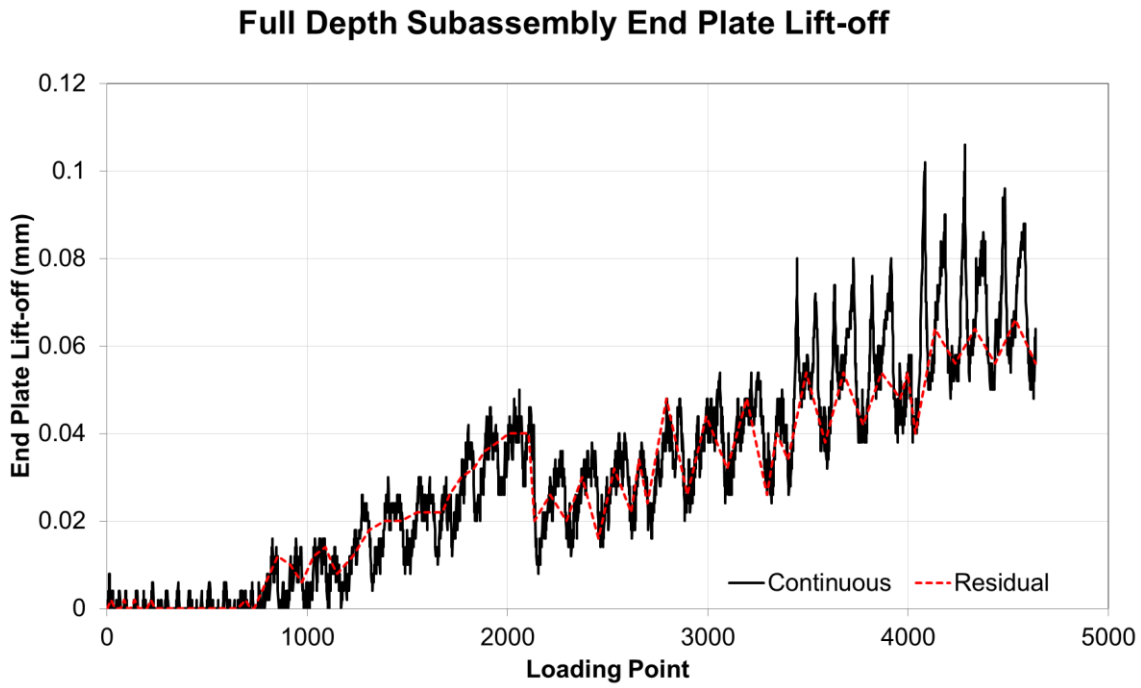

Figure 6-56: Full depth subassembly displacement due to end plate lift-off (mm)

The effect of the panel zone deformation on the overall deformation of the structure is shown in Figure 6-57. As can be seen the panel zone accounted for at most 1.4mm of column top displacement (0.07% drift).

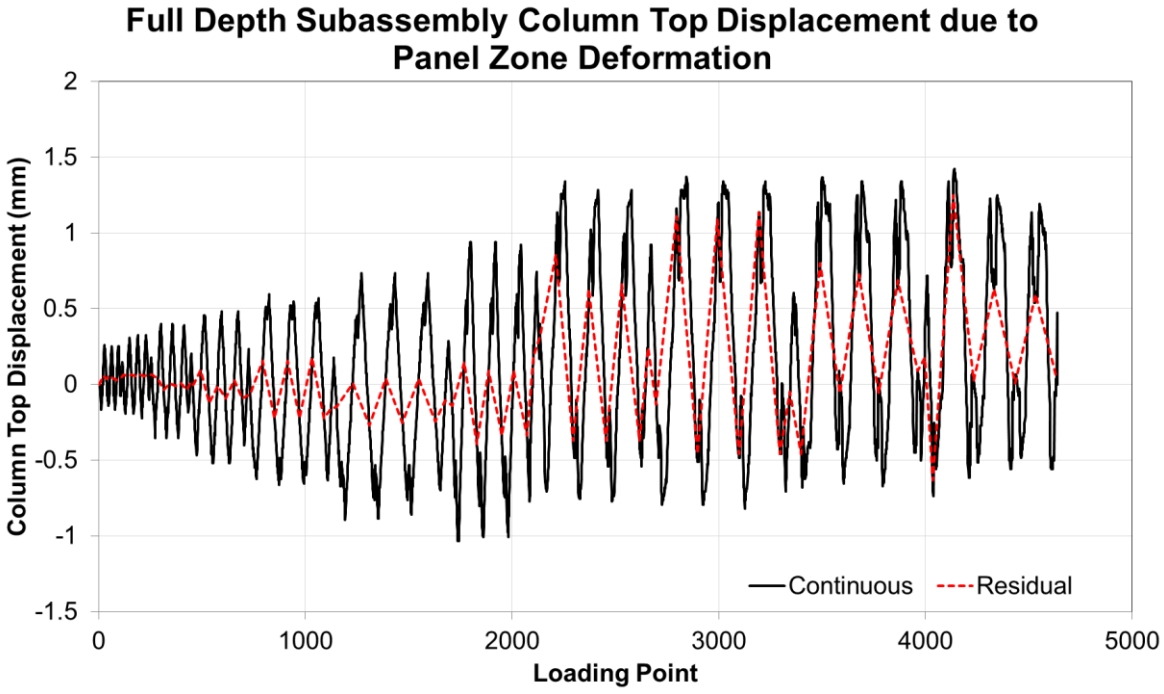

Figure 6-57: SHJ subassembly column top displacement due to panel zone deformation (mm)

6.2.3 Beam Elongation

Unit 1 (Isolated):

The centreline elongation of the beams within the plastic hinge zone is shown in Figure 6-58 and Figure 6-59. The east beam exhibited a gradual elongation of less than 1mm up to the 3.5% drift cycles (load point 3300). Following buckling of the beam flanges at 3.5% drift, elongation of the beam increased to up to 2mm when the bottom flange was in tension whilst buckling of the bottom flange allowed beam shortening of up to 5mm. Residual displacements at zero load following the 5.0% drift cycles were less than 1mm elongation.

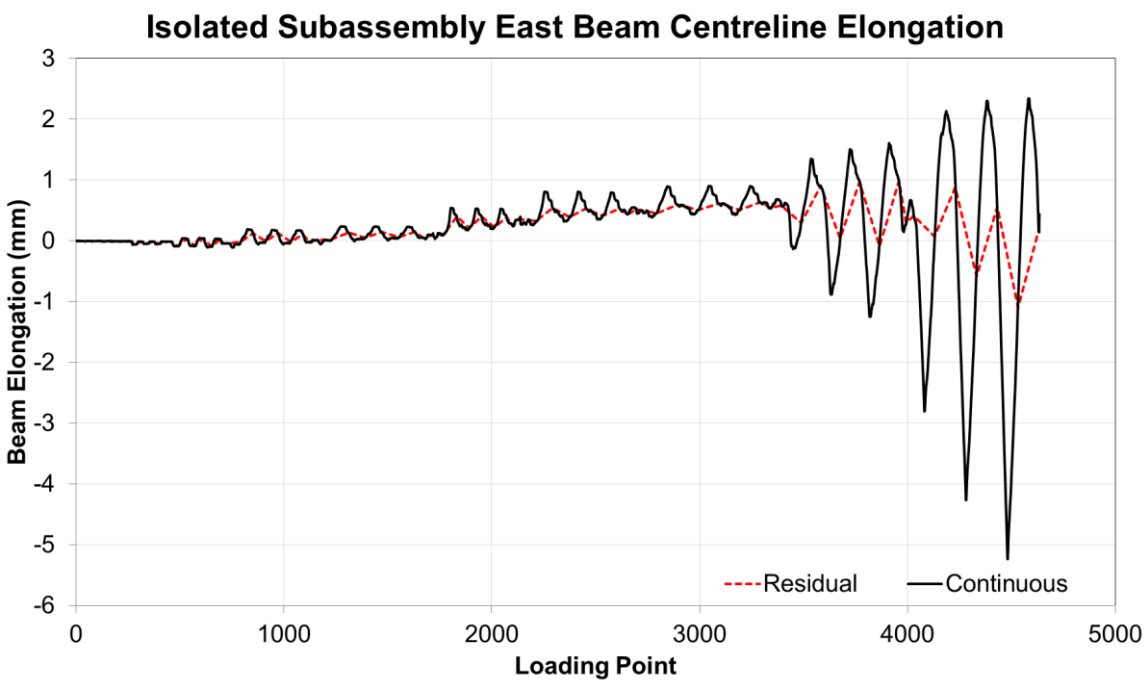

Figure 6-58: Centreline elongation of the east beam, isolated subassembly (mm).

The west beam did not exhibit noticeable elongation under low drift cycles. However, like the east beam, following buckling of the beam flanges at 3.5% drift elongation of the beam increased to up to 1mm when the bottom flange was in tension and shortening by up to 5mm when the bottom flange was in compression. Residual displacements at zero load following the 5.0% drift cycles was approximately 2mm of beam shortening.

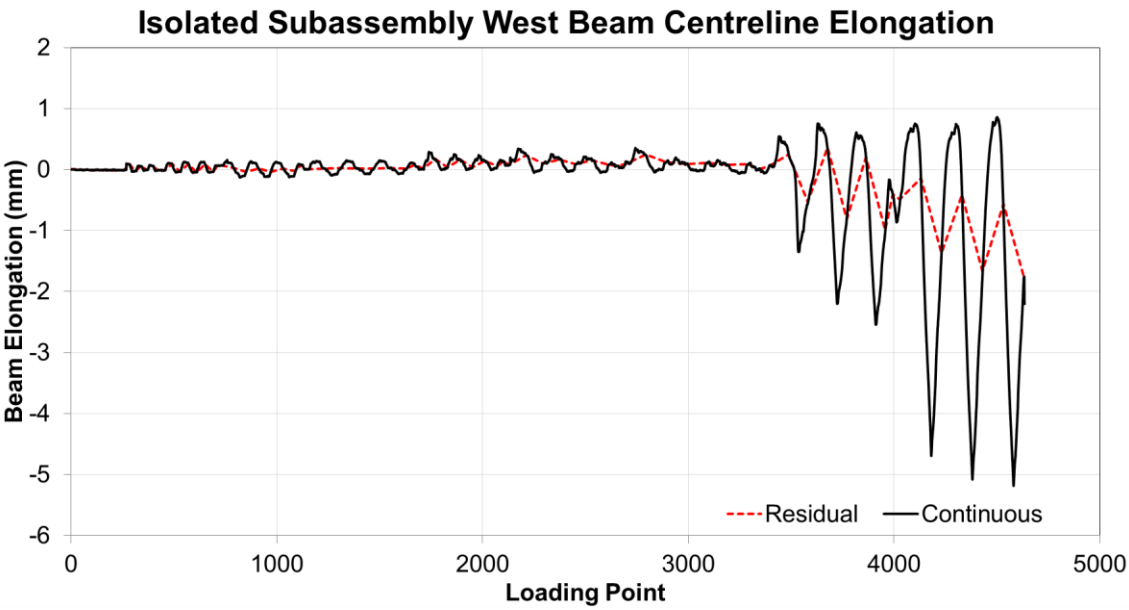

Figure 6-59: Centreline elongation of the west beam, isolated subassembly (mm).

Unit 2 (Transverse):

The centreline elongation of the beams within the plastic hinge zone is shown in Figure 6-60 and Figure 6-61. Below 2.5% drift (load pint 2800) neither beam tended to show any long term elongation with the beams elongating and shortening cyclically with maximum displacements of 1-2mm. Beyond 2.5% drift the east beam exhibited a gradual shortening with a residual beam shortening of 1mm. Peak elongation was 2-3mm whilst peak shortening was up to 8mm.

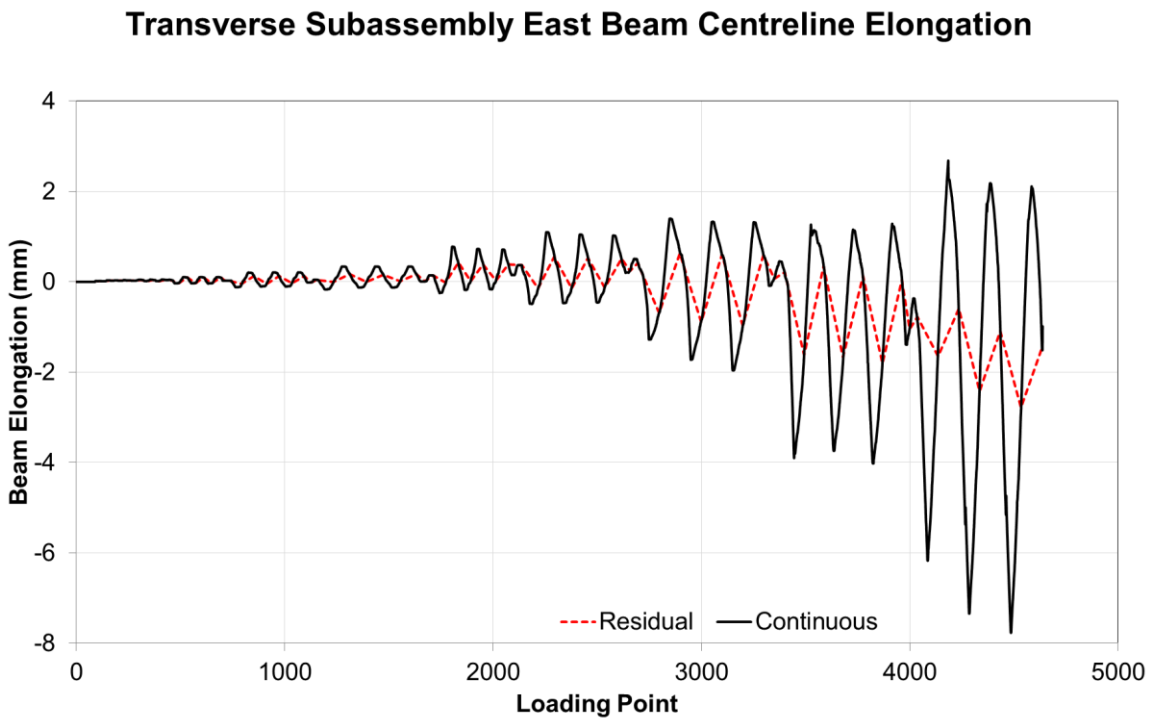

Figure 6-60: Centreline elongation of the east beam, transverse subassembly (mm).

Likewise the west beam did not exhibit noticeable elongation under low drift cycles however following buckling of the beam flanges the beam underwent shortening with a residual reduction in length of 3mm being recorded. Like the east beam peak elongation was 2-3mm whilst peak shortening was up to 9mm.

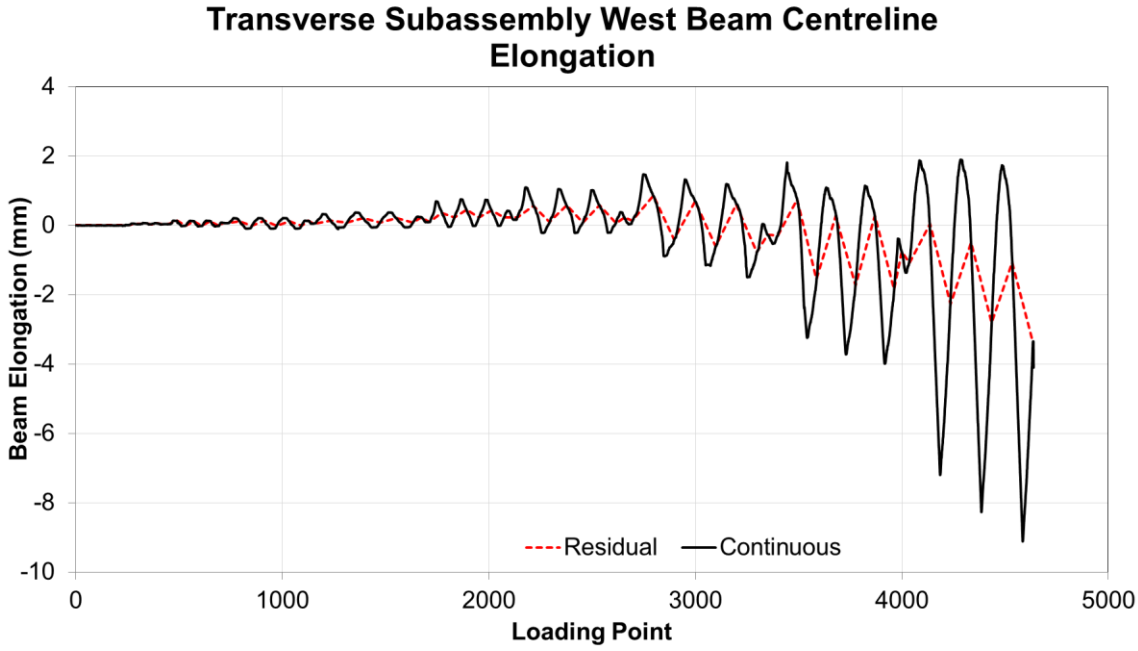

Figure 6-61: Centreline elongation of the west beam, transverse subassembly (mm).

Unit 3 (Longitudinal):

The centreline elongation of the beams within the plastic hinge zone is shown in Figure 6-62 and Figure 6-63. As for the transverse subassembly, below 2.5% drift (load point 2800) neither beam tended to show any long term elongation. Beyond 2.5% drift the east beam exhibited a gradual shortening with a residual beam shortening of 1mm. Peak elongation was just over 2mm whilst peak shortening was up to 9mm.

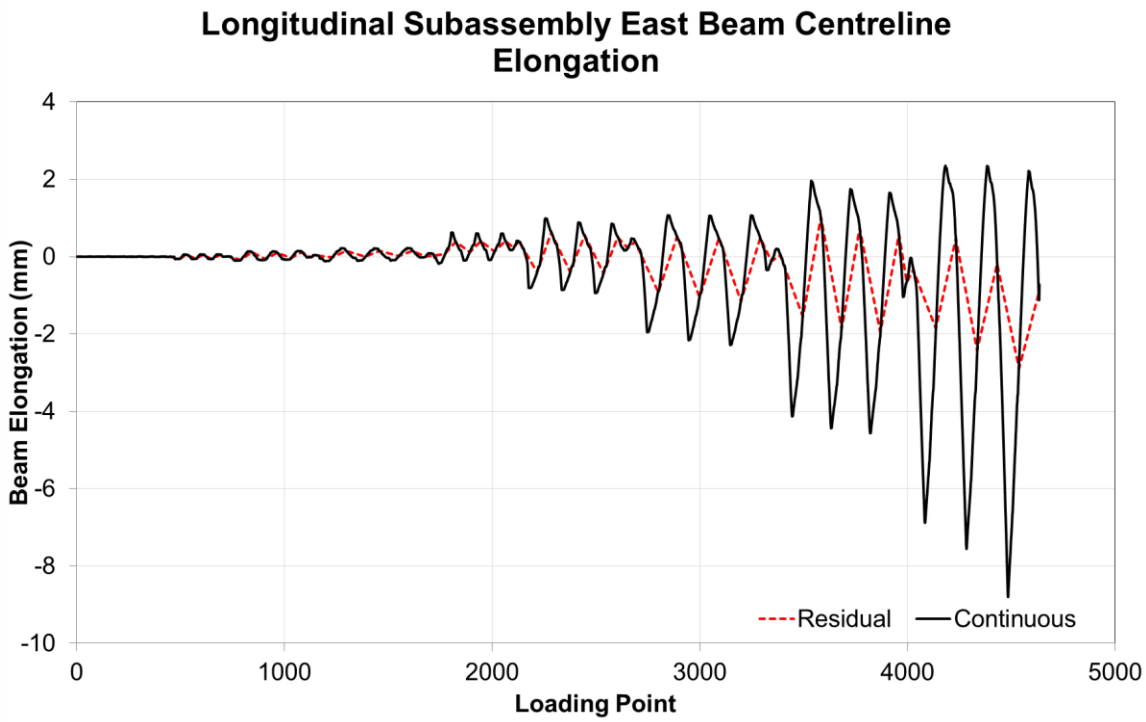

Figure 6-62: Centreline elongation of the east beam, longitudinal subassembly (mm).

Likewise the west beam did not exhibit noticeable elongation under low drift cycles. Unfortunately during the 3.5% and 5% drift cycles the bottom flange instrument mounting point fell within the buckled portion of the beam resulting in a skewed result as shown in Figure 6-63. At 2.5% drift it is apparent that a residual elongation of less than 1mm is present however at higher cycles the elongation increases due to the effect of uplift on the instrument mounting point.

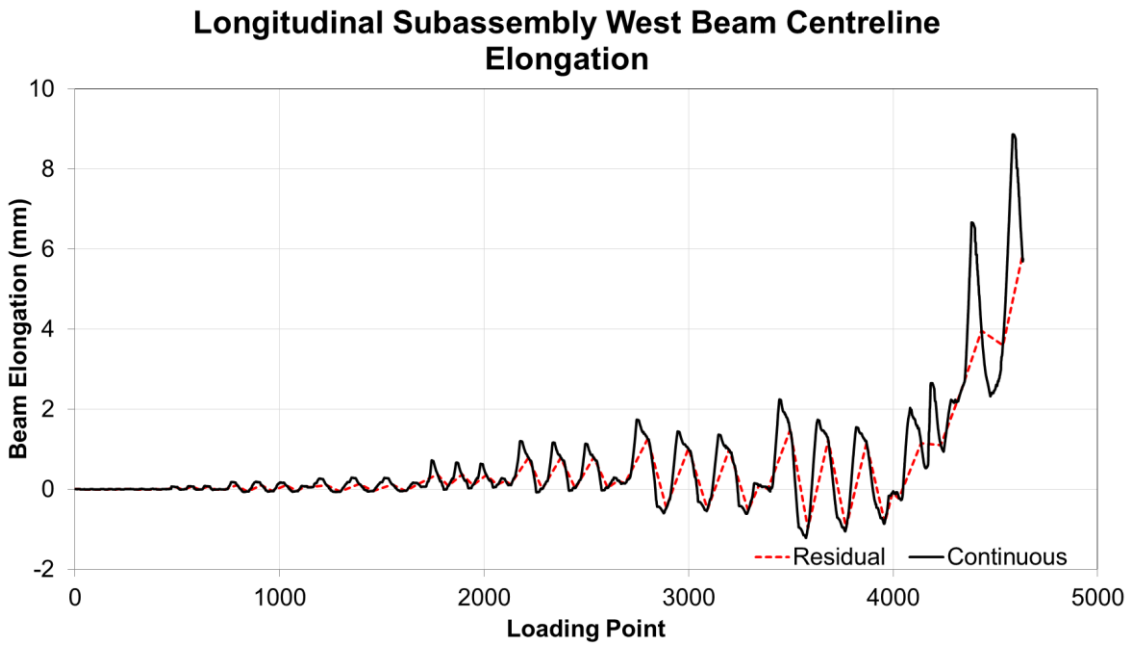

Figure 6-63: Centreline elongation of the west beam, longitudinal subassembly (mm).

Unit 4 (SHJ):

The centreline elongation of the beams within the plastic hinge zone is shown in Figure 6-64 and Figure 6-65. As was expected, the beams showed minimal elongation or shortening as they were never subjected to inelastic deformations. The centreline of both beams moved cyclically by up to 6mm in either direction as the beams rocked in their connections. Some minor residual elongation was noted in both beams however this was due to movement of the bolts in the marginally oversized holes and as such is not representing beam elongation.

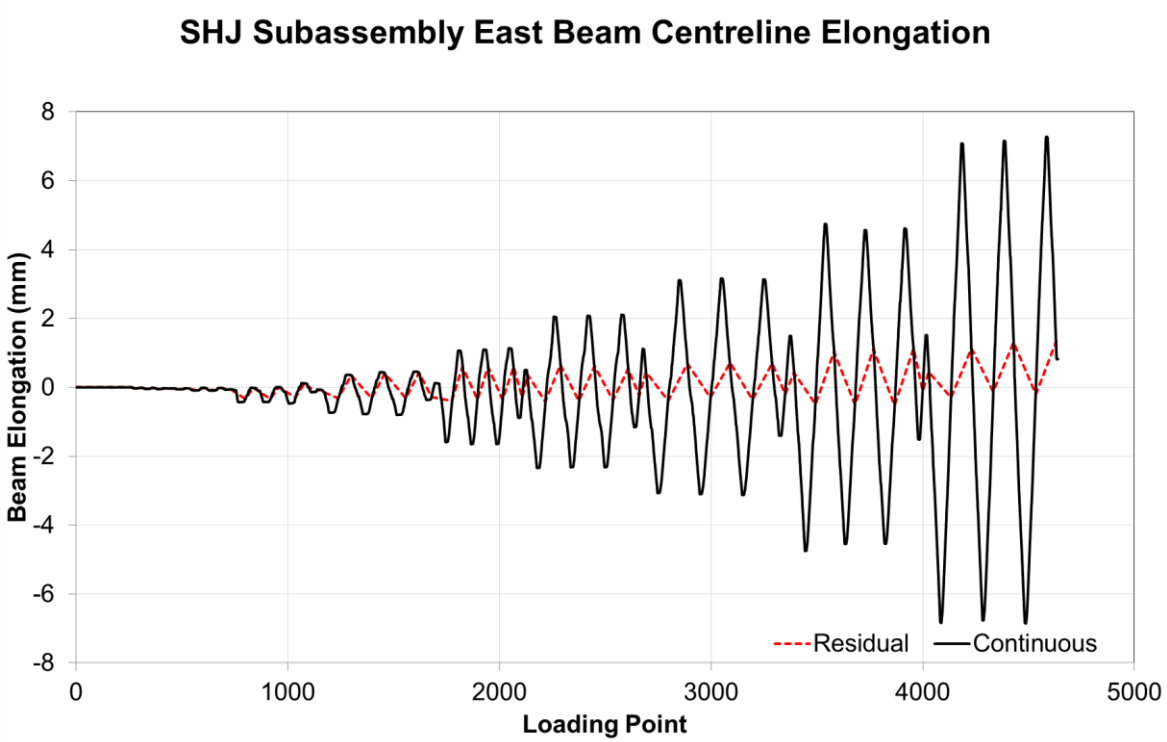

Figure 6-64: Centreline elongation of the east beam, SHJ subassembly (mm).

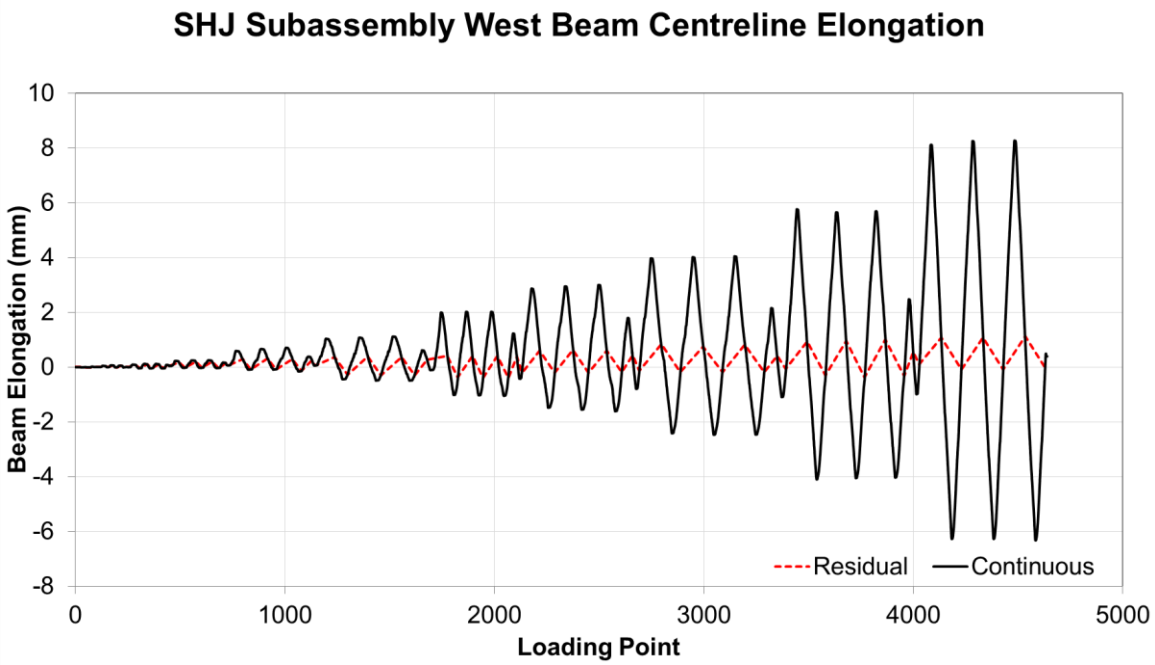

Figure 6-65: Centreline elongation of the west beam, SHJ subassembly (mm).

The centreline elongation of the beams within the plastic hinge zone under extended testing is shown in Figure 6-66 and Figure 6-67. As was observed in the initial testing, the sliding hinge connection continued to prevent beam elongation throughout the extended testing cycles at

2.5% and 5% drift. Some minor elongation was noted during the cycle at 20% drift although this appears to have been primarily from elongation of the bolt holes.

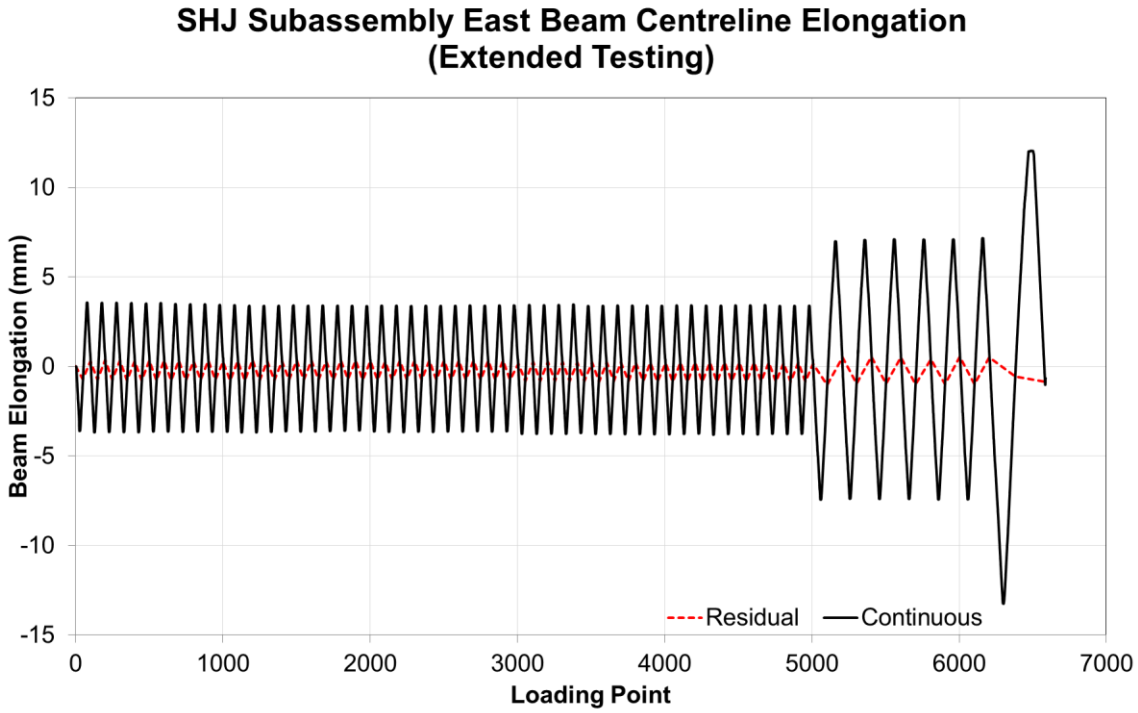

Figure 6-66: Centreline elongation of the east beam, SHJ subassembly under extended testing (mm).

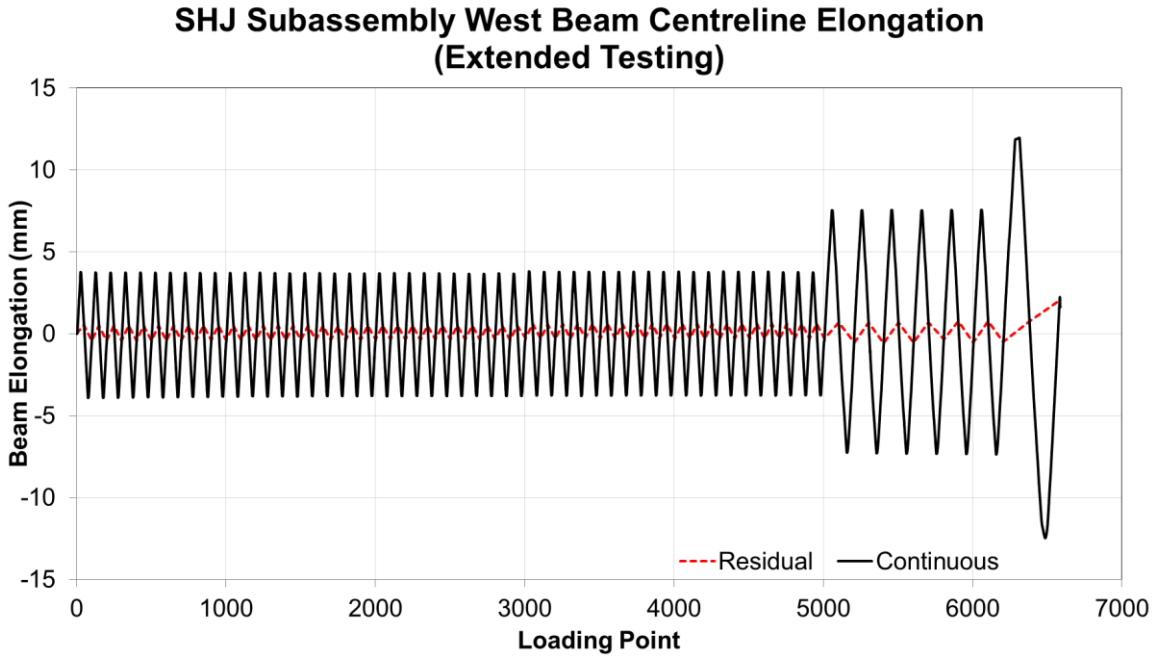

Figure 6-67: Centreline elongation of the west beam, SHJ subassembly under extended testing (mm).

Unit 5 (Full Depth):

The centreline elongation of the beams within the plastic hinge zone is shown in Figure 6-68 and Figure 6-69. Below 2.5% drift (load point 2800) neither beam tended to show any long term elongation. Beyond 2.5% drift the east beam exhibited a gradual shortening with a residual beam shortening of 2mm. Peak elongations was just over 2mm whilst peak shortening was up to 9mm.

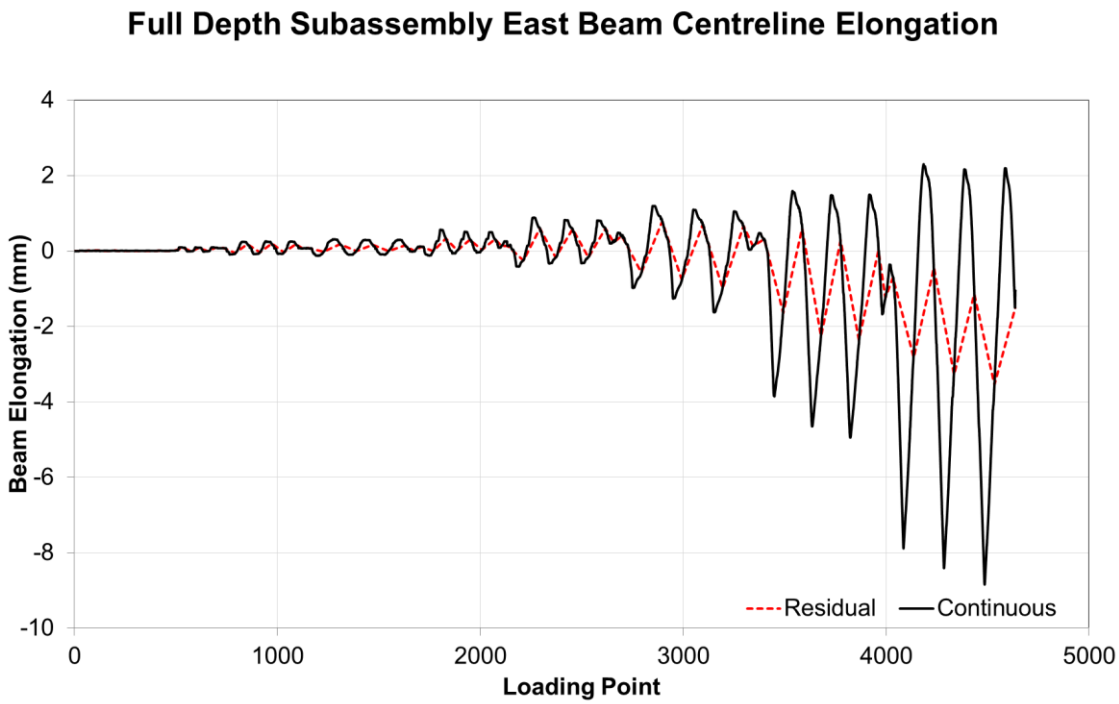

Figure 6-68: Centreline elongation of the east beam, full depth subassembly (mm).

Likewise the west beam did not exhibit noticeable elongation under low drift cycles. Unfortunately during the 3.5% and 5% drift cycles the bottom flange instrument mounting point fell within the buckled portion of the beam resulting in a skewed result as shown in Figure 6-69. At 2.5% drift it is apparent that a residual elongation of less than 1mm is present however at higher cycles the elongation increases due to the effect of uplift on the instrument mounting point.

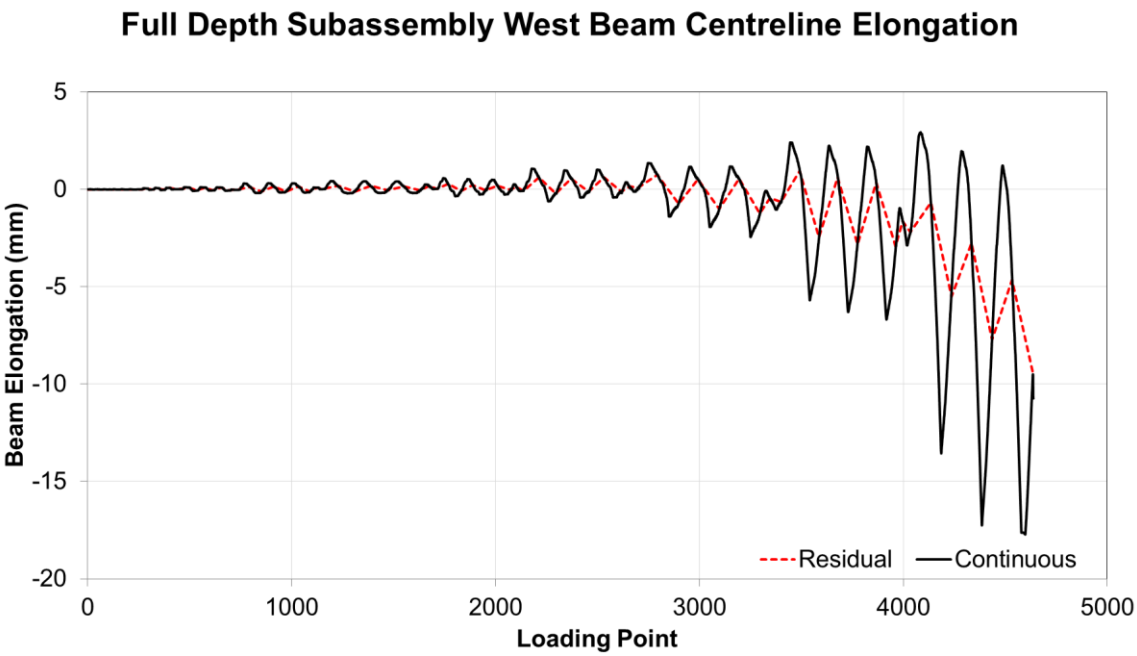

Figure 6-69: Centreline elongation of the west beam, full depth subassembly (mm).

6.2.4 Bending Shear Displacement of the Column Alone

As mentioned in Section 5.3, loss of testing data due to instrument failure meant that a data-based model was required to provide some indication of the column bending displacement. A linear relationship was devised in which the force applied to the column was used to determine the corresponding bending displacement in the column. This was then applied to the applied force data from the first four subassemblies to create the plots below.

Unit 1 (Isolated):

Modelled column deformation from the isolated subassembly, shown in Figure 6-70, indicated that the maximum expected drift from the column alone was around 1.5mm-2mm. Residual deformations peaked at just over 1mm. Beyond 2.5% drift (load point 2800) the column peak displacement plateaued indicating that the total resistance of the system was being governed by the beams which had yielded and begun to buckle.

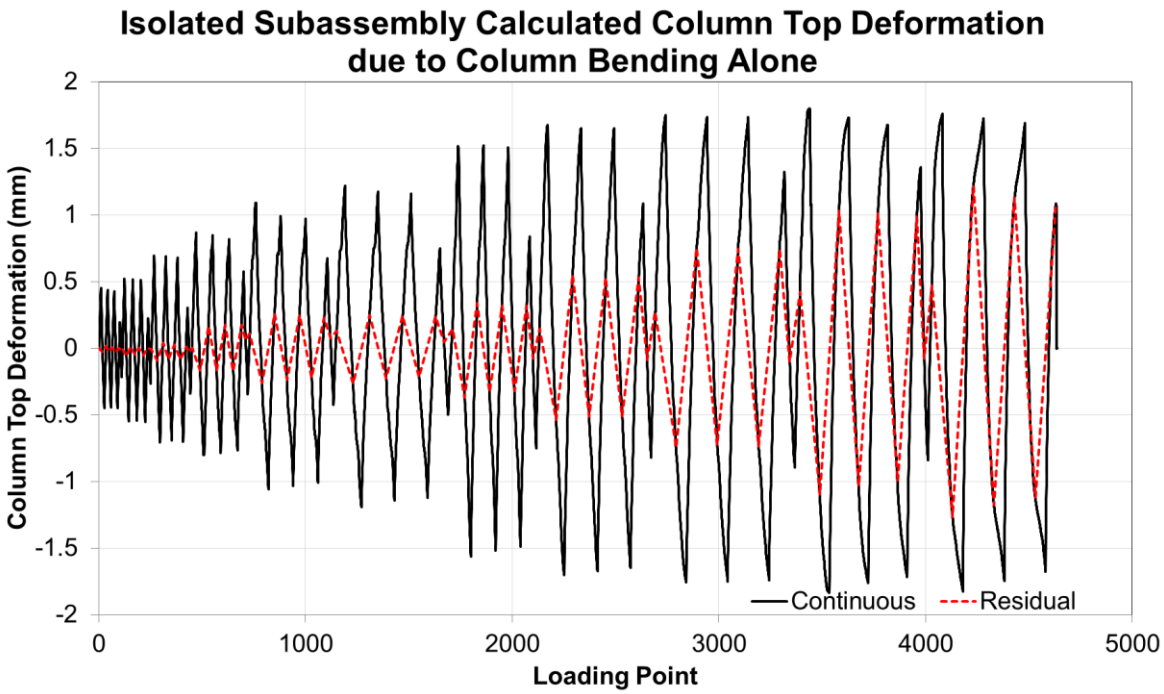

Figure 6-70: Isolated subassembly modelled column bending deformation (mm).

Unit 2 (Transverse):

Modelled column deformation from the transverse subassembly, shown in Figure 6-71, showed a slightly higher peak column drift of just over 2mm. Again residual deformations peaked at just over 1mm during the 2.5% drift cycle (load point 2800). The column peak displacement then dropped, most likely as a result of strength loss due to concrete spalling, to the level observed in the isolated subassembly after the beams had yielded and begun to buckle.

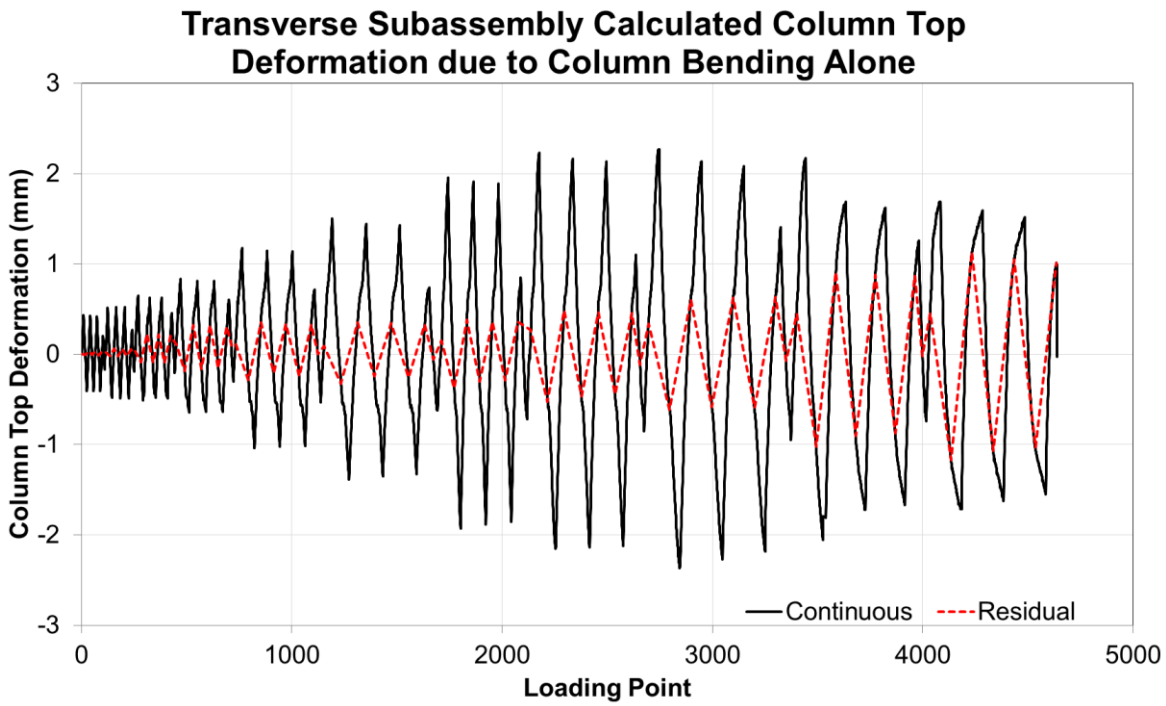

Figure 6-71: Transverse subassembly modelled column bending deformation (mm).

Unit 3 (Longitudinal):

The longitudinal subassembly showed a similar modelled column deformation to the transverse subassembly, shown in Figure 6-72, with a peak column drift of just over 2mm. and a residual deformation of around 1mm. Peak displacements occurred during the 2.0% drift cycle (load point 2200) after which the column peak displacement then dropped as was observed in the transverse subassembly.

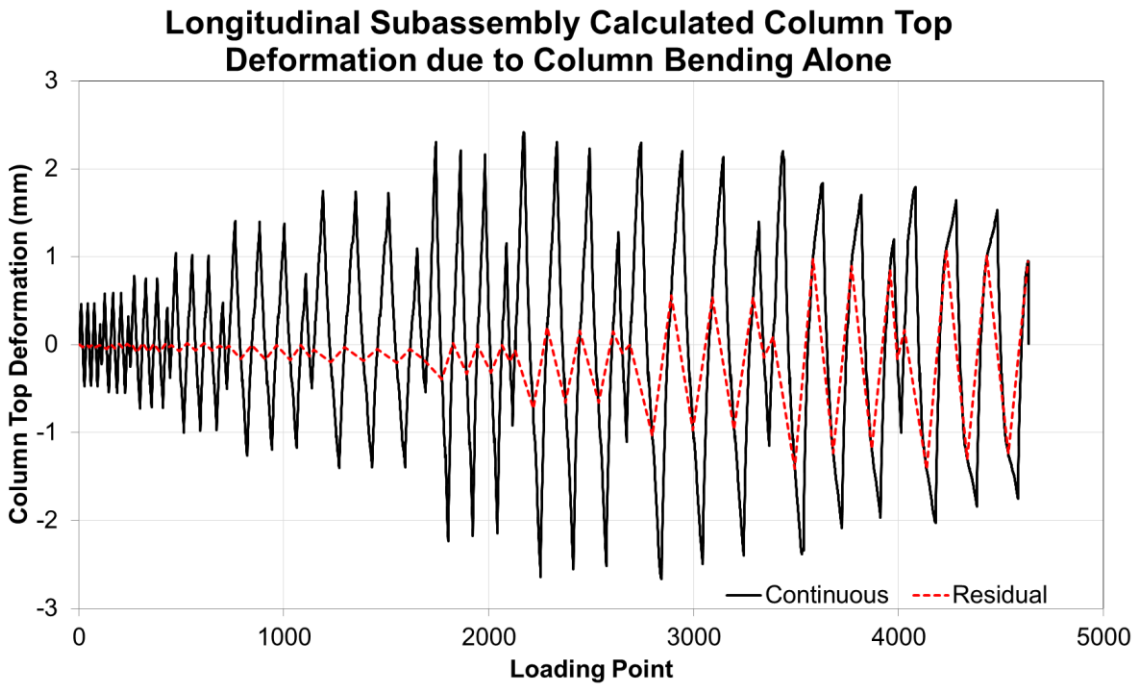

Figure 6-72: Longitudinal subassembly modelled column bending deformation (mm).

Unit 4 (SHJ):

The SHJ subassembly showed a reduced modelled column deformation with a peak column drift of approximately 1.5mm, as shown in Figure 6-73, and a residual deformation of around 0.5mm. Peak displacements occurred during the 2.0% drift cycle (load point 2200) after which a small reduction in column peak displacement was observed.

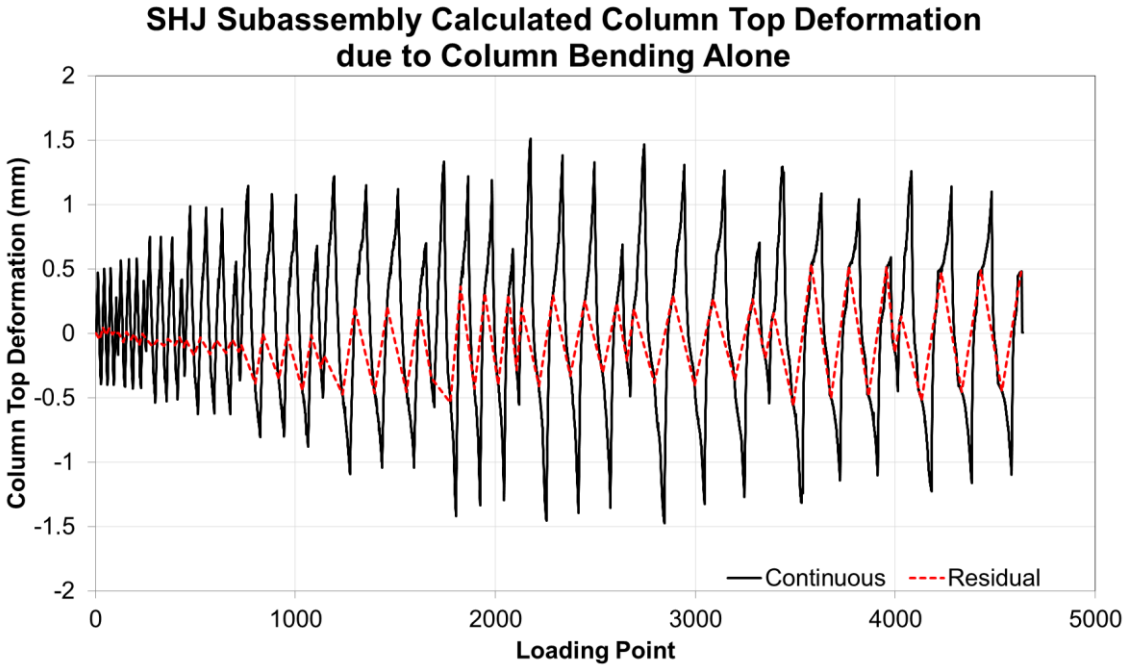

Figure 6-73: SHJ subassembly modelled column bending deformation (mm).

The extended testing of the SHJ subassembly showed a further reduced modelled column deformation with a peak column drift of 0.5mm for the 2.5% drift cycles and up to 2mm for the 10% drift cycle as shown in Figure 6-74. Because concrete spalling had already occurred no further reduction in peak displacement was observed.

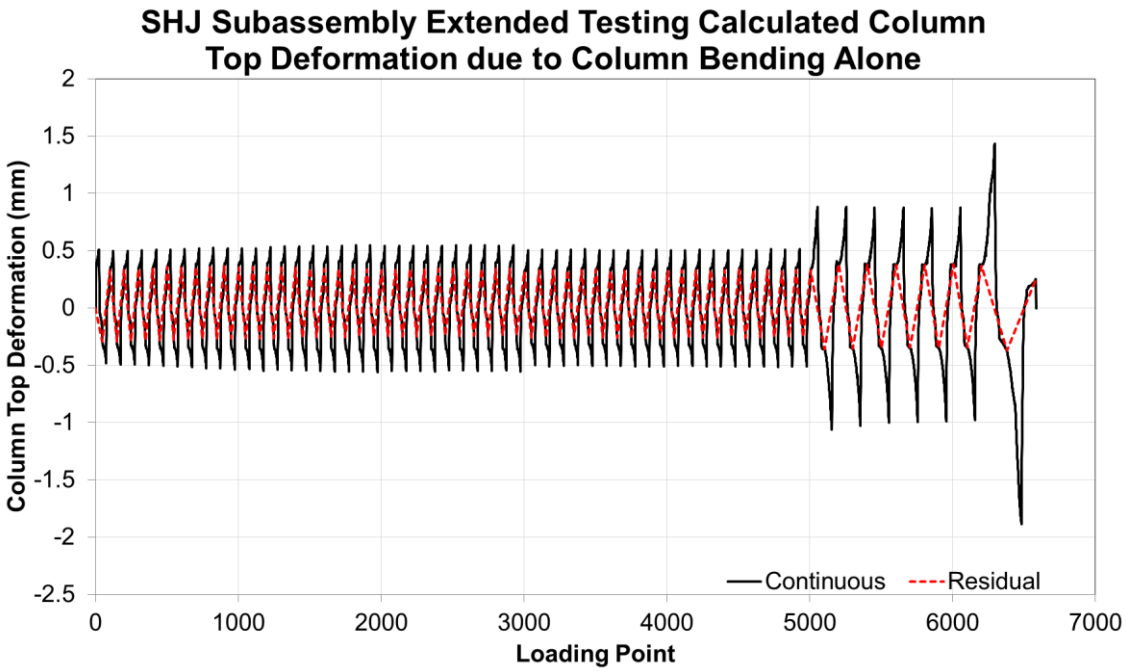

Figure 6-74: SHJ subassembly modelled column bending deformation under extended testing (mm).

Unit 5 (Full Depth):

The full depth subassembly, shown in Figure 6-75, showed a similar modelled column deformation to the transverse and longitudinal subassemblies with a peak column drift of just over 2mm. and a residual deformation of around 1mm. The reduction in displacement after 2.5% drift was more gradual than was observed in previous subassembly and reflected the reduction in damage to the slab surrounding the column.

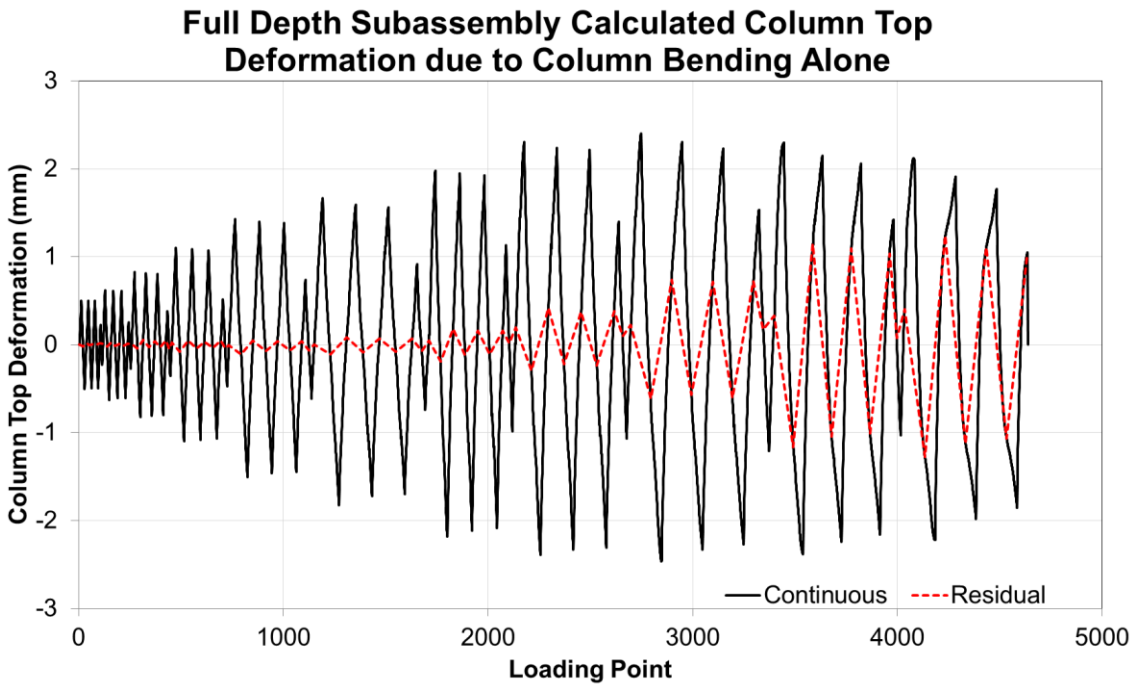

Figure 6-75: Full Depth subassembly modelled column bending deformation (mm).

6.2.5 Components of Displacement

To determine the extent to which column bending and panel zone deformation effect the overall response of the structure, displacement component plots were created for each subassembly. The column top displacement due to panel zone deformation from Section 6.2.2 and the column top displacement due to column bending from Section 6.2.4 were each plotted against the total (measured) column top displacement. These values were also subtracted from the total column top displacement to give an indication of the displacement owing to the bending of the beams. As such the individual values for the column, beam and panel zone displacements for a given measured column top displacement will add to give the column top displacement.

Unit 1 (Isolated):

As shown in Figure 6-76, the majority of the displacement observed in the isolated subassembly can be contributed to the deformation of the beams both elastically and in-elastically. Column top displacement owing to panel zone deformation was less than 1.5mm at maximum drift (5% drift) while column bending displacement was less than 2mm. As such approximately 96% of the total drift was related to beam bending, 2% to column elastic deformation and 2% to panel zone deformation.

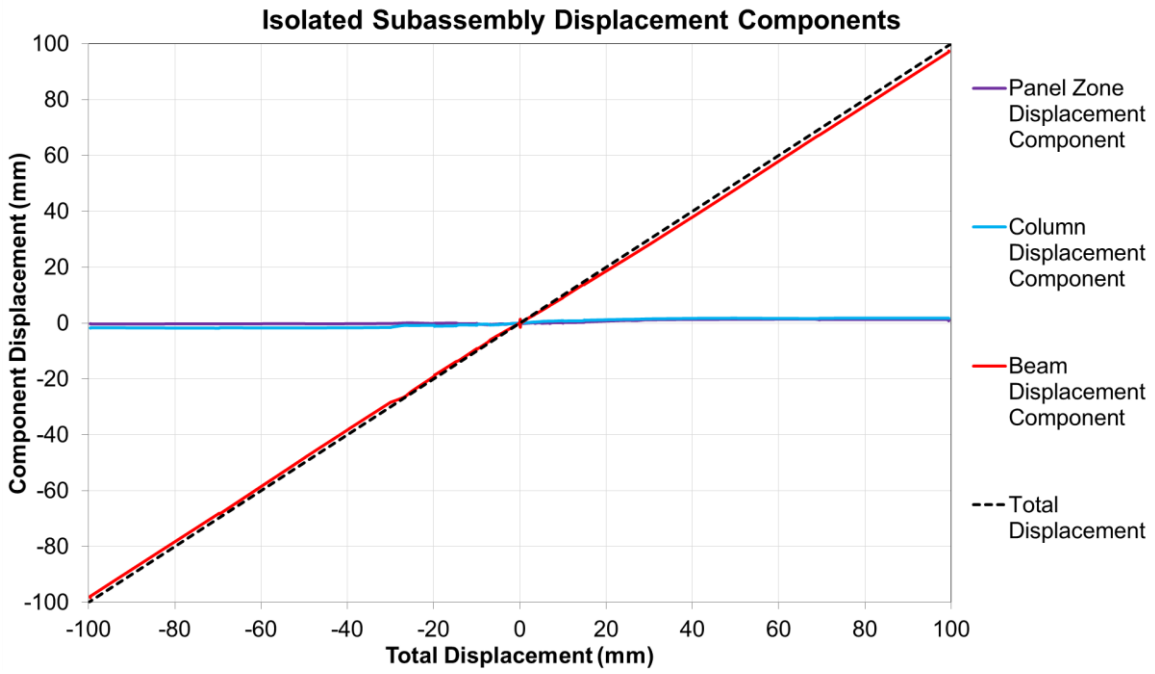

Figure 6-76: Displacements components for the isolated subassembly.

Unit 2 (Transverse):

Like the isolated subassembly, the majority of the displacement observed in the transverse subassembly was contributed to the deformation of the beams as shown in Figure 6-77. Displacement owing to panel zone deformation was again less than 1mm at maximum drift (5% drift) while elastic column displacement was between 2mm and 2.5mm. As such the percentage contributions were approximately 97% beam bending, 2% column elastic deformation and 1% panel zone deformation.

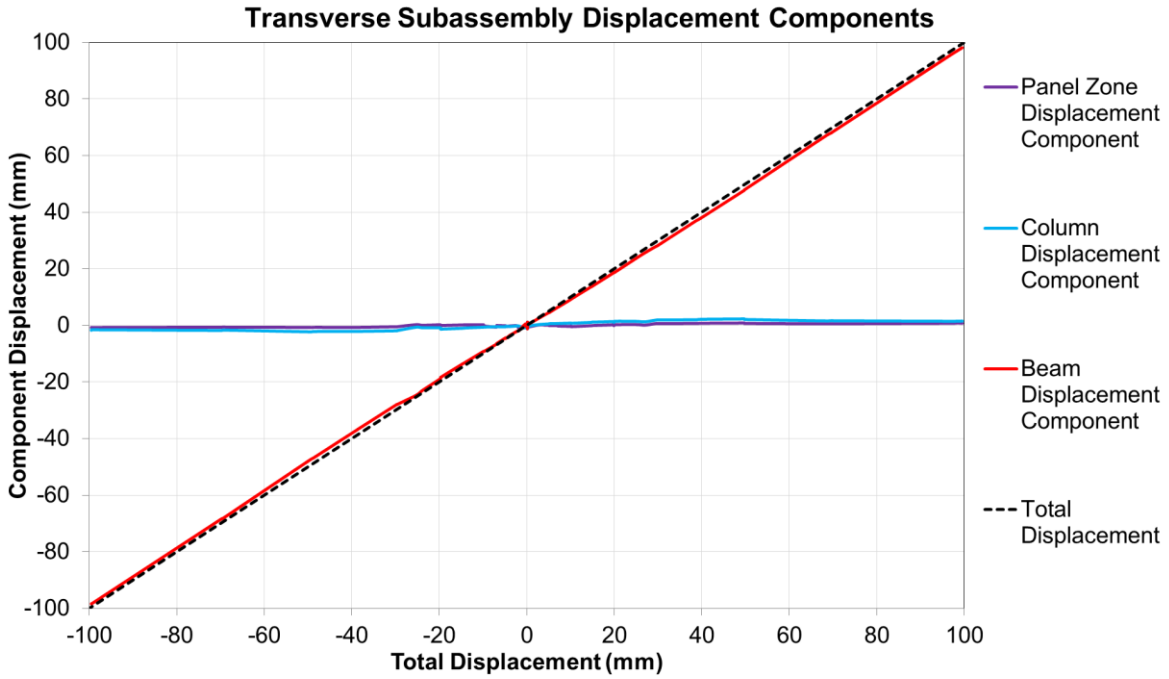

Figure 6-77: Displacements components for the transverse subassembly.

Unit 3 (Longitudinal):

In the longitudinal subassembly an increase in the column contribution was noted as shown in Figure 6-78. Because of incomplete instrumentation the panel zone displacements could not be recorded however it is likely that this too would have increased to 1-1.5mm. Elastic column displacement was up to 2.5mm leaving the remaining 96mm-97mm to beam action. As such the percentage contributions were approximately 96% beam bending, 3% column elastic deformation and 1% panel zone deformation.

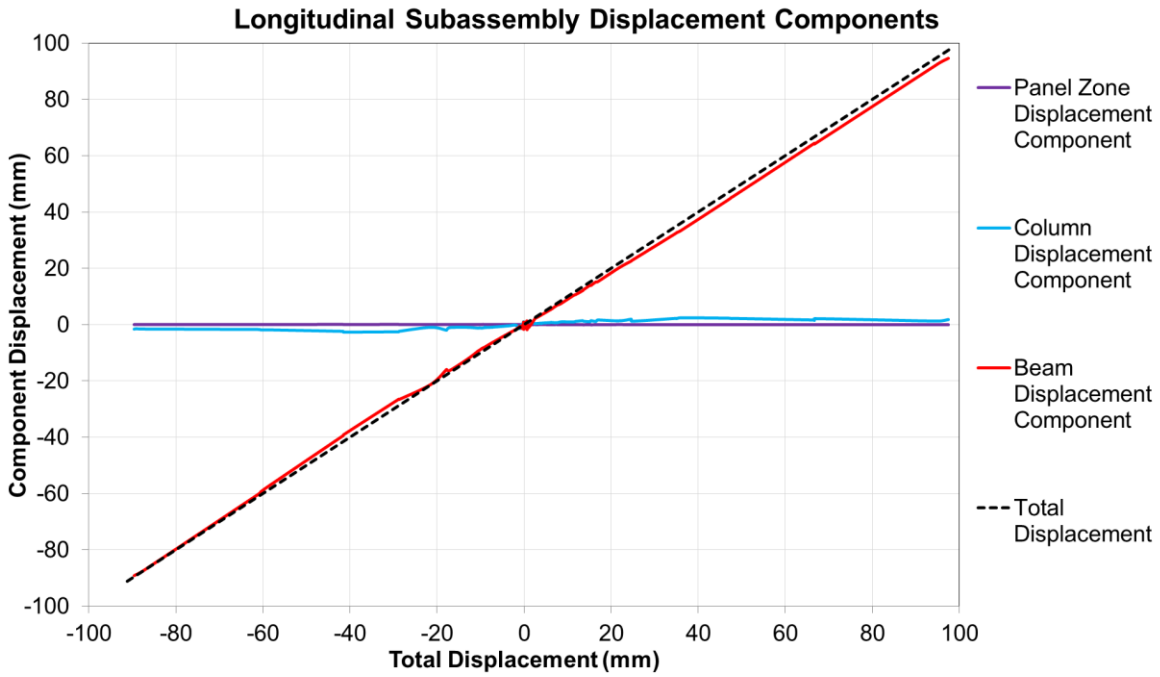

Figure 6-78: Displacements components for the longitudinal subassembly.

Unit 4 (SHJ):

The SHJ subassembly exhibited a lower level of column and panel zone deformation than in the three previous subassemblies. Figure 6-79 shows that the, displacement owing to panel zone deformation was less than 0.5 mm at maximum drift (5% drift) and the elastic column displacement was only 1.5mm. The percentage contributions were therefore around 98% SHJ action, 1.5% column deformation and 0.5% panel zone deformation.

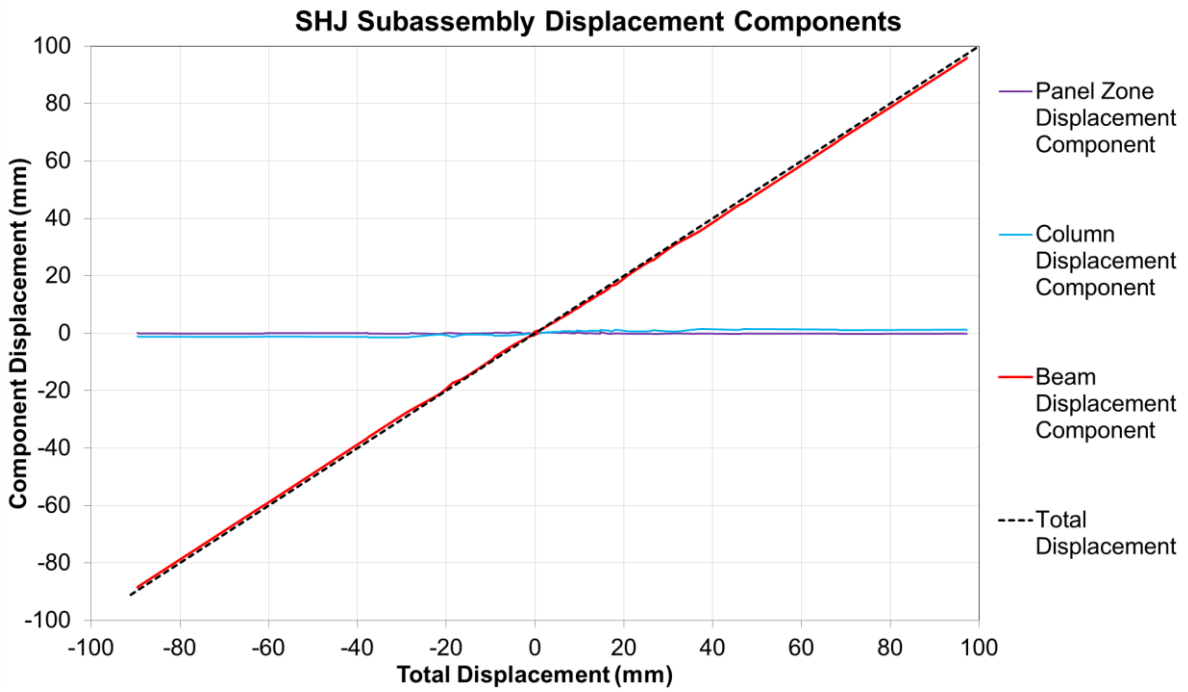

Figure 6-79: Displacements components for the SHJ subassembly.

This trend continued in the extended testing as shown in Figure 6-80. At 10% drift displacement owing to panel zone deformation was still less than 0.5 mm and the elastic column displacement was less than 2mm. This equates to over 99% SHJ action, and less than 1% combined column and panel zone deformation.

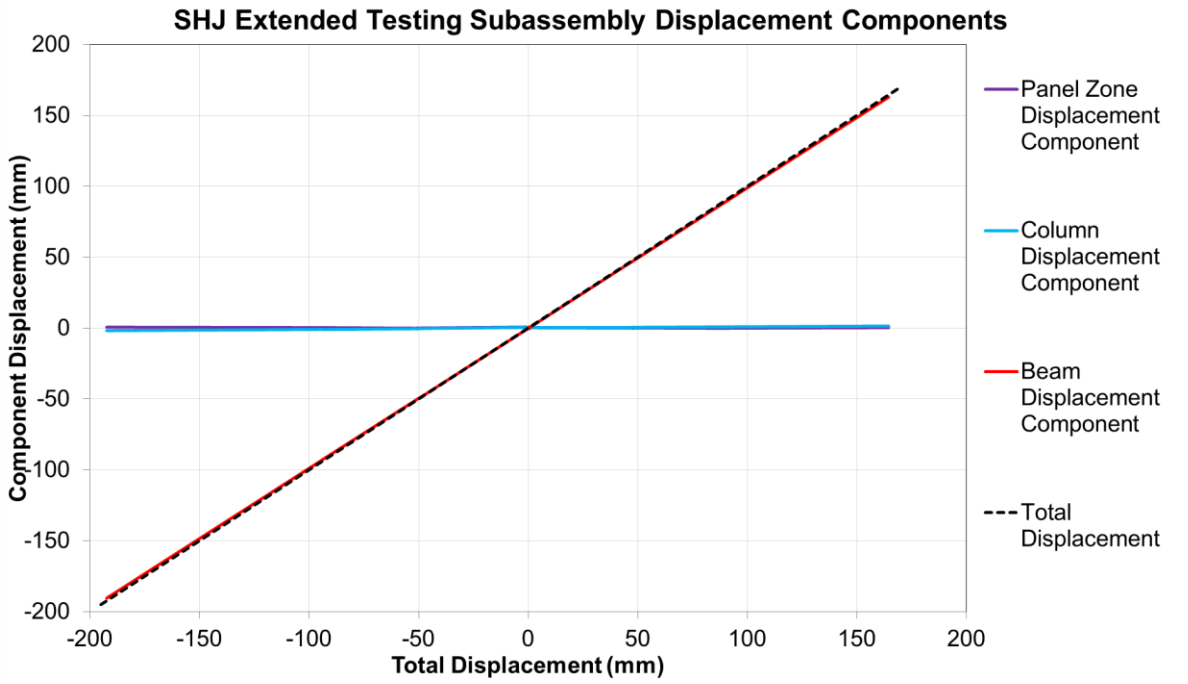

Figure 6-80: Displacements components for the SHJ subassembly under extended testing.

Unit 5 (Full Depth):

In the full depth subassembly showed a similar level of column deformation to the isolated subassembly although the panel zone contribution was reduced. As shown in Figure 6-81, panel zone deformation was around 0.5mm at maximum 5% drift and column displacement was up to 2.5mm. The percentage contributions were therefore approximately 96% beam bending, 3% column elastic deformation and 1% panel zone deformation.

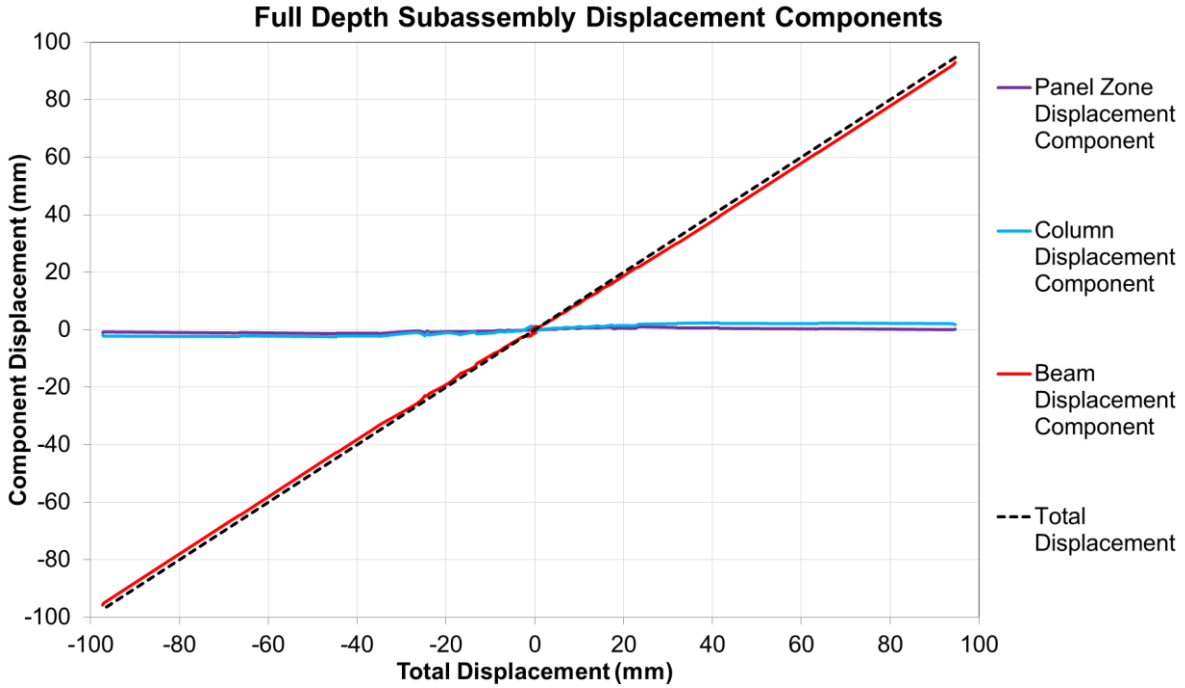

Figure 6-81: Displacements components for the full depth subassembly.

6.2.6 In-Plane Slab Deformations

As described in Section 3.5, the in-plane displacements of the slab surface, relative to its initial position, were determined from the data recorded by the potentiometers on the slab. The plots produced show the total movement of individual points on the grid relative to their initial position (not direction specific). The total displacement (relative to the column centreline) is therefore the sum of the displacements of the individual points between the column and the desired location. The plots displayed below are absolute maximum values and are not specific to any one drift cycle.

Unit 1 (Isolated):

The total horizontal surface displacement of the data points of the slab in the isolated subassembly, taken as the sum of the maximum positive and negative displacements and shown in Figure 6-82, remained less than 2mm throughout the testing. It was also noted that the majority of the movement in the slab occurred between 600m and 1000mm from the column centreline. Furthermore results from the various drift cycle peaks, given in Appendix H, indicate that the majority of the slab surface displacement occurred between 2% drift and 5% drift. This was consistent with the observed crack pattern.

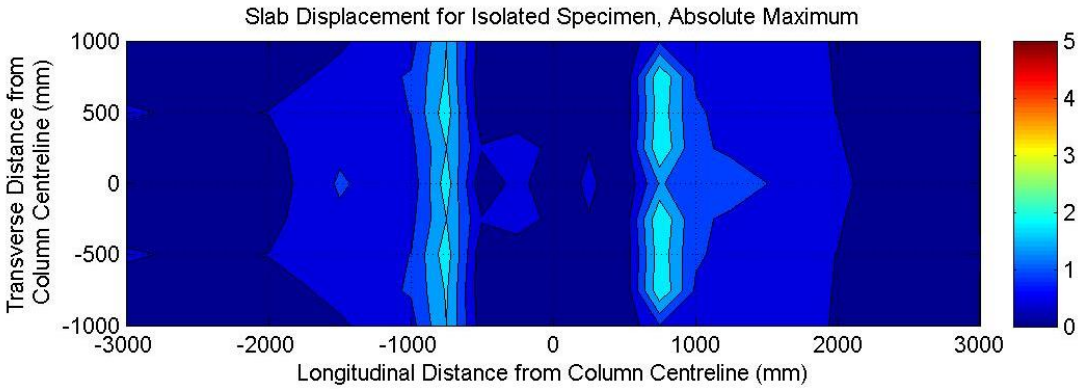

Figure 6-82: Maximum slab surface displacements, isolated subassembly.

Unit 2 (Transverse):

As shown in Figure 6-83, the maximum slab surface displacement of the transverse subassembly increased to around 3mm near to the column. An increased level of slab surface displacement was also noted beyond 1000mm from the column centreline indicating a larger spread of surface cracking. As with the isolated subassembly the majority of the slab displacement occurred between 2% drift and 5% drift as is shown in Appendix H. Again this was consistent with the observed crack pattern and recorded crack widths.

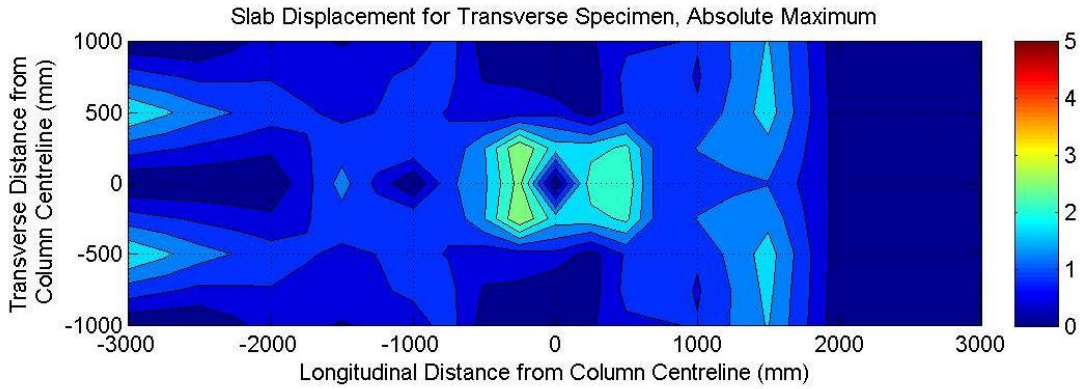

Figure 6-83: Maximum slab surface displacements, transverse subassembly.

Unit 3 (Longitudinal):

In the longitudinal subassembly the maximum slab surface displacement increased to over 5mm near to the column as shown in Figure 6-84. This was primarily due to the large area of surface spalling at high drift levels. A further increased level of slab surface displacement was also noted away from the column centreline. This included over 2.5mm of total displacement at both ends of the primary beam although this was most prominent at the east end of the beam (3000mm). This was unexpected as the secondary beams at the east end of the subassembly were not attached to the deck with shear studs whereas the west end secondary beams (-3000mm) were connected. Significant slab movement, greater than 1mm, began to occur from 0.75% drift as is shown in Appendix H.

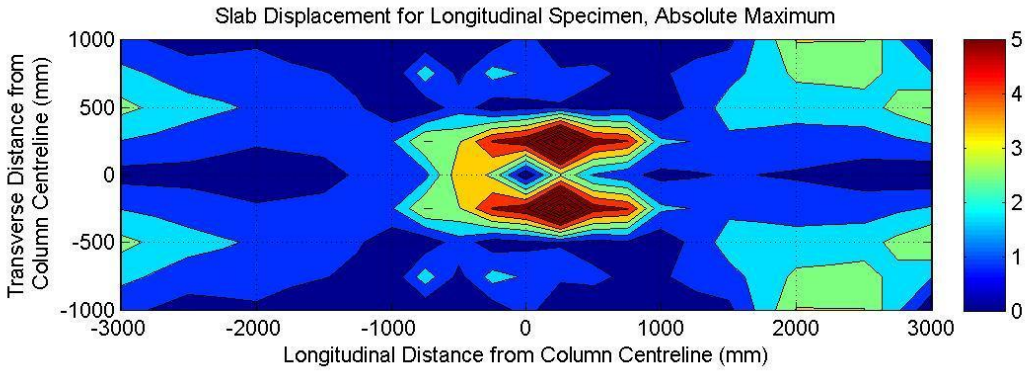

Figure 6-84: Maximum slab surface displacements, longitudinal subassembly.

Unit 4 (SHJ):

As mentioned in section 6.1.4 the SHJ subassembly displayed a reduction in slab damage due to the lack of bending and elongation in the primary beams. This trend was also observed in measurements taken from the slab surface. As shown in Figure 6-85 the outer extremities of the slab showed very little movement whilst the area of slab surrounding the column showed similar levels of movement to the transverse subassembly. Further slab displacement figures can be found in Appendix H. As expected slab surface displacements generally remained below 0.5mm up until sliding was initiated at 0.75% drift. This was followed by gradually increasing displacements around the column and connections as the higher drift cycles progressed.

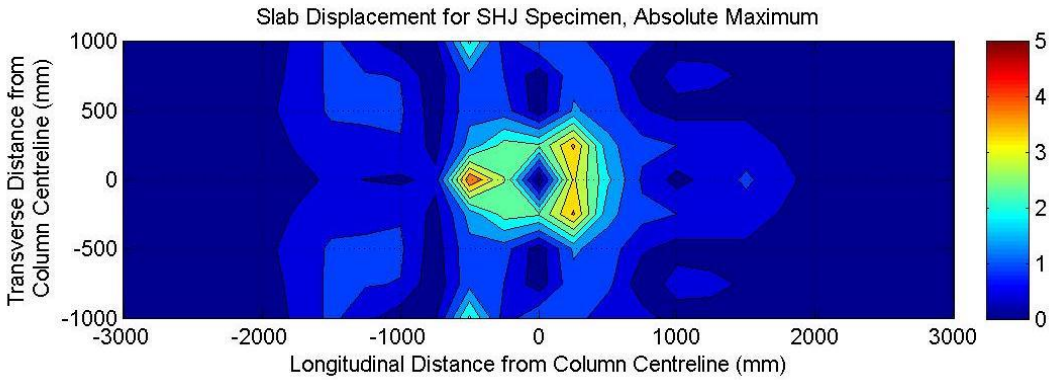

Figure 6-85: Maximum slab surface displacements, SHJ subassembly.

Unit 5 (Full Depth):

The Full Depth subassembly exhibited an increase in crack widths in the area surrounding the column in comparison to the isolated and longitudinal subassemblies and a reduction near the outer extremities of the slab. This was reflected in measurements taken from the slab surface as shown in Figure 6-86. When compared to the transverse and longitudinal subassemblies the outer extremities of the slab showed reduced movement whilst the area of slab surrounding the column showed similar levels of movement to the transverse subassembly. The slab surrounding the column reached peak displacements of around 3.5mm indicating a level of damage between that observed in the transverse and longitudinal tests. Further slab displacement figures can be found in Appendix H.

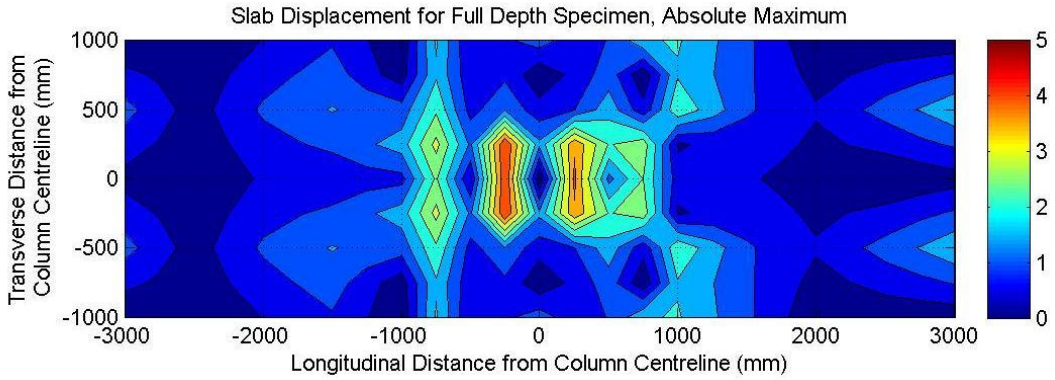

Figure 6-86: Maximum slab surface displacements, full depth subassembly.

6.3 Test Comparison

Comparison of the test data and the model predictions are provided in Table 11 below. In each case the peak and residual strengths are compared along with the initial stiffness of the subassembly (taken as the average stiffness of the 0.2% drift and 0.25% drift cycles). Modelling of the sliding hinge joint was not undertaken hence no model data is available for this. The model values tabulated are those from the models prepared using the measured steel and concrete properties as given in Section 3.

Table 11: Recorded test data and predictions from subassembly models.

	Isolated	Transverse	Longitudinal	SHJ	Full Depth
Actual					
Maximum Recorded Strength (kN)	251	324	365	207	337
5% Drift Residual Strength (kN)	231	212	240	150	254
Initial Stiffness	15400	14100	17300	16800	15700
Model					
Maximum Recorded Strength (kN)	242	271	312	-	271
5% Drift Residual Strength (kN)	242	242	312	-	242
Initial Stiffness	8864	9707	9632	-	9707

The initial stiffness values for the models were taken as the slope of the force-displacement envelope between zero and first yield whereas the initial stiffness values for the test subassemblies were taken as the average slope of the force-displacement envelope up to 0.25% drift (5mm displacement). Force-displacement envelopes for the test subassemblies were created by taking the force at the target drift during the first cycle at each drift level. Further comparison of the model results can be found in the discussion section.

6.3.1 Isolated Subassembly

The model for the isolated subassembly formed an essentially bi-linear hysteresis as shown in Figure 6-87. The initial stiffness of the model was only 58% of that observed in the actual subassembly. This was unexpected as the stiffness of the subassembly should have been lower than the model owing to slop in the support connections. The increased initial stiffness indicates that although the slab was isolated from the column face, some contact still existed between the floor slab and the column. Despite this the bi-linear assumption provides a reasonable fit particularly at higher levels of drift. Table 11 shows that both the peak strength and the residual strength given by the model are within 5% of the actual testing values in both positive and negative loading.

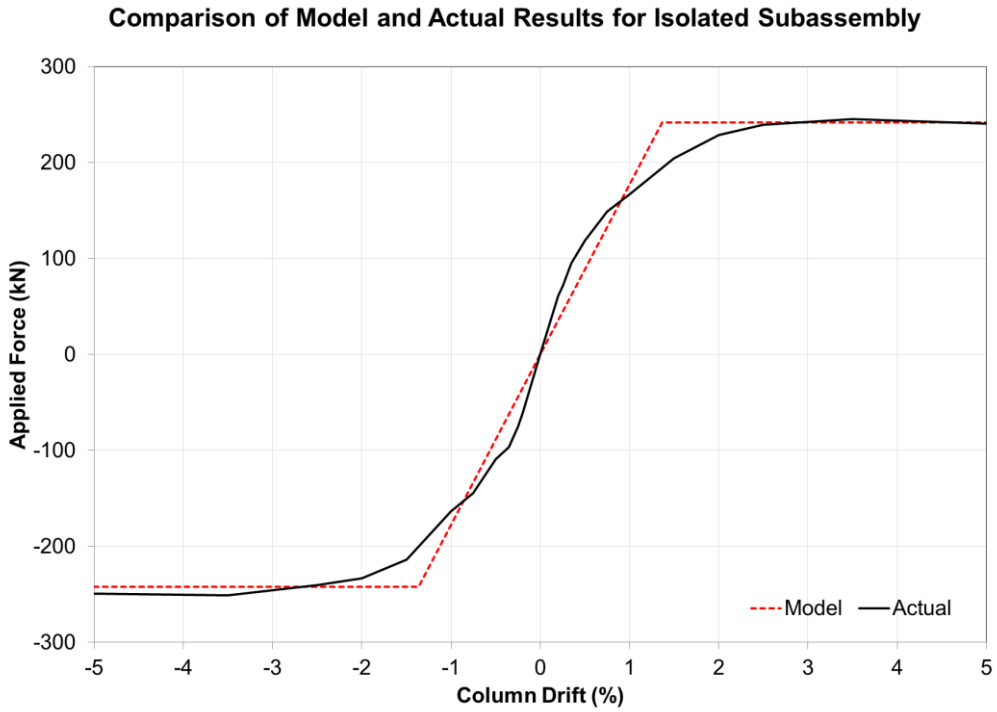

Figure 6-87: Comparison of model and actual results for the Isolated subassembly.

6.3.2 Transverse Subassembly

The model for the Transverse subassembly, shown in Figure 6-88, also predicted a lower initial stiffness than was observed in the actual subassembly although this was less than the isolated subassembly. This indicates that the concrete contact elements in the model had insufficient stiffness or could not replicate the confinement effects present in the test subassemblies. The initial behaviour predicted by the model was a reasonable indication of the actual behaviour up to around 1% drift. Beyond this it is apparent than the model underestimated the resistance provided by the concrete leading to a premature reduction in strength. Table 11 shows that the peak strength predicted by the mode was only 84% of that observed in testing however the residual strength given by the model was within 15% of the actual testing values in both positive and negative loading. The premature strength reduction in the model indicates that the contact mechanism between the column and the slab may not have been modelled with sufficient strength or that other mechanisms may have been increasing the resistance of the slab. It is possible to that the confinement of the concrete in the test subassembly allowed it to sustain higher levels of force than was possible in the model.

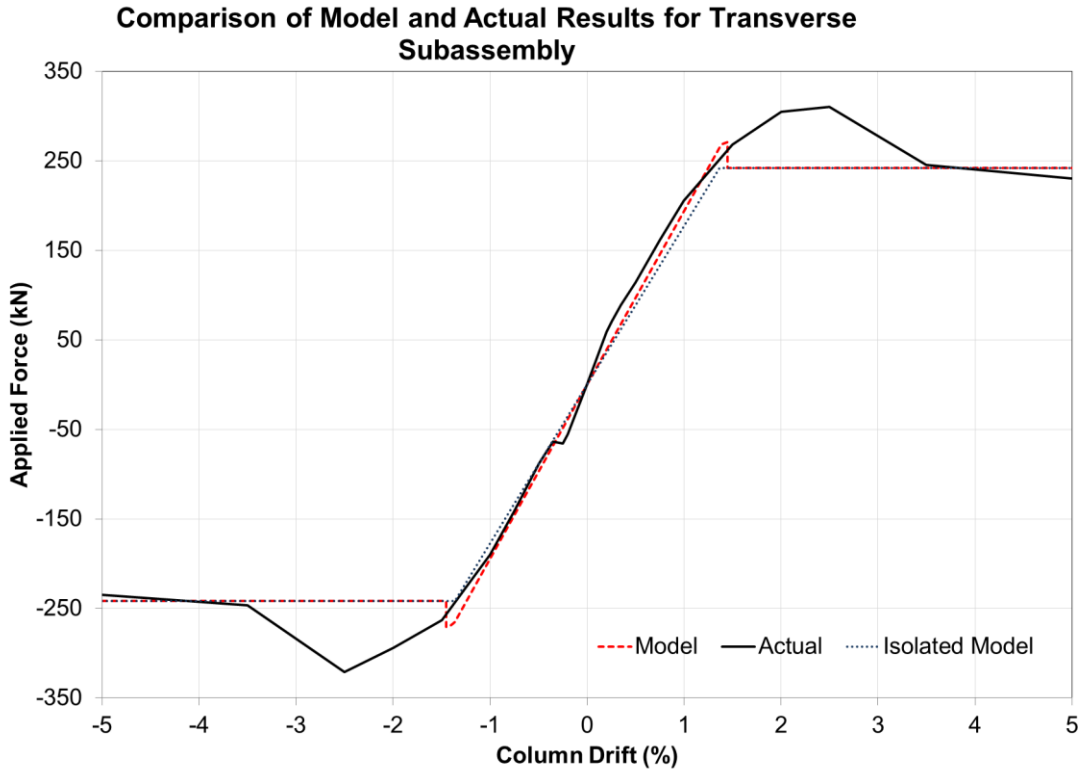

Figure 6-88: Comparison of model and actual results for the Transverse subassembly.

6.3.3 Longitudinal Subassembly

The model for the longitudinal subassembly, shown in Figure 6-89, also predicted a lower initial stiffness than was observed in the actual subassembly. Again this indicates that the concrete contact elements in the model had insufficient stiffness or could not replicate the confinement effects and this appeared to be more significant in the longitudinal subassembly. The initial behaviour predicted by the model was somewhat less accurate than the transverse subassembly with the model predicting a lower strength than was observed in testing. Like the transverse subassembly, the reduction in stiffness due to concrete spalling was premature however the model did continue to gain strength to the point at which it overshot the residual strength. Table 11 shows that the peak strength predicted by the mode was 85% of that observed in testing however the residual strength given by the model was over 25% higher than that observed in testing.

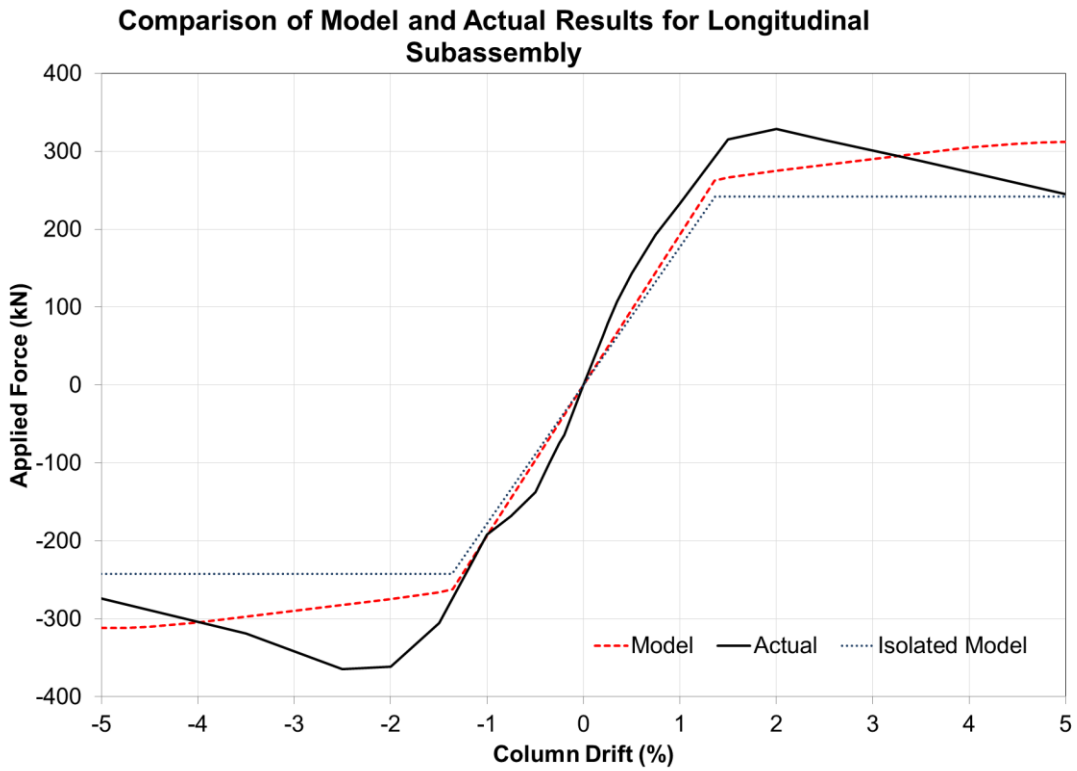

Figure 6-89: Comparison of model and actual results for the Longitudinal subassembly.

6.3.4 Full Subassembly

The results from the full depth subassembly were compared with the model for the Transverse subassembly as shown in Figure 6-90. The increased stiffness of the subassembly owing to the thickened slab was immediately obvious with the model providing a constant underestimate of the performance of the subassembly. Table 11 shows that the initial stiffness of the model was 62% of that observed, the peak strength predicted by the mode was only 80% of that observed and the residual strength given by the model was 95% of the actual testing.

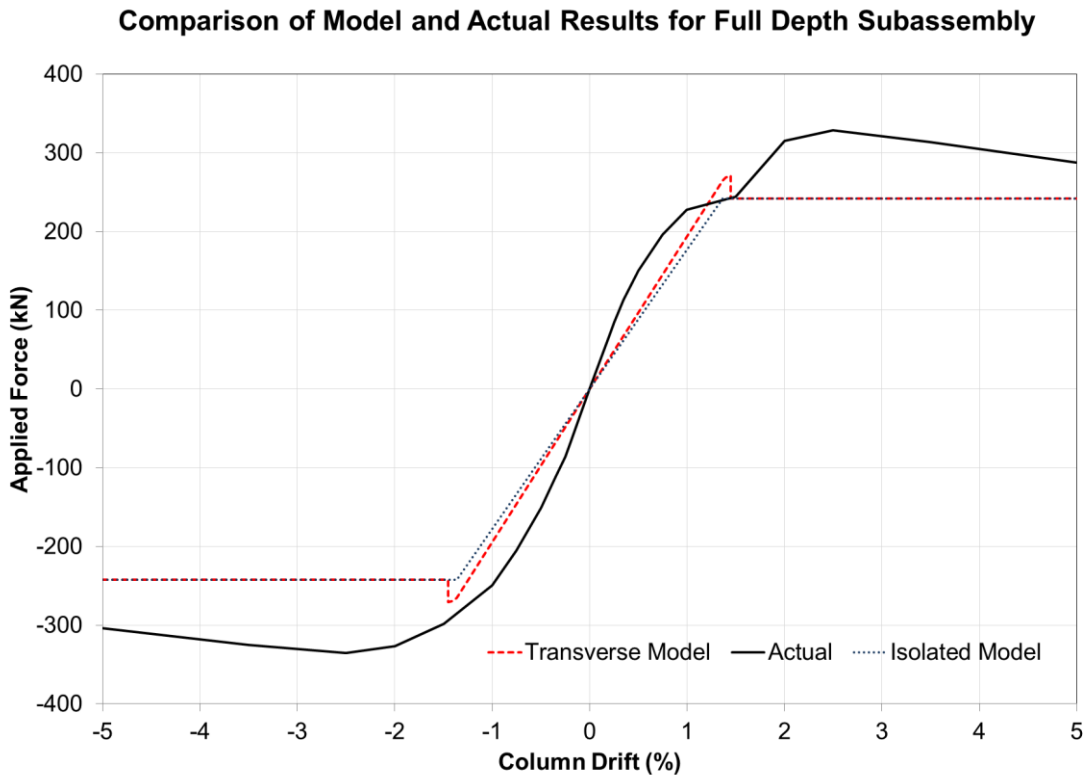

Figure 6-90: Comparison of model and actual results for the Full Depth subassembly.

7 Discussion

7.1 Slab Effects

7.1.1 Isolation detailing

On comparison to the theoretical section capacity of the beams it was noted that the test subassembly strength was higher than the full overstrength capacity of the two beams. This implied that, despite the isolation, some slab effects were still taking place and a connection between the slab and the column face still existed. The polystyrene blocks placed to isolate the slab had been cut to fit around the end plate and the gusset plate on the beam, as shown in Figure 7-1. Because of space limitations the end plate remained exposed as polystyrene blocks could not be fitted into the space.

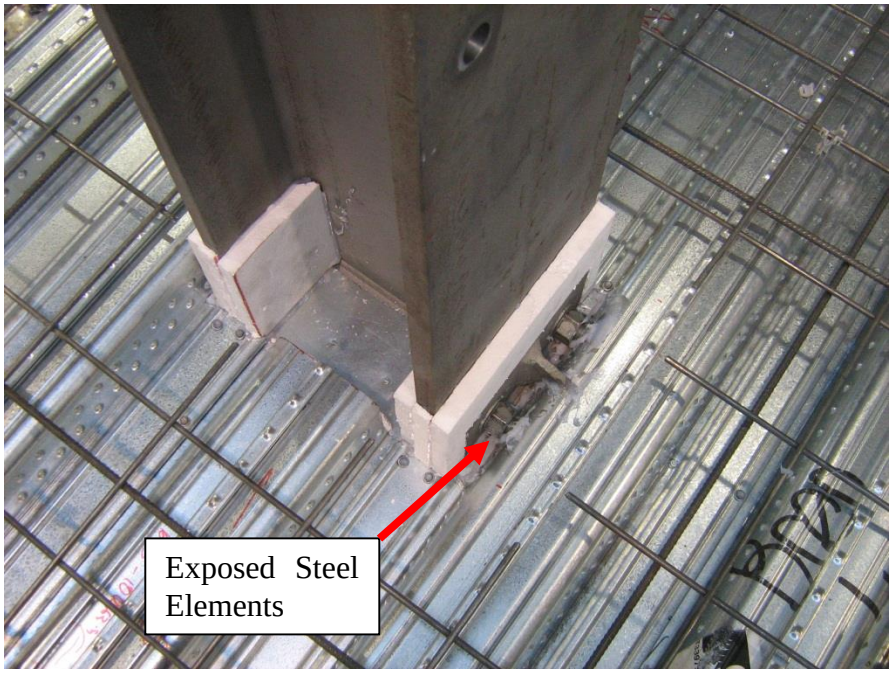

Figure 7-1: Exposed connection steelwork in the isolated subassembly prior to pouring.

As such it was theorised that some interaction between the slab and the column had occurred through these elements. From this we can identify that careful detailing is required to ensure total isolation of the column from the slab.

7.1.2 Isolating the Slab

The effects of isolating the slab from the column face can be determined by comparing the results of the isolated and transverse subassemblies as shown in Figures 7-2 and 7-3. The transverse subassembly exhibited a peak strength 23% higher than that observed in the isolated subassembly although this resulting in higher levels of damage to the subassembly particularly at higher levels of drift.

As shown in Figure 7-2 and Table 11, the slab had minimal effect on the initial stiffness of the structure however as drift levels increased the transverse subassembly showed an increased level of stiffness than the isolated subassembly.

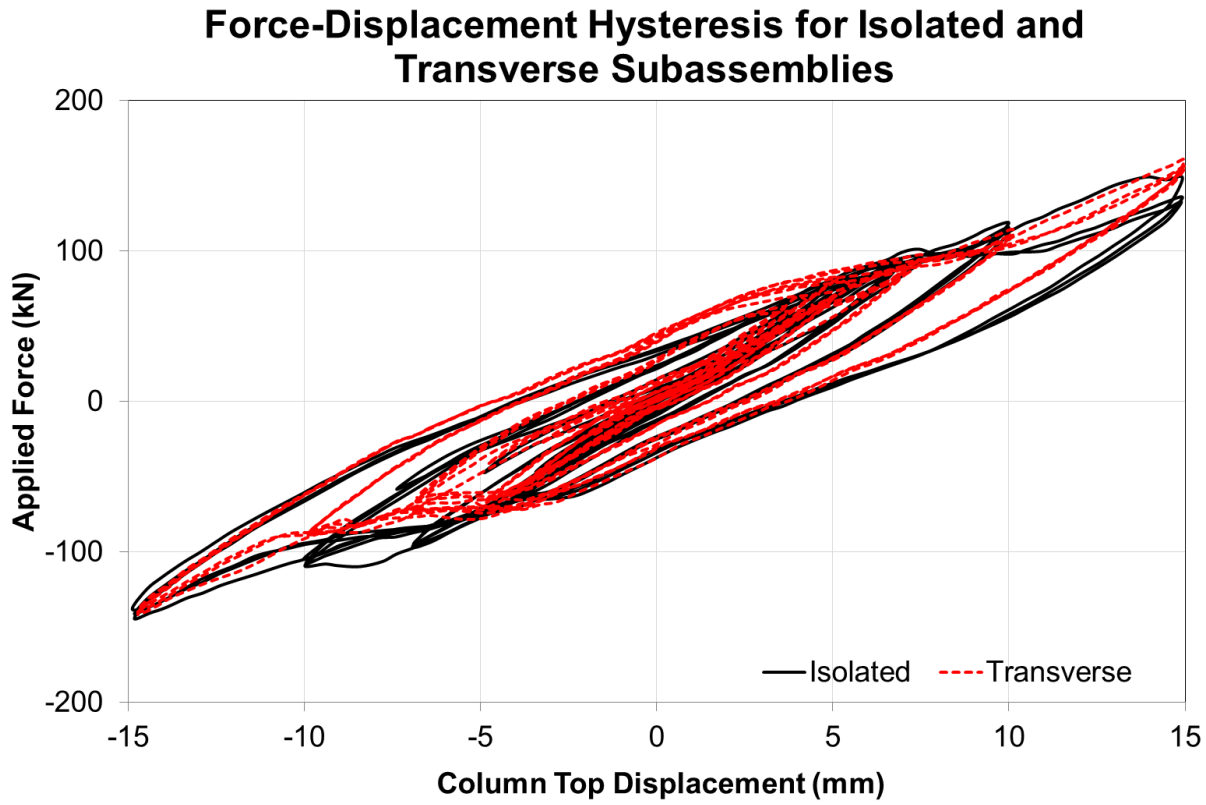

Figure 7-2: Comparison of hysteresis loops for the Isolated and Transverse subassemblies, 0.2%-0.75% Drift.

The transverse subassembly peaked at 2.5% drift as opposed to 3.5% drift for the isolated subassembly. This indicates an earlier onset of yielding and buckling in the beams and was expected given that the presence of the slab increased the lever-arm of the beam-column

connection resulting in greater moments for a given rotation. It was also noted that once the concrete surrounding the column spalled at 3.5% drift the strength of the transverse subassembly dropped suddenly to a similar level as the isolated subassembly. Some reduction in strength below isolated subassembly levels was noticed during the second and third cycles at 3.5% and 5% drift which was likely due to increased yielding damage to the transverse subassembly beams.

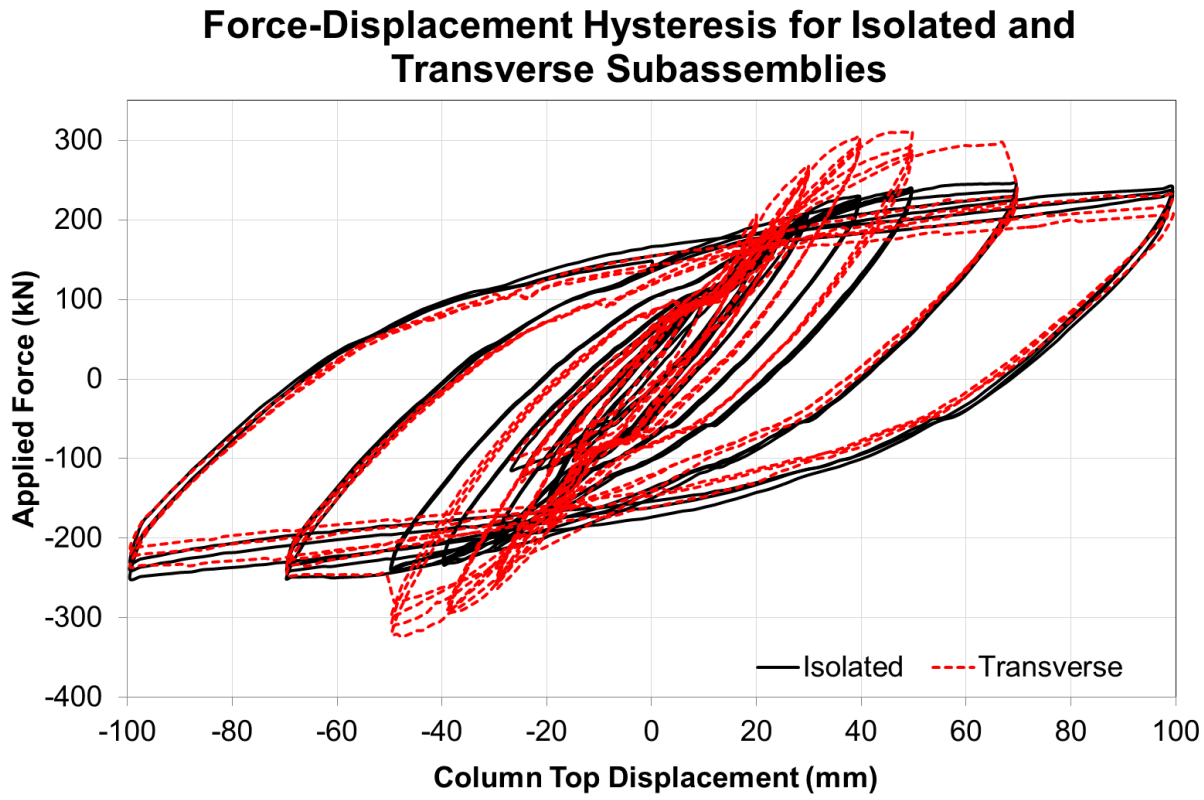

Figure 7-3: Comparison of hysteresis loops for the Isolated and Transverse subassemblies, 1%-5% drift.

The transverse subassembly showed an increased level of slab cracking over that observed in the isolated subassembly. Transverse cracking in the isolated subassembly was limited to the area of slab above and beyond the second rib from the column face. In the transverse subassembly cracking was observed in this area indicating an increase level of movement in the slab. More extensive transverse cracking was also noticed across the slab indicating a greater level of tensile force in the slab. This may have been partially attributed to tensile forced being transferred through the slab via strut and tie mechanisms. Spalling of the slab beside the column in the isolated subassembly was minimal with only surface concrete which had fused to the polystyrene separating. Spalling of the slab beside the column in the transverse

subassembly was confined to the area between the column face and the first rib in the deck. This was likely to have acted as a fuse to prevent further damage in the slab. It should be noted that the cracking in the slab was dispersed with most cracks being of insufficient width to have caused damage to the slab reinforcing.

From this we can identify that the presence of the slab in contact with the column will increase the ultimate strength of the subassembly however this comes at the expense of higher levels of damage to both the beams and the slab. Furthermore the failure of the slab in contact with the column produces a sudden loss of strength although the subassembly will still produce a similar level of residual strength to an isolated subassembly. This slab compression failure however will act as a fuse to prevent more extensive damage to the floor slab.

7.1.3 Deck Tray Direction

The direction of the deck tray had a pronounced effect on both the strength and performance of the system as can be seen by comparing the behaviour of the transverse and longitudinal subassembly. The presence of the length of full depth slab above the primary beams in the longitudinal subassembly resulted in a 10% increase in the ultimate strength of the system over the transverse subassembly however the performance of the system was adversely affected as can be seen in Figures 7-4 and 7-5.

As shown in Figure 7-4 and Table 11 the direction of the deck tray had minimal effect on the initial stiffness of the structure however as drift levels increased the longitudinal subassembly showed a higher level of stiffness than the transverse subassembly.

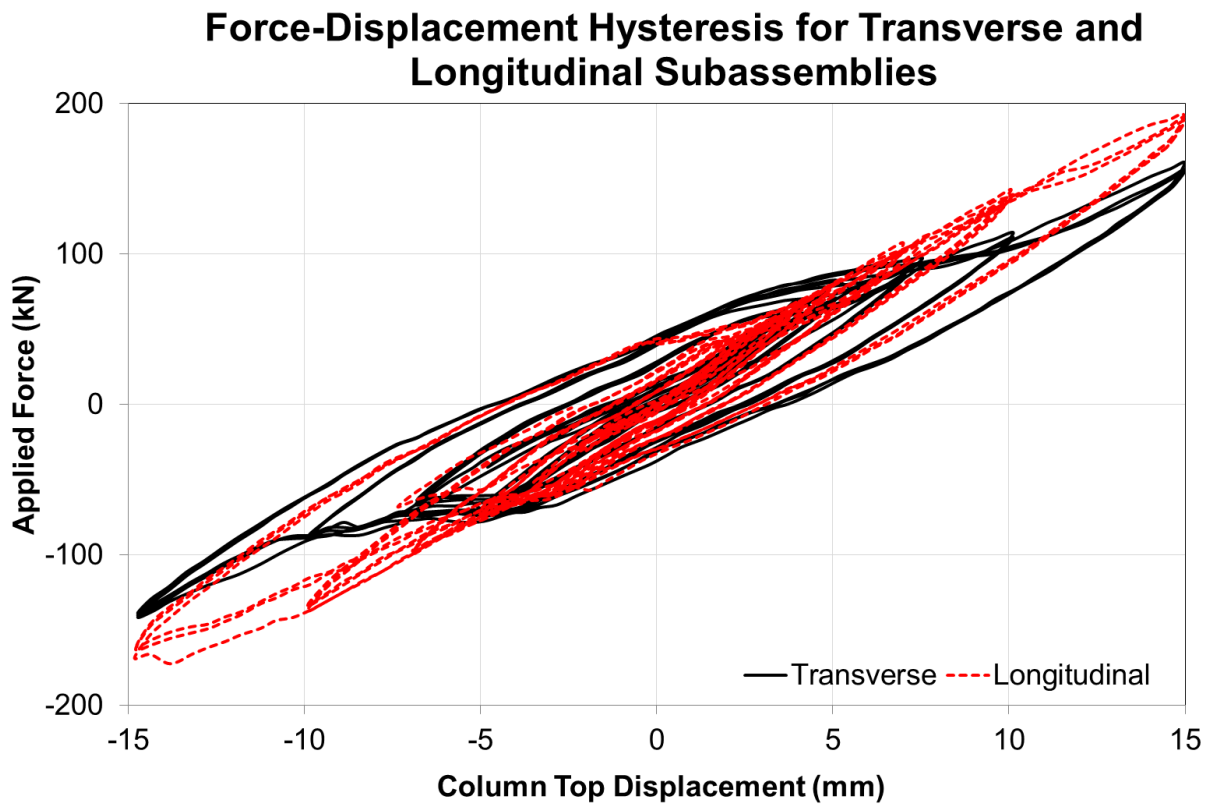

Figure 7-4: Comparison of hysteresis loops for the Transverse and Longitudinal subassemblies, 0.2%-0.75% Drift.

The peak strengths in the longitudinal system occurred at a lower level of drift (40mm) than those in the transverse subassembly (50mm). This was primarily due to an earlier onset of buckling in the bottom flanges of the beams in the longitudinal subassembly. The post-yield decrease in the global stiffness of this subassembly was similar to the transverse subassembly as shown in Figure 7-5.

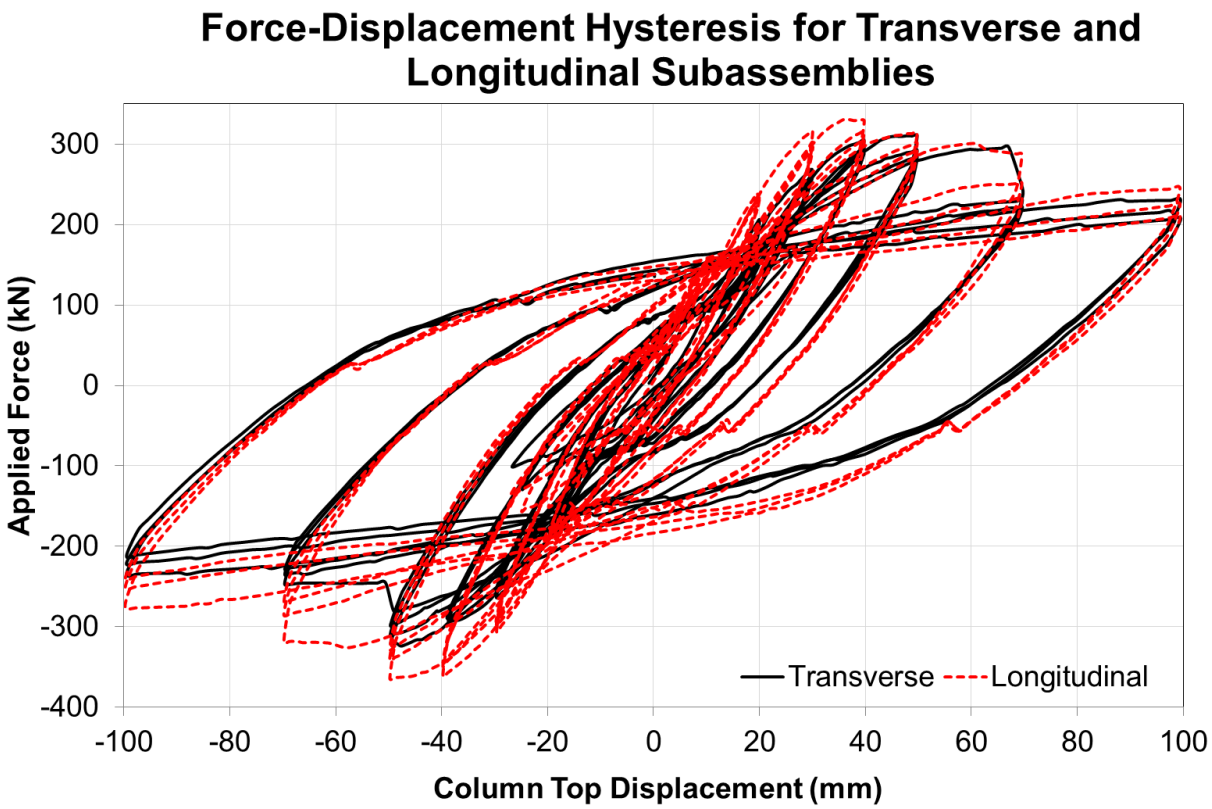

Figure 7-5: Comparison of hysteresis loops for the Transverse and Longitudinal subassemblies, 1%-5% drift.

It should be noted that both sets of data in Figure 7-5 are not corrected. For a comparison of the corrected and uncorrected data for the longitudinal subassembly see Figure 7-6.

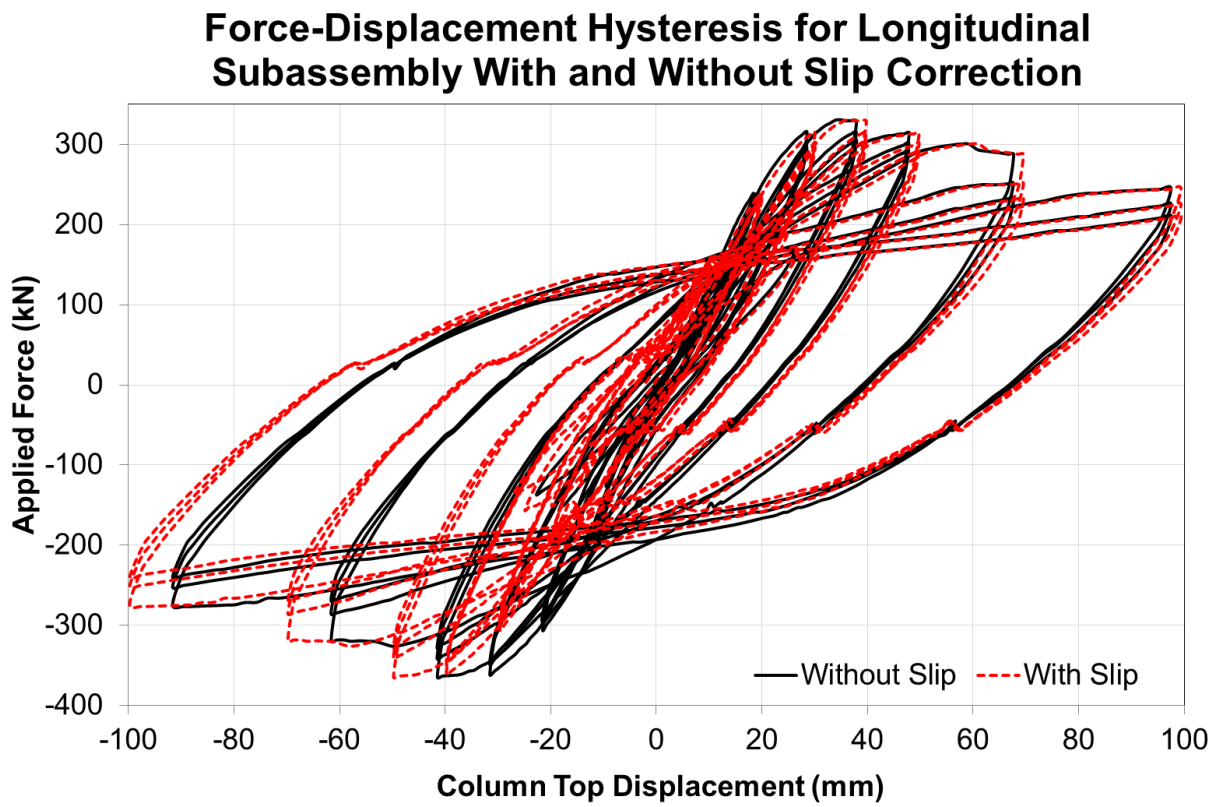

Figure 7-6: Comparison of hysteresis loops for the Longitudinal subassembly with and without correction for slip.

The earlier onset of buckling observed in the longitudinal subassembly would appear to indicate a higher level of yielding deformation (stretch) in the bottom flanges. This in turn indicates that a greater tensile force was being carried by the bottom flanges of the beams than was present in the transverse subassembly. As such it is expected that the slab in contact with the column would be subjected to increased compressive forces which would seek the weakest point in the surrounding slab. In the transverse subassembly this was the first rib in the deck tray from the column face and this is where damage was observed to occur.

In the longitudinal subassembly the weak point is also the first rib in the deck however the orientation of the deck dictates that this must be either a vertical shear failure through the depth of the concrete along the primary beam or a horizontal shear separation of the concrete between the deck ribs along the primary beam (see Figure 7-7). The latter was observed during testing of the longitudinal subassembly and resulted in total separation of the slab surface from the primary beams.

Figure 7-7: Vertical and horizontal concrete shear failure modes in the longitudinal subassembly.

Horizontal shearing was observed close to the column face however the presence of the reinforcing mesh likely prevented this from propagating into the slab. This still leaves the full depth section of slab which is secured to the primary beam to transmit forces into the slab resulting in the more dispersed crack pattern observed and a higher level of damage to the slab. In the transverse subassembly, flexural cracking tended to occur above the ribs in the deck where the slab was thinnest. In the longitudinal subassembly transverse cracks needed to cross both full depth and reduced depth sections of the slab. As such fewer transverse cracks occurred and those that did tended to exhibit higher crack widths than those in the transverse subassembly. This was believed to be primarily a mechanism to distribute surface displacements of the slab (controlled by the deformations of the beams) across fewer cracks. Conversely longitudinal cracking was noticeable greater than in the transverse subassembly with the cracks tending to form over the ribs in the deck.

This increased capacity also puts increased stresses on the rest of the system. Levels of column and panel zone deformation were higher in the longitudinal subassembly indicating that more demand was being placed onto the columns. Likewise the end plate separation was greater for the longitudinal subassembly indicating a higher level of force being transferred through the connection.

It can therefore be concluded that running the deck tray parallel to the primary beams will increase the ultimate strength of the subassembly in this direction however this comes at the expense of higher levels of damage to both the beams and the slab. Failure of the slab in contact with the column will still produce a sudden loss of strength and this loss will be greater than a subassembly with a transverse deck tray as the slab compression failure will occur at a higher level of force. Given the higher level of damage observed in the longitudinal subassembly,

structures with the deck tray laid parallel to the main beams would likely benefit from the isolation of the slab from a durability perspective.

7.1.4 Sliding Hinge Connection

The sliding hinge connection tested had been designed to protect the beams and columns of the structure from inelastic damage at drift levels up to 5% drift. In this respect the sliding hinge joint performed well with no visible beam or column damage observed up to 5% drift. Beyond 5% drift the bolts in the bottom flange plate ran out of travel in their slotted holes and some damage did occur to the beams. However it is believed that with proper design a sliding hinge type connection will prevent inelastic damage from occurring in the beams or columns of a structure.

The vast majority of the damage observed in the sliding hinge joint connections was a result of vertical displacement incompatibility. As the beam rotated prying of the top and bottom flange plates occurred along with shearing of the web plate bolts. The flange plate prying was largely elastic deformation up to 5% drift however some permanent deformation was noted after the 5% and 10% drift cycles as shown in Figure 6-15. This is an inherent design fault of the typical sliding hinge connection and is unlikely to have a significant effect on the connections performance under serviceability load. Under ultimate limit state loading however this plate prying could have a detrimental effect on the connections performance through reduced sliding and axial elongation of the flange plate bolts. Solutions are currently being developed for a non-prying form of sliding hinge connection to remedy this issue.

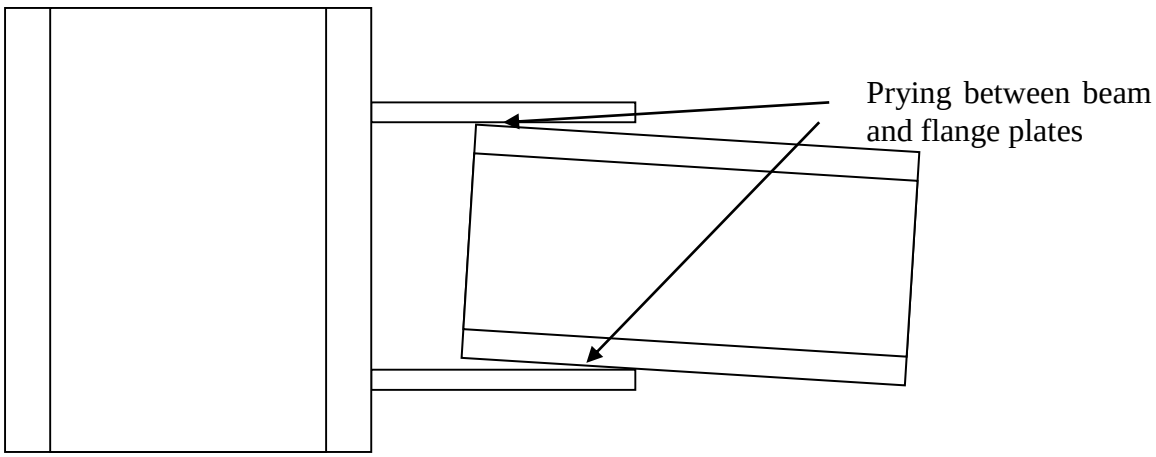

Figure 7-8: Prying of the Sliding Hinge Connection flange plates.

Shearing of the web plate bolts was another form of damaged observed in the SJH connection. As the beams rotated in the connection the web plate bolts moved vertically within the slotted holes as shown in Figure 7-9. This eventually led to binding of the bolts on the top and bottom of the slotted hole. The bolts furthest from the column were the most adversely effected with two bolts failing at 5% drift. This would have reduced the sliding friction resistance generated by the web plate. This issue too is inherent to the traditional design of sliding hinge connections and will require further work to rectify. This may include the need to elongate holes both horizontally and vertically.

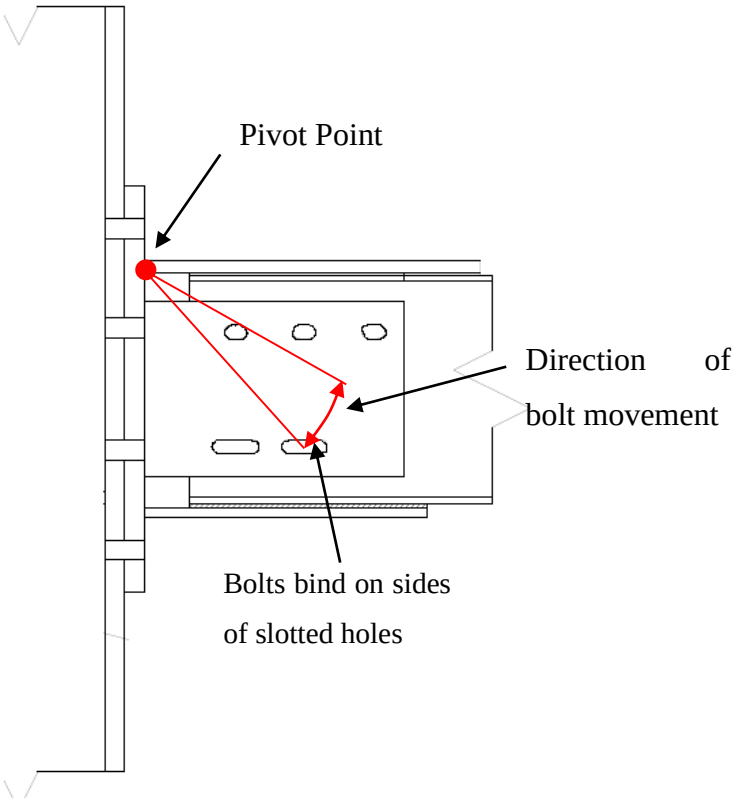

Figure 7-9: Illustration of bolt binding in the SHJ connection.

The slab on the SHJ subassembly sustained a similar level of damage to that observed in the transverse subassembly indicating that elastic deformations of the beam were still occurring. As in the transverse subassembly most of the cracks observed were not wide enough to have damaged the floor slab reinforcing.

7.1.5 Full Depth End Block

The effects of including a section of full depth slab around the column can be determined by comparing the results of the transverse and full depth subassemblies as shown in Figures 7-10 and 7-11. The full depth subassembly exhibited a peak strength 5% higher than that observed in the transverse subassembly with reduced slab damage and a less rapid drop in strength after peak.

As shown in Figure 7-10 and Table 11 the slab had a slight effect on the initial stiffness of the structure. The thinner hysteresis loop in the full depth subassembly below 0.75% drift (15mm displacement) was a result of reduced slip in the column base plate.

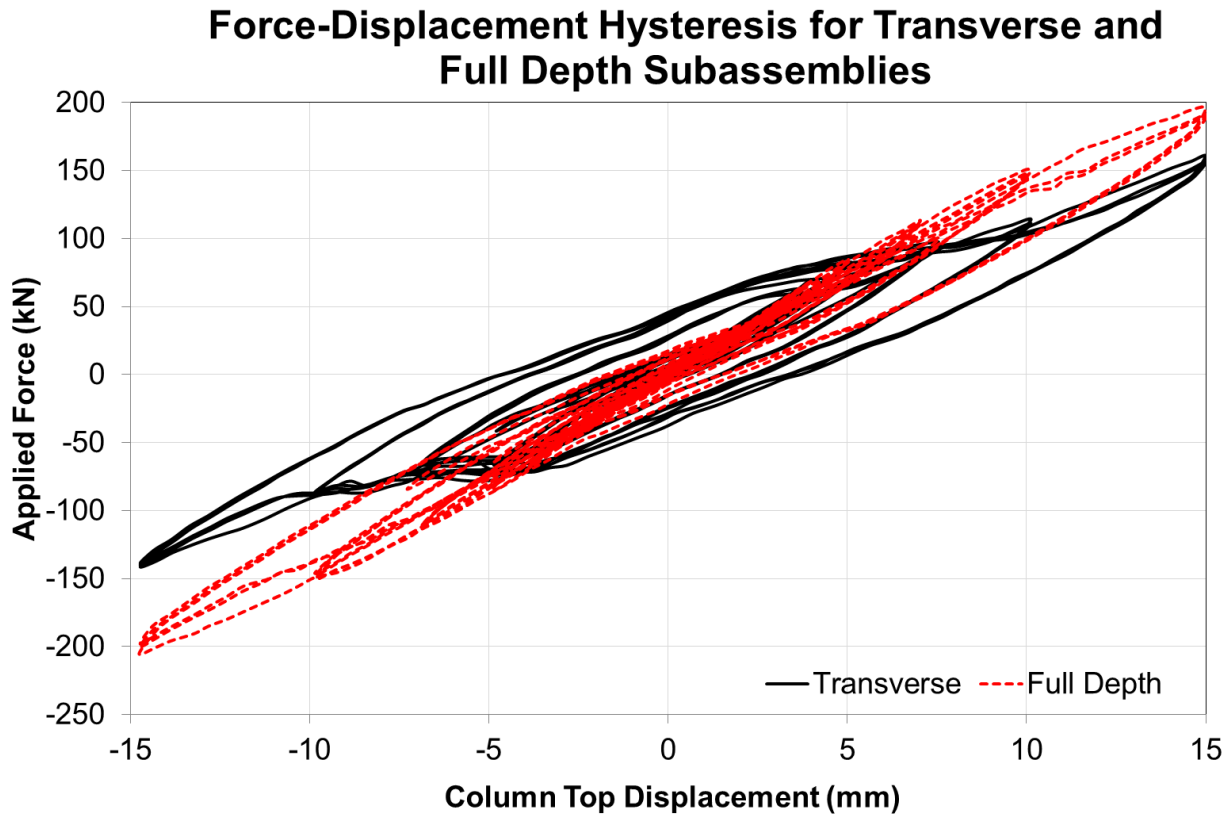

Figure 7-10: Comparison of hysteresis loops for the Transverse and Full Depth subassemblies, 0.2%-0.75% Drift.

Like the transverse subassembly, the full depth subassembly peaked at 2.5% drift (50mm displacement) however as can be seen in Figure 7-11 the strength drop off following peak strength is greatly reduced in the full depth subassembly. Residual strength in the full depth

subassembly was 20% higher than that observed in the transverse subassembly indicating that, at 5% drift, the slab was still providing some resistance.

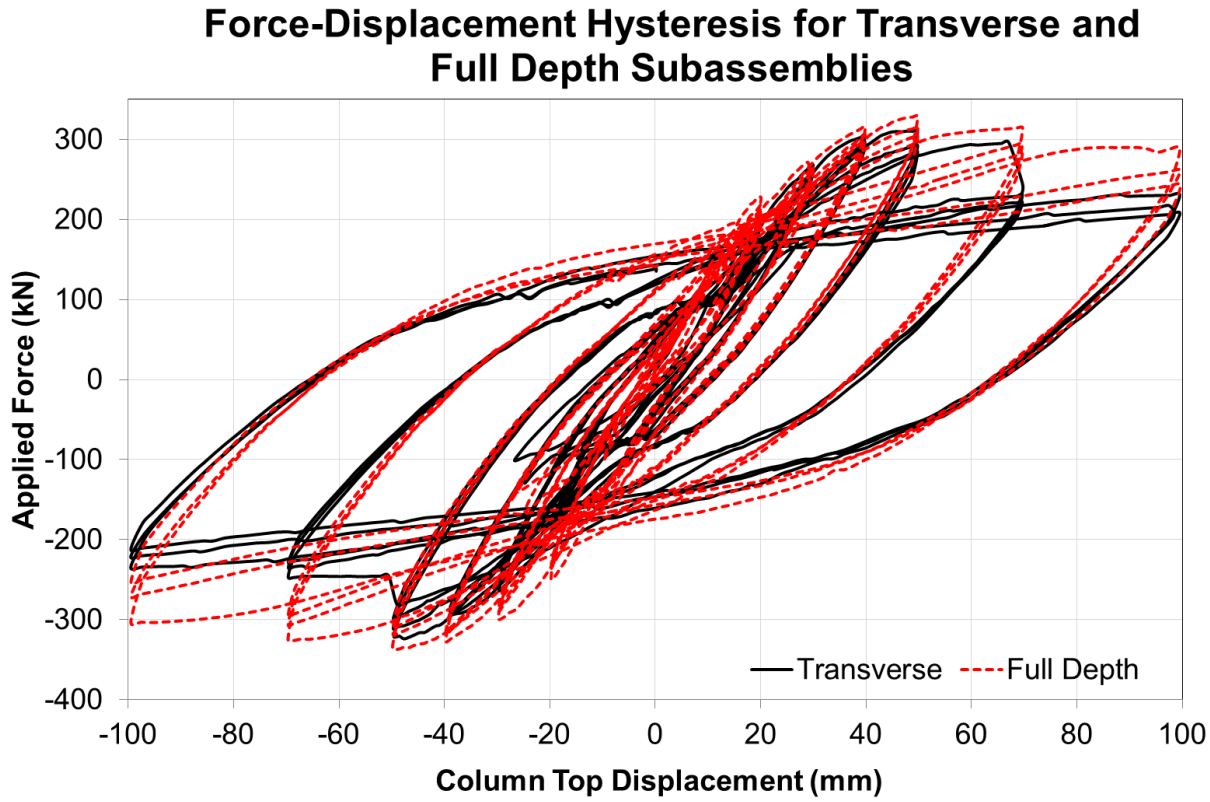

Figure 7-11: Comparison of hysteresis loops for the Transverse and Full Depth subassemblies, 1%-5% drift.

Again it should be noted that both sets of data in Figure 7-11 are not corrected. For a comparison of the corrected and uncorrected data for the full depth subassembly see Figure 7-12.

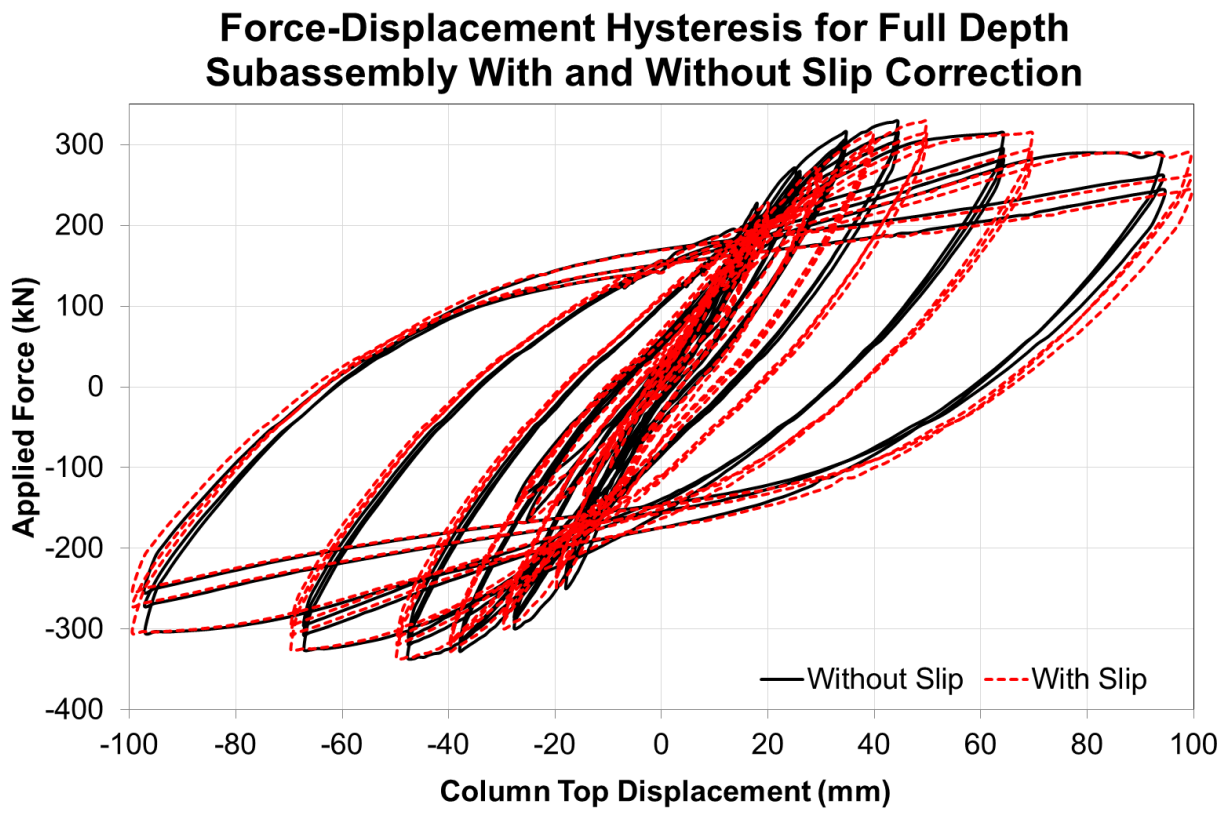

Figure 7-12: Comparison of hysteresis loops for the Full Depth subassembly with and without correction for slip.

It is apparent from these results and from test observations that the section of full depth slab surrounding the column did not exhibit the sudden compression failure observed in the transverse subassembly. This resulted in a more ductile form of strength loss after peak. The increased resistance did however lead to a larger average crack size in the full depth subassembly particularly in the area surrounding the column. Compression or shearing failure of the concrete surrounding the column tended to occur at the edges of the full depth section indicating that the section of concrete above the deck tray ribs is still the weak point in the slab. Outside of this area the crack widths observed were still too small to have caused damage to the reinforcing.

The higher resistance provided by the subassembly also led to an increase in the level of beam flange buckling. This indicates a greater magnitude of tensile force being carried by the beam flanges and hence a greater corresponding compression force being carried by the slab.

7.2 Performance

7.2.1 Steel Strength Degradation

The primary mode of strength loss in the steel components of the MEP subassemblies was buckling of the bottom flange of the beams. This tended to occur between 2% and 2.5% drift with the bottom flange of each beam buckling in compression. During larger drift cycles these buckles remained in the same position and grew in depth. The top flanges of the beams in subassemblies with the slab cast in contact with the columns also buckle however this buckling occurred much later in the testing and was less in magnitude. It should be noted that 2% drift is a commonly accepted level of drift for a steel moment resisting frame. As such the buckling of the beams is occurring earlier than would generally be desired. The 310UB section used is not generally considered a large beam and given this early buckling it may be necessary to limit the size of beam used in structures with composite action to ensure a concrete failure occur before the beams begin to buckle.

The remaining steel components showed minimal degradation. The steel columns remained elastic throughout the test series as did the panel zone. Recorded lift-off of the moment end plates was also minimal and there were no visible signs of elongation to any of the moment end plate bolts. This indicates that the overstrength provisions given by NZS3404 were sufficient to protect the panel zone and connections. Some shear stud failures were noted however in all cases these were owing to poor welding.

7.2.2 Slab Degradation

Flexural cracking of the slab occurred from 0.25% drift in all subassemblies tested. Transverse cracking of the concrete slab tended to occur above the ribs of the deck tray where the slab was shallowest. This tended to lead to a dispersed crack pattern with numerous small cracks occurring above the deck tray ribs. The widths of these cracks tended to increase closer to the column indicating a higher level of slab bending in this region. In the longitudinal direction cracks tended to be less frequent (with the exception of the longitudinal subassembly) owing to the presence of the full depth troughs intersecting these cracks.

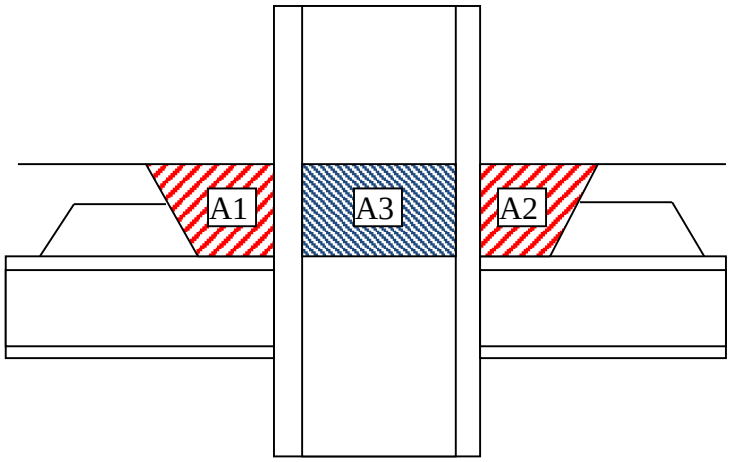

Figure 7-13: Areas of concrete failure in the transverse subassembly.

The most prominent concrete strength loss mode was the compression failure of the concrete at the column faces combined with the shearing of the area of concrete between the column flanges. In the subassemblies with transverse deck trays, the area of concrete between the flanges of the column, A3 as shown in Figure 7-13, was similar to the minimum area of concrete required to shear at the column face (area's A1 and A2). As such, shearing of the concrete between the column flanges was a significant mode of concrete strength loss observed in testing. Similarly in the longitudinal subassembly, shearing failure of the slab along the primary beam occurred at the same level of drift as shearing of the concrete between the column flanges indicating that both failure mechanisms contributed significantly to the resistance provided by the composite slab.

In the full depth subassembly, the shear failure of the concrete between the column flanges was not observed and the compression failure at the column face was less prominent. As such the combination of full depth slab and additional reinforcement close to the column provided the slab at the column face with the additional capacity to resist the column failure and protect the slab between the column flanges from damage. Addition of further reinforcement such as U-bars in the gap between the column flanges would likely have increased this resistance and transferred forces further beyond the full depth section of slab.

As such it is considered that the best practice to reduce slab damage in contacting subassemblies is to provide a fully reinforced, full depth section of slab around the column face and to exercise care when placing the deck tray so as to have the tray spanning perpendicular to the direction of the primary beams.

7.2.3 Beam Elongation

In all moment end plate subassemblies tested some beam elongation was noted however this was very small. Beam elongation peaked at 9mm with residual displacements being 1-2mm at most. It is noted however that in a full SMRF the elongation at one end of the beam would likely be partially offset by the beam shortening at the opposite end. Further restraint would also be provided within a frame by the columns and slabs on either side of the beams. It is theorised that this restraint would likely further reduce the elongation effects in the steel beam. As such results from this set of tests indicate that beam elongation in SMRF structures with composite floor slabs is minimal in comparison to reinforced concrete structures and that the elongation observed can be distributed across the floor slab rather than being lumped at a single crack.

7.3 Predicted Behaviour

7.3.1 Current Code Methods

Current methods for the design of SMRF structures with composite deck trays are set out in NZS3404. Comparison of the subassembly strength predicted using these methods to that observed during testing was made for each different subassembly configuration. These comparisons were made at both ultimate and, perceived, yield level.

Predictions of the strength of the subassemblies were made using the provisions set out in NZS3404 clause 12.10.2.4. These predictions took into account the NZS3404 method for the determination of slab interaction effects and deck tray directionality effects along with the design (no overstrength factor) moment connection and beam buckling capacities. Each subassembly was also assessed using both the nominal material properties and the measured section properties given in Section 4 at both yield and ultimate state. Predictions for the sliding hinge joint connection were made using procedures set out by MacRae et al (2010) with lower and upper bounds for the connection being determined based on friction coefficients of 0.2 and 0.4 respectively as recommended by Chanchi (2013).

The observed design capacity values were taken to be the peak applied forces generated during the first cycle at 2% drift. This was based on the assumption that 2% drift is a typical design level drift for steel moment resisting frame structures. The observed ultimate capacity values are those corresponding to the peak applied force across all drift cycles.

Table 12: Predicted and actual subassembly capacity at design and ultimate level.

	Predicted Design Capacity Using Design Values (kN)	Predicted Design Capacity Using Actual Values (kN)	Observed Design Capacity (kN)
Isolated	140.1	170.4	233
Transverse	218	253	305
Longitudinal	243	278	361
SHJ	-	-	-
Full Depth	243	278	305

	Predicted Ultimate Capacity Using Design Values (kN)	Predicted Ultimate Capacity Using Actual Values (kN)	Observed Ultimate Capacity (kN)
Isolated	205.5	239.8	251
Transverse	294	334	324
Longitudinal	320	360	365
SHJ	203*	256**	207
Full Depth	294	364	337

* Lower Bound value for the Sliding Hinge Connection
** Upper Bound value for the Sliding Hinge Connection

As is shown in Table 12, the predicted design capacities of the structure were all lower than the applied forces at 2% drift. The predicted values tended to be a closer approximation to the level of applied force observed during the 1.5% drift cycles.

The ultimate value for the isolated subassembly was significantly higher than the predicted by NZS3404 however this is likely to be primarily due to the incomplete isolation described in Section 7.1.1. The ultimate capacities of the subassemblies with slab-column contact however were close to their predicted design values. As shown in Table 12, the observed ultimate capacity was either slightly above the predicted value using actual section properties or between the predicted values with nominal and actual section properties. However because progressive yielding occurs in the beams it was theorised that the ultimate capacity of the section should be approximately half way between the design values obtained using nominal

design and ultimate section capacities. As such the design ultimate capacities of the section, shown in Table 13, were 85-95% of the measured ultimate capacity.

Table 13: Predicted capacity half way between design and ultimate and actual ultimate capacity.

	Predicted Ultimate Capacity Using Design Values (kN)	Predicted Ultimate Capacity Using Actual Values (kN)	Observed Ultimate Capacity (kN)
Isolated	172.8	205.1	251
Transverse	256	293.5	324
Longitudinal	281.5	319	365
SHJ	203*	256**	207
Full Depth	268.5	321	337

* Lower Bound value for the Sliding Hinge Connection
** Upper Bound value for the Sliding Hinge Connection

Given that all of the predicted capacities generated using the NZS3404 method were less than the observed peak strengths it is apparent that this design methodology is conservative but within 15% of the actual result. Further work will be required to determine whether changes should be made to this design methodology.

7.3.2 Simple Modelling

Program issues

A number of issues were identified in using the Ruaumoko software which affected the accuracy of the model results.

The Ruaumoko model produced was essentially a line model and although each of the elements has a given area the connections between elements remain single points with no associated area. This introduced difficulties in modelling contact connections such as those between the slab and the column face as the software could not model a gradual failure of the elements as would be expected during spalling of the concrete. This issue also effected the modelling of the connections between the beams and concrete slab via the shear studs.

The control functions used to apply loading to the model were not ideal and although three options were available, individually none where appropriate for the expected hysteresis. The

force based pushover provided an accurate force-displacement hysteresis up to the maximum applied loading however at this point the hysteresis plateaued leaving the behaviour post ultimate unknown. The displacement based pushover method also provided an accurate hysteresis up to peak strength however this option is coded to terminate the analysis once the stiffness of the model reached zero. The final option was a displacement controlled time history analysis which became highly unstable once the stiffness of the model reached zero. As such none of the control options allowed the post-ultimate behaviour to be recorded and a combination of force based modelling of the isolated subassembly and displacement based modelling of the remaining subassemblies up to peak strength was required to produce a rough estimate of the hysteresis.

Stiffness of the Models

One of the largest shortcomings of the Ruaumoko model was its underestimation of the initial stiffness of the subassemblies. Given the slop in the reaction frame and the restraint connections it was expected that the model would predict a higher initial stiffness than would be observed in the test subassemblies.

Table 14: Comparison of model and actual subassembly initial stiffness.

Initial Stiffness	Isolated	Transverse	Longitudinal	SHJ	Full Depth
Actual	15400	14100	17300	16800	15700
Model	8864	9707	9632	-	9707

A number of shortcomings were identified in the model which contributed to the reduced initial stiffness. These included:

- Isolation effects. The model of the isolated subassembly assumed no contact between the concrete slab and the column face. As described in section 7.1.1 however, some contact remained in the test subassembly between the slab and the column. As such the test subassembly would be expected to exhibit a higher initial stiffness than was predicted.
- Confinement effects. Being a 2D line model, the slab and, in particular, the contact elements were unable to recreate the confinement effects provided by the wider slab and the contact between the slab, steel beam and deck tray. A portion of the initial

stiffness deficit in the transverse, longitudinal and full depth subassembly was believed to be attributed to this effect.

- Contact element details. Each of the contact slab elements was separate from the remaining elements and as such strain distribution between the elements could only occur at the column face and at the point where the contact elements converged back into a single slab element. This arrangement tended to engage the lower elements to a lesser extent than the upper elements resulting in a lower global stiffness for the group of elements.

Strength of the Models

The global strength of the Ruaumoko models, with the exception of the isolated subassembly, was also significantly underestimated.

Table 15: Comparison of model and actual subassembly peak and residual capacities.

	Isolated	Transverse	Longitudinal	SHJ	Full Depth
Actual					
Maximum Recorded Capacity (kN)	251	324	365	207	337
5% Drift Residual Capacity (kN)	231	212	240	150	254
Model					
Maximum Predicted Capacity (kN)	242	271	312	-	271
5% Drift Residual Capacity (kN)	242	242	312	-	242

The primary cause for the lower than observed ultimate capacity of the model was the premature failure of the compression elements between the column and the slab. For a 30MPa concrete the estimated compression capacity of the compression elements should have summed to around 1400kN. However as shown in Figure 7-14 (further examples also in Appendix C) the total resistance offered by the contact elements peaked at just under 500kN. As with the initial stiffness, this was believed to be due to the way in which loads were shared between the elements with the upper contact elements being loaded higher than the lower elements. The failure of the uppermost contact element initiated a cascade effect in which the loads were dumped onto the next element causing that to fail. Had better load sharing been achievable it

is believed that the modelling results may have more accurately replicated the observed behaviour of the subassemblies.

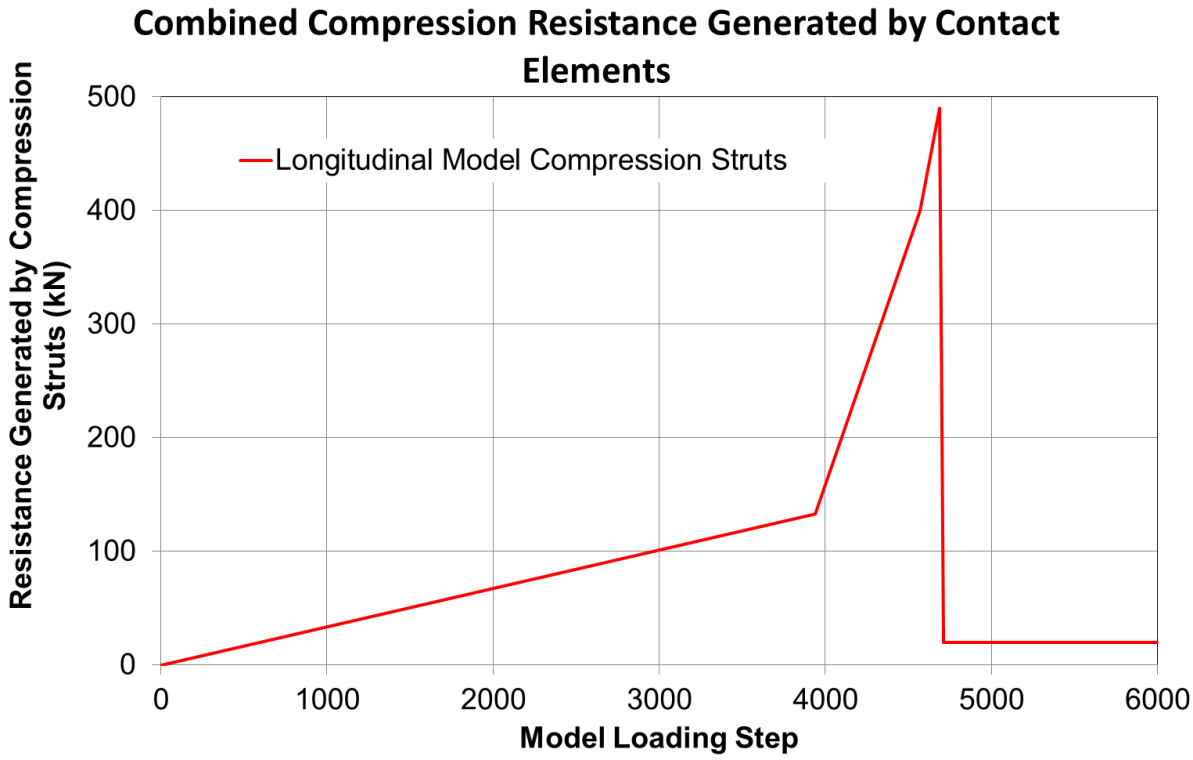

Figure 7-14: Resistance provided by contact elements in the longitudinal model.

Improvements to the Modelling

It is believed that, due to the shortcomings of the modelling software, there are minimal options available for improving the performance of these models significantly. For modelling of systems where contact occurs over any sizable area it is advisable that the modeller utilises a 3D finite element model to better incorporate these effects.

8 Conclusions and Recommendations

8.1 Conclusions

The findings of this study are described in relation to the questions posed in the scope as set out in section 1.3. These are:

a) What is the effect of isolating the floor slab from the column on the performance of the subassembly?

Comparison of Isolated and Transverse subassemblies shows that the provision of a gap between the column flange and the floor slab does effect the performance of the system. The isolated subassembly showed a reduction in ultimate capacity of 25% when compared to the transverse subassembly however yield capacities were similar for both subassemblies. Despite the lower capacities, isolation of the slab produced a more stable global hysteresis with little strength degradation at high drifts. This was reflected in the damage observed with buckling of the beam flanges occurring at higher drift levels in the isolated subassembly than in the transverse subassembly. Likewise slab damage in the isolated subassembly was noticeably less than in the transverse subassembly in terms of crack pattern extent, average crack width and spalling around the column face.

b) What is the effect of the direction of the deck tray on the performance of the subassembly?

Comparison of the transverse and longitudinal subassemblies shows a difference in both the capacities and the performance of subassemblies with different deck tray layouts. The longitudinal subassembly produced a global ultimate capacity 10% higher than that observed in the transverse subassembly. This was primarily attributed to the provision of a full depth section of slab along the length of the beam in the longitudinal subassembly which allowed the transfer of forces from the column face back into the slab. Conversely the transverse subassembly was limited to transferring forces through the reduced slab depth found above the deck ribs hence reducing the capacity of the slab.

The drawback to the longitudinal orientation of the deck tray is the damage sustained by the slab. Damage in the form of extensive cracking and spalling was noted in the longitudinal subassembly. Further investigation also determined significant spalling of cover concrete along the length of the beams indicating the potential for losses in slab strength. The spalling damage in the transverse subassembly, however, was limited to the area of concrete between the column face and the first deck rib.

c) What is the effect of the slab on the low-damage sliding hinge connection?

The sliding hinge connection performed admirable well during testing and produced a very stable hysteresis. The addition of the composite slab did not appear to have any significant impact on the performance of the connection with the behaviour of the subassembly being in line with that observed in the other test subassemblies.

d) What effect does the provision of a full depth slab around the column slab have on the performance of the subassembly?

Comparison of the transverse and full depth subassemblies shows a difference in the post-ultimate performance of subassemblies. The subassembly with a full depth section of slab cast around the column produced a global peak strength which was only 4% higher than the corresponding transverse deck tray subassembly. Beyond peak strength however the full depth subassembly did not exhibit the sudden strength degradation observed in subassemblies without the full depth slab detailing. This was likely due to the additional confinement effect provided by the concrete and the resistance provided by the additional reinforcing placed around the column. The provision of the full depth section of slab also had little effect on the damage obtained by the slab with both the transverse and full depth subassemblies sustaining a similar level of slab damage.

The only drawback to the full depth slab was the amplification of buckling in the beam flanges. The rigid slab resulted in more severe buckling of the beam flanges especially at higher drift levels indicating an increased level of force transfer between the slab and the column face.

e) What are the modes of steel strength loss in the subassemblies with moment end plate connections?

Throughout the testing program, all of the traditional moment end plate subassemblies exhibited similar modes damage to the steel beams. Between 2.0% and 3.5% drift, all subassemblies exhibited buckling of the bottom flanges of the beams near the tip of the gusset plates on the moment end plate. This buckling tended to occur at lower drift cycles in the subassemblies with the slab cast against the columns than in the isolated subassemblies (refer to Table 11). Buckling of the top flanges of the beams was minor in comparison to the bottom flanges and was more prominent in subassemblies with the slab cast in contact with the column. Buckling was usually confined to a single buckle over roughly one beam depth from the gusset plate however in both the longitudinal and full depth tests a second buckle formed on the west beam but remained within 1.5 times the beam depth from the gusset plate.

Neither the columns nor the moment end plate connections of the subassemblies appeared to have undergone significant inelastic deformation.

f) Does the concrete slab contribute significantly to the strength loss of the non-isolated subassemblies and through which mechanisms?

The most prominent modes of strength loss were the shearing of the block of concrete between the column flanges and compression failure of the concrete at the column faces. These two modes of force transfer contributed to up to 30% of the peak capacity of the non-isolated subassemblies tested and contributed to a similar portion of the strength degradation.

The full depth, unreinforced section of slab between the column flanges tended to shear away from the rest of the floor slab at around 3.5% drift. Generally this took the form of a single large shear crack running between the tips of the column flanges and was accompanied by a sudden loss of global capacity. It is believed that this portion of the slab forms a shear key which restrains the movement of the column hence increasing the capacity of the sub-assembly.

Compression failure of the concrete beside the column face occurred at the same time as the shearing of the concrete between the column flanges. In subassemblies with the deck tray run

perpendicular to the primary beams the compression failure was generally limited to the area of concrete between the column face and the first deck rib. Likewise when a full depth section of slab was placed around the column the compression failure was limited to the area of the full depth slab. When the deck tray was run parallel to the main beam an increased level of slab damage was noted with shearing of the layer of concrete above the shear studs occurring along the length of the beam.

Cracking of the slab occurred throughout testing however this did not appear to significantly affect the overall performance of the subassemblies. Cracking of the slab tended to occur over the deck ribs which created a dispersed crack pattern across the slab which would allow for easy repair using crack injection.

g) Are the effects of beam elongation significant in this type of steel moment resisting frame?

Beam Elongation, primarily in the area beside the beam-column joint, was observed in all subassemblies with moment end plate connections. Prior to buckling of the beam, elongation was negligible however higher levels of elongation were observed once buckling of the beam flanges occurred. Whilst most of this elongation was recovered, upon righting of the structure a small amount of residual elongation, usually 2-4mm, remained in all cases. It is theorised that the boundary conditions imposed in a complete structure would likely reduce this further.

h) Is it possible to model this slab column interaction using simplified modelling techniques?

Modelling of the test subassemblies was undertaken using the Ruaumoko modelling package. The models were constructed as 2D representations of the beam-column subassembly with a slab element attached to the beam. This had its limitations particularly in determining the contact force transfer mechanism between the slab and the column flange. The model subassemblies exhibited a reduced initial stiffness and, in the subassemblies with slab contact, a lower peak strength than the physical test subassemblies. The models also failed to reproduce the post-ultimate drop in strength observed in the physical test subassemblies. It is therefore considered that in cases such as this where strength transfer via compression contact is necessary that simplified linear element modelling is not sufficient to accurately predict the performance of the subassembly.

i) Do the current methods used in NZS3404 result in a reasonable approximation of the effects of the composite slab and if not what changes could be made to improve the accuracy of the code calculations?

The design methods given by NZS3404 produced results within 15% of the observed peak strength across all tests with slab-column contact when assessed with the measured section properties. Given the difficulties experienced with the isolated subassembly it would be premature to make meaningful recommendations as to changes to the code without further testing. As such the design methods given by NZS3404 for composite concrete floor slabs should be taken as conservative and continue to be utilised until such time that sufficient data is available to justify making changes to these methods.

Several other aspects of the steel code could also be more closely scrutinised including:

- The overstrength allowance of structural steel members. The steel members tested had a measured overstrength of up to 1.24, close to the NZS3404 prescribed value of 1.25. Limits on the upper bound strength may be required in future to ensure undesirable failure mechanisms do not occur as a result of overstrength in components designed to yield.
- The effect of composite floor slabs on beam strength loss mechanisms. The moment end plate subassemblies tested all exhibited local buckling of beam near the beam-column connection. This would indicate that the provision of a composite floor slab promotes a section strength loss mechanism (local buckling) rather than a member strength loss mechanism such as lateral or torsional buckling. As section failure leads to a higher beam capacity than member failure, consideration should be given as to which design methodology to follow to ensure a ductile failure mechanism.
- The placement of shear studs in plastic hinge zones. Currently the plastic hinge zone for a steel beam is taken as 1.5D from the moment end plate and shear studs are not place within this zone. During testing, the region of beam flange buckling was observed to extend beyond 1.5D from the moment end plate however it remained within 1.5D from the tip of the gusset plates. As such it would be more accurate to take the plastic hinge zone as extending from the moment end plate to 1.5D from the tip of the gusset plates.

8.2 Recommendations

From this study the following recommendations have been made for the design of SMRF structures with composite floor slabs:

- That the design methods given by NZS3404 be taken as conservative and continue to be utilised until such time that sufficient data is available to justify making changes to these methods.
- That slab-column interaction should not be considered in the design of beams in SMRF structures unless specific detailing be incorporated to ensure a ductile failure of the slab in contact with the column. This should be considered on a case by case basis and should include (but not be limited to):
    - Specific design of the slab reinforcing in the concrete surrounding the columns to form a strut and tie mechanism to transfer loads from the column into the slab.
    - Emphasis on the correct placement of the tray deck around the column and the provision of sufficient full depth section of slab around the column.
    - Specific design to ensure the forces imposed on the beams by the floor slab do not cause premature buckling of the beam flanges.
- That the floor slab should only considered to be isolated from the column face if the slab makes no contact with any part of the moment end plate connection including (but not limited to) the end plate, bolts, gusset plates and stiffener plates.
- That shear studs should not be placed within one and a half times the depth of the beam from either the moment end plate of the tips of the gusset plates (if fitted).

9 Further Work

Whilst this study has made large strides toward a better understanding of slab column effects in steel moment resisting frames there are still a number of areas in which future work could be undertaken to further this understanding. These include:

Bare frame test

Owing to time constraints, the opportunity to test a bare steel frame of identical design to those tested as part of this thesis was not available. Further testing of a bare steel frame would provide a valuable comparison point for the effect of a composite slab in the case that the slab is isolated from the column. This would also allow a comparison of the theoretical bare frame strength used in this thesis and in turn better identify the overstrength factors exhibited by these systems.

Further testing of full depth slab

Whilst the performance of the subassembly with the full depth slab surrounding the column was a noticeable improvement over those without, further investigation is required to determine the performance of the full depth slab. In particular future testing on the performance of the full depth slab in subassemblies with longitudinal deck trays and the use of isolation from the inside of the flanges are required to determine the effect on the subassembly. Further tests to determine appropriate placing of reinforcing both in the full depth slab and in the area of concrete between the column flanges could also aid in reducing slab damage and increasing subassembly strength.

Slab Effects in weak bending axis

Whilst this study has focused primarily on interactions in the strong bending axis of the column, interactions in the weak bending axis also have the potential to effect the performance of SMRF structures. This effect may be more pronounced in the weak bending axis especially if the steel connections are designed as shear only type connections.

Sliding Hinge Joint

Further testing of the sliding hinge type connection is required to fully understand the behaviour of this type of connection. Such testing should include:

- Testing of the connection followed by retightening of the connection bolts and re-testing.
- Testing of the connection followed by replacing of the connection bolts and re-testing.
- Further fatigue testing of the connection under multiple cyclic loads.
- Testing of a non-prying SHJ connection.

3D modelling of the Subassembly

Analytical modelling of the subassemblies in this project was simplified to a 2 dimensional model. Further analytical modelling of a 3D subassembly with full slab using a finite element modelling package would likely lead to an improved understanding of the force transfer mechanisms present in the subassembly.

10 References

1. Standards New Zealand, *NZS3404 Structural Steel Standard*. 2009, Standards New Zealand: Wellington.
2. American Institute of Steel Construcxtion (AISC), *AISC341-10 Seismic Provisions for Structural Steel Buildings*. 2010, American Institute of Steel Construction: Chicago, IL.
3. American Concrete Institute (ACI), *ACI318: Building Code Requirements for Structural Concrete and Commentry*. 2011, ACI: Farmington Hills, MI.
4. American Institute of Steel Construcxtion (AISC), *Partially Restrained Composite Connections, A Design Guide*. 1996, AISC: Chicago, IL.
5. American Institute of Steel Construcxtion (AISC), *AISC360-10 Specification for Structural Steel Buildings*. 2010, AISC: Chicago, IL.
6. European Committee for Standardization (CEN), *Eurocode 4: Design of composite steel and concrete structures. Part 1-1: General rules and rules for buildings.* 2004, CEN c2004: Brussels.
7. European Committee for Standardization (CEN), *Eurocode 8: Design of structures for earthquake resistance. Part 1, General rules, seismic actions and rules for buildings.* 2004, CEN c2004: Brussels.
8. European Committee for Standardization (CEN), *Eurocode 3: Design of steel structures. Part 1-8: Design of joints.* 1992, CEN c2005: Brussels.
9. du Plessis, D.P. and J. Hartley Daniels, *Experiment on Composite Beams Under Positive End Moment*. 1972, Lehigh University: Bethlehem PA.
10. du Plessis, D.P. and J. Hartley Daniels, *Strength of Composite Beam-to-Column Connections*. 1973, Lehigh University: Bethlehem PA.
11. du Plessis, D.P., *The Interaction of Floors and Frames in Multistorey Buildings*, in *Civil Engineering*. 1974, Lehigh University: Bethlehem PA.
12. Lee, S.-J. and L.-W. Lu, *Cyclic Tests of Full-Scale Composite Joint Subassemblages.* Journal of Structural Engineering (ASCE), 1989. **115**(8): p. 1978-1998.
13. Han, L.-H. and W. Li, *Seismic performance of CFST column to steel beam joint with RC slab: Experiments.* Journal of Constructional Steel Research, 2010(66): p. 1374-1386.
14. Leon, R.T., *Composite Semi-Rigid Construction.* Engineering Journal (AISC), 1994.
15. Hajjar, J.F., Leon, R.T., Gustafson, M.A., Shield, C.K., *Seismic Response of Composite Moment-Resisting Connections. II: Behaviour*. Journal of Structural Engineering (ASCE), 1998. **124**(8).
16. Leon, R.T., J.F. Hajjar, and M.A. Gustafson, *Seismic Response of Composite Moment-Resisting Connections. I: Performance.* Journal of Structural Engineering (ASCE), 1998. **124**(8).
17. Civjan, S.A., M.D. Engelhardt, and J.L. Gross, *Slab Effects in SMRF Retrofit Connection Tests.* Journal of Structural Engineering, 2001. **127**(3).
18. Sumner, E.A., T.W. Mays, and T.M. Murray, *End-Plate Moment Connections: Test Results and Finite Element Method Validation*. 2002, Virginia Polytechnic Institute: Blacksburg, Virginia.
19. Murray, T.M. and M.W. Seek, *Seismic Strength of Moment End-Plate Connections with Attached Concrete Slab*. 2009, Virginia Tech: Blacksburg, Virginia.
20. Green, T.P., R.T. Leon, and G.A. Rassati, *Bidirectional Tests on Partially Restrained Composite Beam-to-Column Connections.* Journal of Structural Engineering (ASCE), 2004. **130**(2).

21. Liu, J. and A. Astaneh-Asl, *Cyclic Testing of Simple Connections Including Effects of Slab*. Journal of Structural Engineering, 2000. **126**(1).
22. Liu, J. and A. Astaneh-Asl, *Moment-Rotation Parameters for Composite Shear Tab Connections*. Journal of Structural Engineering, 2004. **130**(9).
23. Braconi, A., et al., *Seismic performance of a 3D full-scale high-ductility steel-concrete composite moment-resisting structure - Part II: Test Results and analytical validation.* Earthquake Engineering and Structural Dynamics, 2008(37): p. 1635-1655.
24. Braconi, A., Bursi, O.S., Fabbrocino, G., Salvatore, W., Tremblay, R., *Seismic performance of a 3D full-scale high-ductility steel-concrete composite moment-resisting structure - Part I: Design and testing proceedure.* Earthquake Engineering and Structural Dynamics, 2008(37): p. 1609-1634.
25. Braconi, A., A. Elamary, and W. Salvatore, *Seismic behaviour of beam-to-column partial-strength joints for steel-concrete composite frames.* Journal of Constructional Steel Research, 2010(66): p. 1431-1444.
26. Yamada, S., Suita, K., Tada, M., Kusai, K., Matsuoka, Y., Shimada, Y., *Full Scale Shake Table Collapse Expiriment on 4-Storey Steel Moment Frame*. in *International Conference on Urban Earthquake Engineering & International Conference on Earthquake Engineering*. 2010. Tokyo, Japan.
27. Gunasekaran, U. and G.A. MacRae, *A new concept for consideration of slab effects on building seismic performance.* Journal of Structural Engineering 2007. **34**(1): p. 25-32.
28. Kim, J., J. Stanton, and G.A. MacRae, *Effect of Beam Growth on Reinforced Concrete Frames.* Journal of Structural Engineering (ASCE), 2004. **130**(9): p. 1333-1342.
29. Mago, N. and G.C. Clifton, *Investigation of the Slab Participation in Moment Resisting Steel Frames*. 2008, New Zealand Heavy Engineering Research Assocoation (HERA): Manakau City.
30. MacRae, G., G.C. Clifton, and N. Mago, *Overstrength Effects of Slabs on Demands on Steel Moment Frames*, in *Pacific Structural Steel Conference*. 2007: Wairakei.
31. Clifton, G.C., *Semi-Rigid Joints for Moment-Resisting Steel Framed Seismic-Resisting Systems*, in *Department of Civil and Environmental Engineering*. 2005, University of Auckland: Auckland, New Zealand.
32. MacRae, G.A., Clifton, G.C., Mackinven, H., Mago, N., Butterworth, J., Pampanin, S., *The Sliding Hinge Joint Moment Connection.* Bulletin of the New Zealand Society for Earthquake Engineering, 2010(December).
33. Khoo, H.H., Clifton, G.C., Butterworth, J.W., Mathieson, C.D., MacRae, G.A., *Development of the Self-Centering Sliding Hinge Joint*. in *Pacific Conference of Earthquake Engineering*. 2011. Auckland, New Zealand.
34. Chanchi, J., MacRae, G.A., Chase, J.G., Scott, A., Rodgers, G.W., Clifton, G.C., *Recent Research on Two Low Damage Dampers Applicable to Steel Framing Systems*, in *Steel Innovations Conference*. 2013: Christchurch, New Zealand.
35. Corus New Zealand. *Comflor 80 Composite Floor Decking*. 2005 [cited 2011 26 June]; Available from: http://www.comflor.co.nz/ComFlor-80-Brochure.asp.
36. Corus New Zealand. *Comflor 60/80 Quick Reference Load Span Tables*. 2005 [cited 2011 26 June]; Available from: http://www.comflor.co.nz/ComFlor-60-80-Span-Tables.asp.
37. Heavy Engineering Research Association, *Design properties of 0.7mm CF60 G550, 0.7mm CF80 G550 and 1.15mm CF80 G500 profiled steel decking*. 2008, HERA: Auckland, New Zealand.
38. Khanlou, A., MacRae, G.A., Scott, A.N., Hicks, S.J., Clifton, G.C., *Shear Performance of Steel Fibre-Reinforced Concrete*, in *Steel Innovations Conference*. 2013: Christchurch, New Zealand.

39. Steel & Tube. *SE82 Mesh*. [cited 2013 15 May]; Available from: http://steelandtube.co.nz/product/rei/hrc-mesh/seismic-mesh/se82.
40. Heavy Engineering Research Association, *R4-100: Structural Steelwork Connections Guide*. 2003, HERA: Manukau City, New Zealand.
41. Heavy Engineering Research Association, *R4-142: Eccentric Cleats in Compression and Columns in Moment-Resisting Connections*. 2009, HERA: Manukau City, New Zealand.
42. Bisalloy Steels Pty Ltd. *BISPLATE 500*. 2012 [cited 2013 13 May]; Available from: http://www.bisalloy.com.au/products/18/Wear%20Grades.
43. American Concrete Institute (ACI), *ACI T1.1-01: Acceptance Criterial for Moment Frames Based on Structural Testing*. 2001, ACI: Farmington Hills, MI.
44. OneSteel, *Hot Rolled and Structural Steel Products*. 2003: Port Kembla, Australia.
45. Standards Australia/Standards New Zealand, *AS/NZS3679.1: Structural Steel, Part 1: Hot-rolled bars and sections*. 2010, Standards New Zealand: Wellington.
46. Standards New Zealand, *NZS3112: Specification for Methods of Test for Concrete, Part 1: Tests relating to fresh concrete*. 1986, Standards New Zealand: Wellington.
47. Standards Australia/Standards New Zealand, *AS/NZS1252: High-strength steel bolts with associated nuts and washers for structural engineering*. 1996, Standards New Zealand: Wellington.
48. Han, H., *Tensile Testing of Grade 8.8 Bolts*, University of Auckland: Auckland, New Zealand.
49. Standards Australia/Standards New Zealand, *AS/NZS1554.2: Structural steel welding, Part 2: Stud welding (steel studs to steel)*. 2003, Standards New Zealand: Wellington.
50. Park, R.; Paulay, T. 1975: *Reinforced concrete structures.* John Wiley, New York, 769pp.

11 Appendices

The Appendices for this thesis are presented in CD-ROM form and are attached at the rear of the publication.